UDK 66:54(05) CODEN HMIDA 8 ISSN 0367–598 X

4

Hemijska industrija

Vol. 68

Časopis Saveza hemijskih inženjera

Chemical Industry

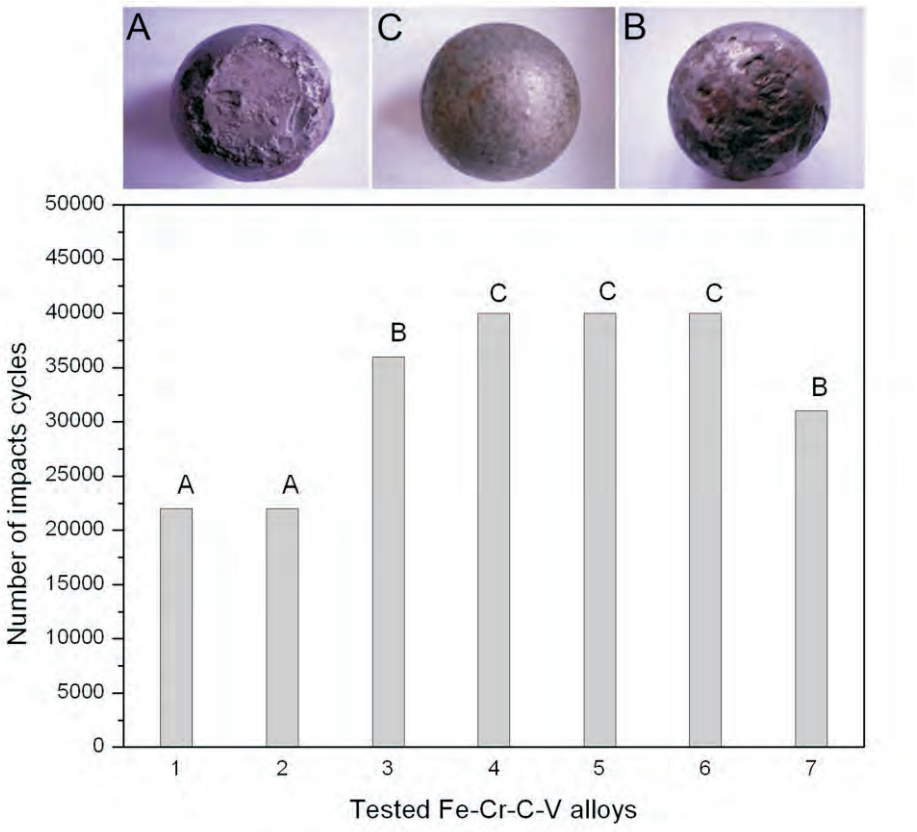

BEOGRAD, JUL-AVGUST 2014. HMIDA 8, 68 (4) 399-517 (2014)

GENERALNI POKROVITELJ

Hemofarm

HEMOFARM KONCERN

VRŠAC, Beogradski put bb, tel. 013/821-345, 821-027, 821-129
BEOGRAD, Prote Mateje 70, tel. 011/344-26-63, faks: 344-17-87
E-pošta: info@hemofarm.com

IZDAVANJE ČASOPISA POMOGLA JE:

INŽENJERSKA KOMORA SRBIJE
Bulevar vojvode Mišića 37
11000 Beograd

SUIZDAVAČI

Tehnološko-metalurški fakultet
Univerziteta u Beogradu, Beograd

Prirodno-matematički fakultet Univerziteta
u Novom Sadu, Novi Sad

Hemijski fakutet
Univerziteta u Beogradu
Beograd

ITNMS
Institut za tehnologiju nuklearnih i drugih
mineralnih sirovina, Beograd

HIP PETROHEMIJA
HIP Petrohemija a.d. Pančevo

Tehnološki fakultet Univerziteta
u Novom Sadu, Novi Sad

NU Institut za hemiju,
tehnologiju i metalurgiju
Univerziteta u Beogradu,
Beograd

nevena
„Nevena Color“ d.o.o.
Leskovac

Tehnološki fakultet Univerziteta
u Nišu, Leskovac

dcp-hemigal®
DCP Hemigal, Leskovac

Chemical Industry
Химическая промышленность

Hemijska industrija

Časopis Saveza hemijskih inženjera Srbije
Journal of the Association of Chemical Engineers of Serbia
Журнал Союза химических инженеров Сербии

VOL. 68 **Beograd, jul–avgust 2014** **Broj 4**

Izdavač
Savez hemijskih inženjera Srbije
Beograd, Kneza Miloša 9/I

Glavni urednik
Branko Bugarski

Zamenica glavnog i odgovornog urednika
Nevenka Bošković-Vragolović

Urednici
Katarina Jeremić, Ivana Banković-Ilić, Maja Obradović, Dušan Mijin

Članovi uredništva
Milorad Cakić, Željko Čupić, Željko Grbavčić, Katarina Jeremić, Miodrag Lazić, Slobodan Petrović, Milovan Purenović, Aleksandar Spasić, Dragoslav Stoiljković, Radmila Šećerov-Sokolović, Slobodan Šerbanović, Nikola Nikačević, Svetomir Milojević

Članovi uredništva iz inostranstva
Dragomir Bukur (SAD), Jiri Hanika (Češka Republika), Valerij Meshalkin (Rusija), Ljubiša Radović (SAD), Constantinos Vayenas (Grčka)

Likovno-grafičko rešenje naslovne strane
Milan Jovanović

Redakcija
11000 Beograd, Kneza Miloša 9/I
Tel/fax: 011/3240-018
E-pošta: shi@yubc.net
www.ache.org.rs

Izlazi dvomesečno, rukopisi se ne vraćaju

Za izdavača
Tatijana Dudukoviċ

Sekretar redakcije
Slavica Desnica

Izdavanje časopisa pomaže
Republika Srbija, Ministarstvo prosvete, nauke i tehnološkog razvoja

Uplata pretplate i oglasnog prostora vrši se na tekući račun Saveza hemijskih inženjera Srbije, Beograd, broj 205-2172-71, Komercijalna banka a.d., Beograd

Kompjuterska priprema
Vladimir Panić

Štampa
Razvojno-istraživački centar grafičkog inženjerstva, Tehnološko-metalurški fakultet, Univerzitet u Beogradu, Karnegijeva 4, 11000 Beograd

Indeksiranje
Radovi koji se publikuju u časopisu *Hemijska Industrija* ideksiraju se preko *Thompson Reuters Scietific®* servisa *Science Citation Index - Expanded™* i *Journal Citation Report (JCR)*, kao i domaćeg *SCIndeks* servisa Centra za evaluaciju u obrazovanju i nauci

SADRŽAJ

CONTENTS

Significance of the structural properties of CaO catalyst in the production of biodiesel: An effect on the reduction of greenhouse gas emissions

Radomir B. Ljupković[1], Radoslav D. Mićić[2], Milan D. Tomić[3], Niko S. Radulović[1], Aleksandar Lj. Bojić[1], Aleksandra R. Zarubica[1]

[1]*Department of Chemistry, Faculty of Science and Mathematics, University of Niš, Niš, Serbia*
[2]*NTC NIS Naftagas – Novi Sad, Novi Sad, Serbia*
[3]*Faculty of Agriculture, University of Novi Sad, Novi Sad, Serbia*

Abstract

The influence of the physicochemical properties of a series of CaO catalysts activated at different temperatures on the biodiesel production was investigated. These catalysts show dissimilar yields in the transesterification of triglycerides with methanol. We have found significant relationships between structural properties (the type of the pore system, the typical CaO crystal phase and the sizes of crystallites (up to 25 nm), the minimal weight percentage of CaO phase, the total surface basicity and potential existence of two types of basic active sites) of CaO prepared and activated by means of thermal treatment at highest temperature and catalytic efficiency. Benefits of this catalyst are short contact time, standard operating temperature and atmospheric conditions, relatively low molar ratios and small catalyst loading. These all together resulted in a very high biodiesel yield of high purity. The properties of different biodiesel (obtained with the use of the prepared CaO catalyst) blends with different diesel and biodiesel ratios indicate that the higher the fraction of biodiesel fuel the better the achieved fuel properties according to the EU standards. A significant reduction of CO_2 and CO emissions and only a negligible NO_x increase occurred when blends with an increased biodiesel portion was used. The use of biodiesel derived blends, and the eventual complete replacement of fossil fuels with biodiesel as a renewable, alternative fuel for diesel engines, would greatly contribute to the reduction of greenhouse gas emissions.

Keywords: biodiesel production, CaO catalyst, greenhouse gas emissions, structural catalytic properties.

Available online at the Journal website: http://www.ache.org.rs/HI/

SCIENTIFIC PAPER

UDC 662.756.3:544.47:66.097.3

Hem. Ind. **68** (4) 399–412 (2014)

doi: 10.2298/HEMIND130612063L

The great attention has been given lately to biodiesel production from renewable energy resources (*e.g.*, vegetable oils and/or animal fats) because of energetic, ecological, geo-political and economic benefits. The production and use of biodiesel provided the means to a net reduction of CO_2, CO, NO_x, SO_x emissions, directly related to the "greenhouse effect", *i.e.*, global warming, then soot particles and unburned hydrocarbons released from diesel engines, and finally the removal of waste greases [1]. Further, it enables the usage of domestic renewable energy/fuel resources and diminishes the dependence on crude oil import. Other advantages of biodiesel use are its lubricant properties, acceptable cetane number, flash point and low temperature properties, making it an alternative, environmental friendly, biodegradable, renewable fuel [2,3], and a direction to sustainable development and economy.

Biodiesel as non-petroleum derived fuel is a mixture of fatty acid methyl or rarely ethyl esters (FAME and FAEE) obtained by catalytic transesterification of vegetable oils/fats with the two short chain alcohols. The present technology of biodiesel production comprises the utilization of homogeneous catalysts (NaOH and/or KOH) [4]. Typically, NaOH or KOH are used as base homogeneous catalysts. Disadvantages of homogeneous catalysis are the recovery of the catalyst used in the transesterification reaction and considerable volume of wastewater discharged from the process utilized to refine the dissolved alkali hydroxide from the produced biodiesel.

Despite the long history of application of homogeneous catalysis in biodiesel production, a great number of benefits of heterogeneous catalysts are recognized. The utilization of heterogeneous catalysts would be a solution for most of environmental and economic drawbacks of homogeneously catalyzed process. A heterogeneous catalyst can be easily and quickly sepa-

Correspondence: A. Zarubica, Faculty of Science and Mathematics, University of Niš, 18000 Niš, Serbia.
E-mail: zarubica2000@yahoo.com
Paper received: 12 June, 2013
Paper accepted: 5 September, 2013

rated and reused and the produced biodiesel and glycerin could be rapidly purified and collected after separation. This easier and cheaper separation process would enable the elimination of consumption of large volumes of wastewaters [5]. In addition, the use of heterogeneous catalyst in biodiesel production makes it possible to simplify the production process by omitting sections from the complete process technology.

However, at present there is only one commercially accepted transesterification process technology. Also, heterogeneous catalysts are not consumed in the production process, whereas homogeneous processes require a fresh batch of catalyst for each new production cycle.

A number of series of basic or acidic heterogeneous catalysts (with and/or without promoters) have been investigated and used in the methanolysis of vegetable oils [6,7]. Basic heterogeneous catalysts give higher reaction rate than acidic ones and are predominantly prepared and tested. Despite the fact that several basic catalysts have exhibited promising activities, such as alkali and alkali earth oxides [8,9], alkali and alkali earth carbonates [10], basic zeolites [11], hydrotalcites [12,13] under the atmospheric pressure, no real replacement was found for the homogeneous process.

Among alkaline earth oxides, CaO and MgO have attracted more attention than the others due to the solubility of BaO in methanol and the tendency of SrO to react with CO_2 and water [14], and due to their dissolution in the reaction medium that makes the process a homogeneous one.

Mootabadi *et al*. [15] have investigated biodiesel production process from palm oil using alkaline earth oxides, *i.e.*, CaO, SrO and BaO calcined at 500 °C for 3 h, as the heterogeneous catalysts. The catalytic activity of the three catalysts was in the sequence of CaO < SrO < BaO. It was registered that the biodiesel yield was about 5% when CaO was used as the catalyst after 60 min of the reaction under following conditions: catalyst/oil mass ratio 0.03, methanol/oil molar ratio 9:1. The results from the study of basicity verified that the basic strength was in the same sequence of CaO < SrO << BaO [15]. The basic properties of the catalysts were established as the major determinant for the catalytic activity among the catalysts employed in the cited work [15].

Chen *et al*. [16] have studied the basicity of the alumina-supported alkaline earth metal oxides calcined at 550 °C for 6 h (CaO/Al_2O_3 was calcined at temperatures in the range: 300–750 °C). The basic properties (*i.e.*, the amount of basic sites) of alkaline earth oxides are influenced by the calcination temperature, while the strength of basic sites is not influenced by the calcination temperature. The calcination temperature of 550 °C yielded the highest amount of basic sites of CaO [16].

Veljković *et al*. [17] have prepared CaO catalyst by calcination at different temperatures (300, 500, 550, 600, 700 and 900 °C) for 2 h in their investigation on the kinetics of sunflower oil methanolysis catalyzed by calcium oxide. The increase of the calcination temperature to a certain value caused the increase of the CaO activity; the optimal CaO calcination temperature of 550 °C was recognized. This result was explained by dehydration of $Ca(OH)_2$ and the transformation of $CaCO_3$ to CaO [16–18], and additionally by the amount of active sites [16–18]. The FAME yield of rather more than 90% was achieved by using the CaO catalyst calcined at 550 °C after 120 min of the reaction under the following conditions: catalyst amount, based on the oil weight, %: 1.0; average catalyst particle size, μm: 2.8; reaction temperature: 60 °C; agitation speed, rpm: 900 [17].

Granados *et al*. [18] have studied biodiesel production from sunflower oil by using the activated calcium oxide by calcinations at: 200, 500 and 700 °C. The maximal FAME yield slightly larger than 90% was obtained over CaO calcined at 700 °C after 90 min of the reaction (conditions applied: catalyst amount, 0.5 g; 50 g of oil; reaction temperature: 60 °C; agitation speed, rpm: 1000) [18]. The catalytic activity of CaO was improved by activation treatment at 700 °C after transformation of the $CaCO_3$ to CaO; the carbonate groups were established as the main catalyst surface poisoning species [18].

Cho *et al*. [19] have considered transesterification of tributyrin with methanol over calcium oxide catalysts prepared from various precursors (calcium acetate monohydrate (CA), calcium carbonate (CC), calcium hydroxide (CH), calcium nitrate tetrahydrate (CN), calcium oxalate monohydrate (CO)). The precursors were calcined for 2 h at a calcination temperature that was varied from 500 to 900 °C at an interval of 100 °C. The activity of the catalysts increased in the following order: CN-800 < CC-800 < CO-800 ≈ CA-800 < CH-800 [19]. The conversion of more than 90% over CH-800 in transesterification of tributyrin (TriB) with methanol was achieved under the reaction conditions: TriB/MeOH mole ratio = 1/6 and reactant/catalyst mass ratio = 16.4/0.010 [19]. The basicity of the prepared calcium oxide catalysts also differed according to the precursors, and the relationship between the conversion level and the basicity of the CH catalysts was established [19].

Kouzu *et al*. [20] have probed CaO catalyst obtained after calcination of pulverized lime stone at 900 °C for 1.5 h as solid base catalyst for transesterification of soybean oil in biodiesel production. The authors have determined that the catalytic activity was in the sequ-

ence of CaO > $Ca(OH)_2$ >> $CaCO_3$. The yield of FAME at reflux of methanol was 93% for CaO, 12% for $Ca(OH)_2$, and 0% for $CaCO_3$ [20]. The basicity of catalysts seemed to be determinant for the catalytic activity among all the samples [20].

In their other work, Kouzu *et al*. [21] have examined the active phase of calcium oxide used as solid base catalyst for transesterification of soybean oil with refluxing methanol. The catalyst was prepared as it was previously mentioned [20]. Calcium oxide combined with the by-produced glycerol gave calcium diglyceroxide that was a major constituent of the collected catalyst. Calcium diglyceroxide would be the active phase in the catalytic reaction with usage of calcium oxide for biodiesel production. This catalyst had the advantage of tolerance to air-exposure [21].

Wei *et al*. [22] have investigated the activity of the eggshell-derived CaO catalyst calcined at different temperatures between 200 and 1000 °C for 2 h in the transesterification of soybean oil to produce biodiesel. They have claimed that the best catalytic performance was achieved for calcination temperature above 800 °C when XRD patterns showed a crystalline CaO phase. CaO was the active phase of the eggshell derived catalysts [22]. When the calcination temperature was 700 °C, a yield of 90% was achieved. One the other side, the experimental results showed that a 9:1 molar ratio of methanol to oil over 3 wt.% of eggshell-derived catalyst (calcined at 1000 °C), 65 °C reaction temperature gave the biodiesel yield that exceeded 95% at 3 h [22].

To the best of our knowledge, there is no complete consensus on different activation procedures applied in the preparation of CaO-based catalysts published and on the relevance of the physicochemical properties of catalysts for beneficial catalytic performances. Additionally, there are no data on the potential effect of the use of pure biodiesel obtained over CaO and/or diesel––biodiesel blends on the CO_x and NO_x emissions. Especially, such data concerning investigations in Serbia are missing in the scientific literature. Thus, in this work we decided to rectify this situation and investigate an impact of structural characteristics of CaO catalyst on the efficiency in the transesterification reaction, and a potential effect of biodiesel usage on the diesel engine performances and greenhouse gases emission.

EXPERIMENTAL

Preparation of catalyst, materials selection, standard characterization of feedstock and fuel

Calcium oxide of technical grade was used as the catalyst precursor. It was further calcined at selected temperatures (500, 750 and 900 °C) for 2.5 h under static air in order to prepare pure CaO-based activated catalysts. After calcination, the CaO-based catalyst powder was pressed into pellets. The pellets were sieved to obtain a fraction 1.0–1.5 mm in size. These fraction dimensions were optimal to avoid potential external diffusion restrictions within the reactor basket. Catalyst samples were labeled CaO-T, where T represented the calcination temperature. Afterwards, the characterization of the catalysts was performed.

Methanol of HPLC grade was used in the test reactions. Sunflower oil from a domestic producer was employed in the transesterification reactions. It was selected because sunflower represents a typical oilseed plant in Serbia and the region.

The particular properties of the feedstock and the obtained biodiesel (density, kinematic viscosity, cetane index, low temperature properties, flash point, sulfur content, water content, heating value) were determined by standardized methods: JUS EN 14214 (SRPS ISO 12185); JUS E K8.028 (SRPS ISO 3104); EN 14104: 2003 (SRPS ISO 4264); EN ISO 5165: 1998; EN 116; SRPS EN ISO 2719; ASTM D 5453; SRPS ISO 12937; ASTM D5865-07.

Catalysts characterization

Textural features of CaO catalytic samples were studied by low temperature N_2 adsorption/desorption method using a Micromeritics ASAP 2010 instrument with He as the carrier gas. Specific surface area was calculated by the Brunauer–Emmett–Teller (BET) equation, pore size distribution was estimated based on the Barrett–Joyner–Halenda (BJH) method, and the average pore diameter was determined as the BJH desorption mean pore diameter.

X-ray diffraction analysis (XRD) was conducted in order to determine the crystal structure of the CaO--based catalysts on an XRD Philips APD-1700 diffractometer with a Cu-anticathode and monochromator (at 40 kV and 55 mA). Crystallite sizes were calculated from the Scherer equation.

Thermogravimetric (TG) and differential thermal analyses (DTA) were done on a Baehr STA 503 apparatus in inert atmosphere. The measurements were performed in the temperature range 25–1000 °C using a heating rate of 10 °C/min.

Surface properties were revealed by FTIR spectroscopy on a Win Bomem 1000 instrument in the region 4000–400 cm^{-1}. Before the recordings, the catalyst samples were exposed to phenol vapors to investigate the basic nature of surface sites, and afterwards exposed to vacuum to remove any physically adsorbed vapors.

Morphological properties of the bulk catalysts were determined by a scanning electron microscope (SEM, JOEL JSM-6460 L), at different magnification (up to 100000×) at the accelerating voltage of 25 kV.

Catalytic test, biofuel products profile determination

Transesterification of sunflower oil was conducted over the prepared CaO catalysts in a stirred, commercial reactor, Parr 4520. The catalyst loading was 1 wt.% relative to the total reagents weight, the methanol to oil ratio 6:1 (*w*/*w*), at reflux conditions of methanol, and mixing rate of 250 rpm. Constant reaction temperature (64 °C) was maintained during 5 h of the reaction run at atmospheric pressure. Reaction products samples were taken after each 1 h of a single reaction run. The batch reactor was heated to the desired temperature with a constant ramp of 5 °C/min starting from ambient temperature, and the zero reaction point was the moment when the desired temperature was reached.

Reaction products, as well as the oil profile, were characterized by gas chromatography (GC HP 5980 Series II with a FID detector) in accordance with the standard procedure given by SRPS EN 14103. Methyl heptadecanoate (>99%, Fluka Co.) was used as the internal standard in quantitative analyses, and a standard mixture of methyl esters in qualitative analyses. The following conditions of the GC analyses were employed: 30 m long capillary column, the flow of 2 ml/min of He as the carrier gas, and the analyte separation isothermally at 210 °C during 10 min. Catalyst activity was ranked as FAME yield calculated as we have reported in our previous work [23].

Engine performances and exhaust gases emissions

Engine performances were investigated on a Tractor type Mahindra 6500. This type of tractor is common in Serbia, and can be used for various purposes in agriculture. The conventional working conditions of the tractor engine with four cylinders (Tier of the second generation) were reached during the investigation: rated power of 48.4 kW at 2200 rpm, compression ratio of 19.5:1, maximal torque of 217.4 Nm. Fuel injection pressure 250–260 bar was used inside the pump MICO Bosch (VE type).

Fuel consumption was determined by the volume--method applying a flow-meter of type Pireburg 2911. Exhaust gas emissions were resolved according to the standard ISO 8178-4 and tracked with the use of Testo 355 portable analyzer.

RESULTS AND DISCUSSION

Structural properties of the CaO catalyst

The textural properties of the prepared catalysts (BET surface area, average pore diameter, BJH cumulative desorption pore volume and maxima in pore size distribution (PSD)) are shown in Table 1. These properties are important characteristics of the solid state CaO-based catalysts because they readily influence the catalytic efficiency in the transesterification of sunflower oil. These catalytic properties are also in correlation with the precursor of the CaO catalyst and thermal history of the activated CaO-based catalyst samples.

Specifically, the increase of the calcination/activation temperature of the CaO catalyst samples has caused a slight decrease of BET surface areas from 5.2 to 4.1 m^2/g and simultaneously an increase of the average pore diameters (Table 1). Accordingly, the mean pore diameter became greater with the increase of the calcination temperature from 500 to 900 °C. Therefore, the sintering process went on to a smaller extent and this probably resulted in a consolidation of the catalyst samples [24].

In this study, the measured specific surface areas of the CaO catalysts had somewhat lower values of BET surface areas when compared to the results of other authors [18,25]. These results may be explained by the fact that the exact origin of the CaO catalysts was unknown, thus, the catalyst features could be completely different despite the comparable gross chemical composition. In addition, we believe that the BET surface area of the CaO catalyst should be correlated with the precursor type and the relevant thermal treatment applied. To the best of our knowledge, there are no reported data on an identical CaO precursor used; hence, no analogous results on the textural properties of CaO catalysts could be expected.

The results indicate that the CaO catalyst samples calcined at the lowest temperature possess a surface area of 5.2 m^2/g and a mean pore diameter of 11.9 nm (Table 1). The corresponding properties of the catalyst samples calcined at higher temperatures (750 and 900 °C) changed but not to a substantial extent. It seems that the textural characteristics of the CaO catalyst samples used in this experiment (from CaO-500 to CaO--900) are favorable for a liquid–solid heterogeneous phase reaction, and provide sufficient reaction surface area for the conversion of large triglyceride molecules.

Table 1. Specific surface areas, average pore diameters, pore volumes and maxima in pore size distribution for CaO-based catalysts

Catalyst	BET surface area, m^2/g	Average pore diameter, nm	BJH pore volume, cm^3/g	Maxima in PSD, nm
CaO–500	5.2	11.9	0.010	10–20; 60–140
CaO–750	4.7	12.7	0.017	12–20; 60–140
CaO–900	4.1	13.8	0.021	13–20; 60–140

Nitrogen isotherms and pore size distribution curves for the CaO-500 catalyst sample are shown in Fig. 1. The N_2 isotherms exhibited a typical *s*-shape behavior of IV-type with a type-H1 desorption hysteresis loop that indicated a potential presence of relatively wide cylindrical pores. The pore system is in the mesopores range between 10 and 100 nm with an average pore diameter around 28 nm according to the BJH desorption isotherms. Based on the PSD curve, a smaller fraction of the surface area is occupied by pores of around 10 nm in size followed with a larger volume fraction of pores of relatively large size between 60 and 140 nm. Such mesopores and near-edge mesopores–macropores are generated as a result of residual areas among particles formed during the catalyst preparation. The IV-type of isotherms is recognized for catalytic materials with porous system in the mesopore range [26] that additionally coincided with a rather spongy-like morphology of CaO particles proved by SEM.

The mentioned two maxima in the PSD curve may be significant during the catalytic run due to an effective mass transfer process in the conversion of relatively large triglyceride reactants. Taking into account that the approximate dimensions of triglycerides along the fatty acid chain (around 2.5 nm based on the dimension of the extended methyl oleate molecule) [18] are several orders of magnitude smaller than the meso––macropores sizes in CaO catalysts, any internal diffusion restrictions cannot be expected.

In the case of catalytic samples calcined/activated at higher temperatures only slight shifts of maxima in the PSD curves towards bigger mesopores were observed (not shown). Therefore, the increase of calcination temperature caused a shift of pore diameters to somewhat higher values for the CaO-based catalysts.

Based on these and reported CaO textural properties, the authors believe that the reactivity of the catalyst is indirectly proportional to the specific surface area, whereas it is in a direct relation with the average pore diameter [27]. Precisely, the pore diameter and/or pore volume play important roles in exhibiting the catalytic efficiency. We strongly believe that these catalytic properties are vital in expressing the catalytic activity, but not the key ones.

XRD patterns of thermally untreated commercial CaO-precursor, and CaO catalyst samples calcined at different temperatures, are given in Fig. 2. The non-calcined starting CaO precursor sample shows X-ray diffraction peaks characteristic for three different crystal phases: $CaCO_3$, CaO and $Ca(OH)_2$. The intensities of the XRD peaks, as well as their volume fractions attributed to CaO and $Ca(OH)_2$ phases, are comparable whereas the intensity of the corresponding $CaCO_3$ peak is considerably lower although still a significant one. The presence of these three crystal phases in the inactivated CaO starting material is related to its chemical composition, present impurities and potential surface interactions with CO_2 and/or humidity in ambient conditions.

The activation procedure through a thermal treatment of the CaO starting sample has caused a decomposition of the precursor used. The XRD pattern of CaO-500 catalyst reveals the peaks of the above-mentioned phases but now where the CaO phase is the principal one, while $CaCO_3$ and especially $Ca(OH)_2$ phases are only detectable having a volume fraction much lower when compared to the CaO phase. The hydroxide is reported to exhibit slight reactivity [28] but the carbonates are known to have no activity [20] in the transesterification reaction of soybean and rapeseed oils. Some previous work states the formation of calcium oxide at the calcination temperature of 800 °C from the

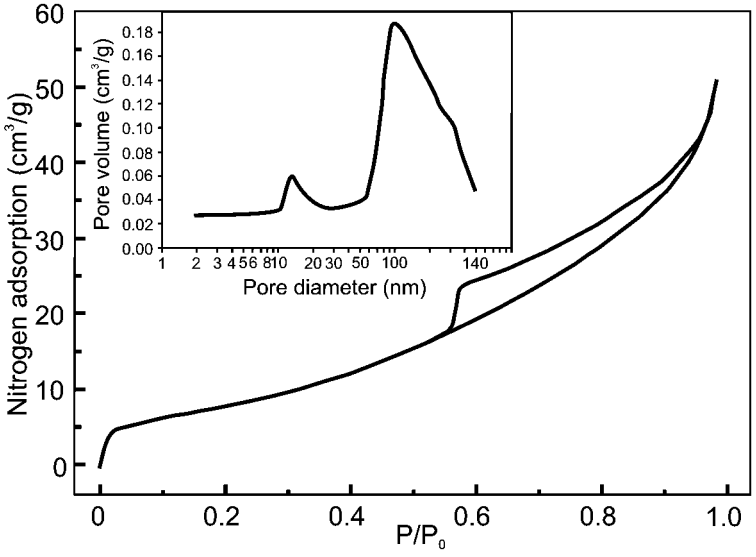

Fig. 1. N_2 Adsorption–desorption isotherms and pore size distribution for CaO-500 catalyst.

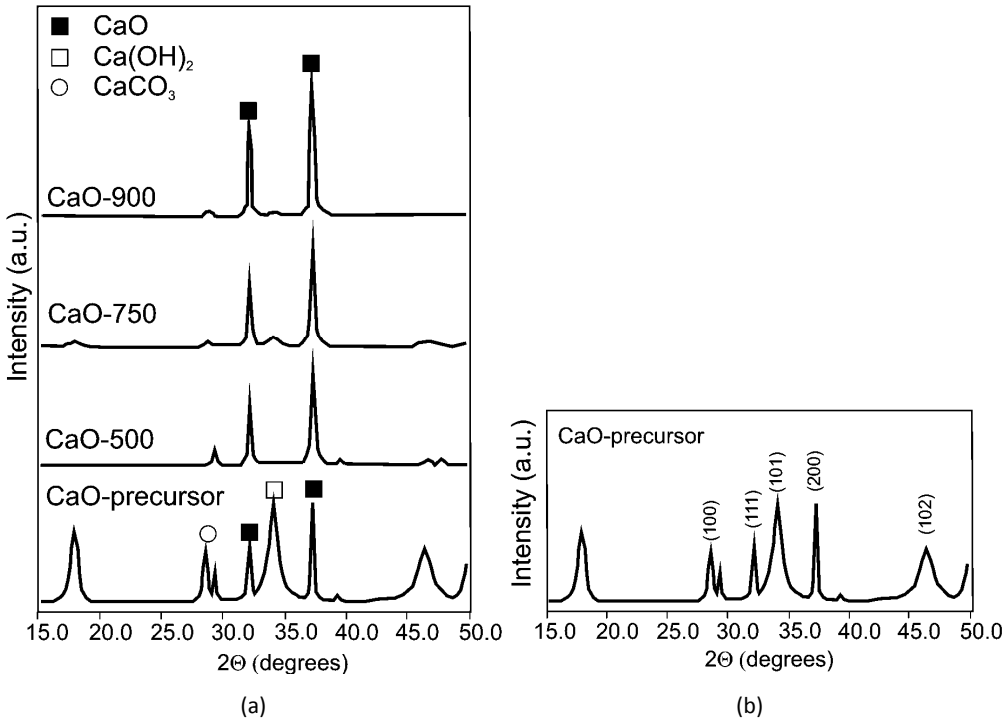

Fig. 2. XRD Patterns for CaO-based catalyst samples: a) CaO-T catalysts samples and b) CaO-precursor.

precursors [29], but we noted a CaO genesis at temperatures lower than 750 °C. Consequently, since the CaO phase may be an essential one for the catalytic activity in biodiesel production [23], it can be expected that a pure CaO catalyst would show a favorable efficiency in the transesterification of sunflower oil.

X-Ray diffraction peaks of the CaO-750 and CaO-900 catalyst samples showed the existence of a pure CaO crystalline phase. The intensity of the typical peaks of the CaO phase is higher when higher activation temperatures were used. These changes in intensity and peak width may indicate somewhat larger dimensions of the CaO crystallites formed at higher activation temperatures (Table 2). Based on the recognized crystalline phases (pure CaO) and crystallite sizes in CaO-catalyst samples calcined at higher temperatures, starting at 750 °C, we can conclude that there is a necessity to activate the CaO-based catalyst by a thermal treatment before its usage. This observation is in agreement with those of other authors [30].

The structural properties of the CaO-based catalysts (Fig. 2 and Table 2) indicate that the catalytic activity in the transesterification reaction of sunflower oil will take the following order: $CaO > Ca(OH)_2 > CaCO_3$. Thus, the catalysts activated at temperatures over 700 °C would perform with a significantly better catalytic efficiency as proven by our results in the test reaction.

The DTA curves of the CaO-based catalytic samples show three relatively broad endothermic peaks (Fig. 3). The first endothermic process occurring to about 120 °C was due to the removal of surface adsorbed and/or chemisorbed water and amounted to a weight loss of 5–15% depending on the particular catalytic sample. The second process was complete up to 430 °C and can be assigned to the dehydration of $Ca(OH)_2$ (Eq. (1)). The third thermal transition at 530–640 °C probably corresponded to the decomposition of $CaCO_3$ (Eq. (2)) formed by a reaction of CaO with CO_2 from the atmosphere. The maximum of these three peaks was positioned at somewhat lower or higher temperatures for each catalyst sample:

$$Ca(OH)_{2(s)} \rightarrow CaO_{(s)} + H_2O_{(g)} \quad (1)$$

$$CaCO_{3(s)} \rightarrow CaO_{(s)} + CO_{2(g)} \quad (2)$$

Table 2. Crystal phases and crystallite sizes

Catalyst	Crystal phases detected	Crystallite size of CaO at 37.4 °C, nm
CaO-precursor	CaO, $Ca(OH)_2$, $CaCO_3$	38.5
CaO-500	CaO, $CaCO_3$	25.5
CaO-750	CaO	25.6
CaO-900	CaO	25.7

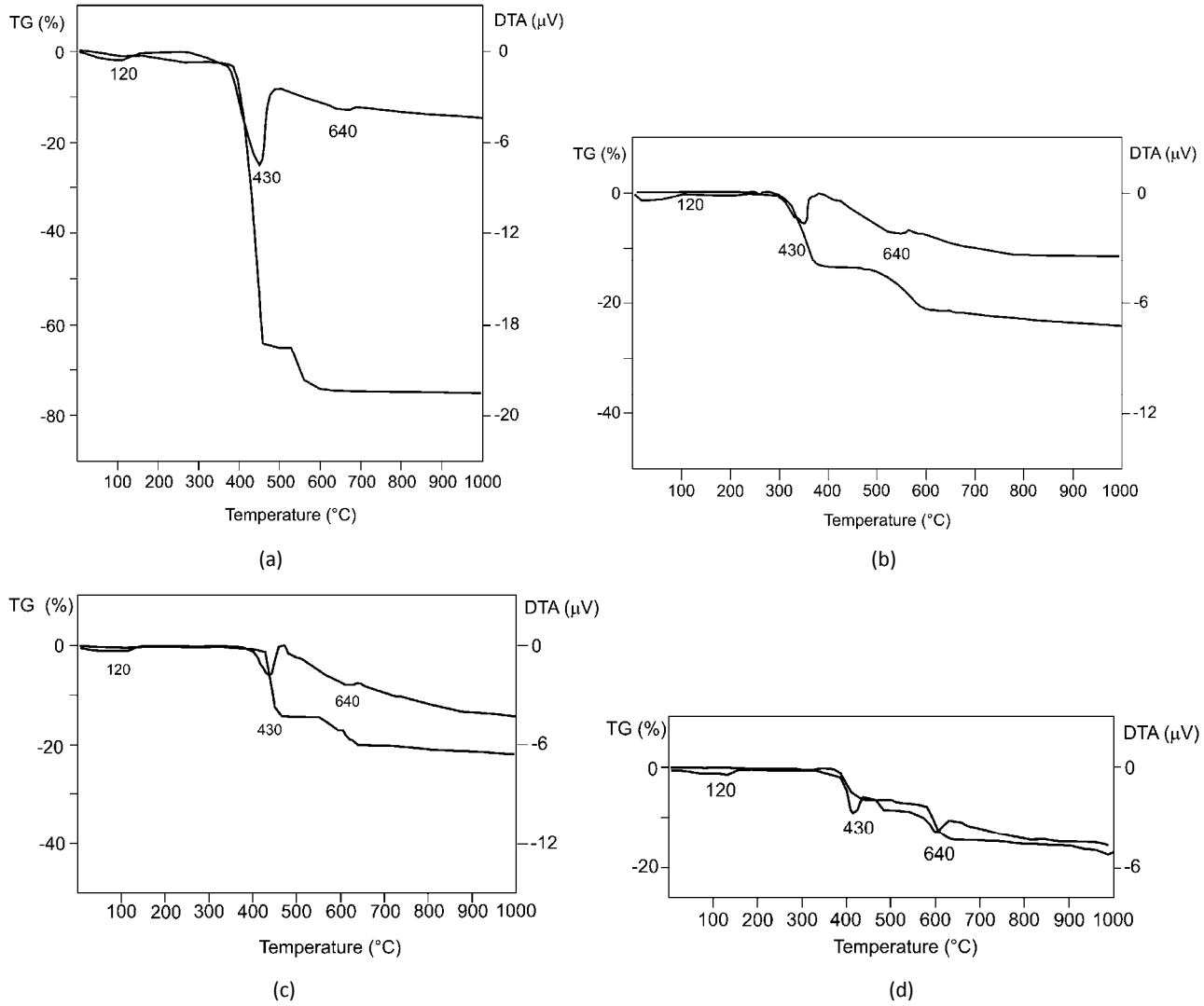

Fig. 3. TG and DTA curves of CaO-based catalyst samples: a) CaO-non-calcined, b) CaO-500, c) CaO-750 and d) CaO-900.

Calcium hydroxide and carbonate might have been present in the starting CaO-precursor material and/or could have formed during the catalyst preparation and testing in ambient conditions. The temperatures of thermal transitions and/or decompositions are somewhat lower than those reported earlier [25,31].

However, it is obvious that the decomposition temperatures of calcium hydroxide and carbonate are shifted to higher temperatures in parallel to the increase of the catalyst activation temperature. This is in line with the thermal stabilization of the catalytic material based on CaO. Additionally, TG curves show three weight losses corresponding to desorption of the physisorbed water onto the catalyst surface, then the mentioned dehydroxylation and decarbonization processes. The percentage weight loss related to the hydroxide degradation is significant only for the non-calcined CaO catalyst sample (around 65%), where the weight percent of carbonate is around 8%. It is clear that as the temperatures of calcination are higher smaller weight percentages of calcium hydroxide and carbonate are expected in the CaO-catalyst samples.

Based on the thermogram (Fig. 3), it seems that the weight percentage of the hydroxide in the CaO-500 sample is 10–15%, and of the carbonate about 5%. CaO samples calcined at higher temperatures possess much lower amounts of the hydroxide and carbonate. These results are consistent with the reported XRD results (Table 2 and Fig. 2). Namely, calcium hydroxide and calcium carbonate phases were detected in the non-calcined CaO sample, and only a small amount of the carbonate phase was registered in the CaO-500 sample (about 5.0% based on the TG results). This can be expected bearing in mind that the chemical species present in weight percentages lower than 5% cannot be seen in XRD patterns. Hence, the obtained XRD and TG/DTA results are entirely in agreement.

We believe that the purity of the CaO catalyst is the most important single factor determining the catalytic activity in the transesterification reaction of sunflower

oil, but we also think that small amounts of $Ca(OH)_2$ and $CaCO_3$ (less than 5%) would not significantly negatively influence the efficiency of the catalyst. However, some authors have given a stricter opinion on the deactivation of CaO-based catalysts with regard to the existence of calcium carbonate in the catalysts. They also claim a negligible catalytic activity in the presence of the hydroxide [20,28]. Namely, after an atmospheric calcination of CaO catalytic samples, deactivation of these CaO catalysts was reported by exposure to air and adsorption of CO_2 [32].

CaO catalytic samples calcined at different temperatures were analyzed by FTIR before and after being exposed to phenol vapors. This was carried out to determine the basic nature of the CaO catalyst, a relevant catalytic property for the transesterification of sunflower oil. Phenol, a rather weak acid, was selected to be the test compound for the estimation of the (active) basic catalytic sites on the catalyst surface [33]. Differences in the FTIR spectra of phenol adsorbed onto CaO surfaces of the catalytic samples differently thermally (pre)treated were observed (Fig. 4). Phenol can interact with basic sites from the catalyst surface via a dissociative adsorption giving probably $C_6H_5O^-$ [34] depending on the presence and strength of the basic catalytic sites. Thus, phenol can be physisorbed molecularly onto the framework of oxygen atoms and/or chemisorbed in the form of phenolate ions.

Vibration bands in the region 1270–1150 cm^{-1} are assigned to OH-groups directly bonded to the phenolic aromatic ring [35]. These vibration bands were detected in the FTIR spectra of the CaO catalyst samples treated at lower temperatures (500 and 750 °C). The clear presence of this vibration in the FTIR spectrum of the CaO--500 sample and also vibrations of smaller intensity in the spectrum of the CaO-750 sample indicated the possible physisorption of phenol in molecular form. We propose that such phenol adsorption may be related to the existence of one specific type of basic sites of relatively low strength. On the other side, the complete absence of this band in the spectrum of the CaO-900 catalyst indicated a probable dissociative adsorption of phenol onto basic sites of the strongest strength and/or other types of basicity. We presume that a deprotonating of phenol on the strong basic sites has occurred leading to a production of phenolates connected with metal oxide surface cations. Our findings are comparable to those previously reported the minimal calcination temperature for the genesis of the maximum amount of electron donating sites/basic sites on the CaO surface is 700 °C [36]. In our experiments this temperature was somewhat higher, *i.e.*, 750 °C.

Greater intensities of vibration bands of OH-groups (around 1650 cm^{-1}) originating from physisorbed water in CaO samples calcined at lower temperatures (500 and 750 °C) indicated that greater volumes of moisture interacted with CaO prior to calcination. These data are consistent with the TG results.

The FTIR bands at about 1475 and 1075 cm^{-1}, assigned to symmetric and asymmetric stretching vibrations of the O–C–O bonds of unidentate carbonate [18], are observable in the CaO samples calcined at lower temperatures (CaO-500 and CaO-750). Higher intensity of these stretching vibrations was observed for the CaO-500 catalyst. The lack of these bands in the CaO-900 catalytic sample corroborates no carbonate or a neg-

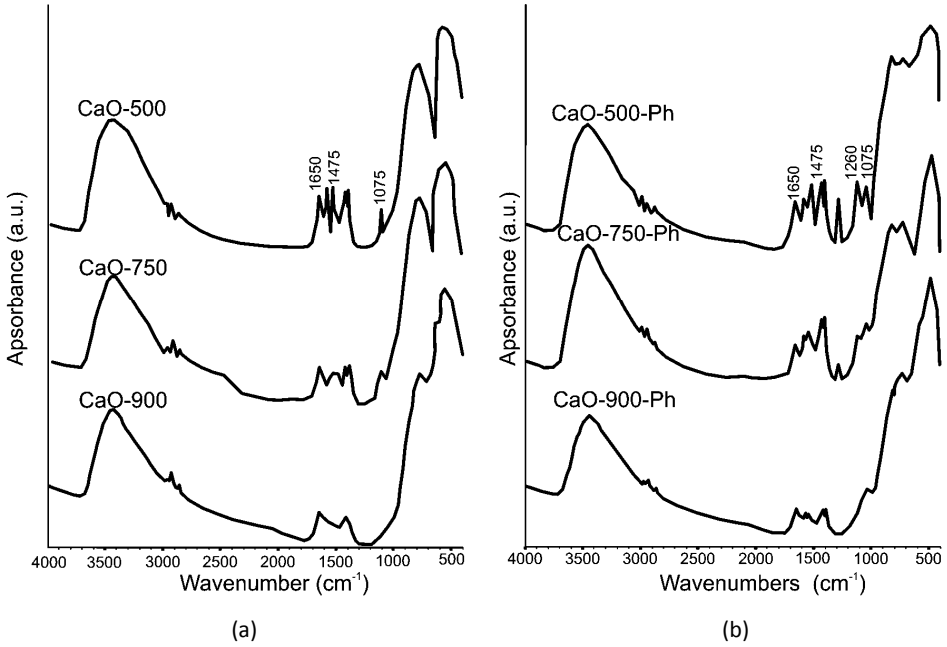

Fig. 4. FTIR Spectra of CaO-based catalyst samples: a) fresh CaO-T catalysts and b) CaO-T catalysts with (pre)adsorbed phenol.

ligible amount of carbonate on the CaO surface. All of this is in accordance with our TG/DTA results (Fig. 3).

SEM images of the CaO catalyst samples show that particle sizes decrease while pore sizes increase after thermal activation (Fig. 5). Non-calcined CaO sample possesses less defined greater particles at the surface surrounded with pores small in size. On the contrary, after the calcination at 500 °C, well defined crystallites of nano-size dimensions were observed whereas larger pores were revealed. These results are consistent with the obtained XRD data on the existing crystal phases and calculated crystallites sizes (Table 2). Such a developed pore system may provide no internal diffusion restrictions for the triglycerides molecules to interact with the catalytically active sites. After the reaction, a coalescence of the catalytic material occurred, and CaO particles were (re)organized in aggregates in a cakes-like sticky structure. These changes in the catalyst bulk morphology led to a deactivation of the catalyst by blocking the contact between the active catalytic sites and the reactants.

Catalyst structure–activity relationships

The transesterification reaction is most often performed at atmospheric pressure, and the heating is consequently limited by the refluxing temperature of the used alcohol. Thus, the reaction temperature cannot be higher than of the boiling point of methanol. If an extensive evaporation of methanol occurred, this would result in a considerable decrease of FAME yield.

Figure 6 presents the fatty acids methyl esters yield, as the function of time-on-stream at atmospheric pressure and temperature of reflux of methanol over the CaO catalysts activated at different temperatures.

The maximum FAME yield of more than 90% (up to 93%) was achieved over CaO-900 catalyst after only 2 h long reaction run. Afterwards, a steady-state was established and maintained during the next 4 h of the reaction progress. A twice lower FAME yield was obtained after as long as 5 h over the CaO-750 catalyst and finally an unsatisfactory FAME yield of 18% was noted for a 5 h long run over the CaO-500 catalyst.

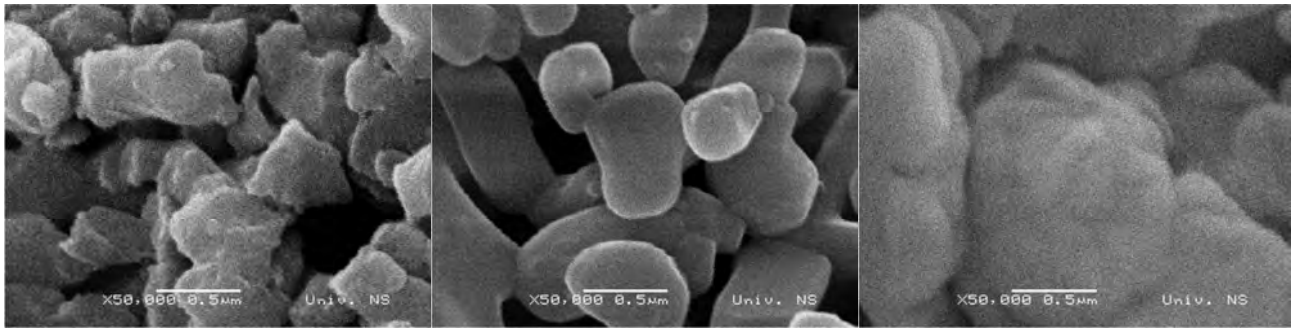

(a) (b) (c)

Fig. 5. SEM Images of the non-calcined CaO (a), CaO-500 (b) and used CaO-900 (c).

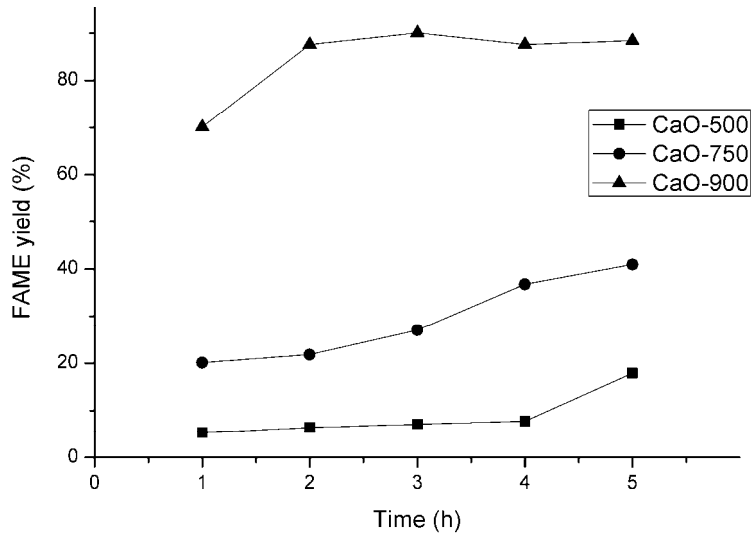

Fig. 6. FAME Yields as a function of time-on-stream over CaO-T catalyst samples.

This is an indication that the establishment of the steady-state is rather slow over CaO-catalysts activated at both lower temperatures. The reason for this is probably in an induction period necessary for the genesis of the catalyst active phases [20,37] followed by the increase of reaction rate and/or FAME yield with the more intense penetration of the reactants to the active sites during the course of biodiesel production.

The catalytic activity of CaO increased with increasing the calcination temperature (Fig. 6), and the optimal CaO calcination temperature was 900 °C in our work, that agreed with the results reported by Kouzu et al. [20,21]. These authors reported that the basicity of catalysts was essential for the catalytic activity. On the other side, we assume that not only the basicity, but adequate balance of specific surface area and pore system, presence of CaO active crystal phase with crystallites of critical dimensions, the total basicity and two types of basic sites are all necessary for the optimal catalytic efficiency. Additionally, we predict that these physico–chemical parameters of the catalysts are influenced with the calcination temperature.

Our results on the optimal calcination/activation temperature were different comparing to the results of some authors [15–19,22]; the reason may be in a fact that precursors of the CaO-based catalysts were various comparing to the compound used in this experiment. Moreover, in our case, the calcination temperatures below 900 °C were not enough high to cause formation of active crystal phase and activation of surface basic sites, while temperatures over 900 °C may induce undesirable sintering of the catalytic material, hence, changes in surface morphology and particle sizes.

A comparison of the textural, thermal, structural, acid–base and morphological properties of the catalysts differently thermally activated along with their observed efficiency suggests that physicochemical properties of the catalysts have a profound influence on the final catalytic performance in the transesterification reaction. We have found a straightforward relationship between the type of the pore system, the typical CaO crystal phase and the sizes of crystallites (up to 25 nm), the minimal weight percentage of CaO phase in the final catalyst, and the total surface basicity related to the catalytic activity.

Firstly, there is a direct link between the catalyst specific surface area and the catalyst activity; however, this property is not crucial for the onset of the catalytic activity. Namely, mesopores and near-edge meso–macropores may be of vital importance in the contact of triglycerides and catalytic active sites. The CaO crystal phase with no more than 5% of the hydroxide and carbonate exhibited very high catalytic activity. Calcinations at higher temperatures resulted in the formation of a higher number of CaO crystallites in the catalyst matrix influencing the density of basic sites required for a catalytically active site.

We wish to draw attention to the potential existence of two types of basic active sites: very strong basic sites (phenolates adsorbed), and rather less strong basic sites (phenol adsorbed). Finally, we believe that the strength of a surface base site plays a vital role in the catalyst efficiency.

The use of conventional diesel fuel and biodiesel fuel blends. Fuel properties, engine performances and exhaust gas emissions

A conventional commercial fossil-based diesel fuel was used for the comparisons with biodiesel fuel blends in order to estimate engine performances and exhaust gas emissions. In addition, a type of low sulfur diesel fuel (LSCDF) (originating from the Refinery–Novi Sad) was also selected for the assessment of the engine working performances, NO_x and CO_x emissions. Biodiesel produced over the CaO catalyst activated at 900 °C from sunflower oil was blended with commercial diesel fuel in different ratios. The selected biodiesel blends were: B25 containing 25% of biodiesel and 75% of diesel, B50, B75, and finally B100 (pure biodiesel fuel). Blends even with 25% of biodiesel are expected to affect exhaust gas emissions and improve fuel properties (Fig. 7 and Tables 3 and 4) based on the previously published report of the data that only 2% of biodiesel in a blend may influence reduction of exhaust gas emissions and some fuel properties [38]. B100 may also provide the mentioned benefits (Tables 3 and 4) and a complete replacement of diesel fuel with biodiesel might be possible if biodiesel becomes available in adequate volumes and at acceptable costs on market [38,39].

The herein laboratory obtained biodiesel (B100) fuel possessed better fuel properties than the LSCDF fuel sample with all of the properties being in the allowed limits (Table 3). Namely, especially the cold filter plugging point (CFPP) of B100 was much closer to the limited value than that of LSCDF fuel, sulfur content was one order of magnitude lower for the B100 fuel sample, and finally the cetane index (CI) was considerably higher for the B100 fuel in comparison to that of LSCDF. CI and CFPP properties of diesel derived fuels are essential parameters that are strictly determined by the fatty acids composition of the feedstock. The measured CI of B100 was higher than the standard value (50-51) and this can be related to the high content of unsaturated fatty acids (oleic and linoleic ones, up to 87%). Conversely, the CFPP value determined could be associated with the amount of mono-unsaturated fatty acids in the feedstock where oleic acid is the most important one dissolving the saturated esters [40].

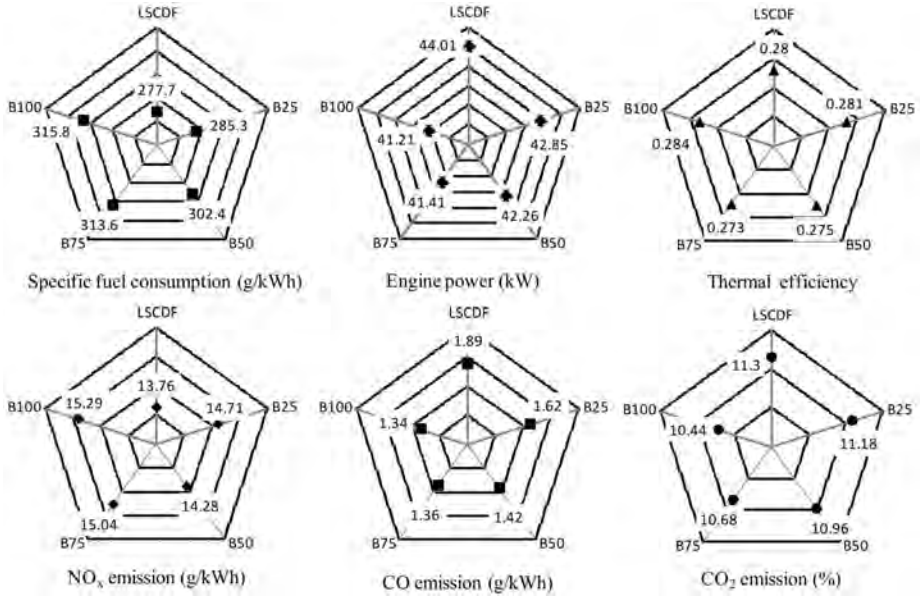

Fig. 7. Greenhouse gas emissions and engine performances.

Table 3. Fuel properties of biodiesel and LSCDF

Fuel property	Unit	Standard value	Value	
			B100	LSCDF
Flash point	°C	Min. 101	154	65
Cold filter plugging point	°C	Max. –5	–4	–19
Sulfur content	mg/kg	Max. 10	0.81	8.2
Water content	mg/kg	Max. 500	279	60
Cetane index	–	>51	51.8	49.7
High heating value	MJ kg^{-1}	–	40.35	46.29

Table 4. Selected fuel properties of biodiesel blends

Fuel property	Unit	Value		
		B25	B50	B75
Density 15 °C	kg/m^3	849.7	861.1	872.6
Viscosity	mm^2/s	3.21	3.44	3.68
Flash point	°C	98	114	132
Sulfur content	mg/kg	6.4	4.5	2.7
Water content	mg/kg	171	219	253
High heating value	MJ kg^{-1}	44.83	43.29	41.70

The properties of different biodiesel blends (Table 4) obtained from the same feedstock and the use of the herein developed CaO-based catalyst but with different diesel and biodiesel ratios indicate that the higher the fraction of biodiesel fuel the better the achieved fuel properties are when compared to the EU established standards [41]. This especially stands for the lower sulfur content, higher viscosity and flash point of the biodiesel blends. These properties are directly linked to the fraction of biodiesel blended in each particular fuel sample.

CO_x and NO_x – "greenhouse gas" emissions

Greenhouse gas emissions (GHGE) for the LSCDF and biodiesel blends are shown in Fig. 7. Increased biodiesel share in particular fuel blends greatly reduced CO_2 emissions. This is easily explainable by the lower content of carbon in biodiesel compared to its content in diesel fossil fuel (Fig. 7). On the other hand, the mentioned reduction leads to a decrease in fuel combustion efficiency. The main reason for such decrease in the combustion efficiency is the higher kinematic viscosity of the higher content biodiesel blended fuel samples.

The increase of kinematic viscosity on low scale may positively affect engine performances, but in general, it has a negative effect on the combustion quality. Viscosity is an important parameter that determines the quality of diesel fuel and its capability to atomize, as well as the smoothness of the injection into the engine, especially at lower temperatures.

The studied increase of biodiesel content in particular blends caused a reduction of CO emissions as well (Fig. 7). The highest CO emission was registered for the LSCDF whereas the lowest one was observed for the B100 fuel sample. One of the reasons for this reduction is the mentioned increase of kinematic viscosity. Another reason might be that biodiesel fuel possesses higher oxygen content that may contribute to a more complete combustion process.

On the side, the rise of the biodiesel fraction in certain blends has caused an increase of NO_x emissions to some extent (Fig. 7). NO_x emissions also grow as the temperatures of the combustion products increase. NO_x emission could be conditioned by the combustion temperature, peak pressure, process time and oxygen concentration. It is most probably in line with properties of the feedstock used for biodiesel production.

Our results on GHGE demonstrated the reduction of CO_2 content for 7.60%, and 29.10% for CO, and finally the increase in NO_x emissions for 11.12%. It is generally known that these gases contribute to global warming. We strongly believe that if renewable energy sources would be used in the future, and especially for transportation, GHGE emissions would be reduced even further. Similar observations and expectations were reported earlier on the production and use of biodiesel in Asia [38,42].

The use of LSCDF resulted in an engine power of 44.01 kW at 2200 rpm. The prepared and tested B25--100 fuels gave power from 42.85 to 41.21 kW, respectively (Fig. 7). The density of fuel samples prepared by blending biodiesel with fossil diesel increased with the addition of biodiesel. A slight increase of kinematic viscosity can positively affect engine working performances [43].

The lowest specific fuel consumption was observed for LSCDF, whereas an increase was experienced with an increase of the biodiesel portion in the blends. Therefore, B100 sample displayed the highest specific fuel consumption (Fig. 7). Such an increase could be explained by the lower heating value and higher fuel density of blends with higher amounts of biodiesel.

All tested biodiesel blends possessed higher thermal efficiency than the LSCDF sample (Fig. 7). Despite the reduced heating value and increased specific fuel consumption, the thermal efficiency was increased for all fuel samples with high biodiesel content, which enables more complete fuel combustion in the engine. The higher cetane number causes a shorter delay in fuel combustion leading to a longer time for the complete combustion [43].

CONCLUSIONS

Calcium oxide prepared and thermally activated at higher temperatures has exhibited itself as a very effective catalyst in short run transesterification reactions of refined sunflower oil with methanol to yield biodiesel. Benefits of this catalyst are short contact time (up to 2h), standard operating temperature and atmospheric conditions, relatively low molar ratios and small catalyst loading. These all together resulted in a relatively high fatty acids methyl esters yield.

A number of key physicochemical features of the CaO catalysts – the great specific surface area and average pore diameter, almost exclusive presence of CaO crystal phase with crystallites up to limited dimensions, the total amount of surface basic sites and the two types of basic active sites – were found to be the reasons for the observed high catalytic efficiency.

The following conclusions can be reached from the comparative use of fossil diesel fuel and biodiesel blends: biodiesel fraction increase in a particular blend leads to a reduced engine power that resulted in a lower heating value and higher viscosity; the specific fuel consumption increases with the increase of the biodiesel fraction; thermal efficiency slightly increases with the increase of the biodiesel share resulting in a more complete fuel combustion; a significant reduction of CO_2 and CO emissions and only a negligible NO_x increase occurred when blends with an increased biodiesel portion was used; CO emissions diminished significantly. All these facts are consequences of better fuel combustion and take place at different engine operating regimes. More oxygen was available for burning with the increase of biofuel share due to the oxygenated nature of biodiesel; hence, decreased amounts of CO were registered in the exhaust gases.

The reduction of emissions of greenhouse gases is of vital interest due to their effect on global warming. The use of biodiesel derived blends with fossil diesel fuel, and the eventual complete replacement of fossil fuels, would greatly contribute to the reduction of greenhouse gases emissions. Further investigations on this topic and on similarly orientated ones would promote the use of biodiesel as a renewable, alternative fuel for diesel engines that could answer the energy demands and traffic transportation needs in Serbia.

Acknowledgement

The authors wish to thank the Ministry of Education, Science and Technological Development of the Republic of Serbia (Project No. 172061 and Project TR 34008) for financial support.

REFERENCES

[1] C. Carraretto, A. Macor, A. Mirandola, A. Stoppato, S. Tonon, Biodiesel as alternative fuel: Experimental analysis and energetic evaluations, Energy **29** (2004) 2195–2211.

[2] M.S. Graboski, R.L. McCormick, Combustion of fat and vegetable oil derived fuels in diesel engines, Prog. Energy Combust. Sci. **24** (1998) 125–164.

[3] A. Srivastava, R. Prasad, Triglycerides-based diesel fuels, Renew. Sust. Energ. Rev. **4** (2011) 111–133.

[4] J. Van Gerpen, Biodiesel processing and production, Fuel Process. Technol. **86** (2005) 1097.

[5] Y. Zhang, M.A. Dube, D.D. McLean, M. Kates, Biodiesel production from waste cooking oil: 1. Process design and technological assessment, Bioresour. Technol. **89** (2003) 1–16.

[6] Y.C. Sharma, B. Singh, S.N. Upadhyay, Advancements in development and characterization of biodiesel: a review, Fuel **87** (2008) 2355–2373.

[7] G. Arzamendi, I. Campoa, E. Arguinarena, M. Snachez, M. Montes, L.M. Gandia, Synthesis of biodiesel with heterogeneous NaOH/alumina catalysts: comparisons with homogeneous NaOH, Chem. Eng. J. **134** (1997) 123–130.

[8] H.J. Kim, B.S. Kang, Y.M. Park, D.K. Kim, J.S. Lee, K.Y. Lee, Transesterification of vegetable oil to biodiesel using heterogeneous base catalyst, Catal. Today **93**–**95** (2004) 315–320.

[9] T. Ebiura, T. Echizen, A. Ishikawa, K. Murai, T. Baba, Selective transesterification of triolein with methanol to methyl oleate and glycerol using alumina loaded alkali metal salt as a solid-base catalyst, Appl. Catal. A: Gen. **283** (2005) 111–116.

[10] G.J. Suppes, K. Bockwinkel, S. Lucas, J.B. Botts, M.H. Mason, J.A. Heppert, Calcium carbonate catalyzed alcoholysis of fats and oils, J. Am. Oil Chem. Soc. **78** (2001) 139-146.

[11] [11] G.J. Suppes, M.A. Dasari, E.J. Doskocil, P.J. Mankidy, M.J. Goff. Transesterification of soybean oil with zeolite and metal catalysts, Appl. Catal. A: Gen. **257** (2004) 213–223.

[12] D.G. Cantrell, L.J. Gillie, A.F. Lee, K. Wilson, Structure-reactivity correlations in MgAl hydrotalcite catalysts for biodiesel synthesis, Appl. Catal., A **287** (2005) 183–190.

[13] W. Xie, H. Peng, L. Chen, Calcined Mg-Al hydrotalcites as solid base catalysts for methanolysis of soybean oil, J. Mol. Catal., A **246** (2006) 24–32.

[14] S. Yan, H. Lu, B. Liang, Supported CaO catalysts used in the transesterification of rapeseed oil for the purpose of biodiesel production, Energ. Fuel. **22** (2008) 646–651.

[15] H. Mootabadi, B. Salamatinia, S. Bhatia, A.Z. Abdullah, Ultrasonic-assisted biodiesel production process from palm oil using alkaline earth oxides as the hetero–ge–neous catalysts, Fuel **89** (2010) 1818–1825.

[16] Y.-W. Chen, H.-Y. Chen, W.-F. Lin, Basicities of alumina-supported alkaline earth metal oxides, React. Kinet. Catal. Lett. **65** (1998) 83–86.

[17] V.B. Veljković, O.S. Stamenković, Z.B. Todorović, M.L. Lazić, D.U. Skala, Kinetics of sunflower oil methanolysis catalyzed by calcium oxide, Fuel **88** (2009) 1554–1562.

[18] M.L. Granados, M.D. Zafra Poves, D.M. Alonso, R. Mar–iscal, F. Cabello Galisteo, R. Moreno-Tost, J. Santamaria, J.L.G. Fierro, Biodiesel from sunflower oil by using activated calcium oxide, Appl. Catal. B: Environ. **73** (2007) 317–326.

[19] Y.B. Cho, G. Seo, D.R. Chang, Transesterification of tributyrin with methanol over calcium oxide catalysts prepared from various precursors, Fuel Process. Tech–nol. **90** (2009) 1252–1258.

[20] M. Kouzu, T. Kasuno, M. Tajika, Y. Sugimoto, S. Yama–naka, J. Hidaka, Calcium oxide as a solid base catalyst for transesterification of soybean oil and its application to biodiesel production, Fuel **87** (2008) 2798–2806.

[21] M. Kouzu, T. Kasuno, M. Tajika, S. Yamanaka, J. Hidaka, Active phase of calcium oxide used as solid base catalyst for trans esterification of soybean oil with refluxing methanol, Appl. Catal., A **334** (2008) 357–365.

[22] Z. Wei, C. Xu, B. Li, Application of waste eggshell as low-cost solid catalyst for biodiesel production, Biores. Technol. **100** (2009) 2883–2885.

[23] Dj. Vujicic, D. Comic, A. Zarubica, R. Micic, G. Boskovic, Kinetics of biodiesel synthesis from sunflower oil over CaO heterogeneous catalyst, Fuel **89** (2010) 2054–2061.

[24] G. Mekhemer, Characterization of phosphated zirconia by XRD, Raman nad IR spectroscopy, Colloids Surfaces, A **141** (1998) 227–235.

[25] Y. Tang, J. Xu, J. Zhang, Y. Lu, Biodiesel production from vegetable oil by using modifies CaO as solid basic catalysts, J. Clean. Prod. **42** (2013) 198–203.

[26] T. Liu, Y. Zhu, X. Zhang, T. Zhang, T. Zhang, X. Li, Syn–thesis and characterization of calcium hydroxide nano–particles by hydrogen plasma-metal reaction method, Mater. Lett. **64** (2010) 2575–2577.

[27] X. Liu, X. Piao, Y. Wang, S. Zhu, H.He, Calcium methoxide as a solid base catalyst for the transesterification of soybean oil to biodiesel with methanol, Fuel **87** (2008) 1076–1082.

[28] S. Gryglewicz, Rapeseed oil methyl esters preparation using heterogeneous catalysts, Bioresour. Technol. **70** (1999) 249–253.

[29] D. Veilleux, N. Barthelemy, J.C. Trombe, M. Verelst, Synthesis of new apatite phases by spray pyrolysis and their characterization, J. Mater. Sci. **36** (2001) 2245–2252.

[30] P.-L. Boey, G.P. Maniam, S.A. Hamid, Performance of calcium oxide as a heterogeneous catalyst in biodiesel production: A review, Chem. Eng. J. **168** (2011) 15–22.

[31] F.X. Yang, Y.Q. Su, X.H. Li, Q. Zhang, R.C. Sun, Prepar–ation of biodiesel from *Idesiapolycarpa* var. vestita fruit oil, Ind. Crop. Prod. **29** (2009) 622–628.

[32] M. Kouzu, M. Umemoto, T. Kasuno, M. Tajika, Y. Aihara, Y. Sugimoto, J. Hidaka, Biodiesel production from soy–bean oil using calcium oxide as a heterogeneous catal–yst, J. Jpn. Inst. Energy **85** (2006) 135–141.

[33] K. Tanabe, Solid acid and bases, Kodansha, Tokyo, 1970, p. 53.

[34] H. Miura, K. Sugiyama, S. Kawakami, T. Aoyama, T. Matsuda, Selective hydration of acrylonitrile on metal oxide catalysts, Chem. Lett. **2** (1982) 183–186.
[35] K. Prepsch, S. Seibl, Tables for identification of the organic compounds by means of spectroscopy methods. Chemistry in Industry, Zagreb, 1982 (in Croatian).
[36] K. Tanabe, New solid acids and bases, Stud. Surf. Sci. Catal. **51** (1989) 27.
[37] A. Demirbas, Comparison of transesterification methods for production of biodiesel from vegetable oils and fats, Energy Convers. Manage **49** (2008) 125–130.
[38] S. Pleanjai, S.H. Gheewala, S. Garivait, Greenhouse gas emissions from production and use of used cooking oil methylester as transport fuel in Thailand**,** J. Clean. Prod. **17** (2009) 873–876.
[39] V.J. Gerpen, C.L. Peterson, C.E. Goering, Biodiesel: an alternative fuel for compression ignition engines, in: ASABE distinguished lecture series No. 31, American Society of Agricultural and Biological Engineers, St. Joseph, MI, 2007.
[40] J. Lopes, L. Boros, M. Krahenbuhl, A. Meirelles, J. Daridon, J. Pauly, Prediction of cloud points of biodiesel, Energ. Fuel. **22** (2008) 747–752.
[41] JUS EN 14214:2004. AJUS EN 14214:2004. Automotive fuels. Fatty acids methyl esters for diesel engines-requirements and test methods. Belgrade, Serbia: Standardization Institute, 2004.
[42] Y. Katayama, Y. Tamaura, Development of new green-fuel production technology by combination of fossil fuel and renewable energy, Energy **30** (2005) 2179–2185.
[43] M.D. Tomić, L.Đ. Savin, R.D. Mićić, M.Đ. Simikić, T.F. Furman, Effects of fossil diesel and biodiesel blends on the performances and emissions of agricultural tractor engines, Thermal Science **17** (2013) 263–278.

IZVOD

Značaj strukturnih karakteristika CaO katalizatora za proizvodnju biodizela: Uticaj na smanjenje emisije gasova staklene bašte

Radomir B. Ljupković[1], Radoslav D. Mićić[2], Milan D. Tomić[3], Niko S. Radulović[1], Aleksandar Lj. Bojić[1], Aleksandra R. Zarubica[1]

[1]*Departman za hemiju, Prirodno–matematički fakultet, Univerzitet u Nišu, Niš, Srbija*
[2]*NTC NIS Naftagas – Novi Sad, Novi Sad, Srbija*
[3]*Poljoprivredni fakultet, Univerzitet u Novom Sadu, Novi Sad, Srbija*

(Naučni rad)

U ovom radu je ispitivan uticaj fizičko–hemijskih svojstava serije CaO katalizatora aktiviranih na različitim temperaturama za proizvodnju biodizela. Pomenuti katalizatori daju različite prinose u reakciji transesterifikacije triglicerida sa metanolom. Utvrdili smo bitnu povezanost između strukturalnih svojstava (tip poroznog sistema, tipična CaO kristalna faza i veličina kristalita do 25 nm, minimalni procenat kristalne faze CaO, ukupna baznost i potencijalno postojanje dve vrste baznih centara) CaO katalizatora pripremljenog i aktiviranog termijskim tretmanom na najvišoj temperaturi i katalitičke efikasnosti. Prednosti korišćenja ovog katalizatora su: kratko kontaktno vreme, standardna radna temperatura i atmosferski uslovi, relativno mali molski udeo reaktanata i mala količina katalizatora. Sve navedeno rezultiralo je veoma visokim prinosom biodizela visokog stepena čistoće. Svojstva različitih namešanih biodizel (dobijenog korišćenjem sintetisanog CaO katalizatora) goriva sa drugačijim udelima dizel i biodizel goriva ukazuju da što je veći udeo biodizela, bolja su ostvarena svojstva goriva imajući u vidu referentne EU standarde. Značajno smanjenje emisija CO_2 i CO gasova, i gotovo neznatno povećanje NO_x emisija, registrovano je kada je upotrebljeno gorivo sa povećanim udelom biodizela. Korišćenje namešanih goriva sa biodizel gorivom, kao i potencijalna totalna zamena fosilnih goriva sa biodizelom kao obnovljivim, alternativnim, ekološki prihvatljivim gorivom za dizel motore, moglo bi u velikoj meri da utiče na smanjenje emisije gasova koji izazivaju efekat "staklene bašte". Smanjenje emisije CO_x i NO_x gasova je od ogromnog značaja imajući u vidu da one izazivaju globalno zagrevanje. Buduća istraživanja na ovu temu i slično orijentisane mogla bi dati odgovor na savremene energetske zahteve i potrebe transporta u Srbiji, korišćenjem novog, alternativnog, obnovljivog izvora. Korišćenje biodizela obezbeđuje nezavisnost u pogledu uvoza sirove nafte, kao i brojne energetske, ekološke, geo-političke i ekonomske benefite.

Ključne reči: CaO katalizator • Emisija gasova koji izazivaju efekat "staklene bašte" • Proizvodnja biodizela • Strukturalna katalitička svojstva

Iron–chromium–carbon–vanadium white cast irons – the microstructure and properties

Mirjana M. Filipović

University of Belgrade, Faculty of Technology and Metallurgy, Belgrade, Serbia

Abstract

The as-cast microstructure of Fe–Cr–C–V white irons consists of M_7C_3 and vanadium rich M_6C_5 carbides in austenitic matrix. Vanadium changed the microstructure parameters of phase present in the structure of these alloys, including volume fraction, size and morphology. The degree of martensitic transformation is also dependent on the content of vanadium in the alloy. The volume fraction of the carbide phase, carbide size and distribution has an important influence on the wear resistance of Fe–Cr–C–V white irons under low-stress abrasion conditions. However, the dynamic fracture toughness of Fe–Cr––C–V irons is mainly determined by the properties of the matrix. The austenite is more effective in this respect than martensite. Since the austenite in these alloys contained very fine $M_{23}C_6$ carbide particles, higher fracture toughness was attributed to a strengthening of the austenite during fracture. Besides, the secondary carbides which precipitate in the matrix regions also influence the abrasion behavior. By increasing the matrix strength through a dispersion hardening effect, the fine secondary carbides can increase the mechanical support of the carbides. Deformation and appropriate strain hardening have occurred in the retained austenite of Fe–Cr–C–V alloys under repeated impact loading. The particles of precipitated $M_{23}C_6$ secondary carbides disturb dislocations movement and contribute to increase the effects of strain hardening in Fe–Cr–C–V white irons.

Keywords: Fe–Cr–C–V white irons, microstructure, hardness, abrasion wear resistance, fracture toughness, repeated impact resistance.

Available online at the Journal website: http://www.ache.org.rs/HI/

REVIEW PAPER

UDC 669.131.2:630.18

Hem. Ind. **68** (4) 413–427 (2014)

doi: 10.2298/HEMIND130615064F

High chromium white cast irons are an important class of wear resistance materials currently used in a variety of applications where stability in an aggressive environment is a principal requirement, including the mining and mineral processing, cement production, slurry pumping and pulp and paper manufacturing industries.

For abrasion resistance, nearly all high chromium cast irons are used as hypoeutectic alloys containing 10–30 wt.% Cr and 2–3.5 wt.% C. The abrasion resistance of these alloys is primarily determined by the features of M_7C_3 carbides, such as their volume fraction [1-6], hardness [1,2], morphology [7,8] and orientation [9–12]. The structure of the matrix that supports the carbides may be extensively altered by alloying and heat treatment [2,3]. It has been already shown that both factors have significant influence on the wear behaviour [1,2,4]. The eutectic carbides play a strong role in influencing the fracture toughness of white irons [1,13–15]. It has been observed that the proportion of eutectic carbides on fracture surfaces is greater than that measured on polished sections [5]. This reflects the brittle nature of the eutectic carbides, with cracks preferentially following the carbide structure. Increasing the carbide volume would increase the number of brittle carbides in the structure, while reducing the amount of matrix material between these carbides. As expected, increased carbide volume decreases the fracture toughness for both austenitic and martensitic matrix [4,13,15].

Extensive industrial applications of high-chromium white cast irons have attracted researchers to try different carbide-forming elements such as tungsten [16,17], niobium [16,18–25], vanadium [16,21,26–34], titanium [19,21,35–39] and boron [40] to further improve this type of material. The addition of an alloying element which confines carbon in the form of a carbide different from cementite, with a greater hardness and more favorable morphology, and which reduces the carbon content of the matrix, allows the simultaneous improvement of both toughness and abrasion resistance [2,21,25,26,29]. By controlling the morphology of the carbide phase and the matrix structure in these materials, significant improvement of toughness and service life may be achieved.

The main goal of adding molybdenum to white cast iron is to improve hardenability. However, only part of the molybdenum contributes to this goal. The presence of carbon in the alloy and its chemical affinity for molybdenum promotes the formation of M_2C or M_6C carbides at the end of the solidification process

Correspondence: Faculty of Technology and Metallurgy, University of Belgrade, Karnegijeva 4, 11120 Belgrade, Serbia.
E-mail: mirjanaf@tmf.bg.ac.rs
Paper received: 15 June, 2013
Paper accepted: 5 September, 2013

[19,41,42]. Addition of the tungsten to high chromium white iron leads to the formation of M_6C carbide (upper than 10% W) that crystallizes in a finely dispersed form as eutectic in the final stage of solidification [16,17]. The introduction of niobium to high chromium white irons resulted in the preferential formation of NbC which is appreciably harder than other carbides present and which forms efficiently since niobium is partitioned fully to these phases [18,19,22,23]. Subsequently, niobium improves the hardness, wear resistance and fracture toughness [20,21,25]. The solubility of titanium to molten cast iron is so small that fine TiC carbides precipitate at higher temperature even in the low titanium-bearing melts, and they likely affect the following solidification [36, 39]. Cerium has limited solubility in austenite and M_7C_3 eutectic carbide [25, 43, 44]. This element formed inclusions in high chromium white irons [45, 46]. In hypoeutectic alloys, around the very fine inclusions of cerium, the carbide particles rich in chromium were formed. The carbide particles can act as the heterogeneous nuclei of austenitic dendrites to enhance nucleation or interfere with their growth and improve the refinement of primary dendrites [45].

Vanadium appeared to be of special interest, due to its double effects, on both the matrix structure and stereological characteristics of carbides. The aim of this paper is to review the microstructural characteristics and properties relevant to the service performance of hypoeutectic Fe–Cr–C–V white cast irons, namely the hardness, abrasion wear resistance, fracture toughness and repeated impact resistance.

MICROSTRUCTURAL DEVELOPMENT

The as-cast microstructure of hypoeutectic F–Cr–C––(V) white irons (chemical composition listed in Table 1) consists of primary austenite dendrites and eutectic colonies composed of M_7C_3 carbides and austenite (Fig. 1).

Also, vanadium rich carbides are found in Fe–Cr–C–V irons containing 1.19–4.73% V (Fig. 2). Vanadium carbide present in these alloys was identified as M_6C_5 type carbide (Fig. 2) and its stoichiometric formula is $V_{3.6}Cr_{1.2}Fe_{1.1}C_5$ [34]. The same type of carbide was found by de Mello *et al.* [28] in cast iron containing 10% Cr and 6% V.

Dupin and Schissler [47] did not detect the vanadium carbide formation in high chromium white cast

Table 1. Chemical composition (mass.%) of Fe–C–Cr–V white irons

Alloy	Element									
	C	P	S	Si	Mn	Mo	Cu	Ni	Cr	V
1	2.89	0.025	0.061	0.85	0.71	0.48	0.99	0.100	19.03	0.0012
2	2.92	0.026	0.063	0.87	0.76	0.45	1.02	0.099	19.01	0.12
3	2.88	0.025	0.061	0.86	0.72	0.42	0.98	0.098	18.89	0.49
4	2.92	0.025	0.061	0.85	0.75	0.43	1.01	0.098	19.04	1.19
5	2.87	0.024	0.063	0.87	0.73	0.44	1.01	0.099	18.92	2.02
6	2.91	0.027	0.061	0.84	0.73	0.44	1.00	0.096	19.05	3.28
7	2.93	0.026	0.062	0.83	0.74	0.43	1.01	0.098	19.07	4.73

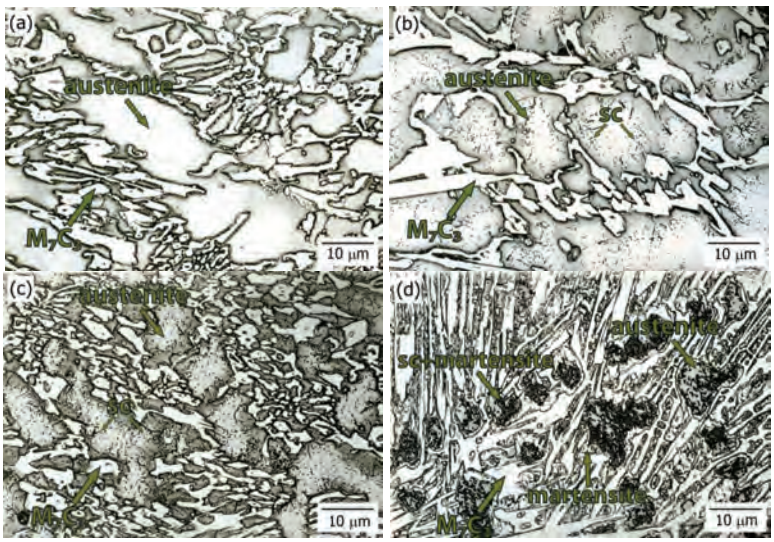

Fig. 1. Optical micrographs of hypoeutectic Fe–Cr–C–V white iron containing: a) 0.12% V, b) 0.49% V, c) 1.19% V, d) 3.28%V.

iron with 1% V. Nonetheless, Bedolla-Jacuinde [21] in 16.9% Cr–2.58% C–1.98% V alloy and Matsubara *et al*. [48] in 17.54% Cr–3.57% C–3.14% V alloy observed that (γ + MC) eutectic solidification did not occur because of lower vanadium content, which was different from the report of Stefanescu and Cracium [49] who indicated that vanadium carbides are present in the microstructure of 14.66% Cr–2.95% C–2.9% V alloy. Furthermore, Sawamoto *et al.* [16] found that vanadium carbides formed in high chromium white cast irons contained more than 5% V. The established disagreement appears to be a result of different cooling conditions, on one hand, and of the fact that vanadium carbides are difficult to notice due to their small volume fraction and size, on the other hand.

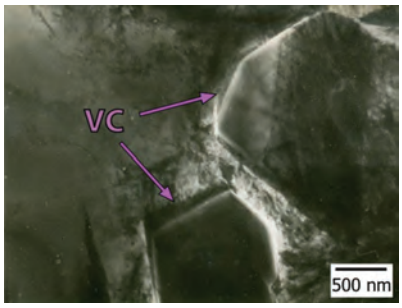

Fig. 2. TEM Micrograph of the Fe–Cr–C–V white iron containing 1.19% V showing vanadium carbide.

Solidification behaviour

With an increase of vanadium content, the alloy composition approaches the eutectic composition in quaternary Fe–Cr–C–V system, causing a decrease of the solidification temperature interval (Table 2).

Solidification starts with formation of *γ*-phase at 1341 °C in Fe-Cr-C alloy with no vanadium addition, at 1319 °C in Fe–Cr–C–V alloy containing 1.19% V, and at 1284 °C in Fe–Cr–C–V alloy containing 4.73% V. In the course of primary γ-phase growth, the composition of the remained liquid was changing. Due to limited solubility of carbon, chromium and vanadium in the austenite, these elements accumulated in front of the progressing solid-liquid interface. At temperatures little bit lower than *liquidus* temperature (1315 °C in alloy containing 1.19% V, 1278 °C in alloy containing 4.73% V) during the eutectic reaction that takes place, in local areas enriched in vanadium, eutectic composed of vanadium rich carbide and austenite was developed. The particles of vanadium carbides disturb or completely block further *γ*-phase growth, with the efficiency depending on their volume fraction, size and distribution [34].

As the temperature falls and solidification progresses, primary austenite dendrites reject solute (carbon, chromium and vanadium) in to the remaining liquid until the eutectic composition is reached and the monovariant eutectic reaction ($L \rightarrow \gamma + M_7C_3$) takes place. From the melt remained in interdendritic regions the coupled austenite–M_7C_3 eutectic was forming at 1244 °C in Fe–Cr–C alloy with no vanadium addition, at 1249 °C in alloy containing 1.19% vanadium, and at 1257 °C in alloy containing 4.73% vanadium. Bedolla-Jacuinde *et al*. [50] found that M_7C_3 eutectic carbides in high chromium white irons nucleated on the surface of the primary and secondary dendrites arms. The eutectic *γ*-phase nucleated side-by-side with the hexagonal M_7C_3 carbides, and both eutectic constituents may then grow more or less at the same rate with bars surrounded by austenite, and coupled growth develops.

The eutectic regions of carbide and austenite grow as colonies, indicating growth of a faceted–non-faceted eutectic [27,51]. Irregular eutectic structures are developed when a non-faceted phase is coupled with a faceted phase. In such eutectics, local morphological adjustment of interphase spacing is severely encumbered by the limited branching ability of the highly anisotropic faceted phase containing planar defects. Thus, the spatially non-uniform or irregular structure that evolves during faceted–non-faceted eutectic solidification is inherently three-dimensional, where the relationship between the growth mechanisms of the faceted phase and the complex non-isothermal interface structure gives rise to a more diverse range of solidification microstructures than that exhibited by regular eutectics [27,51,52]. It has been reported [52] that solute elements, even in trace amounts, may have a strong influence on eutectic growth morphology.

Table 2. DTA Results of the Fe–Cr–C–V white irons during cooling at a rate of 5 °C min^{-1}

Alloy	V in alloy, mass%	Temperature, °C			
		T_L	$T_{E_1(V_6C_5+\gamma)}$	$T_{E(M_7C_3+\gamma)}$	ΔT
1	–	1341	–	1244	97
4	1.19	1319	1315	1249	70
5	2.02	1310	1306	1251	59
6	3.28	1299	1294	1254	45
7	4.73	1284	1278	1257	27

T_L – the start temperature of the austenite reaction (liquidus); $T_{E_1(V_6C_5+\gamma)}$ – the temperature of the eutectic reaction $E_1(L \rightarrow V_6C_5+\gamma)$; $T_{E(M_7C_3+\gamma)}$ – the temperature of the eutectic reaction $E(L \rightarrow M_7C_3+\gamma)$; ΔT – the solidification temperature interval

With increasing vanadium content in the alloy, the volume fraction of primary austenite is decreased, whereas the amount of M_7C_3 and M_6C_5 carbides are increased. In addition, dendrite arms spacing (DAS) and size of eutectic M_7C_3 carbides are decreased, while the size of M_6C_5 carbides is increased with increasing vanadium content (Table 3). When the solidification temperature interval is narrower (as the consequence, in this case, of alloying high chromium white iron with vanadium), around the primary dendrite of the *γ*-phase in the remaining portion of the melt, the temperature and concentration conditions appear more readily, thus enabling the formation of eutectic colony nuclei and their growth which results in the interpretation of further *γ*-phase growth [34]. The eutectic colonies growth rate is well increased with increasing eutectic temperature, *i.e.*, with a lowering of the solidification temperature interval, thus influencing the formation of a larger amount of finer M_7C_3 carbides (Table 3).

Morphology of M_7C_3 eutectic carbide

M_7C_3 carbide has a pseudo-hexagonal structure with lattice parameters a = 13.9820 Å and C = 4.5065 Å, point group *mmm* and space group *Pmna* [53]. M_7C_3 forms as eutectic carbide during solidification with a distinguishable characteristic that it always appears to contain a high concentration of structural faulting [2]. Figure 3 shows a part of the eutectic M_7C_3 carbide containing many twins.

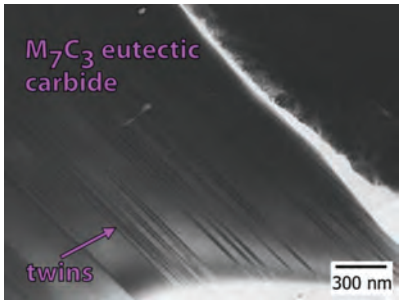

Fig. 3. TEM Micrograph of Fe–Cr–C–V white iron containing 1.19% V showing hexagonal M_7C_3 eutectic carbide.

The SEM micrographs of deep etched sample revealed that single M_7C_3 eutectic carbides in white iron, were rod or blade shaped, where the blades are basically consist of multiple rods (Fig. 4). The hexagonal $(Cr,Fe)_7C_3$ carbides grow as rods and blades, with the fastest [1] growth direction, and form a continuous network within each eutectic colony [9].

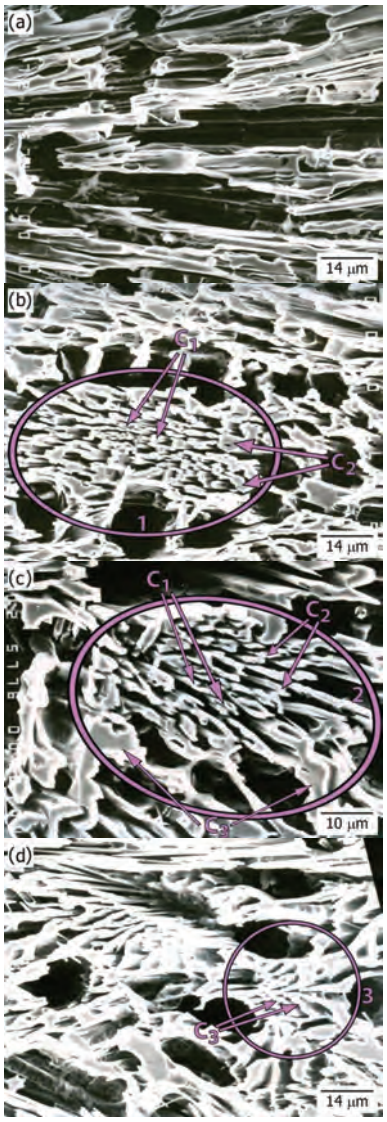

Fig. 4. SEM Micrographs of deep etched sample showing morphology of M_7C_3 eutectic carbides in hypoeutectic Fe–Cr–C–V type alloy containing 1.19% V. Different morphologies of eutectic colonies are marked 1 to 3. M_7C_3 carbides of different compositions marked by arrows C_1 to C_3.

Table 3. The volume fraction and size of phases in the microstructure of Fe–Cr–C–V white irons

Alloy	V in alloy, mass%	Volume fraction, vol.%			Size, μm		
		Primary γ-Fe	M_7C_3	M_6C_5	DAS	M_7C_3	M_6C_5
1	–	50.83	30.97	–	14.08	7.48	–
4	1.19	47.48	31.96	1.58	12.76	6.74	1.26
5	2.02	45.76	32.82	2.31	11.93	6.52	1.31
6	3.28	42.05	34.31	3.12	10.67	5.67	1.45
7	4.73	39.15	35.47	4.27	9.45	5.03	1.52

In the Fe–Cr–C–(V) type alloys, three different compositions of M_7C_3 carbides with different the Fe/Cr ratio of atomic fraction have been found (Table 4). While Fe/Cr ratio of atomic fraction in Fe–Cr–C–V alloy containing 0.12% V is 0.71 for carbides of composition C_1, it is 0.99 for carbides C_2 and 1.31 for carbides of composition C_3. In C_1 and C_2 carbides of the alloy containing 1.19% V, vanadium substitutes chromium atoms in M_7C_3 carbides lattice, while in carbide of composition C_3, it substitutes iron atoms. The Fe/Cr ratio in this alloy is 0.79, 1.03 and 1.26 for carbides of composition C_1, C_2 and C_3, respectively. In alloys containing 3.28% V and 4.73% V, chromium and iron atoms have been substituted by vanadium in all three different compositions of eutectic carbides. In cases of C_1 and C_2 carbies greater number of chromium atoms were substituded by vanadium, while in carbides C_3 greater number of iron atoms have been substituted [27].

In the earlier studies [21,54–57] it has been noticed that Fe/Cr ratio in eutectic carbides depends on carbon content in alloys with the same chromium content (hypoeutectic, eutectic and hypereutectic type alloy) or on the cooling rate. Doğan *et al*. [54] did observe that while the Fe/Cr ratio of atomic fraction in the M_7C_3 carbide of hypoeutectic and eutectic high chromium white iron with 15% Cr is approximately 1, it is 1.3 in 15% Cr hypereutectic iron. Jacuinde [57] has found in the study of iron containing 16.9% Cr, 2.58% C and 1.98% V that for higher cooling rate Fe/Cr ratio is 1.36, and that for slower cooling rate Fe/Cr ratio is 0.97.

Different morphologies of eutectic colonies in the columnar zone of as-cast structure of Fe–Cr–C–V white irons presented in Figs. 4 and 5. The eutectic colony consists of carbides of different compositions (Table 4 and Fig. 4). Blade-like carbides predominantly show C_3 composition [27].

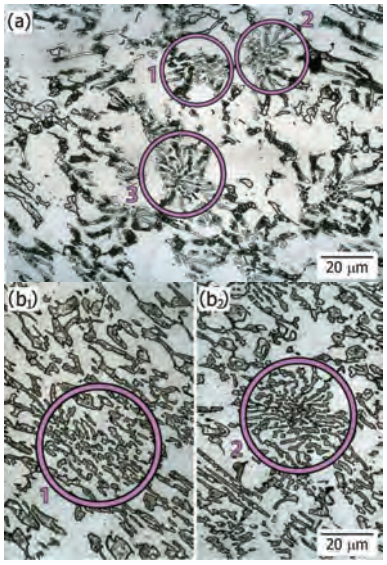

Fig. 5. Optical micrographs of hypoeutectic Fe–Cr–C iron (a) and Fe–Cr–C–V iron containing 3.28% V (b_1 and b_2) in the columnar zone of as-cast structures (5 mm from the surface). Different morphologies of eutectic colonies are marked by 1 to 3.

In the columnar zone of as-cast structures, the eutectic carbides are usually aligned so that the long axis of the carbide rods is parallel with the direction of heat flow (*i.e*., perpendicular to the cast surface), forming a highly anisotropic morphology. The formation of eutectic colonies of different morphologies is assumed to be related to the segregation of alloying elements in the melt. That is confirmed by EDS analysis which indicates different M_7C_3 carbide compositions (Table 4).

Table 4. Chemical composition of M_7C_3 eutectic carbide in Fe–Cr–C–V alloys (mass%). The values are based on an average of thirty different measurements per each of three different chemical compositions of M_7C_3 eutectic carbide in all tested alloys

Alloy	M_7C_3	Element								Formula
		C	Si	Mn	Mo	Cu	Cr	Fe	V	
1	C_1	8.17	0.028	0.673	0.557	0.032	53.36	38.07	–	$Cr_{4.2}Fe_{2.8}C_3$
	C_2	8.55	0.033	0.548	0.674	0.047	45.44	44.68	–	$Cr_{3.6}Fe_{3.3}C_3$
	C_3	8.43	0.019	0.659	0.494	0.053	39.77	50.11	–	$Cr_{3.2}Fe_{3.8}C_3$
2	C_1	8.35	0.031	0.781	0.595	0.020	53.12	37.91	0.111	$Cr_{4.2}Fe_{2.8}C_3$
	C_2	8.18	0.014	0.487	0.538	0.045	45.88	45.29	0.076	$Cr_{3.6}Fe_{3.3}C_3$
	C_3	8.67	0.028	0.663	0.686	0.038	38.87	51.18	0.078	$Cr_{3.1}Fe_{3.8}C_3$
4	C_1	8.23	0.011	0.667	0.541	0.049	48.43	38.13	3.63	$Cr_{3.8}Fe_{2.8}V_{0.3}C_3$
	C_2	8.48	0.032	0.535	0.672	0.029	42.72	44.22	2.76	$Cr_{3.4}Fe_{3.3}V_{0.2}C_3$
	C_3	8.41	0.055	0.671	0.479	0.048	38.72	48.93	2.75	$Cr_{3.1}Fe_{3.6}V_{0.2}C_3$
6	C_1	8.56	0.045	0.461	0.451	0.059	45.46	34.54	10.62	$Cr_{3.6}Fe_{2.6}V_{0.8}C_3$
	C_2	8.62	0.027	0.675	0.564	0.037	38.53	43.92	7.74	$Cr_{3.1}Fe_{3.2}V_{0.6}C_3$
	C_3	8.28	0.029	0.427	0.448	0.056	35.52	46.01	8.35	$Cr_{2.8}Fe_{3.4}V_{0.7}C_3$
7	C_1	8.44	0.016	0.585	0.671	0.061	43.16	32.97	14.19	$Cr_{3.4}Fe_{2.4}V_{1.1}C_3$
	C_2	8.14	0.031	0.643	0.451	0.048	38.03	40.92	11.79	$Cr_{3.0}Fe_{3.0}V_{0.9}C_3$
	C_3	8.37	0.013	0.591	0.493	0.053	34.19	45.24	11.53	$Cr_{2.7}Fe_{3.4}V_{0.8}C_3$

During solidification, solute segregation will influence nucleation and growth kinetics through its influence on constitutional undercooling (the constitutional undercooling of a particular phase is dependent on the *liquidus* and/or eutectic temperature which, in turn, is dependent on the local liquid composition) [27]. Due to different melt composition in particular regions, the constitutional undercooling and also the growth rate are different and the formation of eutectic colonies with different morphologies will be induced (Figs. 4 and 5).

According to solidification theory [51], for a hypoeutectic alloy composition, the alloy *liquidus* is much higher than the eutectic temperature. Thus the corresponding primary phase is highly constitutionally undercooled, due to the long-range boundary layer built up ahead of the solid–liquid interface in this case, and tends to grow faster than the eutectic. Consequently, primary phase will destabilize the solid–liquid interface. At the time when eutectic nucleation and growth occur, the conditions in the melt will in part be imposed by the characteristics of the previous reaction [52]. Since it can be assumed that thermal conditions, such as thermal gradient and cooling rate, are the same, the morphology of the eutectic growth front will depend on melt composition in particular zones. In the regions with a smaller content of alloying elements, the rosette-like eutectic colonies in which carbides are located radially from the center will be formed (Fig. 4d), whereas in regions of enriched melt, the formation of eutectic colonies consisting of a larger number of long M_7C_3 carbide rods will be favored (Fig. 4a).

The morphology of the eutectic carbides vary from the center to the edge of eutectic colonies marked by 1 and 2 in Figs. 4 and 5. The rod shaped carbides are finer at the center of the eutectic colony and become coarser rod-like or blade-like with increased distance from the center (Fig. 4b and c), as indicates that eutectic solidification begins at the center with a certain undercooling and proceeds radially outward. As solidification progresses, the constitutional undercooling decreases, and thus the rod-like or blade-like carbides that form during the later stages of solidification are coarser [27].

This can be explained by the fact that, during M_7C_3/γ eutectic growth, the solute atoms (as carbon, chromium and vanadium), which are rejected by one phase, are usually needed for the growth of the other. Therefore, lateral diffusion along the solid-liquid interface perpendicular to the growth direction, will become dominant and effectively decreases the solute build-up (ΔC) ahead of both phases. This lateral diffusion causes the interphase spacing, λ, in the eutectic structure to be decreased. However, as λ decreases, an opposing force (capillary effect), which arises from the increased energy associated with the increased curvature of the solid/liquid interface, comes into effect. As shown in Fig. 6, the diffusion effect can be expressed in terms of a constitutional undercooling (ΔT_c) while the latter can be expressed in terms of a curvature undercooling (ΔT_r) [27,51,52]. The sum of the solute (ΔT_c) and curvature (ΔT_r) undercoolings must therefore equal the interface undercooling, ΔT. Both undercoolings vary with λ in opposite ways: ΔT_c, which is proportional to ΔC (the driving force for solute diffusion) increases with λ, while ΔT_r decreases. The interphase spacing in the eutectic structure is eventually established by the equilibrium between an attractive force arising from the diffusion effect and a repulsive force arising from the curvature effect. Decrease in growth rates will shift ΔT_c to ΔT_{c1} without changing the ΔT_r curve, leading to a higher spacing value, λ_1. It is also evident from Fig. 6 that for small values of λ, eutectic growth is controlled by capillary effects ($\Delta T_r > \Delta T_c$), while diffusion is the limiting process at large spacing values [51,58]. With increasing λ values the size of M_7C_3 carbides increases.

In the case of eutectic colonies marked 3 in Figs. 4d and 5a, eutectic grows uniformly in all directions and finally a rosette-like structure is obtained.

The morphology of particular M_7C_3 carbides in Fe––Cr–C–V alloys does not significantly change with increasing vanadium content. These carbides are rod or blade shaped. The volume fraction, size and distribution of rod-like and blade-like carbides in the eutectic colonies are changing with increasing vanadium content in the alloy (Fig. 5). The rod type morphology of eutectic carbides is more dominant in Fe–Cr–C–V alloys with higher content of vanadium. These changes in morphology can be explained by the fact that in alloy with higher vanadium content, due to the higher concentration of vanadium in the melt, and subsequently larger constitutional undercooling, the growth rate is faster than in alloys with lower vanadium content, under the same cooling conditions [27].

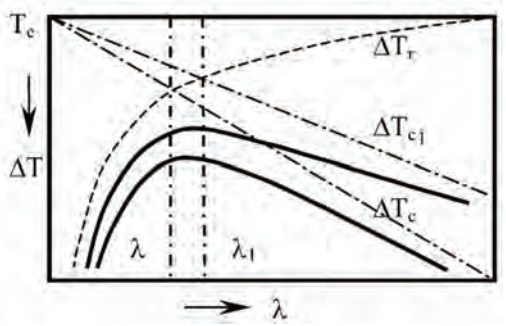

Fig. 6. Adjustment of interphase spacing during eutectic growth.

As-cast matrix microstructure

Vanadium was found to affect the transformation of austenite in as-cast condition of a Fe–Cr–C–V white irons [33]. Changes in the matrix microstructure over

the examined range of vanadium levels are illustrated in Fig. 1.

The austenite remains as a metastable phase at room temperature in Fe–Cr–C alloy with no vanadium addition [1] and Fe–Cr–C–V alloy containing 0.12% V (Figs. 1a), due to the high amount of carbon and alloying elements that lowers the martensite transformation starting temperature M_s.

The inhomogeneity of the dendrites in Fe–Cr–C–V alloys containing 0.49–4.73% V can be clearly seen (Fig. 1b–d). Fine dark particles predominantly located in the middle zone of the austenite (Fig. 1b–d) were identified to be carbides of $M_{23}C_6$ type (Fig. 7a). TEM observation revealed that the secondary carbides were distributed in a regular series (Fig. 7a and b), indicating a precipitation along preferred crystallographic planes. Around the carbide particles, the presence of dislocations (Fig. 7b) or martensite (Fig. 7b and c) was noticed.

As it can be seen from Fig. 1a–c, in alloys containing less than 3.28% V, primary and eutectic austenite is transformed in a narrow zone along the border with eutectic M_7C_3 carbide.

It has been suggested by several authors [1,13,21, 33,39] that during eutectic solidification the M_7C_3 carbide, which grows along the austenite, absorbs carbon from its surroundings and a narrow area at the austenite/carbide interphase becomes impoverished in it. The lack of carbon in these zones of austenite increases the M_s temperature which allows these areas of austenite to transform into martensite, during subsequent cooling.

Nevertheless, in Fe–Cr–C–V alloys containing 3.28 (Fig. 1d) and 4.73% V [33], a remarkably higher degree of austenite transformation can be seen. TEM Analysis identified martensite as a product of this transformation [33].

The chemical composition of austenite changes by changing the vanadium content in high chromium iron (Table 5). Adding more vanadium into the Fe–Cr–C–V type alloys was followed by higher vanadium content in the austenite, as a normal consequence of its wide solubility range in the *γ*-solid solution. The lower carbon content experienced in the matrix in alloy with higher vanadium content was assumed to be related to the larger amount of eutectic with M_7C_3 carbides (Table 3).

At temperatures below solidus, in the course of further cooling after solidification, $M_{23}C_6$ carbides precipitate in austenite (Fig. 7), mainly in areas with lower carbon content. Due to heterogeneity of the matrix composition, the precipitation is heterogeneous, and in alloys with vanadium content lower than 2% they were predominantly located in the surface dendrite zone (Fig. 1b and c).

The carbides precipitation kinetic in austenite of Fe–Cr–C–V alloys depends on the vanadium content in the alloy [33]. In spite of the vanadium content increase in the austenite matrix, the part of the added vanadium was locked in the precipitated $M_{23}C_6$ carbides, whose volume fraction increased in alloys with higher vanadium content.

The transformation of austenite into martensite in the Fe–C–Cr–V alloys is closely related to the precipitation of secondary carbides. Precipitation of $M_{23}C_6$ carbides minimizes the carbon and chromium content in the matrix, and increases the M_s temperaature. The degree of martensitic transformation is determined by the amount of precipitated carbides, i.e. depends on the austenite composition [33].

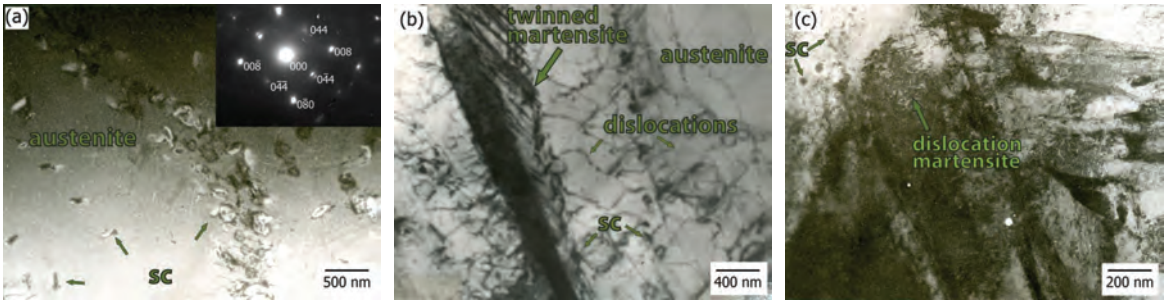

Fig. 7. TEM Micrographs of the Fe–C–Cr–V alloy containing 1.19% V showing: a) secondary carbides and selected-area diffraction pattern (in the corner) from the region in this micrograph showing a [100] zone axis; b) and c) secondary carbides and martensite.

Table 5. Chemical composition of the as-cast matrix in Fe–C–Cr–V alloys (mass%)

Alloy	V in alloy, mass%	Element							
		C	Si	Mn	Mo	Cu	Cr	Fe	V
2	0.12	1.35–1.56	0.82–0.93	0.63–0.68	0.24–0.34	1.43–1.81	11.76–12.89	82.07–83.16	0.014–0.015
4	1.19	1.01–1.31	0.95–1.12.	0.78–0.82	0.22–0.38	1.46–1.82	11.20–12.71	82.92–83.24	0.341–0.346
6	3.28	0.65–0.94	0.88–0.97	0.72–0.81	0.17–0.35	1.74–1.96	11.51–12.42	81.37–82.84	1.26–1.29
7	4.73	0.54–0.79	0.96–1.04	0.78–0.81	0.32–0.47	1.71–1.87	11.62–12.16	81.14–82.35	1.84–1.89

The amount of retained austenite in the Fe–Cr–C–V white irons is found to decrease with increasing vanadium content (Fig. 8).

Microstructure after subcritical heat treatment

After heat treatment (500 °C/4 h) there were no notable changes in the structure of a basic Fe–Cr–C white iron [2, 13]. However, during isothermal holding at 500 °C for 4 h, the secondary carbides precipitated in the austenite of Fe–Cr–C–V white irons. Martensite present in the as-cast structure was also tempered at this temperature. Austenite was then partly transformed into martensite during the cooling process. The amount of precipitated carbides and volume fraction of martensite which formed depended on the basic as-cast structure, *i.e.*, on vanadium content in the alloy [2].

EFFECT OF MICROSTRUCTURE ON THE PROPERTIES OF TESTED Fe-Cr-C-V ALLOYS

Vanadium therefore altered the microstructure characteristics of high chromium white cast iron and affected its properties.

Effect of microstructure on the hardness of tested Fe–C–Cr–V alloys

The matrix microhardness and the alloy macrohardness were improved by increasing the vanadium content in both the as-cast and heat treated state (Figs. 9 and 10).

The improved hardness of the Fe–C–Cr–V white irons by increasing vanadium content in as-cast condition (Fig. 10) was the result of an increased volume

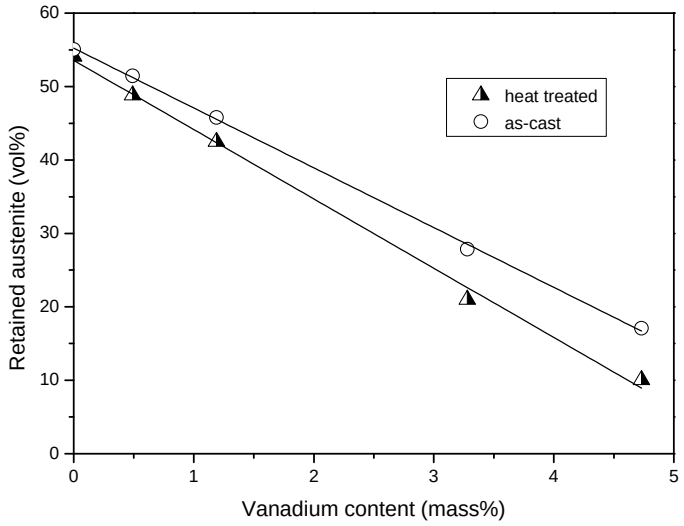

Fig. 8. Volume fraction of retained austenite as a function of vanadium content in Fe–Cr–C–V white irons in both as-cast and heat treatment state.

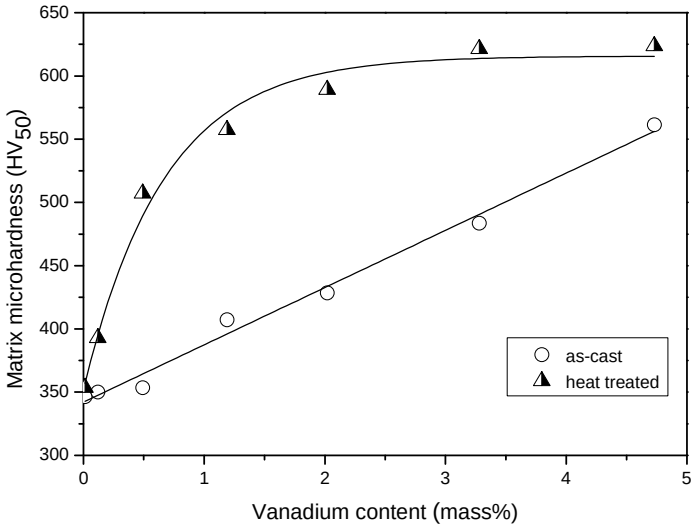

Fig. 9. Matrix microhardness as a function of vanadium content in Fe–Cr–C–V white irons in both as-cast and heat treatment state.

fraction of the eutectic M_7C_3 and V_6C_5 carbide. Nevertheless, an increase in the amount of precipitated carbides in austenite and the formation of a larger amount of martensite, combined with a reduction in the volume fraction of retained austenite (Fig. 8), improved the matrix microhardness (Fig. 9), and consequently the alloy macrohardness (Fig. 10) in both the as-cast and heat treated states [29].

Effects of microstructure on the abrasion wear resistance of tested Fe–C–Cr–V alloys

The influence of vanadium on abrasion resistance* is presented in Fig. 11. Wear resistance improved as the concentration of vanadium increased up to 3.28%, and fell off thereafter. Abrasion wear resistance was slightly higher after heat treatment at 500 °C (Fig. 11).

The abrasion resistance of the carbide phase was more effective than the matrix in white cast irons, since, mainly, the hardness of M_7C_3 (1200–1800 HV [1]) carbides were greater than the hardness of the used abrasive – quartz (900-1080 HV [1]). In white cast irons the matrix was preferentially worn by a cutting action, under low-stress abrasion conditions. Eutectic carbides were then forced to stand in relief and directly obstruct the cutting action of abrasive particles for a period of time until they were partly or completely removed by a

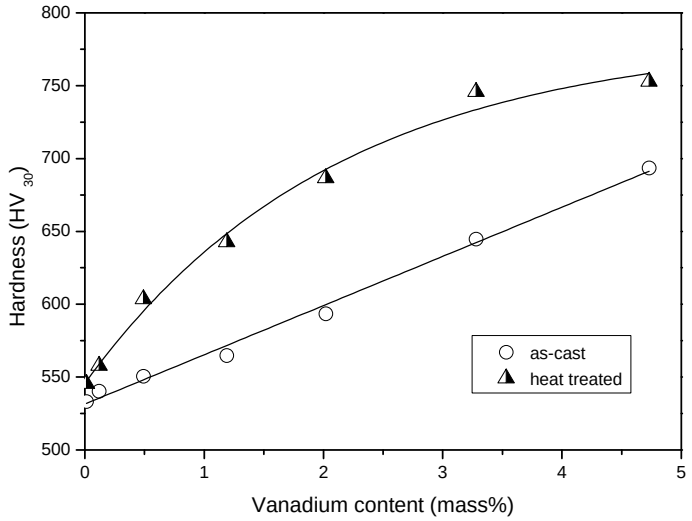

Fig. 10. Hardness as a function of vanadium content in Fe–Cr–C–V white irons in both as-cast and heat treatment state.

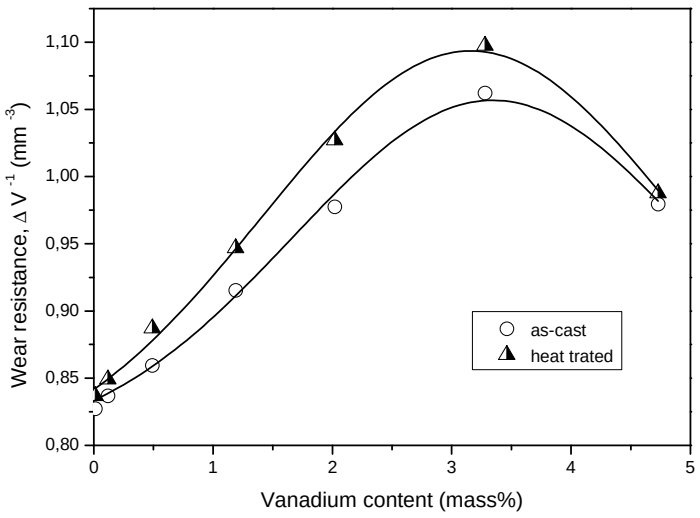

Fig. 11. Wear resistance as a function of vanadium content in Fe–Cr–C–V white irons in both as-cast and heat treatment state.

*Abrasive wear resistance was evaluated according to the ASTM Standard Practice G-65, Procedure B (Dry Sand/Rubber Wheel Abrasion Test).

cutting or chipping action [1,5,29]. In other words, wear under low-stress abrasion conditions, and using a quartz abrasive, was apparently controlled by the rate of removal of the carbide phase since the protruding

carbides protected the matrix from direct attack of abrasive particles [2].

Therefore, increasing the volume fraction of M_7C_3 eutectic carbides up to 35% in the Fe–C–Cr–V white irons, and simultaneously increasing the amount of very hard V_6C_5 carbide (2800 HV), reduced the volume loss caused by abrasive wear (Fig. 11). However, a further increase in the volume fraction of the carbide phase (alloy with 4.73% V, Table 3) reduced wear resistance (Fig. 11), which was most likely attributable to intensive spalling of massive carbides during wear.

In addition to the volume fraction of carbides, the size of phases present in the structure was another microstructure variable which affected the abrasive resistance of the Fe–Cr–C–V alloys. The smaller size of primary austenite dendrites, *i.e.*, the average distance between carbide particles, caused by increasing the content of vanadium in the alloy (Table 3), protected the matrix better from direct attack by abrasive particles. The shorter rods of M_7C_3 carbides (Table 3) also tended to be less severely cracked during wear, thereby improving the wear resistance of the alloys. It must be specified, however, that the effect of controlling wear rate by refining the microstructure depended on abrasive grit size, *i.e.*, the ratio of mean free path to mean abrasive asperity size [4,13,29]. The smaller the ratio, the less likely that grit would undermine the hard particles by penetrating the matrix.

The improved wear resistance of white cast irons after heat treatment, compared with the as-cast condition (Fig. 11) indicated that wear resistance under low-stress abrasion conditions also depended on the matrix microstructure. In addition to the fact that the matrix helped control of the penetration depth of abrasive particles, it also played an important role in preventing bodily removal of smaller carbides and cracking of massive ones [14]. Experimental results indicate that the martensitic or martensite-austenitic matrix microstructure more adequately reinforced M_7C_3 eutectic carbides to minimize cracking and removal during wear than the austenitic matrix [29].

Besides, the secondary carbides which precipitate in the matrix regions of high chromium white irons also influence the abrasion behaviour [2,25]. By increasing the matrix strength through a dispersion hardening effect, the fine secondary carbides can increase the mechanical support of the eutectic carbides. These results agree with those of Liu et al. [59] and Wang et al. [60] who found that the precipitation of fine $M_{23}C_6$ carbides and the more homogeneous carbide distribution as a result of cryogenic treatment is responsible for the improved wear resistance of high chromium white irons.

Effect of microstructure on the fracture toughness of tested Fe–C–Cr–V alloys

The higher content of vanadium in high chromium white iron increases the volume fraction of the carbide phase and reduces fracture toughness. On the other hand, the toughness has been improved by reducing the size of M_7C_3 eutectic carbide. However, the results of fracture toughness tests* in both as-cast and heat treated conditions (Fig. 12) show that the dynamic fracture toughness in white cast irons is determined

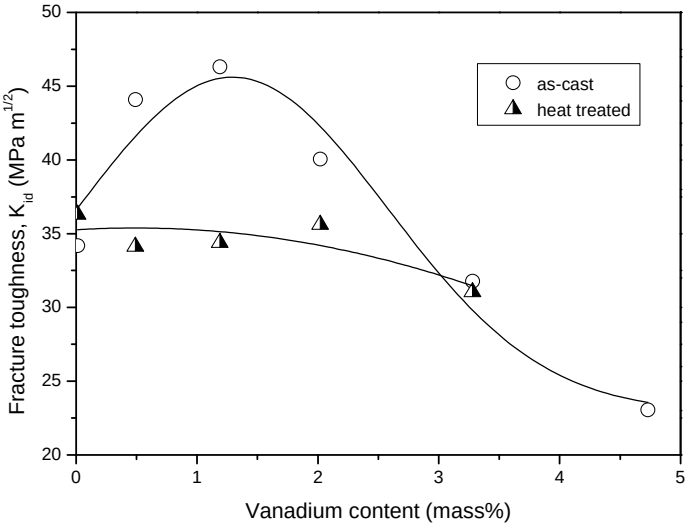

Fig. 12. Fracture toughness as a function of vanadium content in Fe–Cr–C–V white irons in both as-cast and heat treatment state.

*Dynamic fracture toughness was measured at room temperature using an impact test machine equipped with an instrumented Charpy tub. The testing methodology selected was based on the three-point bending tests. The specimens of 10 mm×10 mm×55 mm in size, were notched and precracked by fatigue following ASTM E399 standard.

mainly by the properties of the matrix. The austenite is more effective in this respect than martensite [2,29].

By increasing the vanadium content, the amount of retained austenite decreased, as it shown in Fig. 8, which subsequently reduced toughness. However, the Fe–C–Cr–V alloys containing 1.19% V in the as-cast condition, showed greater dynamic fracture toughness when compared to the basic Fe–C–Cr alloy, Fig. 12. Fracture toughness was determined mainly by the energy that had to be consumed in extending the crack through ligaments of matrix [10,36]. Since the austenite in that alloy contained very fine $M_{23}C_6$ carbide particles, higher fracture toughness was attributed to a strengthening of the austenite during fracture [29]. Hence, the contribution to improving the fracture toughness of the alloy containing 1.19 wt.% V, due to the presence of fine $M_{23}C_6$ carbides within the austenite, was considerably higher than the reduction. Reduction was caused by, on the one hand, increasing the amount of M_7C_3 carbides and reducing inter-carbide distance, and on the other hand, reducing the volume fraction of retained austenite. Where the content of vanadium exceeded 1.19%, fracture toughness decreased (Fig. 12), since the matrix microstructure of those alloys was mainly martensitic.

In heat-treated Fe–C–Cr–V alloys with varying contents of vanadium, lower K_{id} values wear obtained, compared with as-cast alloys (Fig. 12). Several processes which occurred during tempering affected fracture toughness. When held at 500 °C for 4 h, extensive carbide precipitation probably occurred in the martensite present in the as-cast structure, and retained austenite was decomposed [2,13]. Both effects combined to produce a significant drop in fracture toughness. Furthermore, during the cooling process, after it had been held at the tempering temperature, martensite formed, which also contributed to lower K_{id} values.

Effect of microstructure on the impact resistance of tested Fe–C–Cr–V alloys

The results obtained by examination of impact resistance* of Fe–Cr–C–V white irons in as-cast condition are presented in Fig. 13.

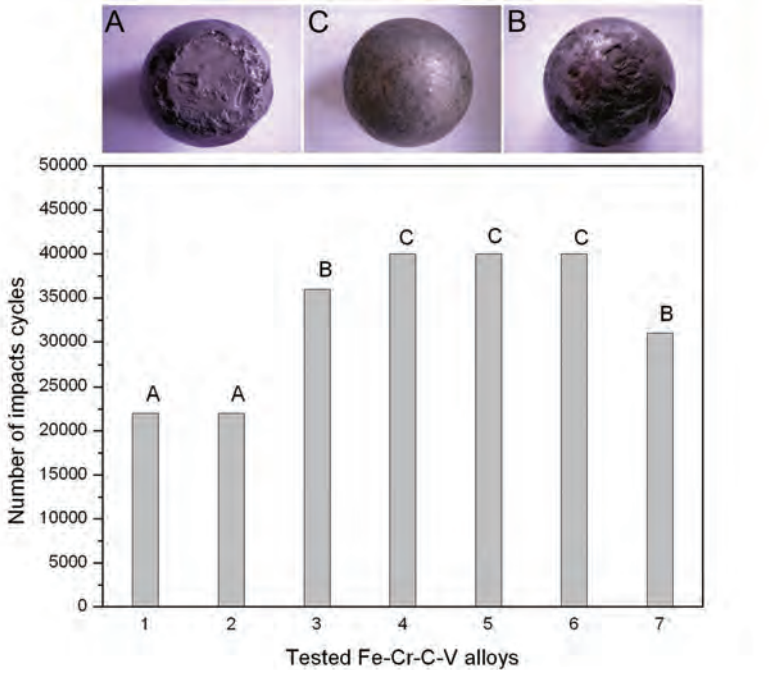

Fig. 13. Impact resistance of Fe–Cr–C–V white irons in as-cast condition. Markings on the graph: A – form of the balls changed, balls gained an elliptic shaped; B – spalling of the balls started; C – testing interrupted, form unchanged and no spalling of the balls.

Fe–Cr–C–V white irons show considerably higher impact resistance compared to the basic Fe–Cr–C white iron (Fig. 13). However, the vanadium content influence on the impact resistance was not unique, as the importance of the specific structural features brought by adding vanadium indicates [26].

*The impact resistance of Fe–Cr–C–V white irons was tested using an impact-fatigue test machine. The test balls (ten balls of each examined alloy) were lifted to a height of up to 6.4 m and allowed to fall freely on the hardened steel anvil. Following impact, each ball was automatically recycled, by means of a bucket-type elevator, and allowed to drop again on the anvil. The impact cycles were repeated until the ball failed (defined either by the ball cracking or the appearance of significant spalls). The number of impacts to failure was taken as a measure of the impact resistance.

TEM Micrographs of the surface layer (4 mm depth from ball surface) of a Fe–Cr–C–V alloy ball, containing 1.19% V, after impact resistance testing, are shown in Fig. 14. In the surface dendritic area, along the border with M_7C_3 carbides, austenite was transformed into martensite (Fig. 14a), and this change was rather similar before and after the impact resistance testing (Fig. 1c).

Micrographs in Fig. 14b and c indicate a clear planar deformation substructure. In the austenitic matrix very fine twinning lamellae (width about 50–60 nm) can be observed, due to the twinning occurring on {111} planes (making the angle ≈70°), and a planar dispositional arrangement produced by slip at the same slip system (Fig. 14b and c).

The hardness was measured at 4 mm depth from ball surface of the Fe–Cr–C–V cast iron containing 1.19% V was 668 HV before the impact test, increasing to the range from 936 to 984 HV, after the test.

The fact that in Fe–Cr–C–V alloys with increasing vanadium content the retained austenite volume fraction decreases (Figs. 1 and 8), the amounts of precipitated $M_{23}C_6$ carbides and martensite increase (Fig. 1), and the fact that the impact resistance of the alloys with 0.49% V and 1.19–3.28% V is 60 and 80% higher, respectively, compared to basic Fe–Cr–C alloy (Fig. 13), indicates the complexity of the hardening process in tested balls.

Deformed substructure revealed in the retained austenite at the surface of the ball after impact test (Fig. 14), indicates that under repeated impact loading, deformation and appropriate strain hardening come into play [26]. The emergence of fine twinning lamellae as a primary deformation mechanism and subsequent activation of planar slip of dislocations are considered to be anomalies in deformation behaviour of austenitic steels with low-stacking-fault energy, which may result in a very strong strain hardening effect [61]. According to the results of TEM examinations (Fig. 14b and c), it was supposed that similar activity of an anomalous strain hardening happened in the retained austenite of the tested balls of high chromium white cast iron alloyed with vanadium. The change in the amount of austenite was assumed to affect the strain hardening process, and obviously in the white iron with 4.73% V the strain hardening effect was weak due to a little retained austenite (Fig. 8).

The particles of precipitated $M_{23}C_6$ secondary carbides disturb dislocations movement and contribute to increase the effects of strain hardening in Fe–Cr–C–V white irons [26].

According to literature [3], the impact resistance of Fe–Cr–C white iron with high chromium content decreases with increasing volume fraction of eutectic M_7C_3 carbides. Nevertheless, in Fe–Cr–C–V white cast irons, regardless of the increased amount of eutectic carbides in the structure, the higher impact resistance for higher vanadium content in alloy up to 3.28% V, can be related to the strain hardening of retained austenite [26]. The alloy with 4.73% V shows a lower impact resistance compared to other Fe–Cr–C–V alloys and it was assumed to be the consequence of, on one hand, the lower amount of retained austenite and the higher amount of martensite and, on the other hand, of a large volume fraction of eutectic M_7C_3 carbides. Thus, the lower impact resistance found in balls with 4.73% V obviously is the result of a complex interaction of all structural features and hardening phenomena.

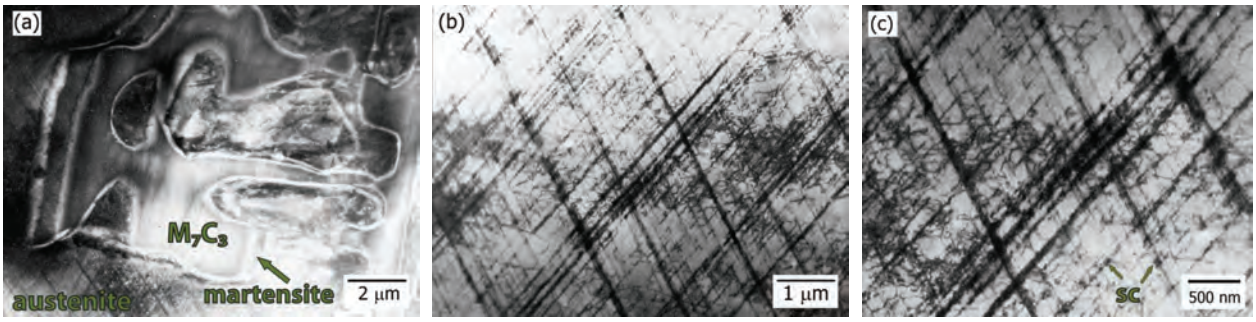

Fig. 14. TEM Micrographs of Fe–C–Cr–V white iron containing 1.19% V after impact resistance testing.

CONCLUSIONS

The microstructure of Fe–Cr–C–V white irons consists of M_7C_3 and vanadium rich M_6C_5 carbides in austenitic matrix.

With an increase of vanadium content the alloy composition approaches the eutectic composition in the quaternary Fe–Cr–C–V system, causing a decrease of the solidification temperature interval, and thereby also changing the volume fraction, size and morphology of the present phases. Vanadium changes the transformation characteristics of austenite in as-cast condition in the Fe–C–Cr–V type alloys. The transformation of austenite to martensite in the Fe–C–Cr–V is closely connected with the secondary carbide deposition.

The volume fraction of the carbide phase, carbide size and distribution had an important influence on the wear resistance of Fe–Cr–C–V white cast iron alloys under low-stress abrasion conditions. However, the dynamic fracture toughness of Fe–Cr–C–V white cast irons is determined mainly by the properties of the matrix. The austenite is more effective in this respect than martensite. Since the austenite in these alloys contained very fine $M_{23}C_6$ carbide particles, higher fracture toughness was attributed to a strengthening of the austenite during fracture. Besides, the secondary carbides which precipitate in the matrix regions also influence the abrasion behaviour. By increasing the matrix strength through a dispersion hardening effect, the fine secondary carbides can increase the mechanical support of the carbides. Deformation and appropriate strain hardening occur in the retained austenite of Fe–Cr–C–V alloys under repeated impact loading. The particles of precipitated $M_{23}C_6$ secondary carbides disturb dislocations movement and contribute to increase the effects of strain hardening in Fe–Cr–C–V white irons.

It was therefore possible, by adding approximately 3 wt.% V to high chromium white iron, to obtain an alloy that will have, in the as-cast condition or after tempering at 500 °C, better properties than high temperature treated alloys with no vanadium addition. This may be very important from a practical point of view, especially for castings with a complex configuration, since the possibility of high residual stresses during high temperature heat treatment and problems related to this process can be avoided.

REFERENCES

[1] C.P. Tabrett, I.R. Sare, M.R. Ghomashchi, Microstructure–property relationships in high chromium white iron alloys, Int. Mater. Rev. **41** (1996) 59–82.

[2] M. Filipovic, Z. Kamberovic, M. Korac, M. Gavrilovski, Correlation of microstructure with the wear resistance and fracture toughness of the white cast iron alloys, Met. Mater. Int. **19** (2013) 473–481.

[3] I.R. Sare, B.K. Arnold, G.A. Dunlop, P.G. Lloyd, Repeated impact-abrasion testing of alloy white cast irons, Wear **162–164** (1993) 790–801.

[4] I.R. Sare, Abrasion resistance and fracture toughness of white cast irons, Met. Technol. **6** (1979) 412–419.

[5] K.H. Zum Gahr, D.V. Doane, Optimizing fracture toughness and abrasion resistance in white cast irons, Metall. Trans., A **11** (1980) 613–620.

[6] C.K. Kim, S. Lee, J.Y. Jung, Effects of heat treatment on wear resistance and fracture toughness of duo-cast materials composed of high-chromium white cast iron and low-chromium steel, Met. Mat. Trans., A **37** (2006) 633–643.

[7] A. Wiengmoon, J.T.H. Pearce, T. Chairuangsri, Relationship between microstructure, hardness and corrosion resistance in 20 wt.% Cr, 27 wt.% Cr and 36 wt.% Cr high chromium cast irons, Mater. Chem. Phys. **125** (2011) 739–748.

[8] Ö.N. Doğan, Columnar to equiaxed transition in high Cr white iron castings, Scr. Mater. **35** (1996) 163–168.

[9] Ö.N. Doğan, J.A. Hawk, Effect of carbide orientation on abrasion of high Cr white cast iron, Wear **189** (1995) 136–142.

[10] G. Powell, V. Randle, The effect of Si on the relationship between orientation and carbide morphology in high chromium white irons, J. Mater. Sci. **32** (1997) 561–565.

[11] R. Correa, A. Bedolla-Jacuinde, J. Zuno-Silva, E. Cardoso, I. Mejía, Effect of boron on the sliding wear of directionally solidified high-chromium white irons, Wear **267** (2009) 495–504.

[12] J.J. Coronado, Effect of load and carbide orientation on abrasive wear resistance of white cast iron, Wear **270** (2011) 287–293.

[13] I.R. Sare, B.K. Arnold, The influence of heat treatment on the high-stress abrasion resistance and fracture toughness of alloy white cast irons, Met. Mater. Trans. **26** (1995) 1785–1793.

[14] C.P. Tabrett, I.R. Sare, Fracture toughness of high-chromium white irons: Influence of cast structure, J. Mater. Sci. **35** (2000) 2069–2077.

[15] A. Kootsookos, J.D. Gates, The role of secondary carbide precipitation on the fracture toughness of a reduced carbon white iron, Mater. Sci. Eng., A **490** (2008) 313––318.

[16] A. Sawamoto, K. Ōgi, K. Matsuda, Solidification structures of Fe–C–Cr–(V–Nb–W) alloys, AFS Trans. **94** (1986) 403–416.

[17] S.H. Mousavi Anijdan, A. Bahrami, N. Varahram, P. Davami, Effects of tungsten on erosion–corrosion behavior of high chromium white cast iron, Mater. Sci. Eng., A **454–455** (2007) 623–628.

[18] H.K. Baik, C.R. Loper, The influence of niobium on the solidification structure of Fe-C-Cr alloys, AFS Trans. **96** (1988) 405-412.

[19] C.R. Loper, H.K. Baik, Influence of molybdenum and titanium on the microstructures of Fe-C-Cr-Nb white cast irons, AFS Trans. **97** (1989) 1001–1008.

[20] M. Fiset, K. Peev, M. Radulovic, The influence of niobium on fracture toughness and abrasion resistance in high chromium white cast irons, J. Mater. Sci. Lett. **12** (1993) 615–617.

[21] A. Bedolla-Jacuinde, Microstructure of vanadium-, niobium- and titanium-alloyed high-chromium white cast irons, Int. J. Cast Metals Res. **13** (2001) 343–361**.**

[22] R. Kesri, M. Durand-Charre, Phase equilibria, solidification and solid-state transformations of white cast irons containing niobium, J. Mater. Sci. **22** (1987) 2959––2964.

[23] X. Zhi, J. Xing, H. Fu, B. Xiao, Effect of niobium on the as-cast microstructure of hypereutectic high chromium cast iron, Mater. Lett. **62** (2008) 857–860.

[24] G.H. Coelho, J.A. Golczewski, H.F. Fischmeister. Thermodynamic calculations for Nb-containing high-speed steels and white cast iron alloys, Met. Mat. Trans., A **34** (2003) 1749–1758.

[25] M. Filipovic, Z. Kamberovic, M. Korac, M. Gavrilovski, Microstructure and mechanical properties of Fe–Cr–C––Nb white cast irons, Mater. Des. **47** (2013) 41–48.

[26] M. Filipovic, E. Romhanji, Strain hardening of austenite in Fe–Cr–C–V alloys under repeated impact, Wear **270** (2011) 800–805.

[27] M. Filipovic, E. Romhanji, Z. Kamberovic, Chemical composition and morphology of M_7C_3 eutectic carbide in high chromium white cast iron alloyed with vanadium, ISIJ Int. **52** (2012) 2200–2204.

[28] J.D.B. De Mello, M. Durand-Charre, T. Mathia, Abrasion mechanisms of white cast iron II: Influence of the metallurgical structure of V–Cr white cast irons, Mater. Sci. Eng. **78** (1986) 127–134.

[29] M. Radulovic, M. Fiset, K. Peev, M. Tomovic, The influence of vanadium on fracture toughness and abrasion resistance in high chromium white cast irons, J. Mater. Sci. **29** (1994) 5085–5094.

[30] A. Bedolla-Jacuinde, L. Arias, B. Hernández, Kinetic of secondary carbides precipitation in a high-chromium white iron, J. Mater. Eng. Perform. **12** (2003) 371–382.

[31] A. Wiengmoon, T. Chairuangsri, J.T.H. Pearce, Microstructural and crytallographical study of carbides in 30wt.%Cr cast irons, Acta Materialia **53** (2005) 4143––4154.

[32] J. Wang, R.L. Zuo, Z.P. Sun, C. Li, K.K. Liu, H.X. Yang, B.L. Shen, S.J. Huang, Influence of secondary carbides precipitation and transformation on hardening behavior of a 15 Cr–1 Mo–1.5 V white iron, Mater. Charact. **55** (2005) 234–240.

[33] M. Filipovic, E. Romhanji, Z. Kamberovic, M. Korac, Matrix microstructure and its micro-analysis of constituent phases in as-cast Fe–Cr–C–V alloys, Mater. Trans. **50** (2009) 2488–2492.

[34] M. Filipovic, Z. Kamberovic, M. Korac, Solidification of high chromium white cast iron alloyed with vanadium, Mater. Trans. **52** (2011), 386–390.

[35] X. Wu, J. Xing, H. Fu, X. Zhi, Effect of titanium on the morphology of primary M_7C_3 carbides in hypereutectic high chromium white iron, Mater. Sci. Eng., A **457** (2007) 180–185.

[36] X. Zhi, J. Xing, H. Fu, Y. Gao, Y, Effect of titanium on the as-cast microstructure of hypereutectic high chromium cast iron, Mater. Charact. **59** (2008) 1221–1226.

[37] A. Bedolla-Jacuinde, R. Correa, I. Mejia, J.G. Quezada, W.M. Rainforth, The effect of titanium on the wear behaviour of a 16% Cr white cast iron under pure sliding, Wear **263** (2007) 808–820.

[38] X. Wu, J. Xing, H. Fu, X. Zhi, Effect of titanium on the morphology of primary M_7C_3 carbides in hypereutectic high chromium white iron, Mater. Sci. Eng., A **457** (2007) 180–185.

[39] A. Bedolla-Jacuinde, R. Correa, J.G. Quezada, C. Maldonado, Effect of titanium on the as-cast microstructure of a 16% chromium white iron, Mater. Sci. Eng., A 398 (2005) 297–308.

[40] Y. Taşgin, M. Kaplan, M. Yaz, Investigation of effects of boron additives and heat treatment on carbides and phase transition of highly alloyed duplex cast iron, Mater. Des. **30** (2009) 3174–3179.

[41] J.W. Choi, S.K. Chang, Effects of molybdenum and copper additions on microstructure of high chromium cast iron rolls, ISIJ Int. **32** (1992) 1170–1176.

[42] C. Scandian, C. Boher, J.D.B. De Mello, F. Rézaï-Aria, Effect of molybdenum and chromium contents in sliding wear of high-chromium white cast iron: The relationship between microstructure and wear, Wear **267** (2009) 401–408.

[43] A. Bedolla-Jacuinde, W.M. Rainforth, The wear behaviour of high-chromium white cast irons as a function of silicon and mischmetal content, Wear **250** (2001) 449––461.

[44] K. Peev, M. Radulovic, M. Fiset, Modification of Fe-Cr-C alloys using mischmetal, J. Mater. Sci. Lett. 13 (1994) 112–114.

[45] M. Radulovic, M. Fiset, K. Peev, Effect of rare earth elements on microstructure and properties of high chromium white iron, Mater. Sci. Technol. **10** (1994) 1057––1062.

[46] Y. Qu, J. Xing, X. Zhi, J. Peng, H. Fu, Effect of cerium on the as-cast microstructure of a hypereutectic high chromium cast iron, Mater. Mater. Lett. **62** (2008) 3024––3027.

[47] P. Dupin, J.M. Schissler, Influence of additions of silicon, molybdenum, vanadium, and tungsten upon the structural evolution of the as-cast state of a high-chromium cast iron (20%Cr, 2.6%C), AFS Trans. **92** (1984) 355–360.

[48] Y. Matsubara, N. Sasaguri, K. Shimizu, S.K. Yu, Solidification and abrasion wear of white cast irons alloyed with 20% carbide forming elements, Wear **250** (2001) 502–510.

[49] D.M. Stefanescu, S. Cracium, Manganese and vanadium cast iron with 15% chromium for abrasive wear resistant castings, Fonderie **32** (1977) 51–60.

[50] A. Bedolla-Jacuinde, B. Hernández, L. Béjar-Gómez, SEM study on the M_7C_3 carbide nucleation during eutectic solidification of high-chromium white irons, Z. Metallkd. **96** (2005) 1380–1385.

[51] W. Kurz, D.J. Fisher, Fundamentals of Solidification, Trans Tech Publication, Dürnten, 1984, pp. 97–116.

[52] M. Asta, C. Beckermann, A. Karma, W. Kurz, R. Napolitano, M. Plapp, G. Purdy, M. Rappaz, R. Trivedi, Solidification microstructures and solid-state parallels: Recent developments, future directions, Acta Mater. **57** (2009) 941–971.

[53] S.D. Carpenter, D. Carpenter, J.D.H. Pearce, XRD and electron microscope study of an as-cast 26.6% chromium white iron microstructure, Mater. Chem. and Phys. **85** (2004) 32–40.

[54] Ö.N. Doğan, J.A. Hawk, G. Laird II, Solidification structure and abrasion resistance of high chromium white irons, Met. Mat. Trans., A **28** (1997) 1315–1328.

[55] K. Ogi, Y. Matsubara, K. Matsuda, Eutectic solidification of high chromium cast iron — mechanism of eutectic growth, AFS Trans. **89** (1981) 197–204.

[56] X. Zhi, J. Xing, Y. Gao, H. Fu, J. Peng, B. Xiao, Effect of heat treatment on microstructure and mechanical

properties of a Ti-bearing hypereutectic high chromium white cast iron, Mater. Sci. Eng., A **487** (2008) 171–179.

[57] R.S.J. Jackson, The austenite liquidus surface and constitutional diagram for the Fe–Cr–C metastable system, Iron Steel Inst. **208** (1970) 163–167.

[58] L. Lu, H. Soda, A. McLean, Microstructure and mechanical properties of Fe–Cr–C eutectic composites, Mater. Sci. Eng., A **347** (2003) 214–222.

[59] H. Liu, J. Wang, H. Yang, B. Shen, Effects of cryogenic treatment on microstructure and abrasion resistance of CrMnB high chromium cast iron subjected to sub-critical treatment, Mater. Sci. Eng., A **478** (2008) 324–328.

[60] J. Wang, J. Xiong, H. Fan, H.S. Yang, H.H. Liu, B.L. Shen, Effects of high temperature and cryogenic treatment on the microstructure and abrasion resistance of a high chromium cast iron, J. Mater. Process. Technol. **209** (2009) 3236–3240.

[61] I. Karaman, H. Sehitoglu, Y.I. Chumlyakov, H.J. Maier, The deformation of low-stacking-fault-energy austenitic steels, JOM **54** (2002) 31–37.

IZVOD

ŽELEZO-HROM-UGLJENIK-VANADIJUM BELA LIVENA GVOŽĐA – MIKROSTRUKTURA I SVOJSTVA

Mirjana M. Filipović

Tehnološko-metalurški fakultet, Univerzitet u Beogradu, Beograd, Srbija

(Pregledni rad)

Mikrostruktura Fe–Cr–C–V belih gvožđa u livenom stanju se sastoji od M_7C_3 karbida i M_6C_5 karbida bogatih vanadijumom u austenitnoj metalnoj osnovi. Vanadijum menja mikrostrukturne parametre faza prisutnih u strukturi ovih legura, uključujući zapreminski udeo, veličinu i morfologiju. Stepen martenzitne transformacije, takođe, zavisi od sadržaja vanadijuma u leguri. Zapreminski udeo karbidne faze, veličina karbida i raspodela ima značajan uticaj na otpornost na habanje abrazijom Fe–Cr–C–V belih livenih gvožđa u uslovima malih naprezanja. Međutim, žilavost Fe–Cr–C–V gvožđa je uglavnom određena svojstvima metalne osnove. Austenit je mnogo efektniji od martenzita. Budući da austenit u ovim legurama sadrži vrlo fine čestice $M_{23}C_6$ karbida, veća žilavost je povezana sa ojačavanjem austenita u toku loma. Pored toga, sekundarni karbidi, istaloženi u regionima metalne osnove, takođe, utiču na ponašanje pri habanju abrazijom. Povećavajući čvrstoću metalne osnove kroz efekat disperznog ojačavanja, fini sekundarni karbidi povećavaju mehaničku podršku eutektičkim karbidima. U uslovima ponovljenih udarnih opterećenja u zaostalom austenitu Fe–Cr–C–V belih gvožđa javlja se deformacija i deformaciono ojačavanje. Čestice istaloženih $M_{23}C_6$ sekundarnih karbida ometaju kretanje dislokacija i doprinose pojačanju efekta deformacionog ojačavanja.

Ključne reči: Fe–Cr–C–V bela livena gvožđa • Mikrostruktura • Tvrdoća • Žilavost • Otpornost na habanje abrazijom • Otpornost na ponovljena udarna opterećenja

Analytical application of the reaction system methylene blue B–$K_2S_2O_8$ for the spectrophotometric kinetic determination of silver in citric buffer media

Sofija M. Rančić[1], Snežana D. Nikolić-Mandić[2], Aleksandar Lj. Bojić[1]

[1]*Department of Chemistry, Faculty of Sciences and Mathematics, University of Niš, Serbia*
[2]*Faculty of Chemistry, University of Belgrade, Belgrade, Serbia*

Abstract

A new, simple, rapid, sensitive and selective spectrophotometric kinetic method for Ag(I) traces determination at room temperature was elaborated in this paper. It is based on catalytic effect of silver ions upon the oxidation of methylene blue B (MBB) by $K_2S_2O_8$ (PPS) in citric buffer (BUF) solution. The method was confirmed by determination of Ag(I) in PbO. The obtained results were compared to those obtained by ICP-OES method and good agreement of results was found.

Keywords: Ag(I) determination, catalyst, kinetic spectrophotometric method.

SCIENTIFIC PAPER

UDC 547.47:546.2:543.272.8:543.422.3

Hem. Ind. **68** (4) 429–434 (2014)

doi: 10.2298/HEMIND130422066R

Available online at the Journal website: http://www.ache.org.rs/HI/

The silver traces determination is present in analytical practice for a long time. At the first time silver was determined in the photographic materials and solutions for black and white films, silver-plating solutions and effluents. Recently, silver has also been analyzed in ayurvedic and other drugs and medicines, chemical substances, natural and waste water samples, electronics, flow-solders, white metals, ores, alloys, biological samples, etc. [1,3,4] The toxico-kinetics of silver is very complex: its ability to form organometalic compounds and chelate complexes with influence on the metabolic processes in living organisms is subject of investigations in biology and environmental studies.

There are different methods for Ag(I) determination, like atomic absorption spectrometry (AAS) [1,2], capillary zone electrophoresis (CZE) [3], fluorimetric [4], high performance liquid chromatography (HPLC) [5], kinetic [16–19], flow injection analysis (FIA) [20], spectrophotometric [21–28], photometric, etc. Silver was also determined using PVC-membrane electrodes based on 18-crown-6 and dibenzo-18-crown-6 ethers [29].

Kinetic methods for Ag(I) determination with spectrophotometric detection, are mainly based on catalytic effect of silver ions upon the reaction rate of oxidation of different reductors by $K_2S_2O_8$ or $(NH_4)_2S_2O_8$ [6–15]. So, silver was determined as a catalyst of Kongo red oxidation in the presence of 1,10-phenantroline as an activator [6], and oxidation of BAPDAB in the presence of 2,2-dipyridyl as an activator [7], oxidation of pyrocathehol-1-aldehide-2-pyridyl hidrazone [8], pyridoxal nicotinyl hydrazone [9], fuchsine [10], SPADNS [11], 7-(antipyrinylazo)-8-hydroxyquinoline [12], indigo carmine, etc. Silver was also determined as the catalyst of chromotropic acid oxidation by bromate, in the range 2–10 μg cm^{-3} [16]. There are only a few kinetic methods for silver determination based on its inhibitory effect. One of the most interesting is the reaction of oxidation of arsenite by Ce(IV), which is catalyzed by iodide ions [17]. As the inhibitor of this reaction, Ag(I) was determined in silicate rocks. Kinetic methods were also published for silver determination in ores and alloys [18], sulfide minerals molybdenite and sphalerite and some other natural materials [19].

FIA method with spectrophotometric detection was published in 2011. for silver determination in silver plating solutions [20]. One of many spectrophotometric methods is the method for silver determination in 2500 soil samples of agricultural areas subjected to cloud seeding in Greece [25]. Also, flotation-spectrophotometric method was developed for silver detection in semiconductors in the process of crystal growth [28].

The main goal of our investigation was to develop new, easy to performance, sensitive kinetic method for silver determination at room temperature, using common and available chemicals. In addition, we wanted to check the method on the real sample in order to discover its possibilities for further applications.

EXPERIMENTAL

Apparatus

Spectrophotometric measurements were performed on UV–Vis spectrophotometer Shimadzu UV-VIS 1650 PC (Shimadzu, Japan). ICP-OES measure-

Correspondence: A.Lj. Bojić, Department of Chemistry, Faculty of Sciences and Mathematics, University of Niš, Visegradska 33, 18000 Niš, Serbia.
E-mail: bojica@gmail.com
Paper received: 22 April, 2013
Paper accepted: 10 September, 2013

ments were performed on ICP-OES, model ICAP 65000 Duo (Thermo Scientific, UK). The cylindrical cells were thermostated at 20.00±0.02 °C using thermocirculating bath (Julabo MP-5A). The pH measurements were performed using a Hach H260G pH-meter with a non-glass pH probe PH77SS (Hach, USA).

Reagents and chemicals

Analytical grade reagents, provided by Merck, Germany, unless indicated otherwise and ultrapure water (18.2 MΩ) (water purification system Thermo Fisher Scientific Smart2Pure Standard) were utilized for solutions preparation. Adequate polyethylene vessels were used for storage of the solutions. Citric buffer solutions were prepared by mixing $NaC_6H_5O_7$ and NaOH or HCl solution (0.1 mol dm^{-3}) according the rule and their pH values were checked using a pH-meter. A stock Ag(I) solution (1×10^{-3} g cm^{-3}) was prepared by dissolving the exactly measured dry $AgNO_3$ in deionised water. The concentration of the stock solution was checked by complexometric determination. The methylene blue B solution was prepared by dissolving the exactly measured substance in deionised water. All the polyethylene containers and the glassware were washed by diluted hydrochloric acid (1:1), solution of potassium hydroxide in ethanol and then repeatedly well rinsed by tap, distilled and deionised water. All concentrations described here are the initial concentrations in the reaction mixture at time zero after mixing. Each kinetic result is the average of five determinations

Procedure

In order to obtain good mechanical and thermal stability, the instruments were run for ten minutes before the first measurement. Selected volumes of reactants and deionized water were poured separately in the reaction mixture vessel with four compartments (Budarin vessel) up to a predeterminated total volume of 10 cm^3. The solution of Ag(I) was measured into one leg of the Budarin vessel for catalytic reaction and the same volume of deionized water was measured for non-catalytic reaction. After thermostating for 10 min, the reagents were mixed and simultaneously the stopwatch was turned on. To properly rinsed spectrophotometer cell with a path length of 10 cm, the solution was immediately added and absorbance was measured every 15 s, starting from the 45th second of reaction, up to 10 min of the reaction. Spectrophotometric measurements were performed at the wavelength of 662.4 nm, and at working temperature of 20±0.02 °C.

The reaction was tested by examination the influence of each component of the reaction mixture upon the reaction rate of catalytic and non-catalytic reaction. The concentration of each component was changing consecutively, while the concentrations of other components, as well as the working temperature, were kept constant.

RESULTS AND DISCUSSION

While the reaction proceeds, the initial blue color of the solution fades and a colorless reaction product is formed. Neither the exact mechanism of reaction nor the chemical nature of the products was of major interest in the investigation. The spectrophotometric measurements were performed at the wavelength of absorption maximum of methylene blue B (662.4 nm) in citric buffer media (Fig. 1). The logarithm of absorbance–time curves is linear during the first five to ten minutes of reaction for different Ag(I) concentrations, so all kinetic results were treated by the integral variant of the tangent method [30]. The rate of reaction was obtained using the slope of the kinetic curves of the absorbance–time plot.

Hence, the influence of the pH value of the selected citric buffer solutions on the rate of both the catalytic and non-catalytic reaction was examined in the pH interval of about 5 to about 6 (Fig. 2). The value of 5.2 was selected as the most appropriate one, because it provides very well difference of reaction rates of the catalytic and non-catalytic reaction and good reproducibility of absorbance measurements in the absorbance area of the least error for spectrophotometric measurements, for both reactions. The same principles

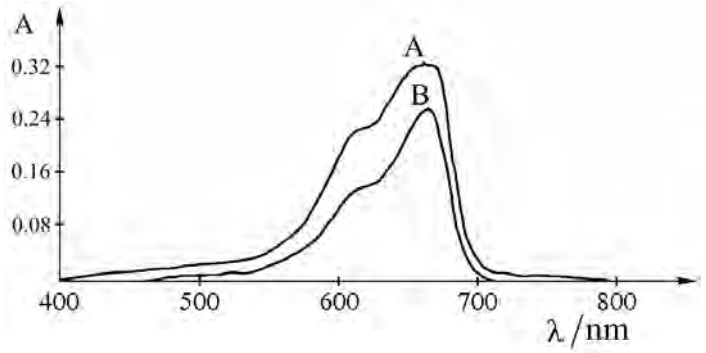

Fig. 1. Absorption spectra of MBB in citric buffer. Initial conditions: MBB, 7.15×10^{-6} mol dm^{-3}; 20±0.02 °C; pH: A – 1.0; B – 7.0.

were used for optimal conditions selection in all further investigations. The citric buffer pH 5.2 was used in subsequent examinations.

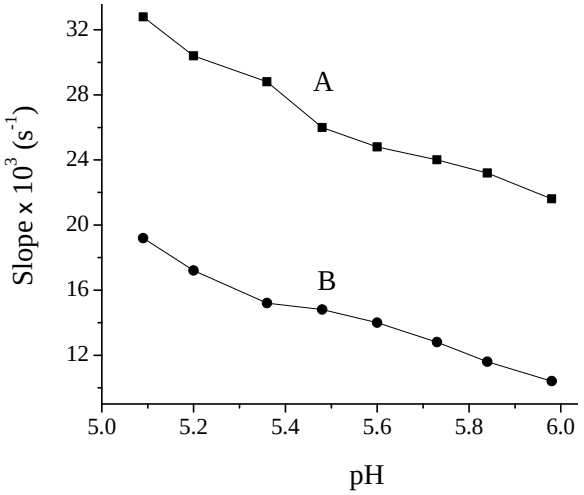

Fig. 2. Dependence of the reaction rate on pH. Initial conditions: MBB, 4.5×10^{-6} mol dm^{-3}; PPS, 7.9×10^{-2} mol dm^{-3}; BUF, 9.2×10^{-3} mol dm^{-3}; Ag(I), 2.1 μg cm^{-3}; 20±0.02 °C; A – catalytic reaction, B – non-catalytic reaction.

The rate of the non-catalytic reaction shows first order dependence on the buffer concentration, while the catalytic reaction rate shows complex dependence (Fig. 3) within the range of 2.6×10^{-3} to 9.2×10^{-3} mol dm^{-3}, and a concentration of 7.9×10^{-3} mol dm^{-3} was selected as the optimal concentration of citric buffer for further measurements.

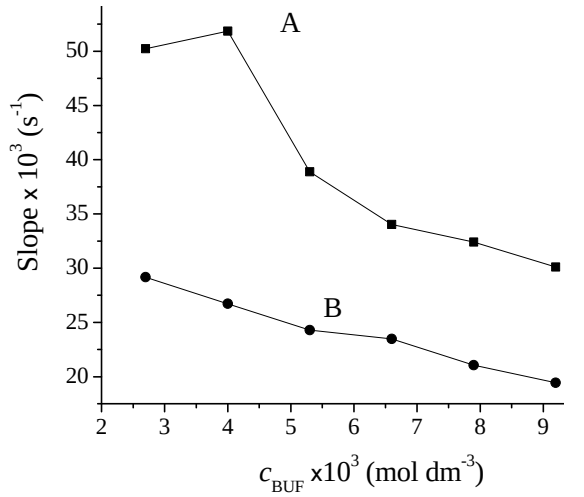

Fig. 3. Dependence of the reaction rate on the BUF concentration. Initial conditions: MBB, 4.5×10^{-6} mol dm^{-3}; PPS 7.9×10^{-2} mol dm^{-3}; pH 5.2; Ag(I), 2.1 μg cm^{-3}; 20±0.02 °C; A – catalytic reaction, B – non-catalytic reaction.

The dependence of the rate of the catalytic and non-catalytic reaction on the reductor concentration was monitored within the concentration range of about 1.5×10^{-6} to about 6.0×10^{-6} mol dm^{-3} MBB. Within this interval, both the catalytic and non-catalytic reaction rate shows a complex dependence of the MBB concentration (Fig. 4). As optimal, a concentration of 4.5×10^{-6} mol dm^{-3} MBB was selected.

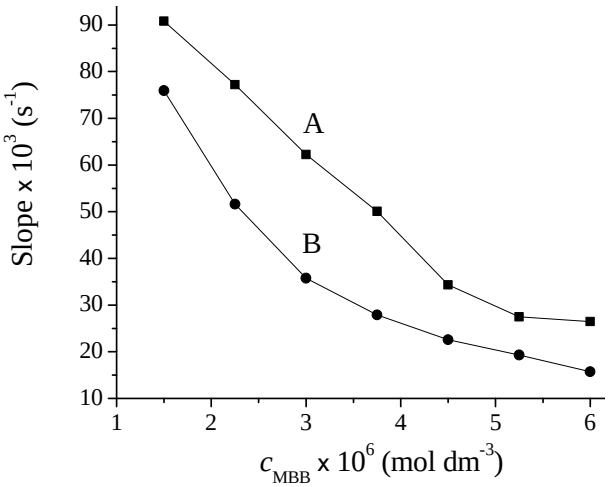

Fig. 4. Dependence of the reaction rate on the MBB concentration. Initial conditions: PPS, 7.9×10^{-2} mol dm^{-3}; pH 5.2; BUF, 7.9×10^{-3} mol dm^{-3}; Ag(I), 2.1 μg cm^{-3}; 20±0.02 °C; A – catalytic reaction, B – non-catalytic reaction.

At last, the influence of the concentration of the oxidant was tested (Fig. 5). Inside the investigated concentration range of $K_2S_2O_8$ of about 6.0×10^{-2} to about 14.0×10^{-2} mol dm^{-3} the catalytic reaction rate exhibited a complex dependence, while the non-catalytic reaction showed first order dependence on oxidant concentration. PPS concentration of 12.6×10^{-2} mol dm^{-3} was selected as the adequate for further work.

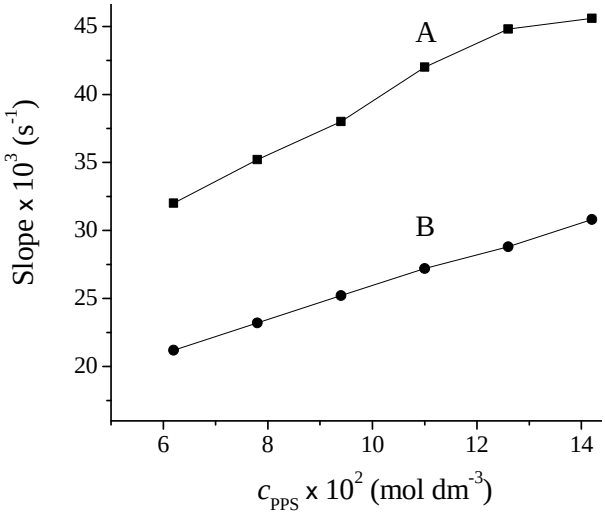

Fig. 5. Dependence of the reaction rate on the PPS concentration. Initial conditions: MBB, 4.5×10^{-6} mol dm^{-3}; pH 5.2; BUF, 7.9×10^{-3} mol dm^{-3}; Ag(I), 2.1 μg cm^{-3}; 20±0.02 °C; A – catalytic reaction, B – non-catalytic reaction.

Hence, the optimal conditions were found to be: pH 5.2, $c_{BUF} = 7.9\times10^{-3}$ mol dm^{-3}, $c_{MBB} = 4.5\times10^{-6}$ mol dm^{-3}, $c_{PPS} = 12.6\times10^{-2}$ mol dm^{-3}.

Under the optimal conditions, the dependence of catalytic reaction rate on the Ag(I) concentration was observed at three temperatures: 20±0.02, 23±0.02 and 25±0.02 °C. The linear dependence of calibration curves falls within the range of 0.4 to 2.1 μg cm^{-3} Ag(I).

The adequate equations of calibration curves for 20±0.02 (Eq. (1)), 23±0.02 (Eq. (2)) and 25±0.02°C (Eq. (3)), were calculated as follows:

$$\text{Slope} = (0.00726\pm0.00001)c + (0.02892\pm0.00010) \quad (1)$$

$$\text{Slope} = (0.01183\pm0.00003)c + (0.03491\pm0.00012) \quad (2)$$

$$\text{Slope} = (0.01502\pm0.00002)c + (0.03811\pm0.00013) \quad (3)$$

where c is Ag(I) concentration in μg cm^{-3}.

The accuracy and precision of the method were checked for three different Ag(I) concentrations within the range of the calibration curve. Five repeated measurements were performed for each concentration. Satisfactory results were obtained. For Ag(I) concentrations of 0.5, 1.0 and 2.0 μg cm^{-3}, *RSD* values were found to be 3.2, 2.4 and 1.3%, respectively.

The selectivity of the method was established by interference studies: selected ions were separately added in the reaction mixture. The tolerance limit was estimated as the concentration of the added ion that gives up to a 3% relative error in the determination of silver. Cations were added as chlorides or nitrates and anions were added as sodium or potassium salts. Each ion was added in six known concentration ratios (0.01:1, 0.1:1, 1:1, 10:1, 100:1 and 1000:1) against the constant Ag(I) concentration of 1.05 μg cm^{-3}. The measurements were performed at 20±0.02 °C, and about 30 most frequently used cations and anions were tested (Na^+, Ca^{2+}, Sr^{2+}, Ba^{2+}, Mg^{2+}, Zn^{2+}, Cu^{2+}, Pb^{2+}, Pd^{2+} Ni^{2+}, Co^{2+}, Hg^{2+}, Sn^{2+}, Bi^{3+}, Fe^{3+}, Al^{3+}, As^{3+}, Sb^{3+}, Au^{3+}, acetates, tartarates, oxalates, molybdates, wolframmates, Br^-, I^-, Cl^-, NO_3^-, SO_4^{2-}, CO_3^{2-} and PO_4^{3-}). The results presented in Table 1 reveal that proposed methods for silver determination have a very good selectivity.

Table1. Selected results of interference studies for silver determination. Initial conditions: pH 5.2; MBB, 4.5×10^{-6} mol dm^{-3}; BUF, 7.9×10^{-3} mol dm^{-3}; PPS, 12.6×10^{-2} mol dm^{-3}; Ag(I), 1.05 μg cm^{-3}; 20±0.02 °C

Added ion	Ion:Ag(I) ratio	Silver determination
Ni(II)	1	Interferes
Co(II)	1	Interferes
Cu(II)	10	Interferes
Molybdate	10	Interferes
Zn(II)	10	Inhibits
Au(III)	1	Catalyses
Pd(II)	10	Catalyses

Only the presence of Ni^{2+} and Co^{2+} in the ratio 1:1 and Cu^{2+} and molybdates in the ratio 10:1, interferes with the determination of silver. The presence of Zn^{2+} in the ratio 10:1 inhibits, while Au^{3+} in the ratio 1:1 catalyzes the determination of silver by proposed method. The ions that interfere determination of silver can be easily removed by standard analytical methods like masking, precipitation, etc., depending of different samples nature.

By application of spectrophotometric technique, at the wavelength of 662.4 nm, a limit of quantification (*LQ*) of 83 ng cm^{-3} Ag(I), was reached, and the limit of detection (*LD*) of 24 ng cm^{-3} Ag(I), was obtained. *LQ* was defined as the ratio signal:noise = 10:1 and *LD* was defined as signal 3:1 against the blank.

The method was successfully applied to Ag(I) determination in PbO (Merck, Germany). Solution containing a known quantity of silver was analyzed by application of both the presented kinetic method and ICP-OES method. As presented in Table 2, there is a good agreement of results.

Table 2. Ag(I) determination in PbO. Initial conditions: pH 5.2; MBB, 4.5×10^{-6} mol dm^{-3}; BUF, 7.9×10^{-3} mol dm^{-3}; PPS, 12.6×10^{-2} mol dm^{-3}; Ag(I), 1.05 μg cm^{-3}; 20±0.02 °C; mean values of five measurements±2SD

Kinetic determination	Recovery %	Determination by ICP-OES	Recovery %
$(5.38\pm0.05)\times10^{-7}$ g cm^{-3}	97.8	$(5.48\pm0.02)\times10^{-7}$ g cm^{-3}	99.6

CONCLUSIONS

The proposed kinetic method for the determination of Ag(I) shows a very good selectivity and provides rapid and easy performance at room temperature, by using available equipment and cheap chemical substances. The obtained results are precise and reproducible. The *RSD* value was found to be in the range 1.3–3.2% for the investigated concentration range of Ag(I).

On the grounds of the obtained results, the new spectrophotometric kinetic method is recommendable for the determination of Ag(I) in chemical substances of high grade purity, and potentially also in different samples from industrial processes and environment. The results suggest that it could also be a good basis for further investigations, not only in the area of kinetic methods development, but also in the area of noble metals determination.

Acknowledgements

The research was supported by the Serbian Ministry of Education, Science and Technological Development (Grant no. 172051).

REFERENCES

[1] G. Chakrapani, P.L. Mahanta, D.S.R. Murty, B. Gomathy, Preconcentration of traces of gold, silver and palladium on activated carbon and its determination in geological samples by flame AAS after wet ashing, Talanta **53** (2001) 1139–1147.

[2] J. Pandey, P. Sudhakar, V.J. Koshy, Determination of silver at submicrogram levels by absorption spectrophotometry, Ind. J. Chem. Tech. **10** (2003) 295–297.

[3] M. Aguilar, A. Farran, M. Martinez, Determination of gold(I) and silver(I) cyanide in ores by capillary zone electrophoresis, J. Chromatogr. **635** (1993) 127–131.

[4] V. Kabasakalis, Fluorimetric determination of silver by brilliant green in aqueous systems and its application in photographic fixing solutions, Anal. Lett. **27** (1994) 2789–2798.

[5] L. Wang, Q. Hu, G. Yang, J. Yin, Z. Yuan, Online solid phase extraction-reverse phase liquid chromatographic determination of lead, cadmium, silver and merkury in water, Fenxi Huaxue **32** (2004) 421–427 (in Chinese).

[6] H.R. Pouretedal, S. Tavakkol, Catalytic kinetic determination of silver through its catalytic effect on kongo red-peroxodisulphate reaction, Iran. J. Chem. **22** (2003) 21–26.

[7] X.J. Guo, Q.L. Deng, B. Peng, J.Z. Gao, J.W. Kang, Catalytic spectrophotometric determination of ultra-trace amounts of silver with solubilizing effect on non-ionic surfacant, Chin. J. Chem. **20** (2002) 39–44.

[8] A.M. Alfonso, J.J. Santana, F. Garcia-Montelongo, Kinetic spectrofluorimetric determination of silver, based on its catalytic effect on the oxidation of pyrocatechol-1-aldehyde 2-pyridylhydrazone by peroxodisulfate in the presence of 1,10-phenantroline as activator, Talanta **33** (1986) 779–783.

[9] M.A. Cejas, A. Gomez-Hens, M. Valcarcel, Kinetic fluorimetric determination of silver by its catalytic effect on the oxidation of pyridoxal nicotinyl hydrazone by potassium peroxidisulfate, Microchim. Acta **84** (1984) 349–352.

[10] N. Pourreza, H. Pahram, F. Hashemi, Kinetic-spectrophotometric determination of trace silver(I) using its catalytic effect on the oxidation reaction of fuchsin by peroxodisulfate in the presence of 1,10-phenantroline as an activator, J. Anal. Chem. **58** (2003) 333–336.

[11] M. Keyvanfard, H.R. Pouretedal, Catalytic spectrophotometric determination of trace amounts of Ag(I) using the oxidation of 1,8-dihidroxy-2-(4-sulfophenylazo)-naphthalene-3,6-disulfonic acid trisodium salt with peroxydisulfate, Asian J. Chem. **19** (2007) 3747–3754.

[12] L.M. Matat, I.B. Myzetskaya, V.K. Pavlova, A.T. Pilipenko, Kinetic determination of silver based on oxidation of 7-(antipyrinylazo)-8-hydroxyquinoline, Zh. Anal. Khim. **37** (1982) 2165–2167.

[13] R.M. Naik, R.K. Tiwari, P.K. Singh, S.B.S. Yadav, A. Asthana, Kinetic determination of silver at trace level based on its catalytic effect on a ligand substitution reaction, Tran. Met. Chem. **33** (2008) 615–623.

[14] K.P.P.R.M. Reddy, P.G. Chowdary, V.K. Reddy, P.R. Reddy, Catalytic-kinetic determination of silver(I) using hexacyanoferrate(II) and 2,4,6-tripyridyl-1,3,5-triazine, Annal. Chim. **97** (2007) 1207–1215.

[15] G.D. Sulka, M. Jaskula, Determination of silver traces in pure metallic copper and zinc by a catalytic photometric method, Croat. Chem. Acta **80** (2007) 147–150.

[16] G.M. Mastoi, A.A. Khaskheli, I.A. Ansari, M.Y. Khuhawar, Kinetic spectrophotometric determination of silver(I) by the catalytic effect on the oxidation of chromotropic acid by bromate, Paks. J. Chem. Soc. **19** (1997) 273–278.

[17] Yu.I. Grosse, A.D. Miller, Highly sensitive kinetic method for determination of silver in rocks, Metody Anal. Redkometal. Miner. Rud. Gorn. Porod. **2** (1971) 52–64.

[18] V.K. Reddy, A. Chennaiah, P.R. Reddy, T.S. Reddy, Kinetic-photometric determination of silver(I) based on its catalytic effect on reaction between potassium ferrocyanide and 2-hydroxy-4-metoxybenzophenone thioemicarbazone, Chem Anal. **48** (2003) 733–740.

[19] Yu.I. Grosse, A.D. Miller, Kinetic determination of silver in natural materiale, Zavodskaya Lab. **40** (1974) 262––263.

[20] K. Fujimura, T. Odake, H. Takiguchi, N. Watanabe, T. Sawada, Flow injection spectrophotometric determination o sub mg/dm^3 silver in a strongly acidic solution containing concentrated copper(II) using a pyridylazo reagent, Anal. Sci. **27** (2011) 1197–1201.

[21] P. Nagaraja, M.S.H. Kumar, H.S. Yathirajan, Silver-enhanced reduction of 2,3,5-triphenyl-2*H*-tetrazolium by semicarbazide hydrochloride (SHC) for the spectrophotometric determination of traces silver(I), Anal. Sci. **18** (2002) 815–820.

[22] C. Ivanova, S. Popova, Spectrophotometric determination of silver with brompyrogallol red (BPR) and 1,10--phenantroline in the presence of gelatin J. Univ. Chem. Tech. Met. **37** (2002) 33–38.

[23] H.W. Gao, L. Wang, M. Tao, Primary-secondary wavelength spectrophotometric determination of trace amounts of silver in waste water with 2,4-dibromo-6--carboxy-benzendiazoaminoazobenzene (DBCBAAB), Paks. J. Chem. Soc. **22** (2000) 275–280.

[24] S.G. Kawatkar, P.S. Manol, A simple and sensitive spectrophotometric method for determination of silver(I) with resacetophenone guanylhydrazone (RAG), Acta Cie. Ind. **24** (1998) 167–169.

[25] S. Tsiouris, F. Aravanopoulos, I. Papadoyannis, M. Sofoniou, N. Polyzopoulos, M. Christodoulou, V. Samanidou, G. Zachariadis, H. Constantinidou, Soil silver content of agricultural areas subjected to cloud seeding with AgI, Frez. Env. Bull. **11** (2002) 697–702.

[26] H.W. Gao, Reanalysis of silver chelate solution and determination of trace amounts of silver in waste water, Asian J. Chem. **11** (1999) 740–745.

[27] F. Salinas, A. Espinosa-Mansilla, A.P. Lopez de Alba, Extraction-spectrophotometric determination of silver in ores, electronic flow- solders and white metals with 2-carboxybenzaldehyde thiosemicarbazone (2CBTSC), Analyst **120** (1995) 2857–2860.

[28] N.N. Ischenko, L.I. Ganago, I.F. Ivanova, Flotation-spectrophotometric determination of silver, J. Anal. Chem. **52** (1997) 768–769.

[29] M.M.Zareh, M.A. Akl, A.K. Gonheim, M.H. Abdel Aziz, PVC membrane electrodes based on 18-crown-6 and dibenzo-18-crown-6 ethers for determination of silver, Turk J. Chem. **31** (2007) 449–456.

[30] D. Perez-Bendito, M. Silva, Kinetic Methods in Analytical Chemistry, John Wiley & Sons, Chichester, 1988.

IZVOD

ANALITIČKA PRIMENA REAKCIONOG SISTEMA METILEN-PLAVO B–$K_2S_2O_8$ ZA SPEKTROFOTOMETRIJSKO KINETIČKO ODREĐIVANJE SREBRA U CITRATNOM PUFERU

Sofija M. Rančić[1], Snežana D. Nikolić-Mandić[2], Aleksandar Lj. Bojić[1]

[1]*Departman za Hemiju, Prirodno-matematički fakultet, Univerzitet u Nišu, Srbija*
[2]*Hemijski fakultet, Univerzitet u Beogradu, Beograd, Srbija*

(Naučni rad)

Predložena kinetička metoda za određivanje Ag(I) pokazuje vrlo dobru selektivnost i lako se i brzo izvodi na sobnoj temperaturi. Uz korišćenje dostupne opreme i jeftinih supstanci, ostvaruju se precizni i reproduktivni rezultati. Spektrofotometrijskim merenjem, na talasnoj dužini od 662,4 nm, postignuta je granica kvantifikacije (*LQ*) od 83 ng cm^{-3} Ag(I), kao i granica detekcije (*LD*) od 24 ng cm^{-3} Ag(I). *LQ* je definisana kao odnos signal:šum = 10:1, a *LD* kao signal 3:1 u odnosu na slepu probu. *RSD* vrednosti se nalaze u rasponu od 1,3–3,2% za ispitivanu oblast koncentracija Ag(I). Na osnovu dobijenih rezultata se može zaključiti da je nova spektrofotometrijsko–kinetička metoda pogodna za određivanje Ag(I) u hemijskim supstancama visoke čistoće, a potencijalno i u drugim uzorcima iz proizvodnih procesa i životne sredine. Takođe, rezultati ispitivanja ukazuju na to da ona može da bude dobra osnova ne samo za dalja istraživanja u oblasti razvoja kinetičkih metoda analize, već i u oblasti razvoja novih metoda za određivanje plemenitih metala.

Ključne reči: Određivanje Ag(I) • Katalizator • Kinetičko spektrofotometrijska metoda

Viscoelastic properties of hydroxyl-terminated poly(butadiene)-based composite rocket propellants

Saša J. Brzić, Ljiljana N. Jelisavac, Jela R. Galović, Danica M. Simić, Jelena Lj. Petković

Military Technical Institute, Belgrade, Serbia

Abstract

In the present study, the viscoelastic response of three composite solid propellants based on hydroxyl-terminated poly(butadiene), ammonium perchlorate and aluminum has been investigated. The investigation was surveyed by dynamic mechanical analysis over a wide range of temperatures and frequencies. The mechanical properties of these materials are related to the macromolecular structure of the binder as well as to the content and nature of solid fillers. The storage modulus, loss modulus, loss factor and glass transition temperature for each propellant sample have been evaluated. The master curves of storage (log G' *vs.* log ω) and loss modulus (log G'' *vs.* log ω) were generated for each propellant. A comparison of log a_T *vs.* temperature curves for all propellants indicate conformance to Williams–Landel–Ferry equation. Choosing the glass transition as the reference temperature, WLF equation constants are determined. Fractional free volume at the glass transition temperature and thermal coefficient of free volume expansion values are in accordance with the consideration that Al is reinforcing filler.

Keywords: composite propellant, hydroxyl-terminated polybutadiene (HTPB), dynamic mechanical analysis, viscoelastic properties.

Available online at the Journal website: http://www.ache.org.rs/HI/

SCIENTIFIC PAPER

UDC 662.1/.4:678.742.4

Hem. Ind. **68** (4) 435–443 (2014)

doi: 10.2298/HEMIND130426067B

Composite rocket propellant formulations based on hydroxyl-terminated poly(butadiene) (HTPB) as a binder, ammonium-perchlorate (AP) and aluminum (Al) as solid ingredients, are at present the state-of-the-art propellants in solid fuel rocket engines. A major component in propellant, by weight and volume, is an oxidizer. AP is currently the most widely employed oxidizer because of its high specific impulse, high density, relatively high availability, low cost, high energy, etc. The function of metal fuel is to increase the flame temperature and generate hot metal particles for improved ignition. By far, the most common metal in use as a solid propellant fuel is fine divided aluminum. The binder, as the name implies, holds the composition together and acts as an auxiliary fuel. Once cured, the binder makes the propellant flexible, which decreases the likelihood that the propellant will fracture under stress and pressure. The binder comprises at least two components. The first one is a liquid or semi-liquid prepolymer and the second one is a curing agent. Hydroxyl-functional prepolymers, such as HTPB, are cured using multifunctional isocyanates. Preferably, the curing agent is an isophorone diisocyanate (IPDI), which is a less reactive isocyanate and, therefore, helpful to pot life. To insure the desired degree of crosslinking, IPDI is added in an amount sufficient to generate a ratio of isocyanate to hydroxyl groups (NCO/OH) of about 0.8 to about 1.20, preferably about 0.85 to about 0.90. The selection of both solid ingredients (AP and Al) and the binder is not dictated by the optimization of the mechanical properties. The optimum choice of these ingredients has to enhance the energetic and ballistic performance rather than mechanical properties. Thus, mechanical properties are, on one hand a result of formulation adjustment, and on the other hand are expected to match the structure integrity requirements with very little means of improvement. For the purpose of meeting the energy and ballistic characteristics for practical applications, the oxidizer is about 70 wt.%, while the metal fuel represents about 15 wt.% of the propellant [1]. In addition, considering process-ability aspect of propellant production, this formulation gives acceptable values of viscosity. In other words, there is sufficient “pot life”, defined as the time the propellant mixture remains sufficiently fluid to permit processing and casting. One of the most common used methods in order to achieve the required mechanical properties is a variation of AP/Al ratios for a fixed solid loading, without drastic influence on energetic and ballistic properties. Being reinforcing (filler strongly interacts with the binder) or non-reinforcing (filler interact only weakly with the binder), viscoelastic properties of composite propellants are strongly affected by the inclusion of solid fillers.

Due to presence of a polymeric binder, as viscoelastic materials, composite propellants show time and temperature dependence of mechanical properties.

Correspondence: S.J. Brzić, Military Technical Institute, Ratka Resanovića 1, 11000 Belgrade, Serbia.
E-mail: sasabrzic@gmail.com
Paper received: 26 April, 2013
Paper accepted: 11 July, 2013

The time–temperature superposition principle (tTTS) is still widely applied to the viscoelastic properties of these energetic materials. The best-known relation is that derived by Williams, Landel and Ferry (so-called WLF equation), which defines the shift factor a_T, temperature change as:

$$\log a_T = -C_1(T - T_0)/(C_2 + T - T_0) \quad (1)$$

where: T – test temperature, T_0 – reference temperature, C_1, C_2 – constants.

If the reference temperature is such that T_0 - T_g = 50 °C, where T_g is the glass transition temperature, then C_1 and C_2 are general constants with values of 8.86 and 101.6, respectively [2]. Since this is a rough approximation, for more accurate calculations it is necessary to determine the values of a shift factor a_T, and constants C_1 and C_2 for each type of rocket propellant. Despite the importance of HTPB-based composite propellant for rocket engines and the obvious concern about structure and properties relationships, very few comprehensive investigations appear to be available in the open literature. De la Fuente *et al*. analyzed unfilled elastomeric binder and the effect of the different types of fillers on the viscoelastic behavior of a several HTPB based solid composites by dynamic mechanical measurements [3]. Cogmez *et al*. compared dynamic data of two HTPB based composite propellants with different solid compositions, one with 86 wt.% of solid loading including 16 wt.% Al, and the other with 86 wt.% solid loading without Al. The former was found to be less stiff and more dissipative than the latter at higher temperatures [4]. Borsus *et al*. showed that Al particles (having OH-groups on the surface) make fine dispersion in polyurethane foams through a molecular bonds between the particles and the binder [5].

The aim of this work was to characterize and evaluate changes in the viscoelastic properties of composite propellants which follow propellant formulation adjustment by variation of AP/Al ratios for a fixed solid loading.

EXPERIMENTAL

Three HTPB-based propellant compositions (Table 1) selected for this study consisted of 85 wt.% of solids loading including 70–73.5 wt.% AP (oxidizer, with two particle sizes, 200 and 10 μm), 11.5–13 wt.% Al (fuel, with 30 and 15 μm particle sizes) and 15 wt.% of polymeric binder.

Table 1. Tested propellant compositions

Sample	AP_{200}/AP_{10}	Al_{30}/Al_{15}	Al %	AP_{tot} %	Solid loading wt.%
CP1	80/20	50/50	13.0	72.0	85.0
CP2	80/20	50/50	15.0	70.0	85.0
CP3	80/20	50/50	11.5	73.5	85.0

The binder composition consisted of 11.08 wt.% of HTPB (R-45HT, Sartomer, viscosity at 23 °C: 8000 mPa s, OH value: 47.12 mg KOH/g, hydroxyl functionality: 2.4–2.6, average molecular weight: 2800 g/mol, specific gravity at 23 °C: 0.901 g/cm^3, glass transition temperature, T_g: –76 °C), 2.77 wt.% of plasticizer (dioctyladipate; Fluka AG, Switzerland), 0.17 wt.% of antioxidant (phenyl-β-naphtylamine; Fluka AG, Switzerland) and 0.06 wt.% of bonding agent (triethylenetetramine, Riedel). Tested propellant samples differed from each other in a solid particle content ratio.

Curing occurs when hydroxyl groups on the prepolymer (HTPB) react with isocyanate groups of the curing agent (IPDI, purity: 98%, Sigma Aldrich, Germany) to form urethane crosslinks (Figure 1).

The NCO/OH ratio between the isocyanate groups of IPDI to the hydroxy groups of the R45HT was 0.87. Mixing of propellant was conducted at a temperature of 60 °C in 1-gallon Baker-Perkins planetary mixer, while the corresponding propellant binder (HTPB) was hand-mixed, degassed, cast and cured in moulds to obtain 4 mm thick slabs. The curing was performed for 5 days at 70 °C.

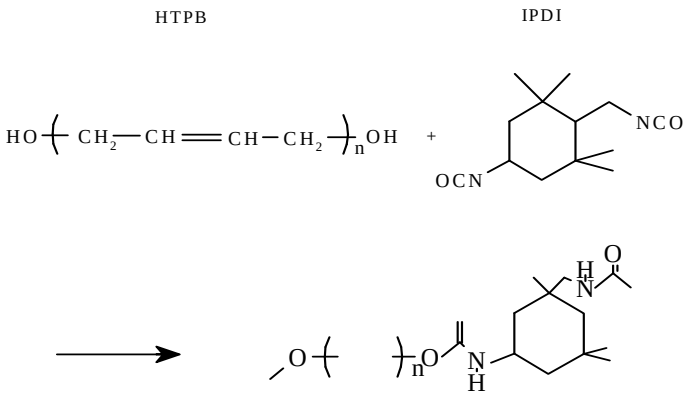

Figure 1. Scheme of urethane reaction.

The DMA tests were carried out by using mechanical spectrometer „Rheometrics“, model RMS-605, in the torsion mode. The temperature range studied was from –90 to 60 °C, the heating rate was 5 °C/min and the single frequency point of 1 Hz was chosen. Strain amplitude was 0.1%. The samples for DMA tests were of rectangular bar shape (63 mm×12 mm×3 to 4 mm). Complex modulus was determined, $G^*(\omega) = G'(\omega) + iG''(\omega)$. Extracted data were the storage modulus (G'), loss modulus (G'') and the loss factor, $\tan \delta = G''/G'$. Each sample was first tested at a constant frequency and temperature over above mentioned range.

The glass transition temperature (T_g) determined by dynamic mechanical measurements was estimated as the temperature at which the loss modulus G'', maximized. Finally, the viscoelastic properties were measured through three decades of frequency over a range of temperatures from –70 to 20 °C.

DSC analyses were carried out using the DSC Q20 manufactured by TA Instruments with liquid nitrogen for low temperatures. The temperature scale was calibrated using the melting temperature of high purity indium. These measurements were made with the purpose to investigate the thermal based glass transition temperature of the tested samples. The small amount of the samples (~5 mg) was scanned with a heating rate of 10 °C min^{-1}, starting from –90 °C and ending at 50 °C. The glass transition temperature, T_g, of the samples were determined from the midpoints of the transitions.

RESULTS AND DISCUSSION

The propellant specimens were analyzed in the dynamic torsion mode. This mode enables determining the binder characteristics without distortions due to the particle–particle contact as it can happen in tensile-compression or in bending mode [6].

Temperature dependence

Based on a weakly cross-linked polymeric matrix, composite rocket propellants show very large changes in mechanical properties with changing temperature. Figure 2 shows the viscoelastic response of tested propellant samples in terms of storage modulus, loss modulus and loss factor at 1 Hz as a function of temperature.

DMA measurements have shown that tested propellants exhibited viscoelastic behavior by passing through glassy transition and rubbery region.

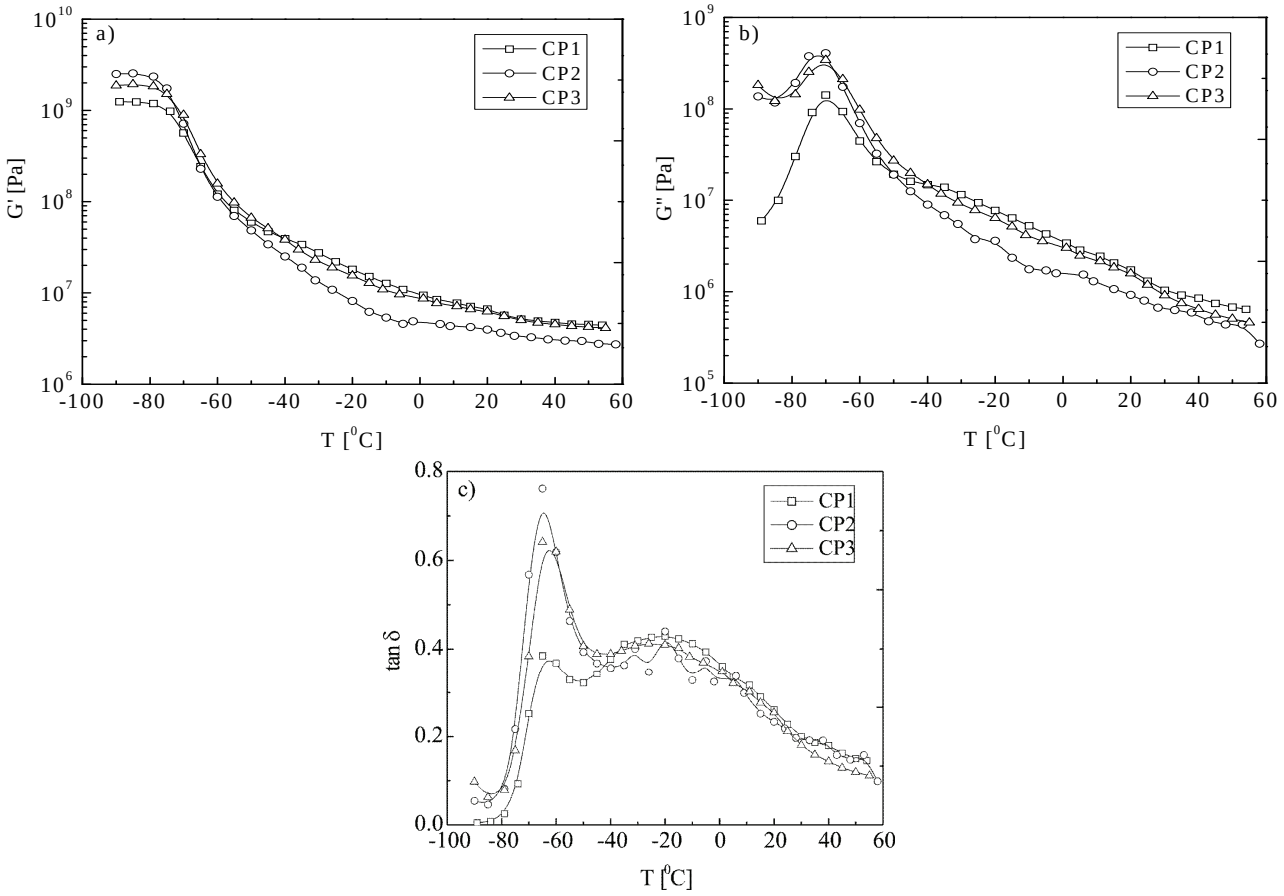

Figure 2. Temperature dependences of a) storage modulus (G'), b) loss modulus (G'') and c) loss factor (tan δ) for tested propellant samples.

Table 2 shows T_g values of the tested samples determined through DMA *via* G'', G', tan δ and through DSC. Also, values of peak widths at half-height (w) of tan δ–temperature dependence are shown.

Tan(δ) is a composed distribution function describing the distributions of the glass transitions of the structural elements of the polymer network in propellant formulations. Polymer network in composite propellant formulations is made of polyurethane elastomer, which contain soft and rigid segments. The soft segments consist of the flexible non-crystalline polymer chains, in this case poly(butadiene), and the rigid or hard segments consist of diisocyanate residues, chain extenders and urethane groups.

Table 2. T_g values determined through G'', G', tan δ and DSC; tan δ_{max} and widths (w) of tan δ peaks

Sample	T_g / °C				T_g^{hard} / °C	tan δ_{max}	w / °C
	G''	G'	tan δ	DSC			
CP1	–69.9	–77.2	–63.1	–78.9	–20.1	0.385	13.2
CP2	–72.0	–79.3	–64.5	–78.3	–19.1	0.762	14.6
CP3	–70.6	–77.6	–62.7	–78.3	–24.1	0.641	14.8
HTPB	–	–	–	–72.7	–	–	–

The differences between T_g values of tested samples determined through DMA *via* G'', G' and tan δ, respectively, are within experimental error. The T_g is easily identified as a peak in the tan δ or the G'' trace. These maxima do not coincide exactly. The maximum in the tan δ is at a higher temperature than that in G'', because the tan δ is the ratio of G'' and G' and both these moduli are changing in the transition region. T_g values based on G'' show that it cannot be observed any regularity of its change with increasing Al content in the tested propellant formulations. However, the lowest T_g is observed for CP2 sample. The T_g of the tested propellants based on the DSC is nearly as same as reported by Cerri *et al.* [6]. The T_g of HPTB cured with IPDI determined by DSC is higher than that of IPDI cured HTPB reported as –83 °C by Bhagawan *et al*. [7]. Although incorporation of fillers significantly modifies the molecular mobility, it is found that T_g of HPTB binder is higher than that of corresponding propellants. The position of T_g depends on the experimental techniques and conditions of the experiment (*e.g*., heating rate of the sample). Phase transitions are time–dependent relaxation processes, so the most reliable values for the phase transition temperatures could be obtained at the lowest cooling rate.

Comparing G' values of tested propellant samples, sample CP2 (AP/Al = 70/15) has the lowest G' values in the rubbery plateau region. Based on the assumed presence of non-homogeneously distributed OH groups on the Al particle surface, that interferes with the curing agent, incorporation more Al particles in propellant formulation with fix solid loading gives less cured propellant [6]. The decrease of G' value is connected with the increase of the macromolecular mobility.

Beside T_g, a molecular interpretation of the viscoelastic behavior can be given considering the tan δ, which is extremely sensitive to all kinds of relaxation processes, structural heterogeneity and the morphology of multiphase systems such as filled or composite materials.

Two maxima in the tan δ curves of all tested propellant samples were observed. The first peak positioned between –80 and –60 °C could be attributed to the main glass transition temperature (α-relaxation peak) in the soft segment regions (HTPB main chain elements). These segments are formed by the reaction of the diisocyanate and the long-chain diol. They have low polarity as they have a very low density of urethane groups, and therefore, they are flexible at room temperature. At this temperature range the molecular rearrangements reach a maximum extend and it is defined as the temperature at which the polymeric material changes from the entropy-elastic rubber behavior to the energy-elastic behaviour or *vice versa*. This temperature is called T_g^{soft}. The intensity of T_g^{soft} for CP2 sample (15 wt.% Al) is the highest, although its temperature location is quite equal to that in the other tested propellants. The highest Al proportion within the solid loadings causes the highest value of T_g^{soft} intensity for the sample CP2. Although Al particles are considered as reinforcing fillers, less AP content means less content of ionic bonds between the bonding agent (triethylenetetramine) and AP particles, which cause increased mobility of the macromolecule chains. Comparing intensity of T_g^{soft} values for CP1 and CP3, although CP1 has a higher proportion of AP, since the Al particles are smaller, they make a stronger adhesion to the polymer matrix, which results in a higher T_g^{soft} value of CP3.

The second peak of the tan δ curves is broader than the first one. It appears at higher temperatures (between –40 and 20 °C) and it can be related to the motions within the polymer short-hard segment units. These segments have a high density of high polarity urethane groups, and for this reason, they are rigid at

room temperature. Temperature range, which corresponds to relaxation related to short-hard segment units is called T_g^{hard}. T_g^{hard} exhibits a small difference in intensity, but its broadness is enlarged in sample CP1, compare to those for samples CP2 and CP3. This can be explained by the free extended HTPB chains (found with GPC) intermixed in the short-hard segment regions and in this way creating more free volume [6]. The fraction of these free chains should be higher in CP1, because of consumption of IPDI by Al particles.

Frequency dependence

An example of the small deformation response properties measured for each of the propellants is presented in Figure 3. The figure shows the effect of temperature and frequency on the storage modulus of the propellant CP3. The response of tested propellants was measured during a frequency sweep for different isothermal temperatures. Frequency was varied from 0.1 to 100 rad s^{-1}, through 16 equidistant values on a logarithmic scale.

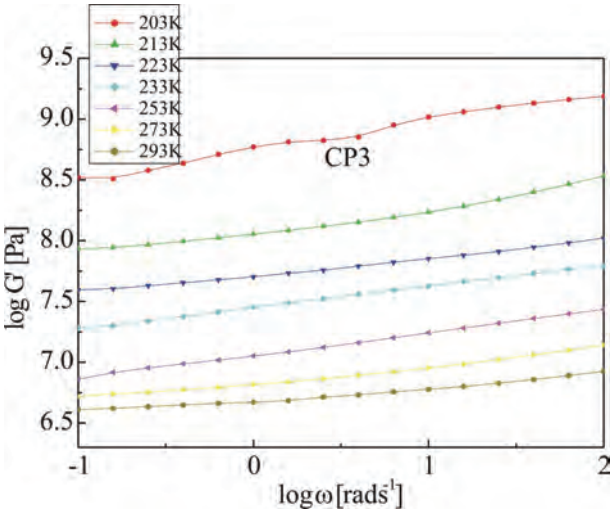

Figure 3. Storage modulus (G') as a function of frequency for CP3 propellant sample.

Storage modulus increases in a regular fashion with increasing frequency or decreasing temperature, suggesting that time–temperature superposition of the data is possible. Similar results were obtained for each of tested propellants.

Figure 4 shows the tan *δ*–frequency dependences for sample CP1.

For sample CP1 the frequency dependence at –60 °C is not observed below 1 rad s^{-1}. Above this value, the tan *δ* increases with increasing frequency. The frequency dependence at –50 °C is scarcely detected in the frequency range from 0.1–10 rad s^{-1}. The frequency dependence at –40 and –20 °C is observed in the whole range of frequencies: tan *δ* decreases with increasing frequency. Above –20 °C, frequency dependence is not observed below 1 rad s^{-1}. Above 1 rad s^{-1}, the value of tan *δ* increases with increasing frequency.

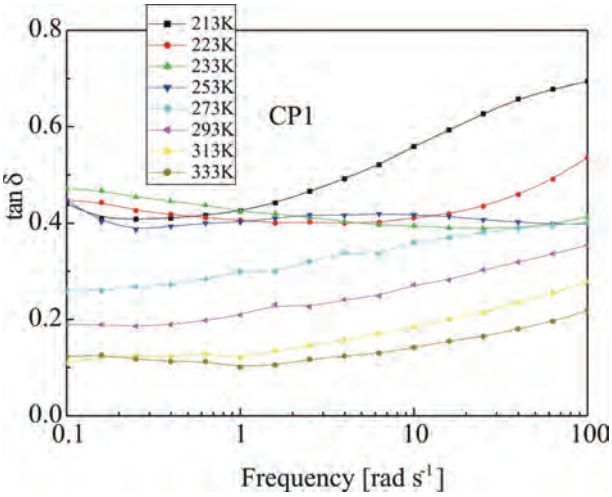

Figure 4. Loss factor tan δ as a function of frequency for sample CP1.

Application of Williams–Landel–Ferry equation

Temperature range for testing was selected so that the lowest testing temperature propellant is in glassy state and that the highest testing temperature is the temperature of use. Temperature step was 10 °C. The master curves represent essential inputs for evaluating the margin of propellant safety usage. The most critical stage during rocket motor operation is the ignition stage. During such conditions, the propellants are exposed to high-speed deformation of the order of 1 to 6 m/s, which corresponds to periodic deformations of 628–3140 rad s^{-1}. Such a high-speed deformation is very difficult to achieve in real life tests.

By dynamic mechanical measurements at small deformation, it is possible to obtain information about the behavior of materials at such high strain rates, because the proper analysis of the measurement results in three decades of frequency can determine the values of these parameters and up to 20 decades for the selected reference temperature. In this way, we can make conclusions about the tested material behavior under conditions of very large or very small strain rates. The master curve reference temperature was T_0 = 20 °C. In addition, it is very important to emphasize that WLF equation is valid in T_g to (T_g+100 °C) region.

Figure 5 shows master curves of storage and loss shear modulus comparison for the tested propellant samples.

Figure 5 shows several important features concerning the viscoelastic response of the tested propellants. For all tested propellants, at low temperatures (high frequencies), *G*' and *G*'' slopes maximize.

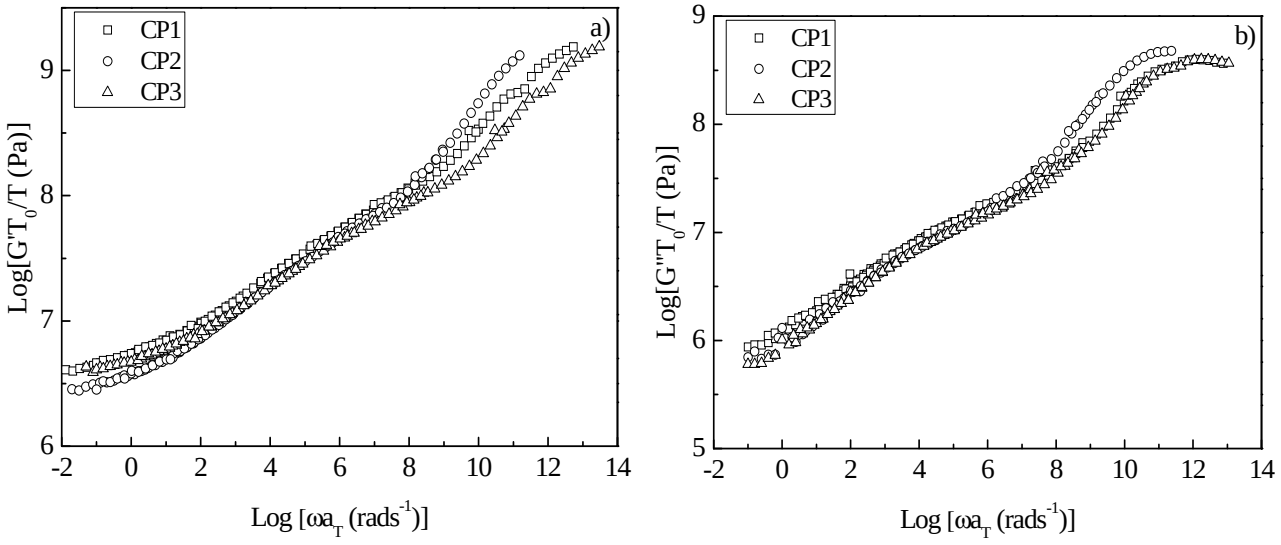

Figure 5. Master curves of a) storage modulus (G') and b) loss modulus (G'') for tested propellant samples.

At higher temperatures, or lower frequencies, *G*'' becomes progressively smaller than *G*', with both curves entering the rubbery plateau. For both moduli change curves, the differences are observed at high and low frequencies for sample CP2. It is observed that the decay of modulus with the reduced frequency (time) is pronounced in CP2 than in other propellant. At higher temperatures or lower frequencies, the value of *G*' is observed to approach the equilibrium value. This portion of the curve is termed the rubbery plateau. The horizontal shift factor values a_T, used to superpose the *G*' and *G*'' experimental data into a master curve for tested propellants are shown in Table 3.

Table 3. Shift factor, log a_T, temperature dependences determined through G' and G'' superposition

T / °C	CP1		CP2		CP3	
	G'	*G''*	*G'*	*G''*	*G'*	*G''*
–69.75	–10.73	–10.88	–9.18	–9.36	–11.47	–11.04
–60.06	–7.99	–8.38	–6.95	–7.25	–8.74	–8.54
–50.37	–6.17	–6.77	–5.21	–5.61	–6.42	–6.66
–40.06	–4.74	–5.25	–3.96	–4.29	–4.94	–5.23
–21.37	–2.72	–2.97	–2.12	–2.28	–2.84	–2.93
–0.06	–1.21	–1.28	–0.81	–0.89	–1.30	–1.33
19.93	0	0	0	0	0	0

Some evidence of thermo-rheological complex behavior was observed as indicated by slightly different shift factors for *G*' and *G*''. This difference is identical to that previously reported by Stacer and Husband [8]. Figure 6 provides a comparative view of the temperature dependences of a shift factor, a_T, the values determined through *G*' and *G*'' superposed to a temperature T_0 = 20 °C for sample CP3.

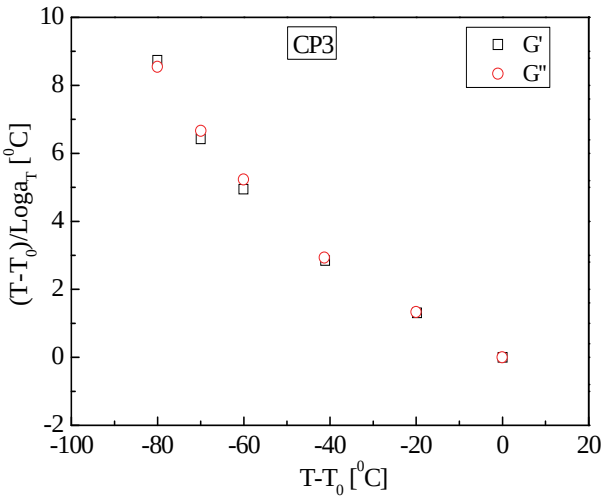

Figure 6. Comparison of the horizontal shift factor values used to superpose G' and G'' data for sample CP3

Temperature dependences of shift factor, a_T, of all tested propellants show that for each of them could be made satisfactory linearization of experimental data, in order to determine WLF constants C_1 and C_2, using transformed WLF equation [9]. Obtained WLF constants C_1 and C_2, are given in Table 4.

Table 4. WLF constants C_1 and C_2 estimated for tested propellants

Sample	*G'*		*G''*	
	C_1	C_2	C_1	C_2
CP1	8.49	164.84	9.31	167.37
CP2	4.79	134.50	5.36	138.43
CP2	9.11	165.98	9.74	171.38

Although these values are in agreement with those reported in literature, WLF constants C_1 and C_2 obtained

via G'' data were slightly different but not significant to affect any of the earlier conclusions. The values are almost comparable for the propellants CP1 and CP3, while propellant CP2 shows the lowest values for both the constants.

All, until now discussed, related to the selected reference temperature T_0 = 20 °C. Ferry proposed an alternative way of representing the temperature dependence of the shift factors, a_T. It consists of choosing the T_g of the sample as the reference temperature and a_T calculation based on the following WLF equations [9]:

$$C_{1,g} = \frac{C_1 C_2}{C_2 + T_g - T_0} \quad (2)$$

$$C_{2,g} = C_2 + T_g - T_0 \quad (3)$$

$C_{1,g}$ and $C_{2,g}$ constants, calculated using Eqs. (2) and (3), and determined experimentally from the shift factors used to superpose the *G'* data to T_g as a reference temperature, are compared in Table 5.

Table 5. WLF constants $C_{1,g}$ and $C_{2,g}$ estimated for tested propellants

Sample	$C_{1,g}$		$C_{2,g}$	
	Calcd.	Exp.	Calcd.	Exp.
Universal[a]	–	17.4	–	51.6
CP1	18.68	17.98	74.90	58.31
CP2	14.40	15.08	44.75	55.97
CP3	19.89	17.95	75.98	52.23

[a]Determined by averaging the values of a wide variety of polymers

The deviation of the WLF equation constants $C_{1,g}$ and $C_{2,g}$ for tested propellants is in agreement with literature data. Unlike the constants $C_{1,g}$, which are approximate, values of $C_{2,g}$ significantly deviate from the ''universal'' values. Regardless of the determining method, $C_{1,g}$ and $C_{2,g}$ values for sample CP2 deviate from the constant values for the other two propellants.

The influence of a reference temperature on the shape and position of storage modulus frequency dependence master curve for propellant CP1 is shown in Figure 7.

Despite the T_{ref}, master curves have the same shape, but the master curve for higher T_{ref} is shifted to a higher frequency. As illustrated in Figure 7, the strain rate of the propellant during rocket motor storage conditions ($\omega \approx 10^{-6}$ rad s^{-1}) is not covered by the master curve superposed to a temperature T_{ref} = 20 °C.

The importance of the WLF constants $C_{1,g}$ and $C_{2,g}$ can be seen through the relationship:

$$C_{1,g} = \frac{B}{2.303 f_g} \quad (4)$$

and

$$C_{2,g} = \frac{f_g}{\alpha_f} \quad (5)$$

where B is a constant in the Doolittle equation assumed equal to unity, f_g is the fractional free volume at the glass transition temperature and α_f is the thermal coefficient of free volume expansion. As the values of the fractional free volume at the glass transition temperature, f_g/B, and thermal coefficient of free volume expansion, α_f/B, are directly associated with known WLF constants $C_{1,g}$ and $C_{2,g}$, these are calculated and the values are given in Table 6.

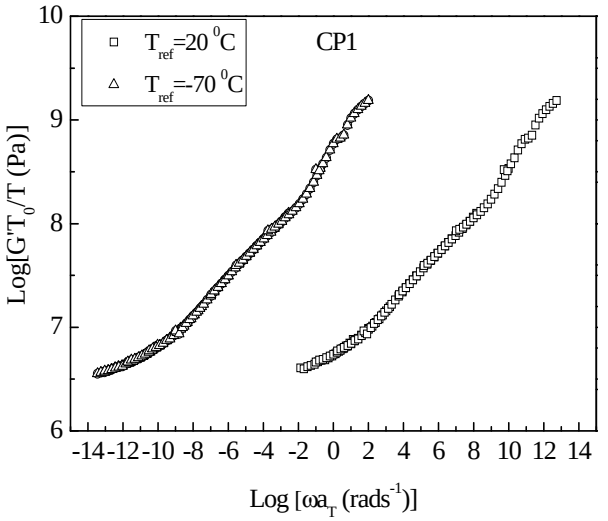

Figure 7. The influence of a reference temperature on the shape and position of G' master curve for sample CP1

Table 6. The values of f_g/B and α_f/B

Sample	$(f_g/B)\times10^{-2}$		$(\alpha_f/B)\times10^{-4}$	
	Calcd.	Exp.	Calcd.	Exp.
CP1	2.155	2.40	2.05	4.14
CP2	2.918	2.88	5.28	5.14
CP3	2.374	2.42	3.53	4.63

f_g/B and α_f/B values are round about the limits given in the literature for the largest number of polymer systems ($f_g/B = 2.5\times10^{-2}$ and $\alpha_f/B = 4.80\times10^{-4}$) [8]. Although they do not match, the trend of these values change is identical.

Comparing the experimentally determined WLF and free volume constants in Table 6 with the “universal” constants (determined by averaging the values of a wide variety of polymers), one may conclude that all tested propellants have a temperature dependent viscoelastic response which is very close to “universal”. Data in Table 6 indicate that Al lowering the glass transition temperature while increasing the thermal

coefficient of free volume expansion. All the tested propellants have values that are less than or equal to the ''universal''.

Dependence of f_g/B and α_f/B as a function of Al content for tested propellant samples is as follows: the values of f_g/B and α_f/B decrease slightly or remain the same with increasing of Al content from 11.5 to 13 wt.%, while over 13 wt.% of Al content these value significantly increases. In conclusion, with the change in the aluminum content there is no linear decrease of α_f/B value confirming that aluminum in composite propellant formulation should be considered as active (reinforcing) filler.

CONCLUSION

The dynamic mechanical analysis in the torsion mode was employed to evaluate the effects of AP/Al content ratio on viscoelastic properties of HTPB-based composite rocket propellants. Temperature and frequency dependences of rheological parameters are determined. Glass transition temperature, T_g, of all tested propellants was nearly –70 °C. DSC measurements could not reveal differences in the tested propellants T_g value. Propellant sample with the lowest content of AP (CP2) has the lowest value of storage modulus in transition and the rubbery plateau region. Storage modulus values in transition region range from 10^6 to 10^9 Pa.

The same trend behavior exhibits loss modulus curve. For all tested propellant the presence of two maxima can be seen on tan δ curve. Master curves have been generated for temperature range from –70 to 20 °C considering the curve at 20 °C, as reference.

The temperature dependence of the shift factors, a_T, obtained by generating master curves of storage energy modulus point out that for each of tested propellant satisfactory linearization of experimental data was achieved.

By introducing glass transition as a reference temperature in the WLF equation, values of “universal” constants, $C_{1,g}$ and $C_{2,g}$, are calculated.

The different AP/Al particle ratio change the temperature dependence of the dominant viscoelastic mechanism as indicated by the change in the free volume constant values, fractional free volume at the glass transition temperature f_g/B, and thermal coefficient of free volume expansion α_f/B.

Values obtained both for fractional free volume at the glass transition temperature f_g/B, and thermal coefficient of free volume expansion α_f/B from 11.5 to 15 wt.% of Al, are in accordance with the consideration that Al is reinforcing filler.

REFERENCES

[1] V. Rodic, Case bonded System for Composite Solid Propellants, Scientific Technical Review, Vol. LVII, No. 3–4, 2007.

[2] R. Jeremic, Some Aspects of Time-Temperature Superposition Principle Applied for Predicting Mechanical Properties of Solid Rocket Propellants. Propellants Explos. Pyrotech. **24** (1999) 221–223.

[3] J.L. de la Fuente, M.F. Garcia, M.L. Cerrada, Viscoelastic Behavior in a Hydroxyl-Terminated Polybutadiene Gum and Its Highly Filled Composites: Effect of the Type of Filler on the Relaxation Processes, J. Appl. Polym. Sci. **88** (2003) 1705–1712.

[4] A. Cogmez, M.Y. Ozen, B. Veral, F. Pekel, S. Ozkel, Comparison of two HTPB-based composite propellants by dynamic mechanical analysis, in Proceedings of the 30th International Conference of ICT, Karlsruhe, Germany, 1999, pp. 1–29.

[5] J.M. Borsus, P. Merckaert, R. Jerome, P.H. Teyssie, Enfacement of Adhesion between Filler and Polymer in Alumina-Filled Rigid Polyurethane Foams, J. Appl. Polym. Sci. **29** (1984) 1857–1863.

[6] M. Bohn, S. Cerri, Ageing behaviour of composite rocket propellant formulations investigated by DMA, SGA and GPC, NDIA 2010, Insensitive munitions & energetic materials Technology symposium, 2010.

[7] S.S. Bhagawan, N. Prabhakaran, S.S. Rao and K.N. Kinan, Viscoelastic behaviour of solid propellants based on various polymeric binders, Defence Sci. J. **45** (1995) 17–23.

[8] R.G. Stacer, D.M. Husband, H.L.Stacer, Viscoelastic response and adhesion properties of highly filled elastomers, Rubb. Chem. Technol. **60** (1987) 227–244.

[9] J.D. Ferry, Viscoelastic properties of Polymers, John Wiley & Sons, New York, , 1970, pp. 292–430.

ИЗВОД

ВИСКОЕЛАСТИЧНА СВОЈСТВА КОМПОЗИТНИХ РАКЕТНИХ ГОРИВА НА БАЗИ ХИДРОКСИ-ТЕРМИНИРАНОГ ПОЛИ(БУТАДИЕНА)

Саша Ј. Брзић, Љиљана Н. Јелисавац, Јела Р. Галовић, Даница М. Симић, Јелена Љ. Петковић

Војнотехнички институт, Ратка Ресановића 1, 11000 Београд

(Научни рад)

У раду је испитан утицај односа удела амонијум-перхлората као оксидатора и алуминијума као металног горива у оквиру дефинисаног садржаја чврсте фазе, на вискоеластична својства композитних ракетних горива на бази хидрокси-терминираног поли(бутадиена), умрежених изофорондиизоцијанатом. Анализиране су и поређене вредности динамичко механичких својстава: температуре остакљивања T_g, модула сачуване (G') и изгубљене енергије (G'') и тангенса угла губитака tg δ. На основу реолошких параметара, експериментално одређених на температурама од –70 до 20 °C, конструисане су збирне (мастер) криве, које прекривају знатно шири интервал фреквенција (14 логаритамских декада) у односу на онај у коме је вршено мерење. Формирањем мастер кривих поступком "редукције" модула сачуване и модула изгубљене енергије, за референтну температуру T_0 = 20 °C, добијене су вредности фактора помераја, a_T, за све температуре на којима је експериментално одређивана фреквенциона зависност овог параметра. Поређене су овако добијене вредности фактора помераја, a_T. Одабиром температуре остакљивања као референтне температуре, одређене су "универзалне"' константе WLF једначине, на основу којих су израчунате вредности парцијалне слободне запремине на температури остакљивања, f_g/B, и коефицијент топлотног ширења слободне запремине, α_f/B. Резултати показују да повећањем удела алуминијума до одређене границе, која за дати удео чврсте фазе износи 13 мас.%, долази до незнатног смањења вредности слободне запремине и коефицијента топлотног ширења слободне запремине. Изнад ове границе, повећање удела алуминијума до 15 мас.% доводи до повећања испитаних вредности. Закључак да променом удела алуминијума не долази до линеарног смањења вредности коефицијента топлотног ширења слободне запремине наводи да се алуминијум у саставу композитног ракетног горива треба посматрати као активни пунилац.

Кључне речи: Композитно ракетно гориво • Хидрокси-терминирани поли(бутадиен) • Динамичка механичка анализа • Вискоеластична својства

Određivanje jonofornog kokcidiostatika salinomicina u premiksima i hrani za živinu tečnom hromatografijom posle post-kolonske derivatizacije

Ljiljana M. Kostadinović[1], Šandor M. Kormanjoš[1], Lazar N. Ružičić[2], Gordana K. Dozet[2]

[1]*Univerzitet u Novom Sadu, Institut za prehrambene tehnologije, Novi Sad*
[2]*Megatrend univerzitet, Fakultet za biofarming, Bačka Topola*

Izvod

U radu je razvijen i validiran postupak tečno-hromatografskog određivanja jonofornog kokcidiostatika salinomicina uz UV spektrofotometrijsku detekciju i post-kolonsku derivatizaciju dimetilaminobenzaldehidom (DMAB). Metoda je zasnovana na ekstrakciji salinomicina iz uzoraka hrane za životinje smešom acetonitril–voda (80:20, *V*/*V*) i prečišćavanju dobijenih ekstrakata na filteru 0.2µm Acrodisc® PSF. Relativna standardna devijacija za preciznost i obnovljivost je bila u opsegu od 2.4 do 8.8%, odnosno od 2.6 do 8.8%, a obnovljivost je bila u opsegu od 89 do 98%. Donja granica detekcije je iznosila 47 µg/kg, a donja granica kvantifikacije 71 µg/kg. Na osnovu dobijenih rezultata, zaključuje se da je opisana metoda tačna, precizna, selektivna i reproduktivna i da se može primeniti za određivanje salinomicina u premiksima i hrani za živinu.

Ključne reči: salinomicin, tečna hromatografija, post-kolonska derivatizacija, validacija metode, hrana za živinu.

Dostupno na Internetu sa adrese časopisa: http://www.ache.org.rs/HI/

NAUČNI RAD

UDK 636.5.085.1:543.544.5

Hem. Ind. **68** (4) 445–448 (2014)

doi: 10.2298/HEMIND130513068K

Intenzivna živinarska proizvodnja se prilagođava profilaksi kokcidioze na osobinama antikokcidijalnih preparata. Kokcidioza je visokoinvaziona parazitska bolest digestivnog trakta i stalan problem u živinarskoj proizvodnji. Izazivaju je protozoe iz roda Eimeria i Isospora. Novija antikokcidijalna sredstva širokog spektra delovanja su jonoforni polietarski kokcidiostatici (antibiotici), koji se osim za suzbijanje kokcidioze, primenjuju i kao promotori rasta farmskih životinja, a dejstvo im se zasniva na sposobnosti prenošenja jona metala kroz biološke membrane ćelija kokcidija. Na taj način oni dovode do jonskog debalansa, prekida metabolizma parazita i izazivaju njihovo uginuće [1].

Salinomicin pripada grupi jednovalentnih polietarskih jonofornih antibiotika, metabolički je produkt plesni *Streptomyces albus*, koji poseduje mikrobiološku aktivnost prema Gram-pozitivnim bakterijama, plesnima i velikom broju virusa. Za prevenciju i kontrolu kokcidioze izazvanu kokcidijama iz roda *Eimeria*, najčešće se koriste jonoforni kokcidiostatici, odnosno njihov najznačajniji predstavnik salinomicin. Salinomicin se u hranu za živinu dodaje u količini od 20–70 mg/kg. U ovoj količini salinomicin ima pozitivan efekat i na proizvodne rezultate tova, odnosno povećanje telesne mase, konverzije hrane i na bolje usvajanje hrane [2].

Za određivanje polietarskih jonofornih kokcidiostatika u premiksima i hrani za životinje najčešće se primenjuje tečna hromatografija sa fluorescentnom [3,4] ili UV detekcijom [5–9]. Ove metode uključuju predkolonsku ili postkolonsku derivatizaciju ili ekstrakciju kolonskom hromatografijom, a obezbeđuju donju granicu detekcije od oko 1mg/kg, osim u slučaju lasalocida i narasina (0,5 mg/kg).

U radu su prikazani rezultati validacije tečno-hromatografske metode za određivanje salinomicina u uzorcima premiksa i hrane za brojlere posle postkolonske derivatizacije, UV spektrofotometrijskom detekcijom. Opisana i validirana metoda može se primeniti i za određivanje ostalih jonofornih kokcidiostatika.

EKSPERIMENTALNI DEO

Materijal

Sve hemikalije i rastvori koje su korišćene u radu, bile su analitičke čistoće za HPLC primenu.

Salinomicin u obliku natrijumove soli (SAL) (~98% čistoće) (Sigma-Aldrich, St. Louis, MO, USA). Aditiv za hranu za životinje koji sadrži salinomicin-natrijum (Sacox® 120 microGranulate, Huvepharma, Edinburg, Škotska).

Acetonitril (ACN) i metanol (MeOH) (HPLC čistoće, Merck Sciences, Darmstadt, Nemačka), sulfatna kiselina, minimum 98% čistoće (VWR BDH Prolabo), dimetilaminobenzaldehid (DMAB), minimum 98% čistoće (Sigma-Aldrich, Steinheim, Nemačka).

Standardni rastvori

Osnovni standardni rastvor salinomicin-natrijuma, koncentracije 1mg/ml pripremljen je u metanolu i ko-

Prepiska: Lj. Kostadinović, Univerzitet u Novom Sadu, Institut za prehrambene tehnologije, Bulevar cara Lazara 1, 21000 Novi Sad, Novi Sad, Srbija.
E-pošta: ljiljana.kostadinovic@fins.uns.ac.rs
Rad primljen: 13. maj, 2013
Rad prihvaćen: 5. septembar, 2013

rišćen je za izradu kalibracione krive sa 50, 100, 200 i 500 μg/ml.

Uzorci za analizu

Za određivanje obnovljivosti metode i efikasnosti ekstrakcije, primenjena je metoda standardnog dodatka. U komercijalne uzorke hrane, koji nisu sadržavali salinomicin dodata je tačno određena količina standardnog rastvora salinomicina, tako da se dobiju uzorci hrane sa koncentracijom salinomicina od 0.025, 0.05 i 0.1 mg/kg.

Metoda standardnog dodatka je primenjena i za dodavanje tačno određene količine aditiva Sacox® 120 u uzorke hrane (25.0±0.1 g uzorka), koji nisu sadržavali kokcidiostatik, tako da se dobiju uzorci hrane sa 15; 30 i 60 mg salinomicina/kg hrane za brojlere, odnosno uzorci sa trećinom, polovinom i profilaktičkom koncentracijom salinomicina.

Priprema uzoraka

Uzorak hrane (25.0±0.1g) se ekstrahuje sa 80 ml smeše acetonitril-voda (80:20, *V*/*V*), dok se pri analizi premiksa odmerava 5.00±0.1 g uzorka i ekstrakcija vrši sa 15 ml smeše. Uzorci se mućkaju 2 sata na vibracionoj mućkalici, dobijeni ekstrakt dekantuje, a ekstrakcija ponovi još dva puta sa istom zapreminom ekstrakcione smeše. Sakupljeni, spojeni ekstrakti se filtriraju kroz filter hartiju (Whatmann No. 1), potom uparavaju u struji azota skoro do suva na temperaturi od 45 °C. Ostatak se rastvori u 1 ml metanola i filtrira propuštanjem kroz 0.2 μm Acrodisc® PSF (Pall Europe Limited, UK) u vialice za automatsko injektovanje. Određivanje svake pojedinačne koncentracije vršeno je po šest puta.

Metoda

Uslovi tečno-hromatografskog određivanja

Sva određivanja su izvršena na hromatografu HPLC 1100 Agilent Technology (Diegm, Belgium) sa spektrofotometrijskim detektorom i reaktorom za postkolonsku derivatizaciju na 92 °C. Primenjena je kolona sa oktadecilsilanom na TSK-gelu: TSK ODS-120T, 10 μm (300 mm×7.8 mm) uz mobilnu fazu: MeOH–voda–sirćetna kiselina (94:6:0.1, *V*/*V*) iz koje je uklonjen ugljen dioksid, držanjem u ultrazvučnoj kadi. Injektovana zapremina je bila 100 μl, protok 0.7 ml/min, a UV detekcija je izvršena na 598 nm. Temperatura kolone je iznosila 38 °C.

Post-kolonska derivatizacija

Za post-kolonsku derivatizaciju mobilna faza se sastojala od 3% (*V*/*V*) sumporne kiseline 3% (*V*/*V*) DMAB. Protok je bio 0.9 ml/min, a temperatura reaktora 92 °C.

Koncentracija salinomicina u ispitivanim uzorcima je izračunata na osnovu kalibracione krive dobijene merenjem koncentracije salinomicina u standardnim uzorcima.

Validacija metode

Validacija metode je izvršena određivanjem donje granice detekcije (DGD), donje granice kvantifikacije (DGK), preciznosti i obnovljivosti. Statistička obrada podataka je izvršena primenom komercijalnog softverskog paketa, Statistica®, verzija 10 (StatSoft, Tulsa, OK, USA).

REZULTATI I DISKUSIJA

Selektivnost

U radu je razvijen i validiran tečno-hromatografski postupak određivanja sadržaja salinomicina u uzorcima premiksa i hrane za živinu uz UV spektrofotometrijsku detekciju posle post-kolonske derivatizacije dimetilaminobenzaldehidom (DMAB). Postupak post-kolonske derivatizacije sa stvaranjem dobro detektabilnih derivata je bilo neophodno razviti, jer salinomicin ne sadrži hromoforne grupe i ne apsorbuje u UV oblasti. Primenom identičnih uslova tečno-hromatografskog određivanja uz post-kolonsku derivatizaciju, uspešno se razdvajaju i određuju i drugi jonoforni kokcidiostatici: monensin i narasin. Retenciono vreme za monensin je 11.5 min, za salinomicin 13,5 min, a za narasin 15,5 min, čime je potvrđena selektivnost i specifičnost primenjene metode [10].

Osetljivost

Utvrđivanje donje granice detekcije (DGD) i donje granice kvantifikacije (DGK) je suštinsko pri validaciji metode i izračunato je na osnovu slepe probe (n = 20). Utvrđena DGDs (vrednost za slepu probu + 3*SD*) je 47 μg/kg, a DGKs (vrednost za slepu probu + 10*SD*) 71 μg/kg, što je dovoljno za osetljivo određivanje sadržaja salinomicina u uzorcima hrane za brojlere. Međutim, metoda tečno-hromatografskog određivanja uz UV detekciju nije dovoljno osetljiva, a samim tim ni primenjiva za određivanje sadržaja eventualnih rezidua salinomicina i drugih jonofornih kokcidiostatika u jajima i tkivima tretiranih životinja. U ovu svrhu treba primeniti sistem tečna hromatografija–masena spektrometrija, koji obezbeđuje znatno nižu DGD i DGK za određivanje salinomicina (0,0017 i 0,012 mg/kg) [11].

Linearnost

Linearnost određivanja je ispitana na četiri koncentracije salinomicina: 50, 100, 200 i 500 μg/ml. Ponavljanje je vršeno svakog dana u toku validacionog postupka, a dobijena kalibraciona kriva predstavljena je kao zavisnost površine hromatografskih pikova od koncentracije standardnog rastvora salinomicina. Koeficijent linearnosti R^2 je bio 0,9995.

Preciznost

Preciznost primenjene metode je određena u više nezavisnih eksperimenata koji su sprovedeni istog

dana, na istom instrumentu, uz iste eksperimentalne uslove, određivanja je izvršio isti operater, a zatim su ponovljeni u više narednih dana. Analize su ponavljane tri dana, a u toku svakog dana eksperimenti su rađeni tri puta. U svakom pojedinačnom eksperimentu, injektovanje iste zapremine pripremljenog uzorka u tečno-hromatografski sistem rađeno je 6 puta, a rezultati su dobijeni kao srednja vrednost 6 pojedinačnih određivanja. Na osnovu dobijenih rezultata zaključuje se da je metoda precizna i da se može primeniti za određivanje koncentracije salinomicina u uzorcima hrane za živinu.

Obnovljivost (*recovery*)

Validacija primenjene metode za određivanje Salinomicina u uzorcima hrane za živinu obuhvatila je ispitivanje obnovljivosti preko metode standardnog dodatka. Obnovljivost se kretala u opsegu od 89 do 98%, a rezultati su prikazani u tabeli 1. Nije utvrđen trend između obnovljivosti i koncentracije standardnog dodatka ili vrste hraniva. Utvrđeno je da je metoda obnovljiva, što se zaključuje i na osnovu prikazanih vrednosti srednje *SD* obnovljivosti.

Tabela 1. Rezultati ispitivanja obnovljivosti tečno-hromatografskog određivanja sadržaja salinomicina u hrani za živinu
Table 1. Recovery test results of liquid-chromatographic determination of salinomycin in poultry feed

Uzorak	Dodato, mg/kg	Nađeno, mg/kg	Obnovljivost, %	RSD, %
Hrana+salinomicin	0,025	0,024	95	7,7
	0,050	0,049	98	7,0
	0,100	0,094	94	8,8
Hrana+Sacox® 120	15,0	13,4	89	2,4
	30,0	29,1	97	2,6
	60,0	54,0	90	2,8

ZAKLJUČAK

U ovom radu je opisana i validirana metoda tečne hromatografije uz spektrofotometrijsku UV detekciju i post-kolonsku derivatizaciju za određivanje sadržaja salinomicina u premiksima i hrani za živinu. Rezultati validacije pokazuju da je primenjena metoda selektivna, osetljiva, precizna i obnovljiva, te se može primeniti za kvantitativno određivanje sadržaja salinomicina u uzorcima hrane za živinu i premiksima, ako je njegov sadržaj viši od 71 μg/kg, koliko iznosi DGK metode. Metoda nije primenjiva za određivanje rezidua salinomicina u jajima i mesu tretiranih životinja. Opisana metoda se može primeniti za određivanje i drugih jonofornih kokcidiostatika.

Zahvalnica

Autori se zahvaljuju Ministarstvu prosvete, nauke i tehnološkog razvoja Republike Srbije koje je finansiralo ova istraživanja u okviru projekta III 46012.

LITERATURA

[1] B.W.W. Braunius, Coccidiosis in Broilers: the Effective use of Anticoccidial drugs, WPSJ **38** (1982) 176–185.

[2] V. Simić, M. Kapetanov, Lj. Kostadinović, S. Pavkov, R. Ratajac, S. Lazić, Mogućnost primene leka Sacox 120 u preveniranju kokcidioze živine, Nauka u živinarstvu **4** (1998) 473–477.

[3] D.K. Matabudul, N. T. Crosby, I. Lumley, S. Sumara, The optimisation of rapid method for the determination of lasalocid in poultry feed using supercritical fluid extraction and high performance liquid chromatography, Food Chem. **75** (2001) 465–471.

[4] C. Focht, H. Campbell, J. Dalgleish, Determination of lasalocid sodium in animal feeds and premixes by reversed phase liquid chromatography: collaborative study, J AOAC Int. **91** (2008) 479–488.

[5] G. Dusi, V. Gamba, Liquid chromatography with ultraviolet detection of lasalocid, monensin, salinomycin and narasin in poultry feeds using pre-column derivatization, J Chromatogr. **835** (1999) 243–246.

[6] A. Thalman, K. Wagner, M. Tomassen, J. Driessen, J. de Jong, Liquid chromatographic method to determine narasin in feedingstuffs and premixtures: development, validation and interlaboratory study, J AOAC Int. **87** (2004) 1278–1286.

[7] J. de Jong, B. Stoisser, K. Wagner, M. Tomassen, J. Driessen, P. Hofmann, H. A. Putzka, Determination of maduramicin in feedingstuffs and premixtures by liquid chromatography: development, validation, and interlaboratory study, J AOAC Int. **87** (2004) 1033–1041.

[8] H. Campbell, G. Nayeri, Determination of monensin, narasin, and salinomycin in mineral premixes, supplements, and animal feeds by liquid chromatography and post-column derivatization: collaborative study, J. AOAC Int. **89** (2006) 1229–1242.

[9] G. Tavcar-Kalcher, K. Pavsic-Vrtac, A. Vengust, Validation of the procedure for the determination of maduramicin in concentrates, premixes and fees by liquid chromatography, Food Addit. Contam. **22** (2008) 1–5.

[10] W.J. Blanchflower, D.A. Rice, J.T.G. Hamilton, Simultaneous high-performance liquid chromatographic determination of monensin, narasin and salinomycin in feeds using post-column derivatisation, Analyst **110** (1985) 1283–1287.

[11] M. Rokka, M. Jestoi, K. Peltonen, Trace level determination of polyether ionophores in feed, Biomed Res. Int. (2013,) http://dx.doi.org/10.1155/2013/151363.

SUMMARY

DETERMINATION OF IONOPHORE COCCIDIOSTAT SALINOMYCINE IN PREMIXES AND POULTRY FEEDING STUFFS BY LIQUID CHROMATOGRAPHY AFTER POST-COLUMN DERIVATISATION

Ljiljana M. Kostadinović[1], Šandor M. Kormanjoš[1], Lazar N. Ružičić[2], Gordana K. Dozet[2]

[1]*University of Novi Sad, Institute of Food Technology, Novi Sad*
[2]*Megatrend University, Faculty of biofarming, Bačka Topola*

(Scientific paper)

Coccidiosis is a common parasitic disease of broiler chickens caused by single-celled protozoan parasites of the genus *Eimeria,* which are commonly referred toas "coccidian". This is an infective disease of the digestive tract which is most frequent amongpoultry, causing a decrease in daily increment, prolonged fattening, poorer skin pigmentation, slower feed conversion and increased mortality. The disease is caused by Protozoas from the genera of *Eimeria, Isospora* and *Cryptospora,* and it is manifested by damaging the intestine epithelial cells, less frequently the bile duct and renaltubuli. Coccidiosis is traditionally controlled by chemotherapy. There are many anticoccidial preparations which are used in the prevention of coccidiosis. Wechose a polyether monocarboxylic acid – salinomycine. Salinomycine consists monovalent carboxyl–polyether ionophores. Salinomycine, produced by *Streptomyces albus,* destroys the cell membranes and causes their lysis. Salinomycineand other ionophoric antibiotics combined with a number of mono and divalent cations and in the form of bi-complexes are capable to transfer metal ionsthrough lipid hydrophobic membrane, and when they areadded to diet, they change bioavailability, gut uptake andabsorption and reserves of nutrient tissues. The validationprocess of liquid chromatography determination of ionophoriccoccidiostatsalinomycine with UV spectrophotometric detection and post-column derivatisation with dimethylaminobenzaldehyde (DMAB) has been developed in this paper. The method is based on extraction of salinomycine in animal feed samples by using the mixture of acetonitrile and water (80:20, *V*/*V*) and by purification of extracts obtained by the filter 0.2 μm Acrodisc®PSF. The relative standard deviation (*RSD*) for reproducibility and accuracy varied from 2.4 to 8.8% and from 2.6 to 8.8%, respectively, and the values for the relative recovery rate ranged from 89 to 98%. The limit of detection (*LOD*) and limit of quantification (*LOQ*) were estimated to be below 47 and 71 μg/kg, respectively. Based on theseresults, it is concluded that the described method is accurate, precise, selective and reproducible and can be applied for determination of salinomycine in feeds and premixes for poultry.

Keywords: Salinomycine • Liquid chromatography • Post-column derivatisation • Method validation • Food for poultry

Prostorna varijabilnost ^{137}Cs u zemljištu Beograda (Srbija)

Ljiljana J. Janković-Mandić[1], Ranko M. Dragović[2], Milan M. Đorđević[2], Maja B. Đolić[1], Antonije E. Onjia[1], Snežana D. Dragović[1], Goran G. Bačić[3]

[1]*Univerzitet u Beogradu, Institut za nuklearne nauke Vinča, Beograd, Srbija*
[2]*Univerzitet u Nišu, Prirodno–matematički fakultet, Departman za geografiju, Niš, Srbija*
[3]*Univerzitet u Beogradu, Fakultet za fizičku hemiju, Beograd, Srbija*

Izvod

U radu je gamaspektrometrijski određena specifična aktivnost ^{137}Cs u neobradivom zemljištu sakupljenom u periodu od 2006. do 2010. godine sa 70 lokacija grada Beograda. Specifične aktivnosti ovog radionuklida varirale su u opsegu od 3 (Senjak) do 87 Bq kg^{-1} (Kosmaj), sa srednjom vrednošću od 23 Bq kg^{-1}, a jačine doze koja potiče od ^{137}Cs od 0,2 do 5,8 nSv h^{-1}, sa srednjom vrednošću od 1,5 nSv h^{-1}. Velika standardna devijacija i velika razlika između minimalne i maksimalne vrednosti specifičnih aktivnosti ^{137}Cs tipične su za zagađujuće supstancije antropogenog porekla.

Ključne reči: cezijum, zemljište, jačina doze gama zračenja, geografsko mapiranje.

NAUČNI RAD

UDK 546.36:539.166: 504.5(497.11Beograd)

Hem. Ind. **68** (4) 449–455 (2014)

doi: 10.2298/HEMIND130124069J

Dostupno na Internetu sa adrese časopisa: http://www.ache.org.rs/HI/

Gradske aglomeracije i konurbacije sa više od 1,5 miliona stanovnika predstavljaju generatore globalnih promena na širem prostoru i ugrožavaju živi svet. Promene na lokalnom nivou takođe predstavljaju neposrednu opasnost za stanovništvo grada. Zdravstveni uslovi u velikim gradovima, čak i u razvijenim zemljama, nisu zadovoljavajući, a kod biljnog i životinjskog sveta zapaženi se mutageni procesi, i to posebno kod pojedinih četinara, ptica i insekata. Kontaminacija životne sredine radioaktivnim materijalima postala je jedan od značajnih problema savremene civilizacije. Tehnološka revolucija koja se ostvaruje primenom nuklearne energije u mirnodopske svrhe, bez obzira na veliki napredak koji je u ovoj oblasti postignut u domenu zaštite životne sredine, neposredno vodi daljem povećanju radioaktivne kontaminacije biosfere. Potencijalna opasnost od primene nuklearnog oružja i opasnost od akcidenata na nuklearnim postrojenjima daje ovom problemu još veći značaj.

Pored velikog broja nuklearnih proba (više od 400 u periodu od 1945. do 1980. godine), od početka primene nuklearne energije dogodilo se i više akcidenata na reaktorima i reaktorskim postrojenjima. Najozbiljniji akcident u istoriji nuklearne energije dogodio se 1986. godine u černobiljskoj nuklearnoj elektrani u bivšem Savezu Sovjetskih Socijalističkih Republika (SSSR). Ovaj akcident pokazao je da postoji mogućnost zagađenja ne samo neposredne okoline mesta akcidenta, već mnogo većih prostora. Procenjuje se da je tokom akcidenta i narednih 10 dana u atmosferu oslobođeno 14×10^{18} Bq, od čega $1{,}8\times10^{18}$ Bq ^{131}I, $8{,}6\times10^{16}$ Bq ^{137}Cs i njegovih drugih izotopa, 1×10^{16} Bq ^{90}Sr i 3×10^{15} Bq plutonijumovih izotopa. Rasejavanje radioaktivnog materijala u najvećoj meri zavisilo je od klimatskih faktora kao što su stalni vetrovi, shema morskih struja, termička i barometarska stratifikacija atmosfere, gustina troposfere, godišnje doba, kao i od pravca pružanja planinskih sistema, pokrivenosti vegetacijom i sl. U vreme prve eksplozije kada je stub izbačenog radioaktivnog materijala dostigao najveću visinu iznad Černobilja su duvali vetrovi različitog smera, tako da se aktivnost prenela i na rastojanja veća od 2000 km od Černobilja. Procenjeno je da je 200000 km^2 Evrope bilo kontaminirano sa 4×10^4 Bq m^{-2} ^{137}Cs. Najveći deo aktivnosti (71%) je deponovan u Ukrajini, Belorusiji i Ruskoj Federaciji [1]. Procenjeno je da je u toku 1986. godine na teritoriji Socijalističke Federativne Republike Jugoslavije (SFRJ) deponovano oko 2,4% od ukupno emitovanih radionuklida iz oštećenog reaktora u Černobilju [2]. Veštački radioaktivni izotopi u zemljištu uključuju se u geološko i biološko kruženje materija u prirodi. Preko vode, vazduha i hrane biljnog i životinjskog porekla radionuklidi dospevaju u organizam čoveka. Nakupljanjem u kostima i drugim tkivima radionuklidi izazivaju dugotrajno ozračenje organizma.

Cezijum (^{137}Cs) je beta–gama emiter sa vremenom poluraspada 30,2 godina. Hemijski je analogan kalijumu i prati njegov metabolizam, nema poseban kritični organ za deponovanje već se distribuira u svim ćelijama organizma (organotropni radionuklid). Biološko vreme poluraspada za čoveka je od 10–110 dana i zavisi od starosnog doba i metabolizma organizma [3,4].

Distribucija veštačkih radionuklida u zemljištu [5] karakteriše se jako izraženom neravnomernošću po dubini profila. U regionima sa umerenom količinom atmosferskih taloga, u zemljištima težeg mehaničkog

Prepiska: S. Dragović, Univerzitet u Beogradu, Institut za nuklearne nauke Vinča, p.pr. 522, Beograd, Srbija.
E-pošta: sdragovic@vinca.rs
Rad primljen: 24. januar, 2013
Rad prihvaćen: 5. septembar, 2013

sastava, najveći deo antropogenih radionuklida se tokom dužeg perioda zadržava u površinskom sloju (do 10 cm dubine) zemljišta, a u oranicama – u oraničnom horizontu. U lakšim, peskovitim zemljištima, naročito onim s procednim tipom vodnog režima, znatan deo radioaktivnih materija za 10–15 godina migrira do dubine 40–50 cm, ali mogu dospeti i do podzemnih voda i dalje s njima do reka i mora.

Prema stepenu pokretljivosti [5] u zemljištu antropogeni radionuklidi dugog vremena poluraspada mogu se svrstati u sledeći niz: ^{90}Sr > ^{106}Ru > ^{137}Cs > ^{144}Ce > > ^{129}I > ^{239}Pu.

Ispitivanja [6–14] su pokazala da se ^{137}Cs vezuje za površinski sloj zemljišta (do 10 cm dubine), da se iz ovog sloja može jonski izmeniti (13–30%) i da njegova koncentracija opada sa dubinom. Vertikalna migracija ^{137}Cs u zemljištu je spor proces i procenjeno je da iznosi oko 0,1 do 1 cm godišnje. Na migraciju cezijuma osim fizičkohemijskih karakteristika zemljišta utiče i lokalna konfiguracija terena. U peskovitim zemljištima je veća brzina prodiranja. Na kinetiku transfera ^{137}Cs utiče i oblik u kome se on nalazi. Ako je u anjonskom obliku, zemljište ga veoma slabo apsorbuje i može vrlo intenzivno da migrira. Na migracionu sposobnost cezijuma utiče prisustvo kalijuma, kao i stabilnog cezijuma (njihov višak usporava migraciju).

U ovom radu gamaspektrometrijski je određena specifična aktivnost ^{137}Cs u površinskom sloju neobradivog zemljišta na teritoriji Beograda, izračunata jačina efektivne doze koja potiče od ^{137}Cs i analizirana prostorna distribucija ovog radionuklida metodom geostatističke interpolacije.

EKSPERIMENTALNI DEO

Istraživani prostor i sakupljanje uzoraka

Beograd se nalazi u peripanonskom pojasu Srbije (φN 44°49'14" i λE 20°27'44"), na ušću Save u Dunav, prosečne nadmorske visine 132 m. U obimu, teritorija Beograda zauzima 427 km, sa najvećom dužinom od 93 km i širinom od 68 km. Površina uže teritorije grada iznosi 3223 km^2, a užeg gradskog područja 360 km^2. Poljoprivredno zemljište zauzima 2235 km^2, od čega oranice i bašte 1807 km^2, voćnjaci 154 km^2, vinogradi 33 km^2, pašnjaci 113 km^2, trstici i bare 18 km^2, ribnjaci 3,25 km^2. Prema Generalnom urbanističkom planu građevinsko zemljište zauzima 457 km^2 [15].

Beograd je važno saobraćajno čvorište, jer preko njegove teritorije prolaze međunarodni putevi koji povezuju centralnu Evropu sa Mediteranom i Bliskim istokom. Beograd je tačka ukrštanja koridora IV i X evropskog značaja i geografski važno međunarodno rečno i vazdušno pristanište. Dužina magistralnih puteva iznosi 66 km, regionalnih 326 km, a lokalnih 32 km. Na teritoriji Beograda šume zauzimaju 13135 km^2, a parkovi u užem gradskom području 521 km^2. Na teritoriji grada ima 5517 ulica od toga u prigradskim opštinama 2288 [15].

Beograd se sastoji od 17 opština, 10 gradskih (Čukarica, Novi Beograd, Palilula, Rakovica, Savski Venac, Stari grad, Voždovac, Vračar, Zemun i Zvezdara) i 7 prigradskih (Barajevo, Grocka, Lazarevac, Mladenovac, Obrenovac, Sopot i Surčin).

Po popisu iz 2011. godine, Beograd ima 1,7 miliona stanovnika, od čega u užoj gradskoj zoni živi više od 1,3 miliona stanovnika [16].

Uzorci neobradivog zemljišta (n = 250) su sakupljeni sa 70 lokacija u Beogradu u periodu 2006–2010. godine, primenom metode sistematskog slučajnog uzorkovanja. Sa svake lokacije, sa površine od 1 m×1 m, do dubine od 10 cm, uzorkovano je 3–4 uzorka u skladu sa preporukama Međunarodne agencije za atomsku energiju [17].

Gamaspektrometrijska analiza

Uzorci zemljišta su očišćeni od mehaničkih nečistoća, uglavnom kamenčića i delova biljnog materijala, zatim su sušeni na 105 °C do konstantne mase, homogenizovani i prosejani kroz sito sa otvorima prečnika 2 mm i zapakovani u Marineli posude. Specifična aktivnost ^{137}Cs određena je korišćenjem gamaspektrometra ORTEC-AMETEK sa 8192 kanala, rezolucije 1,85 i relativne efikasnosti 34% na 1,33 MeV za ^{60}Co, na osnovu gama linije 661,66 keV. Za obradu spektara korišćen je softver Gamma Vision-32 [18].

Izračunavanje jačine efektivne doze koja potiče od ^{137}Cs

Jačina efektivne doze usled spoljašnjeg izlaganja koja potiče od ^{137}Cs (D_{Cs}) u zemljištu na 1 m iznad tla izračunata je uz pretpostavku da je zemljište polu-beskonačna, glatka i ravna površina i da je element mekog tkiva pod konstantnim uticajem fotonskog fluksa koji potiče od ^{137}Cs iz zemljišta, uzimajući u obzir da verovatnoća za emisiju gama zračenja na energiji od 661,6 keV iznosi 85,12%, prema jednačini [19–22]:

$$D_{Cs}(\text{nSv/h}) = 0{,}576 E \Phi(E) \left(\frac{\mu a(E)}{\rho} \right) \quad (1)$$

gde je E energija fotona (MeV), $\Phi(E)$ srednji fluks fotona za datu energiju u elementu zapremine mekog tkiva i $(\mu a(E)/\rho)$ maseni apsorpcioni koeficijent za zapreminski mali element mekog tkiva (cm^2 g^{-1}).

Za procenu maksimalne doze koja potiče od zračenja sa površine tla fluks fotona za datu energiju izračunava se prema jednačini:

$$\Phi(E) = \frac{\gamma A_{Cs}}{2(\mu s(E)/\rho)_{\text{zemljište}}} \quad (2)$$

gde su γ frakciona zastupljenost gama zračenja, A_{Cs} specifična aktivnost ^{137}Cs (Bq/kg) i $(\mu s(E)/\rho)_{\text{zemljište}}$ mase-

ni atenuacioni koeficijent za zemljište za *E* od 661,6 keV ($cm^2\ g^{-1}$).

Maseni atenuacioni koeficijent varira sa sadržajem vode u zemljištu i energijom gama fotona. Maseni atenuacioni koeficijent za tipično zemljište gustine 1,625 g cm^{-3}, koje sadrži 30% vode i 20% vazduha, za energiju od 661,6 keV iznosi 0,0780 $cm^2\ g^{-1}$. Maseni apsorpcioni koeficijent za zapreminski element mekog tkiva malih dimenzija, koji se koristi za procenu efektivne doze u uslovima konstantnog fluksa fotona sa površine tla za energiju od 661,6 keV iznosi 0,0316 $cm^2\ g^{-1}$ [19,23,24].

Geografsko mapiranje aktivnosti ^{137}Cs

Modelovanje geoprostornih podataka urađeno je u softverskom paketu ArcGIS (ESRI, 2009) i njegovom dodatku *Geostatistical Analyst* [25]. Interpolaciona metoda koja je korišćena za prikazivanje prostorne distribucije je kriging. Ona kreće od pretpostavke da udaljenost ili pravac pružanja aktivnosti ili koncentracije nekog elementa odražavaju prostornu korelaciju kojom bi se moglo objasniti prostiranje neke pojave. Ova metoda kvantifikuje međusobne odnose svih parova tačaka, nakon čega na podatke automatski primenjuje najpogodniji model i vrši predikciju vrednosti na neispitanim lokacijama u okviru proučavane oblasti. Brojne studije su pokazale da je, među geostatističkim metodama, *kriging* najpouzdanija interpolaciona metoda za izučavanje prostorne distribucije antropogenih radionuklida [26,27]. Metoda je rezistentna na efekat netipičnih vrednosti i preporučuje se za obradu nehomogenih podataka, što je upravo slučaj sa podacima o kontaminaciji životne sredine [26].

REZULTATI I DISKUSIJA

U tabeli 1 prikazana je deskriptivna statistika specifične aktivnosti ^{137}Cs u uzorcima zemljišta sakupljenog sa teritorije grada Beograda u periodu 2006–2010. godina i njoj odgovarajuća jačine doze.

Na osnovu dobijenih rezultata uočava se izražena varijabilnost specifičnih aktivnosti, a time i jačine doze ^{137}Cs u ispitivanim uzorcima zemljišta. Specifične aktivnosti ovog radionuklida varirale su u opsegu od 3 do 87 Bq kg^{-1}, a srednja vrednost iznosila je 23 Bq kg^{-1}, a jačine doze koja potiče od ^{137}Cs od 0,2 do 5,8 nSv h^{-1}, sa srednjom vrednošću od 1,5 nSv h^{-1}. Velika standardna devijacija i velika razlika između minimalne i maksimalne vrednosti tipične su za zagađujuće supstancije antropogenog porekla [28]. Na slici 1 prikazana je prostorna distribucija specifičnih aktivnosti ^{137}Cs u analiziranim uzorcima zemljišta.

Izražena varijabilnost specifičnih aktivnosti ^{137}Cs posledica je topografskih razlika i nehomogene površinske kontaminacije zemljišta posle černobiljskog akcidenta. Znatno veće specifične aktivnosti ^{137}Cs izmerene su u zemljištima južnog dela istraživanog prostora (oko Kosmaja i Avale) u odnosu na one u severozapadnom delu grada (Bežanija, Novi Beograd, Surčin). Uočena prostorna varijabilnost specifičnih aktivnosti ^{137}Cs može biti posledica prostornih razlika u fizičkohemijskim i biološkim osobinama zemljišta, tipu zemljišta i biljnom pokrivaču. U ranijim studijama na istom prostoru pokazana je značajna korelacija između aktivnosti ^{137}Cs i sadržaja organskih materija u zemljištu [29,30]. Poznato je da depozicija ^{137}Cs varira sa nadmorskom visinom i količinom padavina, ali to nije slučaj sa prostorom istraživanim u ovom radu, jer ne postoje značajne razlike u nadmorskoj visini i količini padavina među lokacijama uzorkovanja. Varijabilnost specifičnih aktivnosti ^{137}Cs može takođe biti objašnjena uticajima mikro- i mezotopografije u kontrolisanju redistribucije ovog radionuklida procesima erozije ili akumulacije. Prostorna varijabilnost distribucije ^{137}Cs na relativnom malim prostorima dokumentovana je brojnim studijama. Navas i Walling su uočenu varijabilnost aktivnosti ^{137}Cs u malom drenažnom basenu u severnoj Španiji objasnili procesima erozije i akumulacije [31]. Velika prostorna varijabilnost aktivnosti ovog radionuklida na malom prostoru na Tajvanu protumačena je kao posledica slučajne distribucije fizičkih i hemijskih osobina zemljišnih horizonata i pluvijalne erozije i akumulacije [32].

Tabela 1. Deskriptivna statistika specifične aktivnosti ^{137}Cs u uzorcima zemljišta sakupljenog sa teritorije grada Beograda u periodu 2006–2010. godina i njoj odgovarajuća jačine doze
Table 1. Descriptive statistics of specific activities of ^{137}Cs in soils collected from the territory of Belgrade during 2006–2010 and corresponding gamma dose rate

Parametar	^{137}Cs (Bq kg^{-1})	D_{Cs} / nSv h^{-1}
Srednja vrednost	23	1,5
Standardna devijacija	20	1,2
Medijana	15	1,0
Opseg	84	56
Mod	11	0,6
Minimum	3	0,2
Maksimum	87	5,8

Geostatističke metode su se pokazale pouzdanim u proceni distribucije ^{137}Cs emitovanom posle nuklearnog akcidenta u Černobilju na lokacijama sa kojih nisu sakupljeni uzorci na osnovu aktivnosti na obližnjim lokacijama. Atlas depozicije ^{137}Cs u Evropi posle akcidenta u Černobilju, izrađen je na osnovu podataka prikupljenih u više od 30 evropskih zemalja, transformisanih u mape korišćenjem interpolacionih tehnika i geografskog informacionog sistema [33]. Geostatističke metode pružaju realnu procenu distribucije ^{137}Cs na neuzorkovanim lokacijama širom sveta [34–37]. Dosadašnja istraživanja su pokazala da je tačnost procene nivoa radioaktivnosti na neuzorkovanim lokacijama u

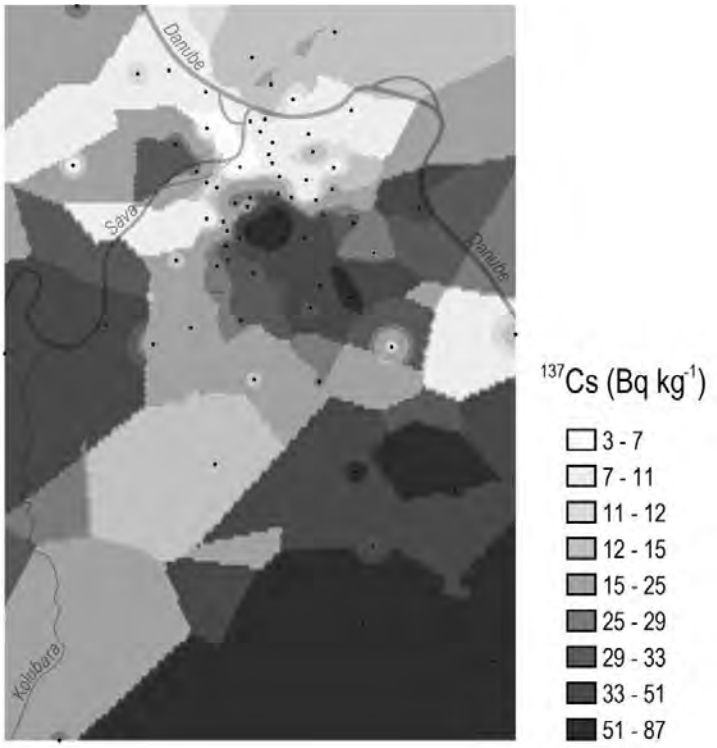

Slika 1. Prostorna distribucija specifičnih aktivnosti ^{137}Cs u zemljištu Beograda.
Figure 1. Spatial distribution of specific activities of ^{137}Cs in soils of Belgrade region.

direktnoj vezi sa brojem podataka na lokacijama koje ih okružuju i validnošću strategije uzorkovanja [27].

Do 1986. godine specifična aktivnost ^{137}Cs u zemljištu u Srbiji [38] bila je manja od 5 Bq kg^{-1}, a u najvećem broju biljaka, sem mahovina i lišajeva, cezijum se nije mogao detektovati. Neposredno posle černobiljskog akcidenta u pojedinim vrstama biljaka, izmerene su aktivnosti ^{137}Cs i do 3 kBq kg^{-1}, a površinska kontaminacija tla bila je veoma nehomogena. U okviru sistematskog ispitivanja sadržaja radionuklida u toku 2007. godine u Beogradu [15] analizirani su uzorci neobradivog zemljišta sa 5 lokacija (Dunavac, Jabučki rit, Zeleno brdo, Lazarevac i Obrenovac), srednja vrednost specifične aktivnosti ^{137}Cs iznosila je 27 Bq kg^{-1}, a varirala je u opsegu od 4 (Dunavac) do 52 Bq kg^{-1} (Zeleno brdo). U istraživanjima sprovedenim 2005. godine u Beogradu [39] u uzorcima sa istih lokacija, srednja vrednost specifične aktivnosti ^{137}Cs bila je 35 Bq kg^{-1}i varirala je u opsegu od 7 (Jabučki rit) do 78 Bq kg^{-1} (Zeleno brdo). Na osnovu ovih podataka srednja vrednost specifična aktivnosti je opala sa 35 na 27 Bq kg^{-1}, za dve godine, dok bi očekivana specifična aktivnost, prema zakonu radioaktivnog raspada, iznosila bi 33 Bq kg^{-1}. Na osnovu eksperimentalnih podataka specifična aktivnost ^{137}Cs za dve godine opala je za 8 Bq kg^{-1}, a ne za očekivanih 2 Bq kg^{-1}, što ukazuje na difuziju cezijuma u zemljištu.

U 2002. godini u uzorcima neobradivog zemljišta sa teritorije Beograda [40] (Dunavac i Jabučki rit) srednja vrednost specifične aktivnosti ^{137}Cs bila je 13 Bq kg^{-1} i varirala je u opsegu od 6 (Jabučki rit) do 23 Bq kg^{-1} (Dunavac).

Rezultati sistematskog ispitivanja sadržaja radionuklida u toku 2002. godine u Republici Srbiji [40] u uzorcima neobradivog zemljišta sa 6 lokacija, pokazali su da srednja vrednost specifične aktivnosti ^{137}Cs iznosi 33 Bq kg^{-1}. Najveći sadržaj ^{137}Cs izmeren je u zemljištima sakupljenim na Zlatiboru (109 Bq kg^{-1}), a najmanji u onim sakupljenom u Novom Sadu (6 Bq kg^{-1}).

Uporedni prikaz vrednosti specifičnih aktivnosti ^{137}Cs dobijene u ovom radu sa vrednostima specifičnih aktivnosti u gradovima različitih regiona sveta dat je u tabeli 2.

Na osnovu podataka iz literature može se uočiti da su vrednosti specifičnih aktivnosti ^{137}Cs znatno veće na prostorima izloženim radioaktivnom oblaku iz Černobilja (Republika Srpska [43], Turska [44], Makedonija [54] i Srbija), dok su znatno niže vrednosti u ostalim delovima sveta, gde su verovatno posledica nadzemnih nuklearnih eksplozija i proba. Uočava se, takođe, da su specifične aktivnosti ^{137}Cs manje na peskovitim terenima [42].

Tabela 2. Pregled specifičnih aktivnosti ^{137}Cs u različitim gradovima sveta (Bq kg^{-1})
Table 2. The summary of specific activities of ^{137}Cs in cities from different parts of the world (Bq kg^{-1})

Lokacija	Vrednost
Adana/Turska [41]	7 (0–28)
Alkharije /Saudijska Arabija [42]	0–3
Banja Luka/Republika Srpska [43]	26 (2–68)
Bursa/Turska [44]	5 (0–15)
Faisalabad/Pakistan [45]	4
Kairo/Egipat [46]	2–19
Istanbul/Turska [47]	2–81
Kalakam/Indija [48]	<0,1–3
Kirklareli/Turska [49]	8
Marmara/Turska [50]	27 (1–153)
Svat/Pakistan [51]	34
Tajvan/Kina [52]	7 (1–6,4)
Trombaj/Indija [53]	0,5–10
Veles/Makedonija[54]	71 (2–358)
Beograd (ovaj rad)	23 (3–87)

ZAKLJUČAK

Uticaj životne sredine na zdravlje odnosi se na sve fizičke, biološke i hemijske spoljašnje faktore koji utiču na ljude i životinje. Kontaminacija životne sredine radioaktivnim materijalima postala je jedan od značajnih problema savremene civilizacije i bez obzira na veliki napredak koji je u ovoj oblasti učinjen u pogledu zaštite životne sredine, tehnološka revolucija neposredno vodi daljem povećanju radioaktivne kontaminacije biosfere.

U svim uzorcima neobradivog zemljišta sa teritorije grada Beograda, utvrđeno je prisustvo ^{137}Cs. Specifične aktivnosti ovog radionuklida, kao i jačina doze koja potiče od njega varirale su u širokom opsegu vrednosti. Velika standardna devijacija i velika razlika između minimalne i maksimalne vrednosti tipične su za zagađujuće supstancije antropogenog porekla. Izražena varijabilnost specifičnih aktivnosti ^{137}Cs posledica je topografskih razlika i nehomogene površinske kontaminacije zemljišta posle černobiljskog akcidenta. Uočena prostorna varijabilnost specifičnih aktivnosti ^{137}Cs može biti posledica prostornih razlika u fizičkohemijskim i biološkim osobinama zemljišta, tipu zemljišta i biljnom pokrivaču.

Zahvalnica

Rad je finansiran sredstvima Ministarstva prosvete, nauke i tehnološkog razvoja Republike Srbije, ugovor broj III 43009.

LITERATURA

[1] International Atomic Energy Agency (IAEA), Environmental Consequences of the Chernobyl Accident and Remediation: Twenty Years of Experience, Report of the Chernobyl Form Expert Group Environment, STI/PUB/ /1239, 2006.

[2] Nivoi radioaktivne kontaminacije čovekove sredine i ozračenost stanovništva Jugoslavije 1986. godine usled havarije nuklearne elektrane u Černobilju, Savezni komitet za rad, zdravstvo i socijalnu zaštitu, Beograd, 1987.

[3] R.L. Kathren, Radioactivity in the Environment: Sources, Distribution and Surveillance, Harwood Academic Publishers, Amsterdam, 1984.

[4] J. Magill, J. Galy, Radioactivity, Radionuclides, Radiation, Springer, Berlin, 2005.

[5] B. Gajić, Fizika zemljišta, Univerzitet u Beogradu, Poljoprivredni fakultet, Beograd, 2006.

[6] D. Krstić, D. Nikezić, N. Stevanović, M. Jelić, Vertical profile of ^{137}Cs in soil, Appl. Radiat. Isot. **61** (2004) 1487––1492.

[7] K. Bunzl, Migration of fallout-radionuclides in the soil. Effects of non –uniformity of sorption properties on the activity-depth profiles, Radiat. Environ. Biophys. **40** (2001) 237–241.

[8] M. Isaksson, B. Erlandsson, S. Mattsson, 10-year study of the ^{137}Cs distribution in soil and a comparison of Cs soil inventory with precipitation-determined deposition, J. Environ. Radioact. **55** (2001) 47–59.

[9] G. Kirchner, Applicability of compartmental models for simulating the transport of radionuclides in soil, J. Environ. Radioact. **38** (1998) 339–352.

[10] G. Matisoff, M.E. Keterer, K. Rosen, J.W. Mietelski, L.F. Vitko, H. Person, E. Lokas, Downward migration of Chernobyl-derived radionuclides in soil in Poland and Sweden, Appl. Geochem. **26** (2011) 105–115.

[11] K.M. Miller, J.L. Kuiper, I.K. Helfer, ^{137}Cs fallout depth distribution in forest versus field sites: implications for external gamma dose rate, J. Environ. Radioact. **12** (1990) 23–47.

[12] K. Rosen, I. Oborn, H. Lonsjo, Migration of radiocesium in in Swedish soil profiles after the Chernobyl accident, J. Environ. Radioact. **46** (1999) 45–66.

[13] P. Bossew, G. Kirchner, Modeling the vertical distribution of radionuclides in soil. Part 1. The converse dispersion equation revisited, J. Environ. Radioact. **73** (2004) 127–150.

[14] A. Clouvas, S. Xanthos, G. Takoudis, M. Antonopoulos-Domis, G. Zinovadis, T. Vidmar, A. Likar, Twenty-year follow-up study of radiocesium migration in soil, Radiat. Prot. Dosim. **124** (2007) 372–377.

[15] Kvalitet životne sredine grada Beograda u 2007. godini, Marija Grubačević sa saradnicima (ur.), Sekretarijat za zaštitu životne sredine, Beograd, 2008.

[16] Popis stanovništva, domaćinstava i stanova 2011. u Republici Srbiji, Stanovništvo, Nacionalna pripadnost – podaci po opštinama i gradovima, ISBN 978-86-6161-023-3, Republički zavod za statistiku, Beograd, 2012, str. 20 (4.1.2013.).

[17] International Atomic Energy Agency (IAEA), Soil Sampling for Environmental Contaminants, IAEA-TECDOC-1415, Vienna, Austria, 2004.

[18] ORTEC, Gamma Vission 32, Gamma-Ray Spectrum Analysis and MCA Emulation, Version 5.3, Oak Ridge, TN, 2001.

[19] S.N. Tahir, K. Jamil, J.H. Zaidi, M. Arif, N. Ahmed, Activity concentration of ^{137}Cs in soil samples from Punjab province (Pakistan) and estimation of gamma-ray dose rate for external exposure, Radiat. Prot. Dosim. **118** (2006) 345–351.

[20] K. Jamil, S. Ali, M. Iqbal, A.A. Qureshi, H.A. Khan, Measurements of radionuclides in coal samples from two provinces of Pakistan and computation of external gamma-ray dose rate in coal mines, J. Environ. Radioact. **41** (1998) 207–216.

[21] S. Ali, M. Tufail, K. Jamil, A. Ahmad, H.A. Khan, Gamma-ray activity and dose rate of brick samples from some areas of North West Frointer Province (NWFP), Pakistan, Sci. Total Environ. **187** (1996) 247–252.

[22] J.R. Lamarsh, Intoduction to Nuclear Engineering, Addision-Wisley, New York, 1983.

[23] P. Jacob, H. Paretzke, Gamma-ray exposure from contaminated soil, Nucl. Sci. Eng. **93** (1986) 248–261.

[24] D. Garber, ENDF-201, ENDF/B Summary documentation, BNL-1754 (ENDF-201) (ENDF/B-IV), Brookhaven National Laboratory, 1975.

[25] ESRI, ArcGIS Desktop: Release 9.3, Environmental Systems Research Institute Redlands, CA, 2009.

[26] N. Diodato, M. Ceccarelli, Geographical information systems and geostatistics for modelling radioactively contaminated land areas, Natural Hazards **35** (2005) 229––242.

[27] L. Mabit, C. Bernard, Assessment of spatial distribution of fallout radionuclides through geostatistics concept, J. Environ. Radioact. **97** (2007) 206–219.

[28] I. Bikit, J. Slivka, M.Vesković, M.Krmar, N. Todorović, D. Mrđa, T. Prodanović, S. Forkapić, G. Šoti, N. Jovančević, J. Hansman, M. Nenin, Određivanje koncentracije aktivnosti radionuklida u poljoprivrednom i nepoljoprivrednom zemljištu na teritoriji grada Novog Sada u 2008. godini, Izveštaj za gradsku upravu za zaštitu životne sredine grada Novog Sada za 2008. godinu, Univerzitet u Novom Sadu, Prirodno–matematički fakultet, Novi Sad, 2008, str. 21.

[29] S. Dragović, B. Gajić, R. Dragović, Lj. Janković Mandić, L. Slavković Beškoski, N. Mihailović, M. Momčilović, M. Ćujić, Edaphic factors affecting the vertical distribution of radionuclides in the different soil types of Belgrade, Serbia, J. Environ. Monit. **14** (2012) 127–137.

[30] J. Petrović, M. Ćujić, M. Đorđević, R. Dragović, B. Gajić, Š. Miljanić, S. Dragović, Spatial distribution and vertical migration of ^{137}Cs in soils of Belgrade (Serbia) 25 years after the Chernobyl accident, Environ. Sci.: Processes Impacts **15** (2013) 1279–1289.

[31] A. Navas, D.E. Walling, Using caesium-137 to assess sediment movement on slopes in a semiarid upland environment in Spain, Erosion, Debris Flows and Environment in Mountain Regions, IAHS Publ. no. 209, 1992, pp. 129–138.

[32] C.-A. Huh, C.-C. Su, Distribution of fallout radionuclides (^{7}Be, ^{137}Cs, ^{210}Pb and ^{239,240}Pu) in soils of Taiwan, J. Environ. Radioact. **77** (2004) 87–100.

[33] M. De Cort, G. Dubois, Sh.D. Fridman, M.G. Germenchuk, Yu.A. Izrael, A. Janssens, A.R. Jones, G.N. Kelly, E.V. Kvasnikova, I.I. Matveenko, I.M. Nazarov, Yu.M. Pokumeiko, V.A. Sitak, E.D. Stukin, L.Ya. Tabachnyi, Yu.S. Tsaturov, S.I. Avdyushin, Atlas of caesium deposition on Europe after the Chernobyl accident. EUR Report 16733, EC, Office for Official Publications of the European Communities, Luxembourg, 1998.

[34] A. Facchinelli, M. Magnoni, L. Gallini, E. Bonifacio, ^{137}Cs contamination from Chernobyl of soils in Piemonte (North-West Italy): Spatial distribution and deposition model, Water Air Soil Pollut. **134** (2002) 341–352.

[35] M.S. Al-Masri, Vertical distribution and inventories of ^{137}Cs in the Syrian soils of the eastern Mediterranean region, J. Environ. Radioact. **86** (2006) 187–198.

[36] A. Chappell, G. Hancock, R.A.Viscarra Rossel, R. Loughran, Spatial uncertainty of the ^{137}Cs reference inventory for Australian soil, J. Geophys. Res: Earth Surf. **116** (2011) F04014.

[37] A. Caro, F. Legarda, L. Romero, M. Herranz, M. Barrera, F. Valiño, R. Idoeta, C. Olondo, Map of predicted deposition of Cs-137 in Spanish soils from geostatistical analysis, J. Environ. Radioact. **115** (2013) 53–59.

[38] D. Popović, V. Spasić-Jokić, Posledice nuklearne nesreće u Černobilju, na teritoriji Republike Srbije, Vojnosanit. pregl. **63** (2006) 481–487.

[39] Kvalitet životne sredine grada Beograda u 2005. godini, Marija Grubačević sa saradnicima (ur.), Sekretarijat za zaštitu životne sredine, Beograd, 2005.

[40] Radioaktivnost životne sredine u Republici Srbiji u 2002. godini, Ministarstvo za zaštitu prirodnih bogatstava i životne sredine, Beograd, 2003.

[41] M. Degerlier, G. Karahan, G. Ozger, Radioactivity concentrations and dose assessment for soil samples around Adana, Turkey, J. Environ. Radioact. **99** (2008) 1018–1025.

[42] H. Orabi, A. Al-Shareaif, M. El Galefi, Gamma ray measurements of naturally occurring radioactive sample from Alkharje City, J. Radioanal. Nucl. Chem. **269** (2006) 99––102.

[43] M. Janković, D. Todorović, M. Savanović, Radioactivity measurements in soil samples collected in the Republic of Srpska, Radiat. Meas. **43** (2008) 1448–1452.

[44] G. Karahan, Risk assessment of baseline outdoor gamma dose rate levels study of natural radiation sources in Bursa, Turkey, Radiat. Prot. Dosim. **142** (2010) 324–331.

[45] M. Tufaila, N. Akhtarb, M. Waqasc, Measurement of terrestrial radiation for assessment of gamma dose from cultivated and barren saline soils of Faisalabad in Pakistan, Radiat. Meas. **41** (2006) 443–451.

[46] R.H. Higgy, M. Pimpl, Natural and man-made radioactivity soils and plants around the research reactor of Inshass, Appl. Radiat. Isot. **48** (1997) 1145–1148.

[47] G. Karahan, A. Bayulken, Assessment of gamma dose rates around Istanbul (Turkey) J. Environ. Radioact. **47** (2000) 213–221.

[48] V. Kannan, M.P. Rajan, M.A.R. Iyengar, R. Ramesh, Distribution of natural and anthropogenic radionuclides and beach sand samples of Kalpakkam, Appl. Radiat. Isot. **57** (2002) 109–119.

[49] H. Taskin, M. Karavus, P. Ayb, A. Topuzoglu, S. Hidiroglu, G. Karahan, Radionuclide concentrations in soil and lifetime cancer risk due to gamma radioactivity in Kirklareli, Turkey, J. Environ. Radioact. **100** (2009) 49––53.

[50] O. Kulic, M. Belivermis, S. Tocuoglu, Y. Cotuk, M. Coskun, A. Cayir, R. Kucer, Radioactivity concentrations and dose assessment in surface soil samples from east and south of Marmara region, Turkey, Radiat. Prot. Dosim. **128** (2008) 324–330.

[51] T. Jabbar, K. Khan, M.S. Subhani, P. Akhter, A. Jabbar, Enviromental gamma radiation measurement in district Swat, Pakistan, Radiat. Prot. Dosim. **132** (2008) 88–93.

[52] J. Lu, Y. Huang, F.Li, L.Wang, S. Li, Z. Hsia, The investigation of ^{137}Cs and ^{90}Sr background radiation levels in soil and plant around Tianwan NPP, China, J. Environ. Radioact. **90** (2006) 89–99.

[53] A. Kumar, R.K. Singhal, J. Preetha, K. Rupali, V.M. Joshi, A.G. Hegde, H.S. Kushwaha, A non-parametric statistical analysis in the measurement of outdoor gamma exposure to residents around Trombay, Radiat. Prot. Dosim. **124** (2007) 378–384.

[54] S. Dimovska, T. Stafilov, R. Šajn, M. Frontasyeva, Distribution of some natural and man-made radionuclides in soil from the city of Veles (Republic of Macedonia) and its environs, Radiat. Prot. Dosim. **138** (2010) 144–157.

SUMMARY

SPATIAL VARIABILITY OF ^{137}Cs IN THE SOIL OF BELGRADE REGION (SERBIA)

Ljiljana J. Janković-Mandić[1], Ranko M. Dragović[2], Milan M. Đorđević[2], Maja B. Đolić[1], Antonije E. Onjia[1], Snežana D. Dragović[1], Goran G. Bačić[3]

[1]*University of Belgrade, Vinča Institute of Nuclear Sciences, P.O. Box 522, Belgrade, Serbia*
[2]*University of Niš, Faculty of Science and Mathematics, Department of Geography, Višegradska 33, Niš, Serbia*
[3]*University of Belgrade, Faculty of Physical Chemistry, Studentski trg 12–16, Belgrade, Serbia*

(Scientific paper)

Among radionuclides in the soil deposited after Chernobyl accident, ^{137}Cs poses considerable environmental and radiological problemdue to its relatively long half-life (30.17 γ), its abundance in the fallout, high mobility and similarity to potassium as the major plant nutrient. In this study the samples of undisturbed surface soil (n = 250) were taken from 70 regions in Belgrade, during 2006–2010. The specific activities of ^{137}Cs were measured by gamma-ray spectrometry. Based on obtained results, the external effective dose rates were calculated according to the internationally accepted activity to dose rate conversion equations. The spe–cific activities of ^{137}Cs were geographically mapped. The presence of ^{137}Cs has been detected in all soil samples, with high variability of its specific activity, ranging from 3 to 87 Bq kg^{-1}.The mean specific activity of ^{137}Cs was 23 Bq kg^{-1} and the corresponding absorbed dose was 1.5 nSv h^{-1}. The observed range reflects the inhomogeneity of the deposition process following the Chernobyl accident. It could also be attributed to topographic differences and spatial differences in physicochemical and biological soil properties, soil type and vegetation cover. The results of the present study could be valuable database for future estimations of the impact of radioactive pollution.

Keywords: Caesium • Soil • Gamma dose rate • Geographic mapping

A comparative analysis of the selected properties of protective filtering masks

Dušan S. Rajić[1], Željko J. Kamberović[1], Radovan M. Karkalić[2], Maja D. Vitorović-Todorović[3], Negovan D. Ivanković[2], Sonja Dj. Bauk[3], Dalibor B. Jovanović[4]

[1]*University of Belgrade, Innovation Center, Faculty of Technology and Metallurgy, Belgrade, Serbia*
[2]*University of Defense, Military Academy, Belgrade, Serbia*
[3]*Military Technical Institute, Belgrade, Serbia*
[4]*Technical Test Center, General Staff of the SAF, Serbia*

Abstract

The results of comparative experimental testing of different filtering masks are presented in this study. Some of the most important functional properties have been tested on available models of Italian, French, British, Canadian, Swiss, American, and three models of Serbian military protective masks (M3 of the latest generation, as well as M2, and M2FV models of the previous generation). The mask models have been tested on protection factor, dynamic resistance of the exhaust valve and its static permeability, the overall inhalation resistance of protective masks, field of view and optical properties, by standardized testing methods. Based on the experimental results obtained, it can be concluded that the Serbian mask M3 is approximately at the same quality level as tested foreign masks, and above Serbian protective masks of the previous generation marked as M2F and M2FV.

Keywords: respiratory protection, filtrating masks, quality characteristics, inner permeability, field of vision.

Available online at the Journal website: http://www.ache.org.rs/HI/

PROFESSIONAL PAPER

UDC 614.894.2:623

Hem. Ind. **68** (4) 457–464 (2014)

doi: 10.2298/HEMIND130612070R

A soldier's personal protective equipment for radiological, chemical and biological (RCB) agents comprises devices that serve to protect his body and respiratory organs [1]. These protective devices, together with other weaponry devices and military equipment, need to be mutually compatible [2]. Respiratory protection is maintained by wearing different types of protective masks, half masks and respirators. A military protective mask is a filtering device which protects the respiratory system, eyes and face of a user from RCB contamination in form of gases, vapour, as well as solid and liquid aerosols [3]. It is also designed to protect a soldier from industrial toxic substances, if used with an appropriate filter.

It is known from experience that manufacturers of weaponry devices and military equipment very often exaggerate the properties of their products for marketing purpose, and it is the same in case of protective masks. Their real properties can be proved only by experimental check of the declared data. Serbian new protective mask M3 (Fig. 1) is expected to be at approximately the same level with the modern armies' IV generation protective masks, in terms of tactical and technical properties.

Correspondence: N.D. Ivanković, MA, University of Defense, Military Academy, Pavla Jurišica Šturma 33, 11000 Belgrade, Serbia.
E-mail: negovan.ivankovic@gmail.com
Paper received: 12 June, 2013
Paper accepted: 17 September, 2013

This hypothesis can only be proved by comparative experimental testing of its relevant properties in relation to military protective masks of other manufacturers. With this aim, this paper offers results of comparative experimental testing of the most important properties of available models of Italian, French, British, Canadian, Swiss, American and Serbian protective mask.

Figure 1. Serbian military protective mask M3, a product of Trayal Corporation, Kruševac, Serbia.

One of the most important properties of a protective mask is the inner permeability on the face piece's fitting line. Often, instead of the term inner permeability, its reciprocal term – protection factor, is being used. Measured value of inner permeability (protection factor) of a protective mask also involves the exhaust valve permeability. Through values of protection factor, the quality of construction of protective mask is being

checked, as well as face piece's airtightness and the quality of its integral elements, thus this property is considered as one of the most important ones.

In this paper, in addition to protection factor, the comparative analysis of the following properties of protective masks and their subsystems has been carried out:

– overall resistance of the mask during exhalation;
– dynamic resistance of the mask's exhaust valve;
– static permeability of the exhaust valve;
– field of view and the most important optical properties.

The aim of this paper is to determine the state of the quality through experimental comparative analysis of the most important properties of the domestic protective mask M3, in relation to available foreign masks, as well as Serbian masks of the previous generation, marked as M2F (phonic) and M2FV (phonic with a subsystem for drinking water) which are in Serbian army's equipment for years.

TEST METHODS

Inner permeability level of protective mask

One of the key parameters for testing the efficacy of the protection mask is monitoring the RBC contaminant aerosol penetration, *i.e*., determining the inner permeability level of the protective mask. Since the testing with real RBC contaminants in laboratory conditions is a high risk activity, the method of testing with generated aerosols of a non-toxic agents such as sodium chloride, paraffin mist, etc., which simulate the presence of contamination in the air is being used [4–6]. The apparatus, shown schematically in Figure 2, which consists of bellow listed devices and tools, is being applied for testing filtration efficacy of the mask in conditions of contamination:

Inner permeability of the face piece is tested by the method described in literature [7]. Value of inner permeability of face piece, tested by sodium chloride aerosols, for each testing activity must not be more than 2×10^{-2}% per a tester [7]. The mean value of inner permeability of face piece, tested by sodium chloride aerosols, for each testing activity must not be more than 1×10^{-2}% per an examinee [8]. The mean value of face piece's inner permeability, tested on 10 face pieces and 10 examinees according to a defined matrix, using sodium chloride aerosol, must not be more than 4×10^{-2}% [8]. During the comparative quality testing of different protective masks, the protective factor has been measured on: Italian protective mask IMMD (size S), Canadian protective mask C4 (size S), American protective mask M40A1 (size S), Swiss protective mask SM3 (size S), Serbian protective mask M2FV (size S) and Serbian protective mask M3 (size S).

Examinees have been volunteers from the Military Technical Institute. The selection of examinees has been conditioned by the specific head measurement: gnathion-nation (measurement A) and frontal bizygomatic width (measurement B). The protection factor of protective masks has been measured by a standard test [7]. The test comprises seven activities which simulate actions from real life conditions:

– Normal breathing without head movement;
– energetic head movements to the left;
– energetic head movements to the right;
– energetic head movements upward;
– energetic head movements downward (towards the chest);

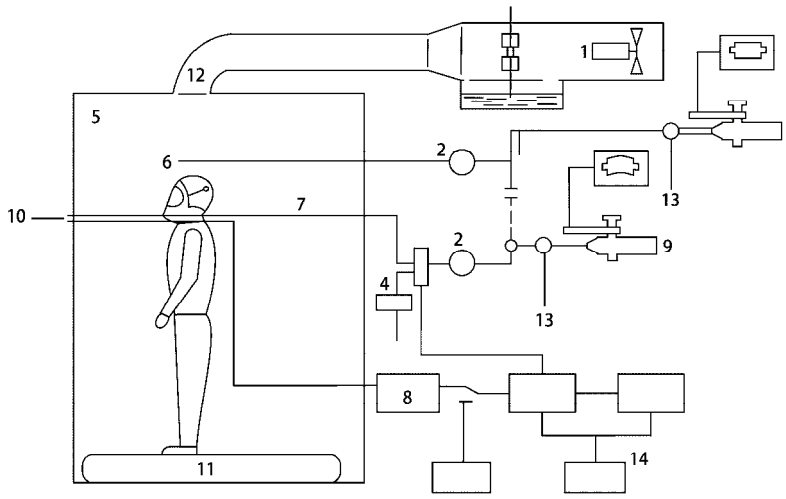

Figure 2. Sodium chloride inner leakage test apparatus. 1. Aerosol generator; 2. pump; 3. valve for sample selection; 4. air filtration filter; 5. testing chamber; 6. aerosol sample from testing chamber C_o; 7. aerosol sample under the mask C_m; 8. pressure sensor; 9. flame photometer; 10. universal filter simulator; 11. treadmill; 12. aerosol inlet; 13. extra air for aerosol dilution; 14. sampling impulse interface.

– Opening and closing the mouth with a deep inhale when the mouth is open to the maximum (hereinafter deep breathing);
– Normal breathing without head movement.

For each test activity the measurement of protective mask factors has been carried out separately and the mean value has been calculated for all examinees.

Total resistance of the protective mask during inhalation has been measured according to the method described in [7]. For measuring total resistance of the protective mask during inhalation, a standard method has been applied, the method which uses a vacuum pump (provides sub-pressure at the flow of 120 dm^3/ /min), flow meter (Rota meter) 0–120 dm^3/min, resistance meter 0–1500 Pa and artificial head with anthropometric dimensions which correspond to the size of the tested protective mask. Before testing the resistance of each protective mask, it is necessary to carefully seal the mask along the fitting line onto the artificial head. Due to the lack of the original filters for all tested protective masks, and thanks to compatibility of the filters of all the mentioned masks, the measurement of resistance of the foreign masks has been carried out by using the American and domestic filters, whereas the Italian protective mask has been tested only with the original filter.

The exhaust valve resistance has been measured according to the method described in [7]. For measuring dynamic resistance of the exhaust valve a standard method has been applied, the method which uses the source of the airflow, flow meter, tray subassembly of the exhaust valve and instruments for measuring the resistance.

The method of static permeability of the subassembly of the exhaust valve is described in the literature [7].

Field of view and optical properties

The field of view means the total spatial extent of stationary sources of visual information that causes irritation of the stationary eye. Total field of view is the field which is obtained by looking with both eyes. Folded or stereoscopic field of view is part of the total field of view which can be seen by one eye. Viewing angle is the angle that is formed by peripheral and central visible beam [7]. The average values of visual angles in the main directions are:

– on the temple: 85°;
– above the temple: 55°;
– above: 45°;
– up on the nose: 55°;
– on the nose: 60°;
– down on the nose: 50°;
– down: 65°;
– down on the temple: 85°.

The flow of the process with the order of activities is described in the literature [9]. Equipment for measuring the field of view comprises apertometer, apertogram and planimeter. The required optical characteristics of protective masks are defined through their tactical and technical requirements, a check is given to the criteria [5,7–10]. Due to the unavailability of these data for the foreign protective mask, tactical and technical requirements for protective mask M3 are to be referred to on this occasion [8]. Ocular transparency to visible light wavelength of 420 to 780 nm must be at least 85%. Spectral transmissions through the oculars in the field of visible light must not deviate more than 5% compared to the average value of the transmission in entire range. Distortion of figure, by passing of visible light through the oculars, must not be greater than ±2%.

The oculars should not have an optical intensity, whereas the following deviations are allowed:

– spherical intensity: ±0.25 Dpt;
– astigmatism: ±0.25 Dpt;
– prismatic effect: ±0.25 PrDpt.

The optical characteristics were studied on the optical bench Salvadoris Firence, Officcine Galileo, Italy manufacturer, with collimator f = 1781 mm, except for the integral transparency in the visible part of spectrum, which was measured on the device "Odeltron", Old Deft USA manufacturer, with photocathode S 20 and green filter for correction of the spectrum to the human eye.

RESULTS AND DISCUSSION

Inner permeability (P) is calculated from aerosol concentration average values in the last 100 s of every test session. Inner permeability expressed in percentage is calculated by using the formula (1):

$$P = \frac{100 C_m}{C_o} \frac{t_{\text{in}} + t_{\text{ex}}}{t_{\text{in}}} \quad (1)$$

C_m – NaCl aerosol concentration under the mask, determinate in the inhalation phase (mg/m^3); C_o – average NaCl aerosol value in the testing chamber (mg/m^3); t_{in} – overall inhalation time (s); t_{ex} – overall exhalation (s).

Results of the calculated mean values of the protection factor for all tested protective masks are shown in Table 1 and Figure 3, where: *PF* (1) – protection factor mean value for normal breathing at the beginning of the testing, *PF* (2) – protection factor mean value for head movements to the left, *PF* (3) – protection factor mean value for head movements to the right, *PF* (4) – protection factor mean value for the upward head movements, *PF* (5) – protection factor mean value for the downward head movements, *PF* (6) – protection factor mean value for deep breathing, *PF* (7) – pro-

Table 1. Protection factor mean values of the tested protective masks

Protection factor	IMMD (S)	M2FV (S)	C4 (S)	SM3 (S)	M40A1 (S)	M3 (S)
PF (1)	141024	43228	96960	58630	≥100000	109213
PF (2)	147911	59832	99550	62725	≥100000	250318
PF (3)	234526	53004	82567	67215	≥100000	92590
PF (4)	216836	52643	86687	67065	≥100000	101349
PF (5)	167453	53613	85247	67930	≥100000	109645
PF (6)	165753	44564	70003	62690	74820	109325
PF (7)	119903	50852	68490	59960	≥100000	89650
PFm	170487	51105	84215	63744	95930	123156

tection factor mean value for normal breathing at the end of testing and *PFm* – protection factor mean value for all test activities of all the examinees.

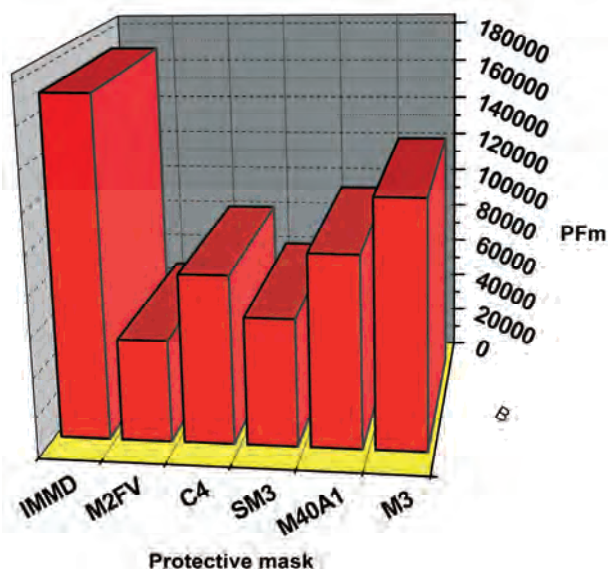

Figure 3. Protection factor mean values of the tested protective masks.

It needs to be pointed out that the number of foreign masks have been limited to one sample per each of the listed, except for the Italian and American (two samples), and number of filters from 1 to 5 pieces. For a valid Quality Score of protective masks in relation to the protection factor, it is needed to have at least 10 protective masks and 30 examinees. Despite the number of foreign masks being insufficient as well as number of measuring, it can still be concluded from the results shown in Table 1 and Figure 3 that the tested protective masks completely fulfil protection factor requirements [8].

During the testing of mask resistance, mostly 4 different airflows have been applied: 30, 60, 90 and 120 dm^3/min, and given results are shown in Figure 4.

By analyzing given results of the total resistance of protective masks during inhaling, it can be concluded that the lowest resistance during inhaling, in complete applied flow range of 30 to 120 dm^3/min, gives Serbian protective mask M3, then Swiss protective mask SM3, and a slightly higher and mutually almost equal, American M40A1 and English AVON S10. The highest level of resistance has been measured in Serbian mask M2FV. It can also be concluded that the resistance during inhalation in all three types of the tested foreign protective masks is higher with domestic than with American filter, which is logical, since the Serbian filter provides higher resistance than the American in total monitored airflow range.

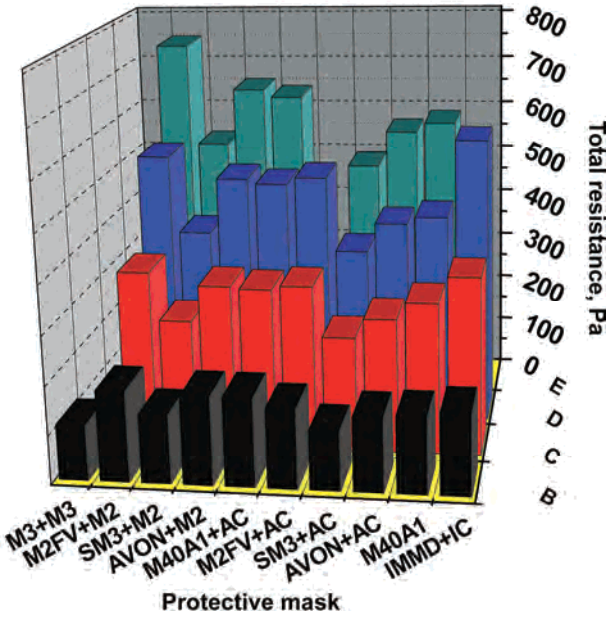

Figure 4. Total resistance during inhalation in tested protective masks IMMD, C4, SM3, M40A1, AVON, M2FV and M3 in combination with different filters at different airflows. B bars: 30 l/min, C bars: 60 l/min, D bars: 90 l/min and E bars: 120 l/min.

Italian protective mask fulfils tactical and technical requirements, which a new generation of protective masks needs to fulfils when it comes to total resistance of protective mask at the flow of 30 dm^3/min, even though it is significantly higher than in Swiss protective masks with the American filter, and somewhat higher

(6–10 %) than in the remained tested protective masks. However, the highest that the mask has been tested on, at the airflow of 90 dm3/min, was the Italian protective mask with the original filter that provided the highest resistance during inhalation, which is a negative property.

The following masks' exhaust valves have been tested simultaneously: Italian IMMD (panorama with transparent face piece and elastomeric border), French ARFA (panorama), English AVON S10, Canadian C4, domestic M2FV and M3. During testing, mostly two different airflows have been applied: 30 and 90 dm^3/min. The results are shown in Table 2.

Table 2. Results of the testing of the dynamic exhaust valve resistance (Pa) of protective masks

Exhaust valve	Flow, dm^3/min		
	30	60	90
IMMD	49.6	81.3	133.9
ARFA	28.4	–	176.6
AVON S10	46.1	–	106.9
C4	78.5	–	206.0
M2FV	52.0	–	133.4
M3	60.4	96.0	123.9

According to the results given in Table 2, it is concluded that the lowest dynamic exhaust valve resistance provide the valve of the French ARFA (panorama) mask at the flow of 30 dm^3/min and English valve AVON S10 at the flow of 60 dm^3/min, whereas the Canadian mask C4 valve provides the highest dynamic resistance at both applied airflows. Dynamic exhaust valve resistance of the Italian protective mask is at the same level as measured in the protective mask M2FV. Considering that in literature [8] is stated that dynamic resistance which has to fulfil the exhaust valve, at the airflow of 30 dm^3/min, is below 70 Pa, from Table 2. It can be concluded that all tested exhaust valve samples fulfil this criteria, except the Canadian protective mask C4.

Static permeability of the exhaust valve has been measured by a method described in literature [8], on IMMD and domestic protective mask M2F, on original apparatus, and Canadian protective mask C4, after the adjustment of exhaust valve's mount on the apparatus. It has been found out that the tested samples fulfil the criteria from [8]. Also, 10 exhaust valve samples of the protective mask M3 have been tested, and it has been found out that there is no static permeability in the time of 30 and 60 s and that according to this parameter they fulfil tactical and technical requirements [8]. Namely, static permeability of the exhaust valve subassembly has to be less than 15 cm^3, when the valve is exposed to the sub pressure of 250 Pa for 30 s. Measurement of static permeability of the exhaust valve in other foreign protective masks (ARFA, AVON S10, M40A1, SM3) couldn't be conducted due to decision according to which the exhaust valve should not be disassembled.

Total field of view with a protective mask M3 on the model of the head must be at least 80%, compared to the total field of view without protective masks [10]. For foreign protective masks this parameter as a tactical–technical data are not available. Field of view is measured on the following protective masks: Italian (IMMD), French (ARFA), British (AVON S10), Canadian (C4), U.S. (M40A1), Swiss (SM3), Serbian (M2F), (M2FV) and (M3). All measurements and processing of the results were performed according to the standard [9]. Measured values of the field of view are shown in Figure 5.

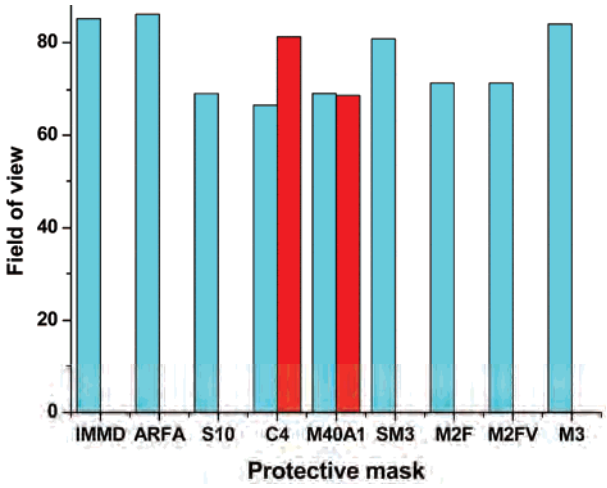

Figure 5. Field of view of tested protective masks. First red bar indicates unclear expanded field of view of C4 mask, and two bars for M40A1 mask represent the results for the basis and protective version of the oculars.

Figure 5 shows that the total field of view of protective mask M3 is 84% and it is greater than the total field of view of protective masks M2F and M2FV, where the value was about 70 %. The value of the total field of view of a protective mask M3 is at approximate level as in some foreign protective masks of IV generation: Swiss mask SM3 (80%), Finish mask M95 (80%), Swedish masks F2 (88%), and better than field of view measured at S10 (69.2%), C4 (66.7 %) and M40A1 (69.2%).

Comparing the results in Fig. 5 it was observed that the protective masks marked IMMD, ARFA and SM3 have bigger fields than others. Protective masks IMMD and ARFA are panorama type, so bigger field of view was expected. Increased field of protective mask SM3 is probably result of its small size, which is incompatible with the size of the artificial head which is used to determine field of view of mid-sized protective mask on the existing apparatus, and from that point the obtained

result is unreliable and may be rejected. In C4 protective mask oculars are a specific form of "cup", where in Fig. 5 unclear field of view is indicated (only unclear contours of the characters can be seen from the sides).

In M40A1 protective mask (Fig. 5) clearly shows the result of measuring of field of view with basic and protective ocular which is used for protection against mechanical damages and sunlight. Based on the results obtained from these measurements, it can be concluded that the literature data for the field of view, for some foreign protective masks that are not panorama type (*e.g.*, C4-field of view greater than 90%), are of marketing character and unrealistic.

The results of measuring optical properties of the oculars are shown in Table 3 and include determination of:

– integral transparency in the whole visible spectrum, *T* (%);
– spherical optical intensity, *P* ($D_p t$);
– astigmatism, *A* ($D_p t$);
– prismatic or cornering light beam, *D* ($P_r D_p t$);
– distortion of image, *Dist* (%).

Based on these results we can conclude that the oculars of all tested protective masks have satisfying transparency (except flexible polyurethane mask type panorama (ARFA) and satisfying optical characteristics, except for oculars of the American protective masks, which have a great value for deflecting a light beam, which causes deformation of the image. Comparative study of materials, components and complete foreign and domestic protective masks, enabled to reach quantitative indicators to compare their characteristics and evaluate and fulfil mounted tactical and technical requirements for protective mask M3 (all of this is done under the same experimental conditions). Number of foreign masks was limited to one sample of medium size, except the Italian (two samples). Due to the limited number of samples, obtained results are accepted with some caution. Despite these problems, the results were used to perform certain conclusions. It was found that the Italian and French masks have the largest field of view, which was expected since both are the panorama type. Among binocular protective masks, Swiss SM3 has the largest field of view. These protective masks satisfy mounted tactical and technical requirement for the field of view of protective mask M3.

By construction of protective mask M3 face piece, *i.e.*, by installation of two small valves in the nasal insert, steady flow of air into interior of nasal insert is enabled, as well as better evanescent of oculars by separation of the hot and cold air.

CONCLUSION

Serbian protective mask M3 has significant improvements compared to Serbian masks of previous generations, M2F and M2FV, in the field of RCB agent protection, as well as in terms of being comfortable to wear. Protective mask M3 has been improved in terms of material quality by choosing brombuthyl rubber instead of natural rubber for making the face piece and nasal inset, then by choosing the natural rubber for making the inhalation and exhaust valve and transparent single-layered polycarbonate for making the ocular (eyepiece). By inserting new subassemblies, its functions are enriched. For example, by getting a new construction of the subassembly of the exhaust valve and its mount, a more reliable work and better hermetic have been achieved, which can be seen from the given results of measuring the protection factor. System of elastic straps at the top of the head of protective mask M3 provides evenly fitting, which also helps improve the masks hermetic.

The field of view of the protective mask M3 is 84% and it is at the level of the latest protective masks generation IV, and is significantly higher in relation to the protective mask M2F and M2FV, where the value is 70%. Based on the obtained results of optical properties testing, it can be concluded that the protective mask M3 oculars and all other investigated protective masks, have satisfying transparency (except flexible polyurethane mask type panorama ARFA) and satisfying optical characteristics (except oculars of American protective mask which has a great value for deflecting a light beam, which causes deformation of the image).

Table 3. Oculars' optical characteristics of foreign and domestic protective masks

Characteristic	*T* / %	*P* ($D_p t$)	*A* ($D_p t$)	*D* ($P_r D_p t$)	*Dist* / %
M40A1	89	0	0	1.3	0
Protective glass M40A1	91	0	0	0	0
M40A and protective glass M40A1	82	-	-	1,3	0
C4	89	0	0	0.14	0
M2F, M2FV	89	-0.25	0.25	0.20	0
M3	96	≤ 0.1	≤ 0.1	≤ 0-8	0
AVON S10	91	0	0	0.58	0
ARFA	83	0	0	0.29	0

The increase of protective mask M3 total comfort is achieved by a new construction of face piece body and nasal implant, by new constructional solution to tighten the mask's strap system on the users head and by new construction and selection of the oculars position on mask's face piece body. The functions of protective masks M3 have expanded by addition of a new filters carrier subassembly, on the right side, which allows more efficient use of mask for left-handed users with targeting, by addition of correction glasses carrier for users with impaired vision and the addition of auxiliary voice membrane for better voice transmission in the use of means of communication. The possibility of using combined filters on the left and right side, and possibility of correction glasses usage significantly facilitates the performance of users' combat actions, especially left-handed persons' and those with weaker eyesight.

Protective mask M3 fulfils all the requirements of tactical and technical quality and in this sense represents a significant improvement in relation to the Serbian military protective masks of previous generations, marked M2F and M2FV. According to their optical and total characteristics, protective mask M3 is at the level of most modern devices of personal respiratory protection generation IV.

Acknowledgements

Ministry of Education, Science and Technological Development of the Republic of Serbia supported this work, Grant No. TR34034 (2011-2014).

REFERENCES

[1] N. Ivankovic, D. Rajic, M. Ilic, M. Vitorovic-Todorovic, N. Pajic, Testing of the efficiency of military devices for personal respiratory protection in relation to sub-micron particles of biological agents, Dig. J. Nanomater. Bios. **7** (2012) 1089–1095.

[2] D. Rajic, Method of testing compatibility of devices for personal NBC protection, Military Tech. Courier **57** (2009) 43–57.

[3] EN 134:1998, Respiratory Protective Devices – Nomenclature of Components. CEN -European Committee for Standardization.

[4] SRPS EN 13274-1:2008, Respiratory protective devices - Methods of test - Part 1: Determination of inward leakage and total inward leakage. Institute for Standardization of Serbia.

[5] SRPS EN 136:2007, Respiratory protective devices - Full face masks - Requirements, testing, marking. Institute for Standardization of Serbia.

[6] SRPS EN 14387:2007 Respiratory protective devices – Gas filter(s) and combined filter(s) – Requirements, testing, marking. Institute for Standardization of Serbia.

[7] SORS 8746:2005, Personal RCB protection devices – Protective mask – Methods of testing. Direction for Standardization, Codification and Metrology, Ministry of Defense, Republic of Serbia.

[8] Draft PKP 6590:2009, Personal RCB protection devices – Protective mask M3. Direction for Standardization, Codification and Metrology, Ministry of Defense, Republic of Serbia.

[9] SORS 7684:1999, Personal RCB protection devices-Laboratory method for testing the field of view in protective masks. Direction for Standardization, Codification and Metrology, Ministry of Defense, Republic of Serbia.

[10] [SORS 8831:2005, Mask protective M3, polycarbonated-Technical requirements. Direction for Standardization, Codification and Metrology, Ministry of Defense, Republic of Serbia.

[11] SRPS EN 166:2008, Personal eye protection-Specifications, Institute for Standardization of Serbia.

IZVOD

UPOREDNA ANALIZA ODABRANIH KARAKTERISTIKA ZAŠTITNIH MASKI FILTRIRAJUĆEG TIPA

Dušan S. Rajić[1], Željko J. Kamberović[1], Radovan M. Karkalić[2], Maja D. Vitorović-Todorović[3], Negovan D. Ivanković[2],Sonja Dj. Bauk[3], Dalibor B. Jovanović[4]

[1]*Univerzitet u Beogradu, Inovacioni centar Tehnološko–metalurškog fakulteta, Beograd, Srbija*
[2]*Univerzitet odbrane, Vojna akademija, Beograd, Srbija*
[3]*Vojnotehnički institut, Beograd, Srbija*
[4]*Tehnički opitni centar, Generalštab Vojske Srbije, Beograd, Srbija*

(Stručni rad)

U radu su prikazani eksperimentalni rezultati komparativnih ispitivanja određenih modela zaštitnih maski na principu filtracije vazduha. Osnovne funkcionalne karakteristike zaštitnih maski potrebne za ocenjivanje njihovog kvaliteta, testirane su na modelima italijanske, francuske, britanske, švajcarske i američke proizvodnje, kao i na tri modela vojnih zaštitnih maski domaće proizvodnje (model M3 najnovije generacije i modeli M2 i M2FV prethodne generacije). Primenom standardizovanih metoda ispitivanja, dostupni modeli zaštitnih maski testirani su na faktor zaštite, dinamički otpor i statičku propustljivost ventila izdisaja, ukupan otpor pri udisaju, karakteristike vidnog polja i optička svojstva. Na osnovu rezulata ispitivanja, može se zaključiti da je zaštitna maska M3 na približnom nivou kvaliteta sa testiranim modelima sa inostranog tržišta i značajno višeg kvaliteta u odnosu na modele ranije generacije M2 i M2FV.

Ključne reči: Respiratorna zaštita • Filtrirajuće maske • Karakteristike kvaliteta • Unutrašnje propuštanje • Polje vida

The influence of detergent and its components on metabolism of *Fusarium oxysporum* in submerged fermentation

Violeta D. Jakovljević[1], Jasmina M. Milićević[1], Jelica D. Stojanović[1], Slavica R. Solujić[2], Miroslav M. Vrvić[3]

[1]*University of Kragujevac, Faculty of Science, Institute of Biology and Ecology, Kragujevac, Serbia*
[2]*University of Kragujevac, Faculty of Science, Institute of Chemistry, Kragujevac, Serbia*
[3]*University of Belgrade, Faculty of Chemistry, Belgrade, Serbia*

Abstract

The influence of detergent and its components (sodium tripolyphosphate and ethoxylated cetyloleyl alcohol) at 0.1% concentration on the enzymatic and metabolic activity of *Fusarium oxysporum* during exponential growth was investigated in this paper. The fungus *Fusarium oxysporum* was isolated from wastewater originating from households which contain detergent. The following biochemical parameters were analyzed: pH, redox potential, proteolytic activity, production of carbohydrates, free and total organic acids, proteins and total dry weight biomass. The detergent had influence on the significant decrease of redox potential, slight increase of pH and quantity of glucose and total organic acids, while the proteolytic activity was triple insensitive in relation to control. The sodium tripolyphosphate had influence on the slight decrease of pH, significant increase of redox potential and quantity of glucose and free and total organic acids, whereas the proteolytic activity was intensive only 5th and 6th day. The total dry weight biomass of the fungus *F. oxysporum* was slightly inhibited by ethoxylated alcohol, but significantly inhibited by detergent and sodium tripolyphosphate.

Keywords: biomass, carbohydrates, ethoxylated cetyloleyl alcohol, organic acids, proteins, proteolytic activity, sodium tripolyphosphate.

Available online at the Journal website: http://www.ache.org.rs/HI/

SCIENTIFIC PAPER

UDC 661.187:582.28:66

Hem. Ind. **68** (4) 465–473 (2014)

doi: 10.2298/HEMIND130620071J

Over 2000 years, mankind has used surface-active components or their ingredients in the various aspects of daily life, personal care products, laundry washing, chemical cleaning and cosmetics. Chemical surfactants are amphiphilic compounds, which can reduce surface and interfacial tension by accumulating at the interface of immiscible fluids, and increase the solubility and mobility of hydrophobic or insoluble organic compounds [1,2]. Their main application is used by the manufacturers of detergents. A modern detergent powder is complicated multicomponent mixture consisting of active substances (surfactants), builders (sodium phosphates, sodium carbonate, sodium silicate and zeolite), bleach (perborate and percarbonate), wetting agents, optical brighteners, softeners, enzymes [3]. Based on ionization of polar head the surfactants are divided into four groups: anionic, cationic, nonionic and amfotheric. The most widely used in all regions of the world are linear alkyl benzene sulfonates (LASs), alcohol ether sulfates (AESs), aliphatic alcohols (AEs), alcohol sulfates (ASs) and alkaline salts of fatty acids (soap). The linear chain alkylbenzene sulfonate types (LAS) are the most popularly used synthetic anionic surfactant as major ingredient in domestic and industrial detergents more than 30 years [4]. Alcohol ethoxylated are presently the largest volume nonionic surfactants. Growth in use of linear primary AE has been rapid over the past 20 years because of their many desirable qualities such as rapid biodegradation, low to moderate foaming ability, superior cleaning of manmade fibers, tolerance of water hardness and ability to perform in cold water [5]. Builders boost the efficiency of surfactants by counteracting hard water, emulsifying oil and grease, and preventing soil from redeposition. Phosphates are an environmentally delicate chemical and a commonly used detergent builder. Phosphorus is in the form of sodium tripolyphosphate ($Na_5P_3O_{10}$) and is used to soften hard water and suspend dirt in the water. But, by dissolving in water phosphates create orthophosphates which are more toxic and because of that phosphates can be substituted with a phosphate free zeolite ($Na_2Al_2Si_3O_{10}\cdot 2H_2O$ – aluminum silicate) [6]. Increased use of household's detergents leads to their accumulation in the wastewater and natural aquatic ecosystems, causing a number of harmful effects on the microbial community and hydrobionts [7]. Numerous investigations showed that detergent causes anaerobic condition in aquatic ecosystems, disrupts cells structure of live beings, changes activities of their enzymes, *etc.* [8]. Various reports are available on the simulative effect of nonionic and ionic surfactants in fermentation

Correspondence: V.D. Jakovljević, University of Kragujevac, Faculty of Science, Institute of Biology and Ecology, Kragujevac, Serbia.
E-mail: jakovljevicvioleta@gmail.com
Paper received: 20 June, 2013
Paper accepted: 6 September, 2013

broth of microorganism, this resulted in many fold increases in the production and secretion of enzyme such as cellulase [9], phytase [10] and amylase [11]. Inclusion of nonionic surfactants, Tween 80 into culture medium increases extracellular protease activity without altering of enzyme properties [12]. Also, it was found that addition of detergent have enhancing effects on extracellular production of some metabolites with microorganism [13] and may be useful method for over-production of hydrophobic compounds by means of biological process. The *Fusarium oxysporum* is mesophilic fungus ubiquitous in soils worldwide. It commonly inhabits aquatic ecosystems and wastewater with high rate of organic matter. The fungus *F. oxysporum* produces severe hydrolytic enzymes which were found to be active on a wide range of natural substrates of either vegetable or animal origin, *e.g.*, lipases, cellulases, hemicellulases, pectinases, xylanases, *etc*. Lignocellulolytic enzyme produced by *F. oxysporum* has been used for conversion of lignocellulosic material to ethanol [14].

The aim of this study was to investigate how commercial detergent (Merix, Henkel, Serbia) and its mainly components at concentration of 0.1% influence on metabolic process of fungus *Fusarium oxysporum* under submerged fermentation during exponential growth phase. The submerged culture technique is widely used for biotechnological application as it is intrinsically less problematic, making it more reliable and reproducible easier to monitor and to control key operational parameters and it is more flexible.

EXPERIMENTAL

Isolation of *Fusarium oxysporum* and cultivation

The fungus species *F. oxysporum* was isolated from the river basin of Lepenica (the place of wastewater flood, sewage). Identification of fungus from a sample of wastewater was carried out at the Institute for Biology and Ecology, University of Kragujevac. The fungus was maintained in a chamber with a constant temperature at 4±0.5 °C, on potato-dextrose agar slant (PDA), in sterile conditions. A monosporial culture was developed by the method of exhaustion on a poor agar, in Petri dishes, in sterile conditions. Meat peptone agar was used for sterility control. During the experiment, the fungus was cultivated in the sterile Czapek Dox liquid medium of the following composition (Table 1).

Erlenmeyer flasks with growth mediums were sterilized at 120 °C for 20 min (autoclave pressure, 0.14 MPa). The pH control was adjusted about 4.70 before sterilization with 0.1 mol/dm^3 HCl.

Inoculation and sampling

The liquid growth mediums were stored in Erlenmeyer flask (100 ml of medium in 250 ml flask). Each flask was inoculated with one ml spore suspension of (1×10^4 CFU ml^{-1}) in three replicates. Erlenmeyer flasks were placed on an electric shaker (Kinetor-m, Ljubljana) thus enabling uniform and constant mixing. All experiments were carried out at room temperature, under alternate light and dark for 8 days. Sampling was started at 4th day after inoculation and repeated every day until the 8th day of the experiment which corresponding exponential growth phase of fungus. The exponential growth phase was confirmed by screening test on solid state fermentation (results of this test were no shown in this paper).

Measurement of pH and redox potential

pH-meter (type MA-5705, the product "Iskra", Kranj) was used for measuring value of pH and electrochemical potential. Redox potential was determined by Petersen's method [15].

Assays of proteolytic activity

Activity for the alkaline protease was determined spectrophotometrically by Anson's method, with casein as substrate [16]. Reaction mixture incubated at 37 °C for 10 min and arrested by addition of 1 ml 5% trichloroacetic acid (TCA). The mixture was centrifuged at 4000 rpm and the supernatant 5 ml of 6 % Na_2CO_3 and 1ml diluted Folin–Ciocalteu phenol reagent were added. The resulting solution was incubated at room temperature for 30 min and absorbance of the blue color developed was read at 660 nm using tyrosine standard. One unite enzyme activity (IU) was defined as the amount of enzyme that liberated 1μg of tyrosine from casein per minute under assay condition.

Table 1. Composition of growth media in 1000 ml distilled water

Growth medium	Mark	c / g dm^{-3}				Sucrose	Detergent[a]	TTP[b]	AOC[c]
		$NaNO_3$	K_2HPO_4	$MgSO_4\cdot7H_2O$	$FeSO_4\cdot7H_2O$				
Control	K	3	1	0.5	0.01	30	–	–	–
K + 0.1 % D	D	3	1	0.5	0.01	30	1		–
K + 0.1% TTP	TTP	3	1	0.5	0.01	30	–	1	–
K + 0.1 % AOC	AOC	3	1	0.5	0.01	30	–	–	1

[a]Detergent "Merix", Henkel, Kruševac; [b]sodium tripolyphosphate; [c]ethoxylated cetyloleyl alcohol

Protein assay

Protein was determined according to Kjeldahl, on the basis of the nitrogen amount present in the fungus tissue [17], according to the Eq. (1):

The quantity of proteins (mg) =
= 6.25×Quantity of nitrogen (1)

Determination of concentrations total and free organic acids

Concentrations of free and total organic acids were determinate by ion exchange chromatography method. To 10 ml of fermentation broth was added 50 ml of ethanol (70 %) and reaction mix was incubated at 70 °C in water bath for 1 h. The mixture was filtered through Whatman filter paper No. 1 and filtrate was concentrated at 50–60 °C under reduced pressure to final extract volume of 40 ml. Active charcoal was added to extract following by incubation (30 to 45 min) in the water bath at 70 °C. After incubation, the extract was filtrated to remove active charcoal, the residue was made up to a volume of 100 ml with distilled water. Ten milliliters aliquots of filtrate were sampling for determination of concentration the free organic acids by titration 0.1 mol/dm^3 NaOH. Phenolphthalein (0.1%) was used as indicator. The residual of sampling (90 ml) was passed through a cationic column (Amberlite IR-120) previously activated, to the volumetric flask of 250 ml. By washing the column with distilled water volumetric flask was supplemented to 250 ml. To determination of concentration the total organic acids, 25 ml aliquots were sampling and titration was carried out as previously described [18]. The results were presented as a percentage.

Determination of monosaccharides quantity

Monosaccharides, glucose and fructose were determined after passing 225 ml of filtrate through a previous activated anion column of type Amberlite IR-120 and after evaporation of filtrate to volume 5 to 10 ml. A small volume of sample was inflicted on paper chromatography Whatman No.1 and descending chromatography was performed. The quantity of glucose and fructose was measured by the spectrophotometer at 600 nm, followed by reaction with suitable reagent to produce a blue-green complex [19].

Determination of dry weight biomass

The mycelia previously removed from fermentation broth were washed with sterile distilled deionized water several times. Both filter paper and mycelia were then dried in an oven at 80 °C to a constant weight. The dry weight of the mycelia was determined by subtracting the initial weight of the filter paper from the weight of mycelia and filter paper.

RESULTS

The effects of detergent and its main components at a concentration of 0.1% on the metabolism of fungus *Fusarium oxysporum* are presented on Figs. 1–7. These effects were observed by the following biochemical parameters: pH, redox potential, proteolytic activity, quantity of proteins, organic acids and carbohydrates from 4th to 8th day, whereas total dry weight biomass was measured on 8th day.

The fungus *F. oxysporum* showed the express or slight decrease of pH value of fermentation broth. The maximum values of pH measured on 4th day in all variation of liquid growth medium except in control. The maximum deviation of pH value was observed in the medium with D and TTP at 0.1% concentration compared to control. The detergent at 0.1% concentration influenced on the significant increase of pH value whereas the TTP at 0.1% concentration influenced on the significant decrease of pH value, as shown in Fig. 1.

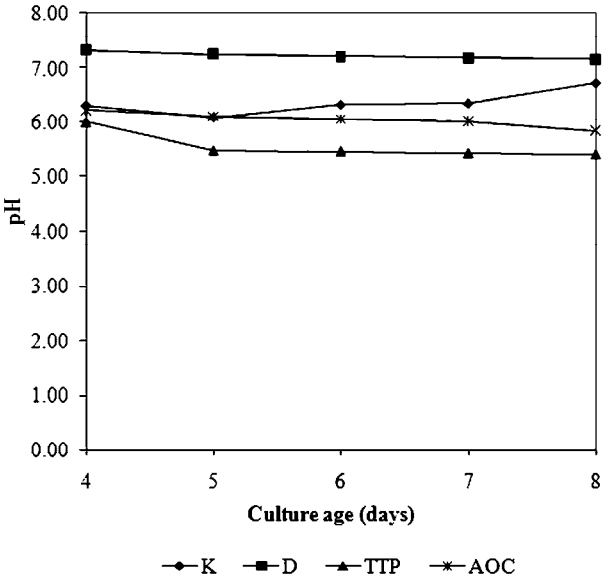

Fig. 1. pH value of different media during growth of fungus F. oxysporum.

Redox potential of the fungus *F. oxysporum* grown in all variants of liquid nutrient medium had a positive value throughout the experimental period, with exception in medium with detergent (negative value). Increasing values of redox potential proceeded in parallel with the development of mycelia, the maximum values were measured on 7th day (control medium) and on 8th day (TTP and AOC media). The results are shown in Fig. 2.

The proteolytic activities of the fungus *F. oxysporum* in the liquid growth medium according to Czapek (the control) and the variants of liquid medium with D, TTP and AOC were particularly expressed on 6th or on 7th day. Presence of AOC in medium had stimulating effect

while the presence of detergent had inhibitory effect on proteolytic activity during the experimental period. The results are shown in Fig. 3.

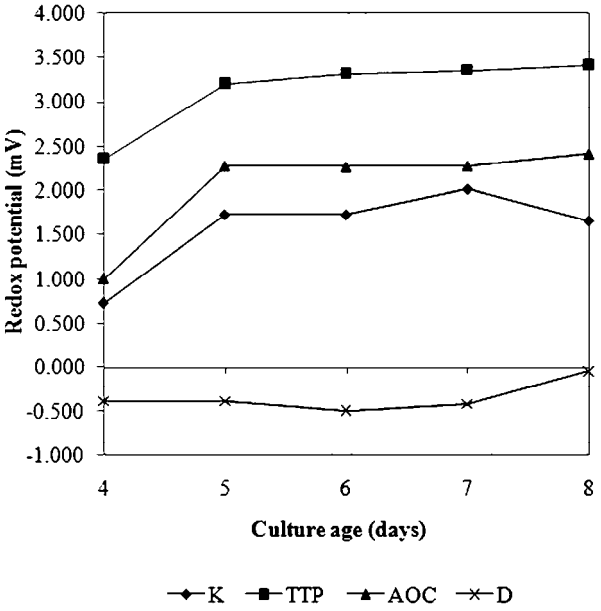

Fig. 2. Redox potential of different media during growth of fungus F. oxysporum.

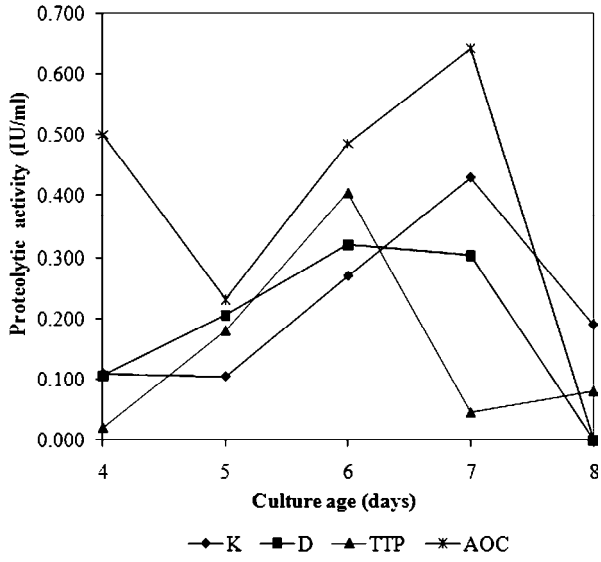

Fig. 3. Profile of proteolityc activity of F. oxysporum in different media during exponential growth.

Protein production increased in parallel with exponential mycelium growth, but concentrations of total protein was different in relation with type of medium. The highest amount of protein was produced by fungus in medium with TTP on the 7th day whereas the least amount of protein measured in medium with detergent at the same time of experiment. The results are shown in Fig. 4.

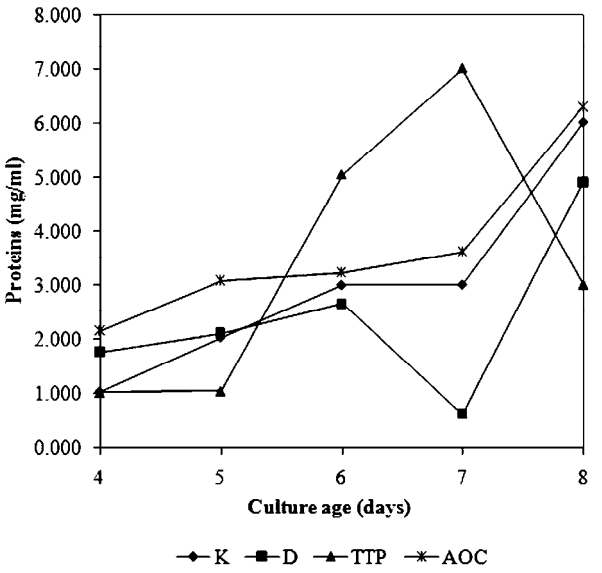

Figure 4. Concentrations of total proteins measured in different media during exponential fungal growth.

The concentration of total organic acids in the control medium and in the medium with AOC was considerably or significantly smaller on the 8th day compared to the 4th day. Contrary, the fungus *F. oxysporum* produced higher percent of total organic acids in the medium with D and TTP, at the same time. The fungus produced different concentration of free organic acids depending on the type of medium. The percentage of free organic acids was lesser in medium with detergent, but it was higher in the medium with TTP and AOC. The TTP showed strong inhibitory effect on the production of free organic acids in the early exponential growth phase, but a strong stimulatory effect in the late exponential growth phase. The results are shown in Fig. 5.

The concentration of glucose, produced by the fungus *F. oxysporum,* was significantly higher in the growth medium with D and AOC at concentration of 0.1% on the 8th day in relation to the control. The presence of AOC in growth medium reduced the concentration of fructose to half while the presence of D influenced on increase of concentration of fructose. The detergent showed the strongest stimulating effect on the bioproduction of glucose whereas ethoxylated cetyl-oleyl alcohol was the strongest stimulator of the fructose bioproduction compared to control, as shown in Fig. 6.

The amount of the total dry weight biomass of the fungus *F. oxysporum* grown in the control nutritious medium was significantly or slightly higher compared to the biomass of the same fungus grown in the variants of liquid media with D, TTP and AOC. Detergent and the sodium tripolyphosphate of 0.1% concentration showed the most significant inhibitory effect on the total dry weight biomass bioproduction in relation to the control (about 50%). The results are shown in Fig. 7.

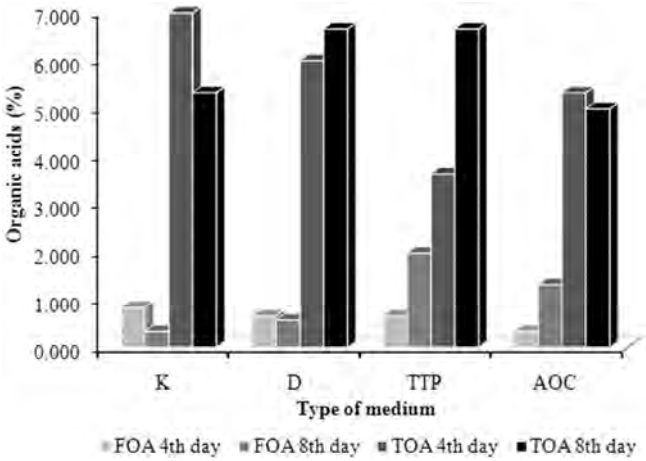

Fig. 5. Concentrations of free (mark-FOA) and total (mark-TOA) organic acids in different media in early and late exponential growth phases.

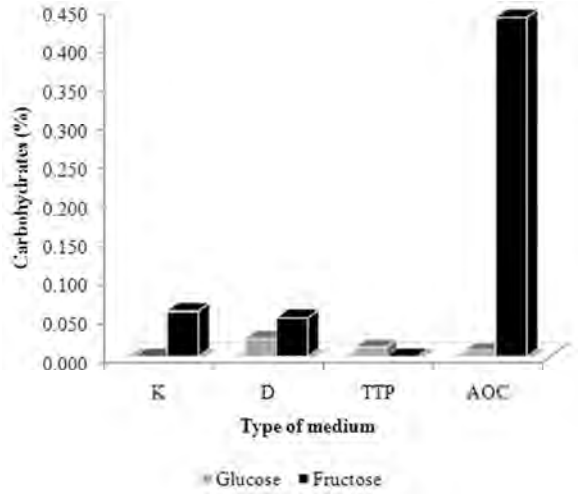

Fig. 6. Concentrations of glucose and fructose measured in different media.

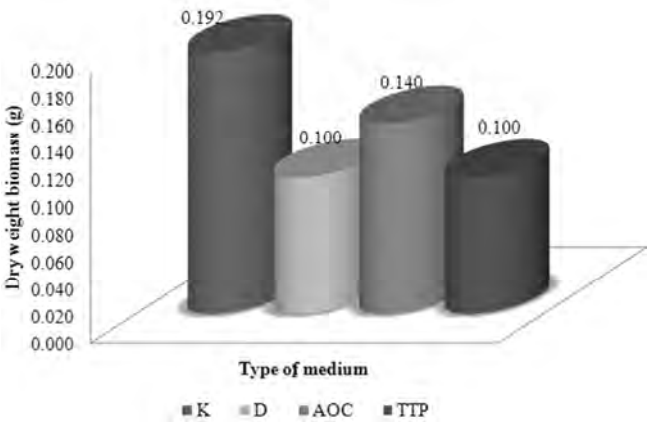

Fig. 7. The total dry weight biomass of fungus F. oxysporum produced in different media at 8th day.

DISCUSSION

The optimal pH environment is necessary for the regular growth and development of microorganisms. It affects the morph-physiological characteristics and biochemical properties of microorganisms. The different initial pH value occurs with addition of detergent and its components in growth media, but these differences aren't influence on the spores germinating and development of mycelia. St Leger *et al.* [20]

observed that *F. oxysporum* tolerated a wide range of pH values. However, these pollutants change metabolic activity of fungus on different ways, which reflects on fungal growth and total dry weight biomass. The utilization of nutrients from growth media changes the pH values. Simultaneously, with changes in pH values and redox potential is changing too. This implies the role of organic acids in pH homeostasis and growth of fungus in a flexible media with detergent and its components. Increase of glucose and fructose concentration in the medium leads to acidification or pH reduction indicating that the acidity of medium originates from organic acids which are released by glycolysis and Krebs cycle. Production of organic acids depends both on the microorganism and source of P in which the microorganism is grown. Many researchers observed that the accumulation of oxalic acid in the cytoplasm can help regulate cytoplasmic pH. Strasser *et al.* [21] reported that oxalic acid is produced in citoplasm of *Aspergillus niger* with little or no participation of the tricarboxylic acids cycle. The chemical composition of commercial detergent is very complex and consists of a mixture of active components, builders, fillers, phosphates, bleach, *etc*. Each of these components can react with active center of the enzyme, leading to their inhibition or activation, which reflects on growth and development of fungi. On the other hand, the individual components of detergent, as substrates for nutrition, are far more acceptable for fungi. As we predicted, the treatment with detergent, AOC and TTP, led to the production of different amounts of free and total organic acids. The quantity of free organic acids was insignificantly lesser in the medium with detergent, but it was significantly higher in the medium with TTP and AOC at the end of experimental period. Many researchers observed that many fungi species produce different organic acids in medium with polyphosphates because of solubilization of P. In the case of the total organic acids bioproduction, the TTP is behaving as a significant stimulator while the detergent is insignificant stimulator of bioproduction. At the same time, the AOC is behaving as an inhibitor of the total organic acids bioproduction.

The presence of detergent, AOC and TTP, in the liquid growth medium affects the production of different protein concentration during the fungal exponential growth. With culture aging, fungus produced higher amount of proteins in control and AOC media probably due to increasing of N consumption from these media. On the 7^{th} day of the experiment, significant changes of proteins bioproduction were observed in medium with D and TTP. The production of protein was rapidly decreased in D medium whereas the opposite effect was observed in TTP medium. These results are in accordance with the results of other authors which observed that. According to Scervino *et al.* [22] consumption of N increases with decreasing of phosphates concentration, which is in agreement with results of this study. Also, our previous studies on other filamentous fungi [23,24] confirmed that pollutants such as LAS detergent type have inhibitory effect on protein bioproduction.

The proteolytic activity of the fungus *F. oxysporum* was expressed in late exponential phase of fungal growth (6^{th} or 7^{th} day). Inclusion of AOC in growth medium showed significant stimulatory effect on proteolityc activity whereas the treatment with the detergent and TTP had inhibitory effect on proteolytic activity. As well known, numerous microorganisms have ability to synthesized different proteases depending on type of medium. The protease of *Bacillus* species showed excellent stability and compatibility with some commercial detergents [25]. However, anionic surfactants, such as SDBS and SDS, express strong inhibitory effect on enzymes activity in the most of microorganisms [26,27]. Polar heads of SDS or SDBS bind to the active site of the enzyme through ionic interaction which causes conformational changes of enzymes. Nonionic surfactants type of ethylene oxides bind to the active site of enzymes through hydrogen bonds in order to enhance the conformation flexibility. In agreement with observations of Pradhan and Sukla [28] and Scervino *et al.* [29] our experiment confirms the hypothesis that solubilization of P is related with releasing of organic acids in medium. Many researchers observed relation between the beginning of autolysis after depletion of the exogenous carbon source and proteolytic activity to a greater or lesser degree in various species of filamentous fungi [30–32]. However, it is not uncommon for the maximum of proteolytic activity to coincide with the growth phase [33], which it was confirmed by our investigation. Similar observations with *A. fumigatus* and *N. crassa* suggest that this phenomenon can be widespread among fungi.

The concentration of carbohydrates (glucose and fructose) was measured in fermentation broth of growth medium on the 8^{th} day. Fungal metabolism of carbohydrates is influenced by the composition of growth medium. When sucrose is only carbon source, the fungus utilizes preferably glucose than fructose for its metabolism which is consistent with the results of Peynaud and Domercq [34]. Because of that, the concentration of glucose is very low compare to fructose in liquid medium by Czapek. As well known, under aerobic condition the fungus *F. oxysporum* metabolizes glucose *via* Embden–Meyerhof–Parnas (EMP) pathway, resulting in high acetic acids production, while under anaerobic condition of the glucose is metabolized via pentose phosphate pathway (PPP) resulting in high ethanol production [35]. The inclusion of D, AOC and TTP leads to decreasing of glucose incorporation in biomass and

its higher concentration in medium. The detergent shows the highest inhibitory effect on glucose metabolism. Interesting, TTP and detergent added in medium showed the stimulatory effect on fructose metabolism and its incorporation in fungal biomass. On the contrary, AOC shows the highest inhibitory effect on metabolism fructose and its incorporationin biomass. This striking difference in the utilization of sugars could be caused either by differences in the transport systems or by the subsequent intracellular metabolism of the sugars [36]. Probably, detergent and TTP influence on synthesis of inducible enzymes involving in regulation of carbohydrates metabolism or some degradation products have a role of competitive inhibitor of these enzymes. These results are in accordance with the results of other authors and our previous studies on other filamentous fungi [37,38].

The total dry weight biomass which the fungus *F. oxysporum* produced during the exponential growth was measured on 8th day. The total amount of biomass of the fungus grown in control is higher compare to media with the detergent, AOC and TTP. These results confirm that these compounds behavior as inhibitors on the bioproduction of biomass. Detergent and the sodium tripolyphosphate at 0.1% concentration show the significant inhibitory effect on the total biomass (about 50%), while the AOC showed little inhibitory effect compared to control.

CONCLUSION

Based on the obtained results it can be concluded that detergent and its components influence on fungal metabolism in different way. These pollutants didn't express fungicide effect, but they have inhibitory influence on total dry weight biomass production at different rates. Inclusion of pollutants in growth medium causes production of different metabolites which could have practical application in biotechnology. The alkaline protease from fungus is stimulated by the presence of AOC, so it could have potential utilization for catalysis and application in detergent formulation. High solubilization of P in medium with TTP indicated the potential role of *F. oxysporum* in bioremediation of environment. The production of higher amount of organic acids is stimulated by detergent and its components, so the fungus could be applied in different industrial area. The fungal ability to produce different amount of glucose and fructose could be practically applied in biotechnology.

Acknowledgments

This research was financially supported by Ministry Education, Science and Technological Development of the Republic of Serbia (Grant No. III 43004).

REFERENCES

[1] E.Z. Ron, E. Rosenberg, Biosurfactants and oil bioremediation, Curr. Opin. Biotechnol. **13** (2002) 249–252.

[2] C.N. Mulligan, Environmental applications of biosurfactants, Environ. Pollut. **133** (2005) 183–198.

[3] J. Palicka, Development and trends in the European laundry detergent market, in Proceedings of 3rd International Symposium "Forum Chemiczne", Warsaw, Poland, 1997, pp. 37–42.

[4] G.-G. Ying, Fate, behaviour and effects of surfactants and their degradation products in the environment, Environ. Int. **32** (2006) 417–431.

[5] S.S. Talmage, Environmental and Human Safety of Major Surfactants Lewis Publishers, Boca Raton, FL, 1994.

[6] V. Pattusamy, N. Nandini, K. Bheemappa, Detergent and Sewage Phosphates entering into Lake Ecosystem and Its Impact on Aquatic Environment, Int. J. Adv. Res. **1** (2013)129–133.

[7] V. Chaturvedi, A. Kumar, Toxity of sodium dodecyl sulfate in fishes and animals, IJABPT **1** (2010) 630–633.

[8] J.L. Berna, J. Ferrer, A. Moreno, D. Prats, F. Ruiz, The fate of LAS in the environment, Tenside Surf. Det. **26** (1989) 101–107.

[9] A.G. Pardo, Effect of surfactants on cellulose production by *Nectria catalinensis*, Curr. Microbiol. **33** (1996) 275––278.

[10] A. Ebune, S. A1-Asheh, Z. Duvnjak, Effects of phosphate, surfactants and glucose on phytase production and hydrolysis of phytic acid in canola meal by *Aspergillus ficuum* during solid-state fermentation, Bioresource Technol. **54** (1995) 241–247.

[11] R.N.A. Rahman, L.P. Geok, M. Basri, A.B. Sale, Physical Factors Affecting the Production of Organic Solvent-tolerant Protease by *Pseudomonas aeruginosa* strain k, Bioresource Technol. **96** (2005) 429–436.

[12] E.C. Evans, A. Abdullahi, Effect Of Surfactant Inclusions On The Yield and Characteristics Of Protease From *Bacillus Subtilis*, Proc. Rom. Acad. Series B **2** (2012) 108––112.

[13] M. Muramatsu, C. Ohto, S. Obata, E. Sakuradani, S. Shimizu, Various oils and detergents enhance the microbial production of farnesol and related phenyl alcohols, J. Biosci. Bioeng. **106** (2008) 263–267.

[14] C. Xiros, P. Christakopoulos, Enhanced ethanol production from brewer's spent grain by a *Fusarium oxysporum* consolidated system, Biotechnol. Biofuels., 2009, doi: 10.1186/1754-6834-2-4.

[15] G.K. Petersen, Redox measurements: Their Theory and Technique, Radiometer A/S, Copenhagen, 1966.

[16] M.L. Anson, The estimation of pepsin, trypsin, papain and cathepsin with hemoglobin. J. Gen. Physiol. **22** (1938) 79–89.

[17] J.J. Laukevics, A.F. Apsite, U.E. Viesturs, R.P. Tengerdy, Solid substrate fermentation of wheat straw to fungal protein, Biotechnol. Bioeng. **26** (1984) 1465–1474.

[18] W.A. Bulen, J.E. Varner, R.C. Burrell, Separation of organic acids from plant tissues, Anal. Chem. **24** (1952) 187–190.

[19] D. Veličković, A contribution to Study of Aminoacidic Composition Dynamics of the Protein Complex and Free Amino Acids in Apple Fruits During the Vegetative Period and Storage, PhD Thesis, University of Belgrade, Belgrade, 1971.

[20] R.J. St Leger, L. Joshi, D. Roberts, Ambient pH is a major determinant in the expression of cuticle-degrading enzymes and hydrophobin by *Metarhizium anisopliae*, Appl. Environ. Microbiol. **64** (1998) 709–713.

[21] H. Strasser, W. Burgstaller, F. Schnner, High-yield production of oxalic acids for metal leaching process by *Aspergillus niger*, FEMS Microbiol. Lett. **119** (1994) 365––370.

[22] J.M. Scervino, V.L. Papinutti, M.S. Godoy, M.A. Rodriguez, I. Della Monica, M.J. Pettinari, A.M. Godeas, Medium pH, carbon and nitrogen concentrations modulate the phosphate solubilization efficiency of *Penicillium purpurogenum* through organic acid production, J. Appl. Microbiol. **110** (2011) 1215–1223.

[23] P.E.A. Asea, R.M.N. Kucey, J.W.B. Stewart, Inorganic phosphate solubilization by two *Penicillium* species in solution culture and soil, Soil Biol. Biochem. **20** (1988) 459–464.

[24] J. Stojanović, F. Barbič, D. Veličković, J. Vučetić, Z. Prolić, Influence of detergent on the biochemical processes of some fungi under in vitro conditions, Acta Veterinaria **44** (1994) 329–336.

[25] M. Mala, S. Srividya, Partial purification and properties of a laundry detergent compatible alkaline protease from a newly isolated *Bacillus* species Y, Indian J. Microbiol. **50** (2010) 309–317.

[26] S.Ž. Grbavčić, D.I. Bezbradica, I.M. Karadžic, Z.D. Knežević-Jugovic, Lipases And Proteases Produced By Indigenous *Pseudomonas Aeruginosa* Strain As Potential Detergent Additives, Hem. Ind. **63** (2009) 331–335.

[27] L.T. Izrael Zivkovic, G.D. Gojgic-Cvijovic, K.R. Gopcevic, M.M. Vrvic, I.M. Karadzic, Enzymatic characterization of 30 kDa lipase from *Pseudomonas aeruginosa* ATCC 27853, J. Basic Microbiol. **49** (2009) 452–462.

[28] N. Pradhan, L.B. Sukla, Solubilization of inorganic phosphates by fungi isolated from agriculture soil, Afr. J. Biotechnol. **5** (2005) 850–854.

[29] J.M. Scervino, M.P. Mesa, I.D. Mónica, M. Recchi, N.S. Moreno, A. Godeas, Soil fungal isolates produce different organic acid patterns involved in phosphate salts solubilization, Biol. Fertil. Soils. **46** (2010) 755–763.

[30] S. White, M. McIntyre, D.R. Berry, B. McNeil, The autolysis of industrial filamentous fungi, Crit. Rev. Biotechnol**. 22** (2002) 1–14.

[31] F. Santamaria, F. Reyes, Proteases produced during autolysis of filamentous fungi, Trans. Br. Mycol. Soc. **91** (1988) 217–220.

[32] F. Reyes, R. Lahoz, P. Cornago, Autolysis of *Neurospora crassa* in different culture conditions and release of *β*-*N*--acetyl-glucosaminidase and chitinase, Trans. Br. Mycol. Soc. **68** (1977) 357–361.

[33] G.U.L. Braga, R.H.R. Destefano, C.L. Messias, Oxygen consumption by *Metarhizium anisopliae* during germination and growth on different carbon sources, J. Invert. Pathol. **74** (1999) 112–119.

[34] E. Peynaud, S. Domercq, Sur les espbces de levures fermentant selectivement le fructose, Ann. Institut Pasteur **89** (1955) 346–351.

[35] G. Panagiotou, S.G. Villas-Bôas, P. Christakopoulos, J. Nielsen, L. Olsson, G. Panagiotou, Intracellular metabolite profiling of *Fusarium oxysporum* converting glucose to ethanol, J. Biotechnol. **115** (2005) 425–434.

[36] W. Emmerich, F. Radler, The Anaerobic Metabolism of Glucose and Fructose by *Sucharomyces bailii*, J. Gen. Microbiol. **129** (1983) 3311–3318.

[37] J. Stojanović, V. Jakovljevic, I. Matović, O. Gajović, Z. Mijušković, T. Nedeljković, Influence of detergent on metabolic activity of fungi Aspergillus niger, Natural Sci. **3** (2011) 466–470.

[38] J. Stojanović, J. Milićević, O. Gajović, V. Jakovljević, I. Matović, Z. Mijušković, T. Nedeljković, The effects of detergent, sodium tripoly-phosphate and ethoxyled oleylcetyl at metabolic parameters of the fungus *Trichothecium roseum* Link**,** Arch. Biol. Sci. **63** (2011) 1001––1006.

IZVOD

UTICAJ DETERGENTA I NJEGOVIH KOMPONENTI NA METABOLIZAM *Fusarium oxysporum* U SUBMERZNOJ FERMENTACIJI

Violeta D. Jakovljević[1], Jasmina M. Milićević[1], Jelica D. Stojanović[1], Slavica R. Solujić[2], Miroslav M. Vrvić[3]

[1]*Univerzitet u Kragujevcu, Prirodno–matematički fakultet, Institut za biologiju i ekologiju, Kragujevac, Srbija*
[2]*Univerzitet u Kragujevcu, Prirodno–matematički fakultet, Institut za hemiju, Kragujevac, Srbija*
[3]*Univerzitet u Beogradu, Hemijski fakultet, Beograd, Srbija*

(Naučni rad)

U ovom radu ispitivan je uticaj detergenta (“Merix”, Henkel, Kruševac) i njegovih komponenti (natrijum-tripolifosfata i etoksilovanog cetil-oleil alkohola) 0,1% koncentracije na enzimsku i metaboličku aktivnost gljive *Fusarium oxysporum* tokom eksponencijalne faze rasta. Ova vrsta gljive je izolovana iz rečnog korita reke Lepenice na mestu ulivanja otpadnih voda u reku. Praćene su promene sledećih biohemijskih parametara: pH, redoks potencijala, proteolitičke aktivnosti, produkcije ugljenih hidrata, slobodnih i ukupnih organskih kiselina, proteina i ukupne suve biomase. Dodatak detergenta u hranljivu podlogu je izazvao značajno smanjenje redoks potencijala, blago povećanje pH, koncentracije glukoze i ukupnih organskih kiselina, dok je proteolitička aktivnost bila trostruko intenzivnija u odnosu na kontrolu. Dodatak natrijum-tripolifosfata u hranljivu podlogu uticao je na blago smanjenje pH, značajno povećanje redoks potencijala i količine glukoze, slobodnih i ukupnih organskih kiselina, dok je proteolitička aktivnost bila izražena samo 5. i 6. dana. Ukupna suva biomasa gljive *Fusarium oxysporum* bila je blago inhibirana prisustvom etoksilovanog cetil-oleil alkohola ali značajno inhibirana prisustvom detergenta i natrijum-tripolifosfata u podlozi.

Ključne reči: Biomasa • Etoksilovani cetil-oleil alkohol • Natrijum-tripolifosfat • Organske kiseline • Proteini • Proteolitička aktivnost

Uklanjanje magnezijuma iz izvorske vode pomoću prirodnog zeolita u protočnom sistemu

Slavica Tomić, Milena Knežević, Nevenka Rajić, Dragan Povrenović

Univerzitet u Beogradu, Tehnološko–metalurški fakultet, Karnegieva 4, Beograd, Srbija

Izvod

Cilj ovog rada je ispitivanje mogućnosti primene srpskog prirodnog zeolita (ležište „Igroš Vidojević“ kod Brusa) za poboljšanje kvaliteta izvorske vode. Koncentracija magnezijuma u izvorskoj vodi u regionu Raška (jugozapad Srbije) je veća od 100 mg/dm^3 i nepogodna za svakodnevnu upotrebu. U eksperimentima su izvršena fluidomehanička ispitivanja čestica zeolitskog tufa prečnika 1,5, 4 i 6 mm u koloni prečnika 65 mm, dok su ispitivanja adsorpcije/desorpcije magnezijuma izvedena u koloni prečnika 110 mm. Dobijeni rezultati su pokazali da se upotrebom zeolita koji je obogaćen natrijumom i uz odgovarajuće fluido mehaničke parametre sistema, koncentracija magnezijuma u sirovoj vodi može smanjiti ispod maksimalno dozvoljene koncentracije (MDK) u vodi za piće od 50 mg/dm^3.

Ključne reči: magnezijum, zeolit, adsorpcija, hemijska modifikacija, protočni sistem.

Dostupno na Internetu sa adrese časopisa: http://www.ache.org.rs/HI/

NAUČNI RAD

UDK 549.67(497.11–14):556:66.081.3

Hem. Ind. **68** (4) 475–482 (2014)

doi: 10.2298/HEMIND130709073T

Zbog rasprostranjenosti u zemljinoj kori, magnezijum je prisutan u prirodnim vodama, gde zajedno sa kalcijumom čini ukupnu tvrdoću vode. Koncentracije Mg jona su posebno visoke na području gde dominiraju dolomitske stene, što je slučaj sa podzemnim vodama u okolini Raške (jugozapadna Srbija). Na ovom području prirodne vode se odlikuju visokim sadržajem Mg čija koncentracija može biti i do 200 mg/dm^3, što ih čini nepovoljnim za upotrebu u javnom vodosnabdevanju, pošto je maksimalna dozvoljena koncentracija Mg u vodi za piće prema važećim pravilnicima ograničena na 50 mg/dm^3 [1].

U eksperimentima prikazanim u ovom radu razmatrano je smanjenje koncentracije magnezijuma u vodi koja izvire u napuštenom rudarskom oknu „Potkop“. Ova voda je pokazala stabilan sastav i zanemarljivo prisustvo mikroorganizama, pa je kao takva uvedena u sistem vodosnabdevanja grada Raške. Jedini nedostatak predstavlja visok sadržaj Mg koji se kreće i do 100 mg/dm^3. Do sada se ovaj problem prevazilazio mešanjem vode sa rečnom vodom kako bi se vrednost Mg svela u dozvoljene okvire. Međutim, kako je rečna voda promenljivog sastava, to je ona često uzrokovala smanjenje kvaliteta sirove vode, a time i povećanje utroška velikih količina koagulanata i flokulanata kako bi se obezbedila njena fizičko-hemijska ispravnost.

Prirodni zeoliti su već poznati kao dobri adsorbenti i jonoizmenjivači, [2,3]. Takođe, različiti sintetički zeoliti (NaX, NaY i NaA) našli su primenu u postupcima omekšavanja vode. Međutim, efikasnost sintetičkih zeolita u smanjenju koncentracije Mg u tvrdoj vodi različita je za različite zeolite, pa se upotrebom zeolita NaA koncentracija može smanjiti za 24%, dok se upotrebom NaY postiže efikasnost od 52% [4].

U ovom radu za smanjenje koncetracije magnezijuma u sirovoj vodi iz izvorišta „Potkop“ ispitan je zeolitski tuf iz ležišta „Igroš Vidojević“ kod Brusa, koji sadrži oko 90% klinoptilolita. Prethodnim ispitivanjima [5], utvrđen je hemijski sastav klinoptilolitne faze u tufu. S obzirom na to da se efikasnost uklanjanja magnezijuma iz vode povećava kada se klinoptilolit obogati natrijumom, u eksperimentima je korišćen zeolitski tuf obogaćen jonima natrijuma (NaZ). U laboratorijskim eksperimentima koji su izvedeni u pojedinačnim serijama, prethodno je utvrđeno da NaZ može maksimalno da veže 2,5 mg Mg /g [5].

EKSPERIMENTALNI SISTEM

U eksperimentima je korišćen zeolitski tuf (Z) u sirovom obliku, sa frakcijama ekvivalentnih prečnika zrna 1,5, 4 i 6 mm. Za određivanje fluido-mehaničkih parametara korišćena je kolona prečnika 60 mm i visine 2 m, slika 1a. Ova kolona je omogućavala režime rada od nasutog i fluidizovanog sloja pa do uslova hidrauličkog transporta. Kroz kolonu (1) sa nasutim slojem zeolita (2), je kroz distributor na dnu (3), dovođena voda iz rezervoara (5), pomoću centrifugalne dozir pumpe (6). Merenje protoka je vršeno elektromagnetnim meračem protoka (7), a protok je regulisan pomoću ventila sa finom regulacijom (8). Vrednosti padova pritisaka na dnu kolone i na visini od 1 m, merene su pomoću piezometarskih cevi (9). Voda je iz kolone izvođena preko prelivnika (4), koji je imao i funkciju sakupljanja čestica u režimu rada sa hidrauličkim transportom, a nakon toga ponovo vraćana u rezervoar (5).

Prepiska: D. Povrenović, Univerzitet u Beogradu, Tehnološko–metalurški fakultet, Karnegieva 4, Beograd, Srbija.
E-pošta: povrenovic@tmf.bg.ac.rs
Rad primljen: 9. jul, 2013
Rad prihvaćen: 26. septembar, 2013

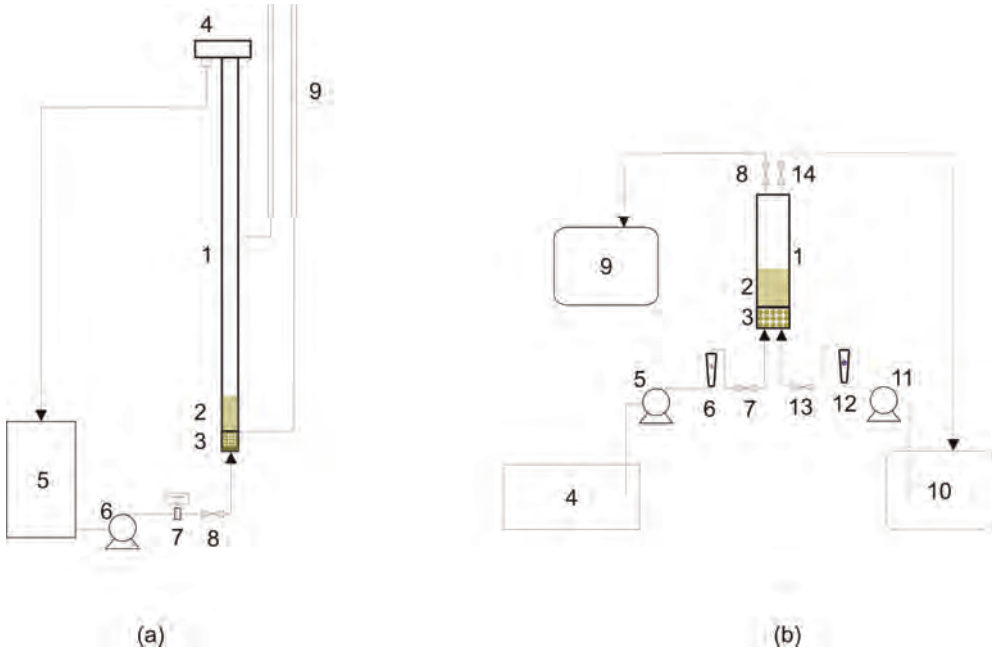

Slika 1. Šema eksperimentalne aparature za: a) određivanje fluido-mehaničkih parametara čestica zeolita (1 – kolona, 2 – sloj zeolita, 3 – distributor fluida, 4 – prelivnik, 5 – rezervoar, 6 – dozir pumpa, 7 – elektromagnetni merač protoka, 8 – regulacioni ventil, 9 – piezometri) i b) filtriranje vode kroz zeolitsku ispunu, i njegova regeneracija pomoću rastvora NaCl (1 – kolona, 2 – sloj zeolita, 3 – distributor fluida, 4 – rezervoar, 5 – dozir pumpa, 6 – rotametar, 7 – regulacioni ventil, 8 – ventil, 9 – sabirni rezervoar, 10 – rezervoar za NaCl (aq), 11 – dozir pumpa, 12 – rotametar, 13 – regulacioni ventil, 14 – ventil.
Figure 1. Scheme of the experimental units for: a) determination of the fluid-mechanical parameters of the zeolite particles (1 – column, 2 – zeolite bed, 3 – fluid distributor 4,5 – overflow tank, 6 – dosing pump, 7 – electromagnetic flowmeter, 8 – control valve, 9 – piezometers) and b) water filtering through the zeolitic filler, and recovering of the filler with a solution of NaCl (1 – column, 2 – zeolite bed , 3 – fluid distributor, 4 – tank, 5 – dosing pump, 6 – rotameter, 7 – control valve, 8 – valve, 9 – collection tanks, 10 – tank for NaCl (aq), 11 – dosing pump, 12 – rotameter, 13 – control valve, 14 – valve).

U eksperimentima adsorpcije, korišćena je staklena kolona prečnika 110 mm i ukupne radne zapremine od 3,9 dm^3, slika 1b. Na osnovu fluido-mehaničkih ispitivanja, za ispunu u koloni (1) odabrana je frakcija zeolita sa česticama prečnika 1,5 mm, ukupne mase 1 kg, koji je zauzimao zapreminu od 1,3 dm^3, odnosno 1/3 radnog dela zapremine kolone (2). Izmerene vrednosti gustina i nasipna gustine zeolita iznosile su 1915 i 763 kg/m^3, redom. Voda je u kolonu dovođena kroz raspodeljivač od inertnih staklenih sfera prečnika 6 mm, postavljenog na dnu kolone (3), iz rezervoara sirove vode (4), pomoću centrifugalne dozir pumpe (5). Protok vode je meren rotametrom (6), a regulacija protoka je vršena pomoću ventila (7). Na izlazu iz kolone je postavljen ventil (8) koji je imao funkciju da zatvori liniju vode, prema sabirnom rezervoaru za prečišćenu vodu zapremine 50,0 dm^3 (9). Brzina proticanja vode u izvedenim eksperimentima kretala se u intervalu od 0,05 do 0,15 mm/s, što odgovara uslovima tzv. spore filtracije.

Nakon zasićenja sloja zeolita magnezijumom, vršena je njegova regeneracija u protočnom sistemu sa recirkulacijom, pri čemu je brzina proticanja rastvora za regeneraciju odgovarala vrednosti brzina vode u koloni, pri kojoj je eksperiment izvođen, odnosno u intervalu od 0,05 do 0,15 mm/s. Nakon zatvaranja ventila (7) i (8), otvarani su ventili (13) i (14) i iz tanka sa rastvorom NaCl, koncentracije 2 mol/dm^3 (10), je pomoću dozir pumpe (11), uz merenje protoka rotametrom (12) i regulacijom protoka ventilom (13) dovođen rastvor za regeneraciju u sloj zeolita. Nakon određenog vremena regeneracije, ventili (13) i (14) su zatvarani i sistem je bio spreman za novi ciklus adsorpcije.

Koncentracija Mg u vodi određivana je pre i nakon prolaska kroz kolonu. Koncentracija Mg i Ca u alikvotima filtrata analizirana je svakih sat vremena. Za analizu je korišćena kompleksometrijska titracija pomoću EDTA uz indikatore eriohromcrno T i mureksid prema standardnom postupku [6]. Izvedene su najmanje tri analize pri svakom određivanju koncentracije. Koncentracija Na u sirovoj vodi i u filtratu odredjivana je metodom atomske apsorpcione spektroskopije (AAS).

REZULTATI I DISKUSIJA

Uz pomoć elektronskog mikroskopa koji obezbeđuje pored konvencionalne SEM fotografije i jasniji uvid o distribuciji elemenata na površini minerala, a na osnovu analize hemijskog sastava odabranih tačaka na zeolitu EDXS mapiranjem, određen je prosečan hemijski sastav uzoraka klinoptilolitne faze, koji je izražen preko oksida prisutnih elemenata prikazan u Tabeli 1 [5]. U zagradi su date vrednosti standardnih devijacija.

Tabela 1. Sastav klinoptilolitne faze u zeolitskom tufu (Z) i tufu obogaćenom natrijumom (NaZ) izražen preko oksida elemenata u mas.%
Table 1. Composition of clinoptilolitne phase in the zeolitic tuff (Z) and of the tuff enriched with sodium (NaZ) expressed as the mass% oxide of the elements

Oksid	Z	NaZ
SiO_2	67,9 (3)	67,04
Al_2O_3	11,9 (1,3)	11,97
Na_2O	0,12 (0,2)	4,08
K_2O	1,03 (0,4)	0,83
MgO	1,32 (0,2)	1,04
CaO	4,38 (0,1)	1,54
H_2O	13,4	13,5

Na osnovu rezultata prikazanih u Tabeli 1 može se zaključiti da je proces obogaćivanja zeolitskog tufa jonima natrijuma zapravo jonska izmena u kojoj se joni K, Mg, i Ca iz klinoptilolitne faze zamenjuju jonima natrijuma iz rastvora.

Osnovni cilj u fludo-mehaničkim ispitivanjima je bilo određivanje vrednosti minimalne brzine fluidizacije, U_{mf}, i ekspanzije zeolitskog sloja u funkciji brzine kretanja vode. Na osnovu urađenih eksperimenata sa različitim granulometrijskim vrednostima, dobijene su vrednosti minimalne brzine fluidizacije, Tabela 2.

Tabela 2. Vrednosti minimalne brzine fluidizacije za čestice prirodnog zeolita
Table 2 Minimum fluidization velocities of the zeolite particles

Ekvivalentni prečnik, mm	1,5	4,5	6
Minimalna brzina fluidizacije, m/s	0,013	0,035	0,054

Primenom krupnijih čestica, većim od 1 mm, stvaraju se uslovi za lakšu manipulaciju sa njima u samom adsorpcionom sloju, a uradjeni eksperimenti potvrđuju fluidno-mehaničku stabilnost sistema i reproduktivnost dobijenih rezultata. U eksperimentima procesa adsorpcije radjeno je sa najsitnijom raspoloživom granulacijom zeolita, srednjeg ekvivalentnog prečnika zrna, d_p = = 1,5 mm, jer je u procesu adsorpcije potrebna i što veća specifična površina ispune.

Analizom oblika zrna, nakon fotografisanja i analizom slike pomoću programa „Sigma Scan“, ustanovljena je njegova nesferičnost, što je i očekivano pošto se dobija drobljenjem mineralnih sirovina.

Za početnu visinu sloja od H_0 = 19 cm, vrednosti pada pritiska u funkciji brzine proticanja vode kroz kolonu prikazani su na slici 2, pri čemu se uočava nepostojanje izraženog pika vrednosti pada pritiska neposredno pre minimalne fluidizacije, a što je posledica polidisperznosti same ispune [7].

Pri uvođenju vode u sloj kroz dno kolone, dolazi do njegove blage ekspanzije i povećanja visine nasutog sloja do određene vrednosti. Daljim povećanjem protoka vode na dnu, odnosno brzine u koloni, dostignuta visina se ne menja sve do trenutka dok se ne dostigne vrednost minimalne brzine fluidizacije. Ta visina se označava kao visina sloja pri kojoj dolazi do pojave minimalne fluidizacije čestice, H_{mf}, za dati nasuti sloj čestica. Daljim povećanjem brzine strujanja vode kroz sloj čestica, dolazi do njegove ekspanzije, pa se u uslovima kada je brzina vode u sloju jednaka dvostrukoj vrednosti minimalne brzine fluidizacije, $U = 2U_{mf}$, može dostići ekspanizija sloja i preko 30% od one pri minimalnoj fluidizaciji, Slika 3.

Ekspanzija sloja, ne dovodi do povećanja pada pritiska u sloju, ali usled intenzivne mikrocirkulacije čestica u sloju, povećavaju se smicajne sile koje mogu dovesti i do drobljenja čestica zeolita. Stoga je u eksperi-

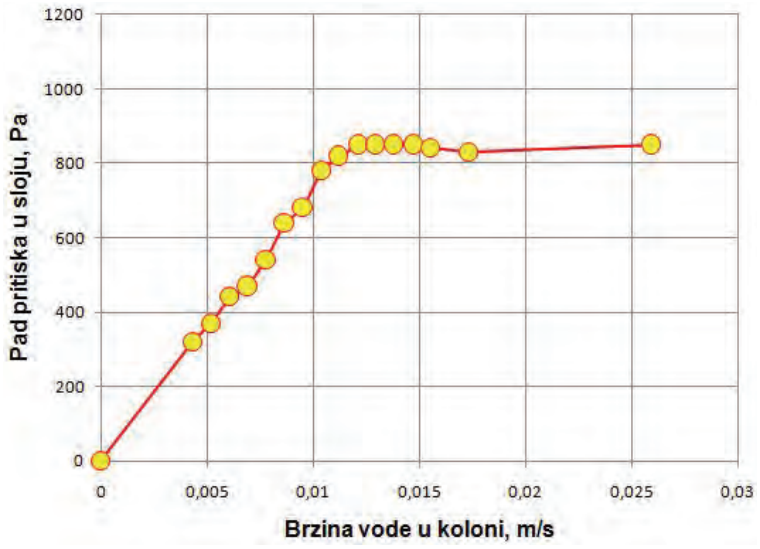

Slika 2. Određivanje vrednosti minimalne brzine fluidizacije čestica zeolita; d_p = 1,5 mm, H_0 = 19 cm.
Figure 2. Determination of the minimum fluidization velocity for the zeolite particles; d_p = 1,5 mm, H_0 = 19 cm.

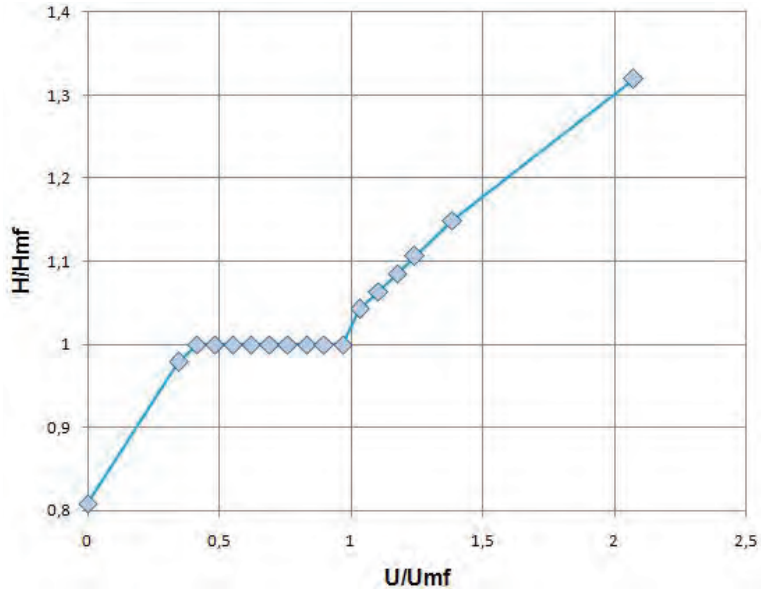

Slika 3. Ekspanzija sloja zeolita u funkciji povećanja brzine vode u koloni; d_p = 1,5 mm, H_0 = 19 cm.
Figure 3. The expansion of the zeolite bed as a function of increasing the water velocity through column; d_p = 1,5 mm, H_0 = 19 cm.

mentima adsorpcije korišćen opseg protoka daleko ispod vrednosti U_{mf}, od 0,05 do 0,15 mm/s, kako bi se utvrdila samo dinamika adsorpcije Mg na zeolitu, a izbegla pojava mogućeg drobljenja zrna i drugih uticaja fluidomehaničkih parametara. Adsorpcija u režimu visokih brzina vode i izražene turbulencije je predmet novih istraživanja.

U eksperimentima adsorpcije, rađeno je sa sirovom vodom iz izvorišta „Potkop“ u okolini Raške, čiji je kvalitet praćen u periodu od pet godina svakog dana za većinu parametara, dok je koncentracija teških metala određivana četiri puta godišnje i ti su rezultati prikazani u Tabeli 3.

Prikazane su maksimalne izmerene vrednosti nekih parametara u vodi iz izvorišta „Potkop“ u prethodnih 5 godina. Analize su vršene svakog dana za većinu parametara, dok su teški metali kontrolisani po četri puta godišnje. Određivanje pojedinih parametara rađeno je u pogonskoj laboratoriji vodovoda Raška, standardnim instrumentalnim i volumetrijskim metodama propisa-

Tabela 3. Maksimalne vrednosti osnovnih hemijskih parametara vode izvorišta Potkop analiziranih u periodu 2008–2012
Table 3. Maximum values of the basic chemical parameters of water from „Potkop“ spring analyzed for the period 2008–2012

Parametar	Vrednost ili koncentracija mg dm^{-3}	Maksimalna dozvoljena vrednost ili koncentracija mg dm^{-3}
pH	9.5	6.8–8.5
NTU	0.5	1.2
$KMnO_4$	8	8
Ca^{2+}	10	200
Mg^{2+}	90	50
SO_4^{2-}	7	250
NO_3^-	5	50
NO_2^-	0.005	0.03
NH_4^+	0.05	0.1
PO_4^{3-}	0.002	0.003

Element	Vrednost µg dm^{-3}	Maksimalna dozvoljena vrednost ili koncentracija µg dm^{-3}
B	2	300
Al	0.45	200
Cr	1.2	50
Mn	0.15	50
Fe	35	300
Ni	0.4	20
Cu	0.15	2000
Zn	0.4	3000
As	0.22	10
Se	0.26	10
Mo	0.02	70
Cd	0.003	3
Sb	0.01	3
Ba	0.41	700
Hg	0.05	1
Pb	0.02	10

nim za pojedine parametre [8]. Analiza sadržaja teških metala rađena je tehnikom masene spektrometrije sa indukovano spregnutom plazmom, na ICP-MS uređaju.

Rezultati adsorpcije dobijene pri brzini proticanja vode kroz sloj prirodnog zeolita od 0,05 mm/s, prikazani su na slici 4. Zapaža se da koncentracija jona kalcijuma u vodi, na početku procesa adsorpcije raste, dok u istom periodu koncentracija magnezijuma opada.

Ovo navodi na zaključak da tokom vezivanja Mg jona za prirodni zeolit dolazi do jonske izmene u kojoj Mg-joni zamenjuju Ca jone u rešetki zeolita. Zbog toga ne dolazi do značajne promene ukupne tvrdoće vode, već samo do promene molskog odnosa Ca/Mg. Takođe, ni u nastavku procesa ne dolazi do značajnije promene u tvrdoći vode što je prikazano na slici 5, gde je stepen tvrdoće vode izražen u sadržaju $CaCO_3$.

Ukupna količina vezanog Mg za zeolit iznosi 0,35 mg Mg/g Z, što je u skladu sa prethodnim ispitivanjima [3––5].

U protočnom sistemu sa istom kolonom gde je zeolit zamenjen modifikovanim zeolitom, NaZ, pri brzini strujanja vode od 0,05 mm/s, došlo je do povećanja stepena sorpcije Mg iz sirove vode bez srazmernog povećanja sadržaja Ca, Slika 6.

Sadržaj Mg je sa 85 mg/dm^3 u sirovoj vodi smanjen na 49 mg/dm^3 u zbirnom filtratu tj. za oko 42%. Ukupna količina vezanog Mg na NaZ iznosi 1,8 mg/g.

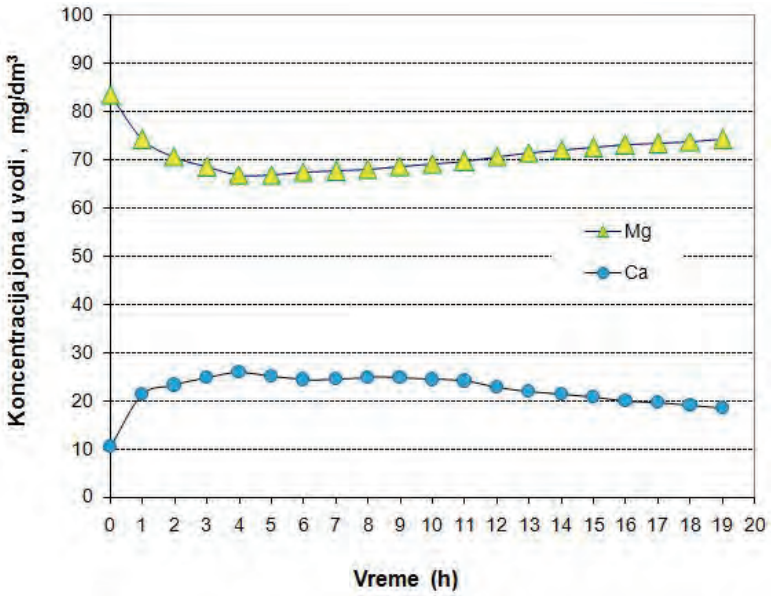

Slika 4. Promena koncentracije Mg i Ca u ukupnom filtratu u funkciji od vremena uzorkovanja.
Figure 4. Change of the concentration of Mg and Ca in the total filtrate volume as a function of time sampling.

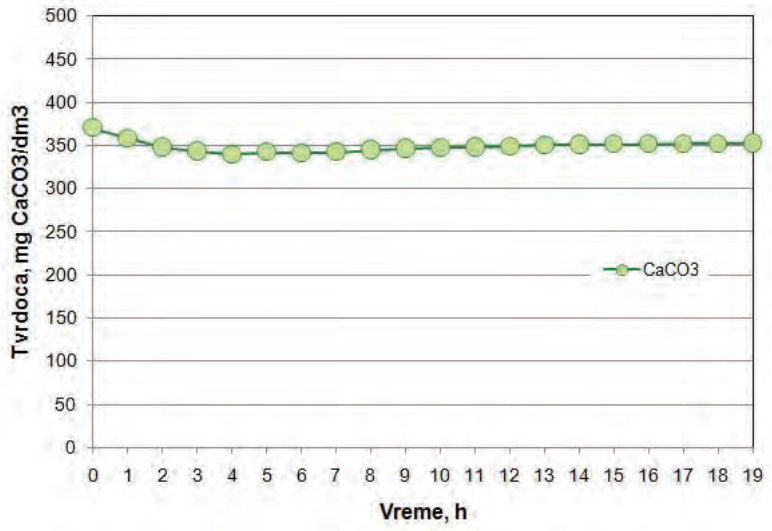

Slika 5. Zavisnost promene tvrdoće vode u ukupnom filtratu od vremena uzorkovanja.
Figure 5. Water hardness change in total filtrate volume as a function of time sampling.

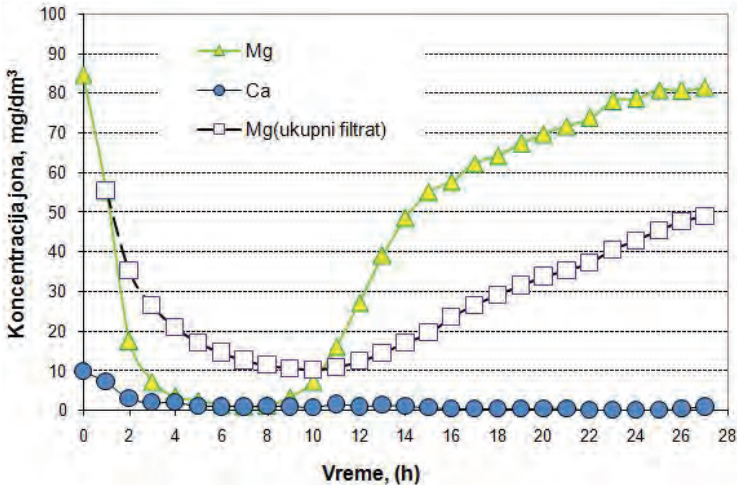

Slika 6. Promena koncentracije Mg i Ca u alikvotima filtrata sakupljanim na svakih sat vremena i koncentracija Mg u zbirnom filtratu.
Figure 6. Change of the concentration of Mg and Ca in aliquots collected every hour, and concentration of Mg in total filtrate volume.

Sadržaj Ca u filtratu je u odnosu na sirovu vodu smanjen sa 9,9 na 0,9, tj. oko 90%. Količina adsorbovanog Ca na 1 g zeolita je 0,45 mg/g. Sadržaj Ca u filtratu se smanjuje tokom filtriranja, što ukazuje da se i joni Ca vezuju za NaZ, što ima za posledicu smanjenje ukupne tvrdoće vode za oko 45 % , izražene u mg $CaCO_3$, slika 7.

Rezultati ukazuju da se upotrebom modifikovanog NaZ umesto prirodnog zeolita, Z, kao filterske ispune, povećava efikasnost zeolitskog filtra, na šta je ukazano i u dosadašnjim istraživanjima [9–12].

S obzirom na to da u filtratu dolazi do smanjenja sadržaja i Ca i Mg, može se zaključiti da NaZ istovremeno izmenjuje jone natrijuma iz rešetke sa jonima Ca i Mg iz vode. Ovo potvrđuje povećan sadržaj Na u filtratu u odnosu na sirovu vodu.Tako je određen sadržaj natrijuma u sirovoj vodi 0,698 mg/dm^3, a u zbirnom filtratu je povećan do koncentracije 24,09 mg/dm^3. No, kako je po važećem Pravilniku o higijenskoj ispravnosti vode za piće u Srbiji maksimalno dozvoljena koncentracija Na u vodi 150 mg/dm^3, to ovo povećanje njegove koncentracije ne predstavlja ograničavajući faktor za primenu NaZ u pripremi vode za piće.

Mogućnost regeneracije ispune zasićene magnezijumom (MgZ) ispitivana je tretiranjem MgZ pomoću 10 dm^3 rastvora NaCl koncentracije 2 mol/dm^3 u kružnom toku u toku 24 h i u predstavljenim rezultatima rađeno je sa brzinom u koloni od 0,05 mm/s.

Nakon završene regeneracije, radi utvrđivanja stepena desorpcije i efikasnosti procesa regeneracije, vršeno je ponovno filtriranje sirove vode u kojoj je koncentracija Mg i Ca iznosila 86, odnosno 10 mg/dm^3, pri istim fluidomehaničkim uslovima kao u prethodnom eksperimentu.

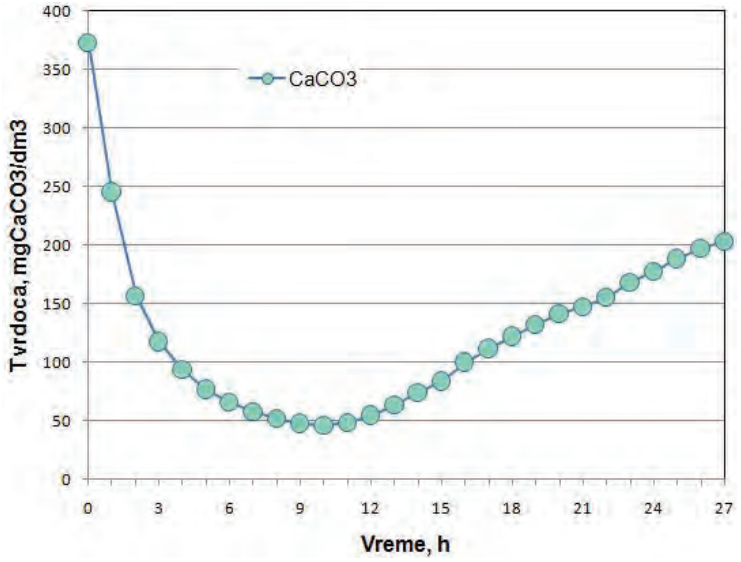

Slika 7. Promena ukupne tvrdoće u filtratu nakon prolaska kroz ispunu NaZ.
Figure 7. Change of the total hardness in the filtrate after passing through the NaZ bed.

Sadržaj Ca i Mg u alikvotima filtrata koji su sakupljani na svakih sat vremena nakon prolaska kroz regenerisanu ispunu, prikazan je na slici 8.

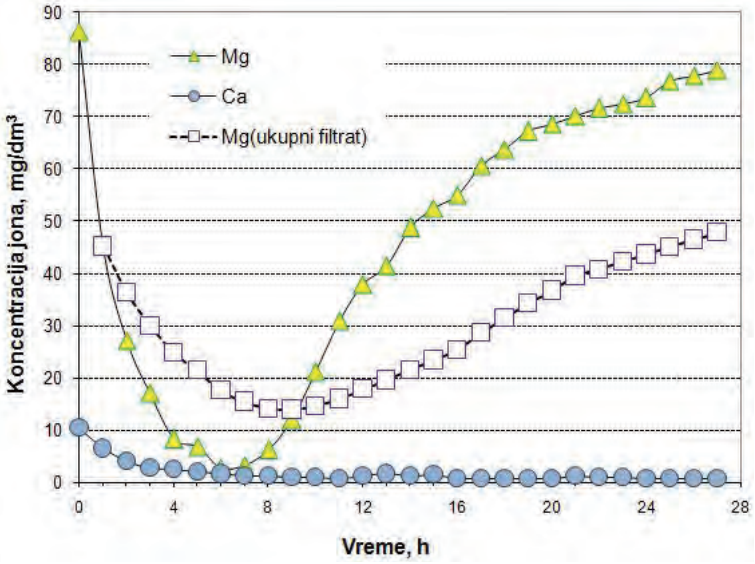

Slika 8. Promena koncentracije Mg i Ca u alikvotima filtrata sakupljanim na svakih sat vremena i koncentracije Mg u ukupnom filtratu, nakon prolaska kroz regenerisanu ispunu NaZ.
Figure 8. Change of the concentration of Mg and Ca in aliquots collected every hour and the concentartion of Mg in total filtrate volume, after passing through the recovered NaZ.

Zapaža se da je efikasnost zeolita nešto povećana u odnosu na predhodno filtriranje.

Ukupna količina vezanog Mg po g NaZ iznosila je 1,92 mg/g, za razliku od prvog filtriranja gde je ova vrednost bila 1,8 mg/g. Regeneracija ispune tokom 24 h sa povratnim tokom rastvora NaCl dovela je do povećanja efikasnosti NaZ za oko 6,7%. Količina vezanog Ca po g zeolita nepromenjena je u odnosu na onu pre regeneracije (0,45 mg/g).

Pri promeni brzine strujanja vode kroz kolonu, u pogledu efikasnosti izdvajanja Mg na zeolitnoj ispuni, kao i smanjenja ukupne tvrdoće vode, dolazi do pojave maksimuma na vrednosti od 0,09 mm/s, pri čemu je u svim slučajevima uočeno povećanje kapaciteta vezivanja Mg nakon regeneracije sloja, tabela 4.

Iz dobijenih rezultata može se zaključiti da fluidomehanika sistema voda–zeolit ima uticaja na kapacitet uklanjanja Mg iz vode. Ovo nameće potrebu razvoja reaktora sa razvijenim fluidizovanim, fontanskim ili fontansko-fluidizovanim slojem sa recirkulacijom toka, nakon ispitivanja stepena otiranja čestica zeolita pri različitim uslovima u sistemu i njihova primena za smanjenje sadržaja Mg, odnosno ukupne tvrdoće vode.

ZAKLJUČAK

Rezultati prikazani u ovom radu potvrdili su predhodna laboratorijska ispitivanja koja su ukazala da se prirodni zeolitski tuf obogaćen natrijumom može koristiti za sniženje koncentracije magnezijuma u sirovoj vodi izvorišta „Potkop“, koja se koristi u vodosnabdevanju grada Raške.

Osim toga, modifikovani zeolit, NaZ, je efikasan i u protočnom sistemu i može se primenjivati kao ispuna u filterskim jedinicama sa mogućnošću regeneracije i ponovnog korišćenja. Primena zeolita u protočnom sistemu ne umanjuje stepen sorpcije magnezijuma, ali smanjuje vreme uspostavljanja ravnoteže.

Uočeno je da brzina protoka kroz filtersku jedinicu utiče na stepen sorpcije Mg i Ca na NaZ, te da se primenom različitih protoka mogu postići optimalni rezultati u procesu uklanjanja Mg i Ca iz vode.

Za upotrebu modifikovanog zeolita, NaZ, u sistemima za pripremu vode značajna je mogućnost pot-

Tabela 4. Uticaj promene brzine strujanja vode na kapacitet uklanjanja Mg jona i smanjenje tvrdoće vode
Table 4. The influence of water velocity on the removal capacity of Mg and on reduction of the water hardness

Brzina strujanja vode kroz nasuti sloj zeolita, mm/s	Početni kapacitet uklanjanja Mg, mgMg/(g zeolita)	Kapacitet uklanjanja Mg regenerisanog sloja mgMg/(g zeolita)	Stepen povećanja kapaciteta, %	Ukupno smanjenje tvrdoće vode, %
0,05	1,8	1,92	6,7	45
0,09	2,4	2,6	8,3	59
0,15	1,96	2,35	20	44

pune regeneracije u protočnom sistemu. Protočna regeneracija pokazala se kao veoma efikasna, pošto se tako postiže ne samo regeneracija zeolita, već se u izvesnoj meri povećava i stepen sorpcije Mg na NaZ. Takođe, maksimalni kapacitet sorpcije u protočnom sistemu nakon regeneracije postiže se za kraće vreme, što dodatno opravdava i stimuliše dalja istraživanja u cilju korišćenja zeolitskog tufa u postupcima omekšavanja vode.

Na osnovu dobijenih rezultata nože se zaključiti da su postavljeni jasni pravci budućih istraživanja u cilju potpune primene domaće sirovine, zeolitskog tufa iz rudnika Igroš Vidojević iz Brusa, u tretmanu voda na prostorima Srbije.

Zahvalnica

Finansijska sredstva za ova istraživanja obezbedilo je Ministarstva prosvete, nauke i tehnološkog razvoja Republike Srbije (projekti: OI-172022, OI-172-018 i IP--451-03-00605/2012-16/143).

LITERATURA

[1] Pravilnik o higijenskoj ispravnosti vode za piće, Službeni list SRJ, br. 42/98, 1998 I 44/99, 1999, list IIIa.

[2] S. Wang, Y. Peng, Natural zeolites as effective adsorbents in water and wastewater treatment, Chem. Eng. J. **156** (2010) 11–24.

[3] I. Arrigo, P. Catalfamo, L. Cavallari, S.D. Pasquale, Use of zeolitized pumice waste as a water softening agent, J. Hazard. Mater. **147** (2007) 513–517.

[4] R.L. VanMao, N. Thanh Vu, S. Xiao, A. Ramsaran, Modified zeolites for the removal of calcium and magnesium from hard water, J. Mater. Chem. **4** (1994) 1143–1147.

[5] S. Tomić, N. Rajić, J. Hrenović, D. Povrenović, Removal of Mg from spring water using natural clinoptilolitem, Clay Miner. **47** (2012), 81–92.

[6] Determination of Hardness of Water, Method WHO/M/ /26.R1, revised 10 December 1999.

[7] D.V. Vuković, Dvofazni i trofazni fontanski i fontansko--fluidizovani slojevi kao novi sistemi višefaznog kontakta", Doktorska disertacija, Tehnološko–metalurški fakultet, Beograd, 1983.

[8] B. Poček, Voda za piće: Standardne metode za ispitivanje higijenske ispravnosti, Privredni pregled, 1990.

[9] S. Cerjan Stefanović, N. Zabukovec Logar, K. Margeta, N. Novak Tusar, I. Arcon, K. Maver, J. Kovač, V. Kaučić, Structural investigation of Zn^{2+} sorption on clinoptilolite tuff from the Vranjska Banja deposit in Serbia, Microporous Mesoporous Mater. **105** (2007) 251–259.

[10] N. Rajić, Dj. Stojaković, S. Jevtić, N. Zabukovec Logar, J. Kovač, V. Kaučič, Removal of aqueous manganese using the natural zeolitic tuff from the Vranjska Banja deposit in Serbia, J. Hazard. Mater. **172** (2009) 1450–1457.

[11] M. Loizidou, R.P. Townsend, Exchange of Cadmium into the Sodium and Ammonium Forms of the Natural Zeolites Clinoptilolite, Mordenite and Ferrierite, J. Chem. Soc. Dalton Trans. (1987) 1911–1916.

[12] N. Vukojević Medvidović, J. Perić, M. Trgo, Column performance in lead removal from aqueous solutions by fixed bed of natural zeolite–clinoptilolite, Sep. Purif. Technol. **49** (2006) 237–244.

SUMMARY

REMOVAL OF MAGNESIUM IN SPRING WATER USING THE NATURAL ZEOLITE IN A CONTINUOUS FLOW SYSTEM

Slavica Tomić, Milena Knežević, Nevenka Rajić, Dragan Povrenović

University of Belgrade, Faculty of Technology and Metallurgy, Belgrade, Serbia

(Scientific paper)

The aim of this work is an investigation of the possible application of Serbian natural zeolitic tuff („Igroš Vidojević“ deposit, Brus, Serbia) for improvement of the spring water quality. The concentration of magnesium in spring waters in Raška area (in Southeast Serbia) is grater than 100 mg/dm^3 and is unsuitable for everyday consumption. The experiments included investigation of fluid-mechanics tests of the zeolite particles with diameters of 1.5, 4 and 6 mm in a column with diameter of 65 mm and magnesium adsorption/desorption experiments in the column with a diameter of 110 mm. The results showed that the concentration of magnesium in the spring water can be decreased below the maximum allowed concentration of 50 mg/dm^3 byusing the sodium enriched zeolite bed and optimal fluid-mechanics parameters.

Keywords: Magnesium • Zeolites • Adsorption • Clinoptilolite • Continuous flow

Uticaj fluido-mehaničkih karakteristika sistema na zapreminski koeficijent prenosa mase i disperziju vazduha u trofaznom sistemu

Milena M. Knežević, Dragan S. Povrenović

Univerzitet u Beogradu, Tehnološko–metalurški fakultet, Karnegijeva 4, Beograd, Srbija

Izvod

U ovom radu je proučavana distribucija mehurova i zapreminski koeficijent prenosa mase, k_La, u trofaznom sistemu, sa sferičnim česticama od stakla i keramike različitog prečnika pod različitim operativnim uslovima. Brzine gasa su se kretale u intervalu 0,03–0,09 m/s, a brzine tečnosti 0–0,1 m/s. Ispitivanja su se izvodila u kolonama od pleksiglasa različitih geometrija. 2D kolona dimenzija 278 mm×20,4 mm×500 mm i cilindrična kolona, prečnika 64 mm i visine 2000 mm. Rezultati su pokazali da prisustvo čestica u sistemu doprinosi povećanju zapreminskog koeficijenta prenosa mase, a da sa povećanjem brzine gasa i tečnosti njegova vrednost nastavlja da raste. Vrednost povećanja zapreminskog koeficijenta prenosa mase, u konkretnim fluido-mehaničkim uslovima, zavisi od karakteristika samih čestica.

Ključne reči: zapreminski koeficijent prenosa mase, trofazni sistem, staklene i keramičke čestice.

Dostupno na Internetu sa adrese časopisa: http://www.ache.org.rs/HI/

NAUČNI RAD

UDK 66.06:544

Hem. Ind. **68** (4) 483–490 (2014)

doi: 10.2298/HEMIND130629072K

Proučavanje trofaznih sistema sa fluidizovanim slojem kao i odgovarajućih fenomena prenosa od velikog je značaja kod operacija multifaznog kontakta u hemijskoj, petrohemijskoj, biohemijskoj industriji i metalurgiji.

Ovakvi sistemi se sve više ispituju i koriste za mikrobiološke procese jer omogućavaju veliku specifičnu površinu za rast mikroorganizama kao i intezivan prenos mase. U biotehnologiji višefazni sistemi sa pokretnim slojem čestica se često primenjuju za aerobne tretmane otpadnih voda. U aerobnim bioreaktorima, limitirajući faktor u podešavanju optimalnih uslova sredine mikroorganizmima je prenos mase kiseonika, zbog posledice slabog rastvaranja kiseonika u vodi, odnosno, u fermentacionim medijumima. Efikasnost prenosa mase kiseonika iz gasne u tečnu fazu, se najbolje opisuje preko vrednosti zapreminskog koeficijenta prenosa mase k_La [1–3].

U trofaznim sistemima sa pokretnim slojem čestica, brojni istražvači [4–6], ispitivali su uticaj distributora vazduha, protoka vazduha, difuzivnosti gasa kroz tečnost, protoka i viskoziteta tečnosti na prenos mase kiseonika [4–6]. Istraživanja su pokazala da zapreminski koeficijent prenosa mase zavisi od distribucije i veličine mehurova u sistemu [7], kao i da ponašanje mehurova u sistemu, koje je uglavnom uslovljeno načinom disperzije, ima direktan uticaj na prenos mase i hidrodinamiku sistema [8]. U dosadašnjom istraživanjima ispitivan je uticaj različitih tipova ispune poput kamene, staklene, keramičke, plastične i sintetske, na prenos mase kiseonika u trofaznim sistemima [4,6,9–16]. Ova ispitivanja su pokazala da osobine čestica koje čine ispunu, gustina i prečnik, kao i njihova količina, utiču na pojavu koalescencije, odnosno na prečnik mehura i zadržavanje gasa u sistemu [4,6,9–16].

Pregledom literature, može se uočiti dosta suprostavljenih rezultata i različitih tumačenja uticaja ispitivanih parametara na prenos mase kiseonika u trofaznim sistemima, zbog toga je nemoguće osloniti se na postojeće analize, pa je neophodno izvršiti eksperimentalne provere za svaki ispitivani sistem sa ciljem detaljnijeg utvrđivanja interakcija čestica i mehurova vazduha u trofaznom sistemu.

Cilj eksperimenta je bio da se odredi uticaj različitih tipova čestica na efikasnost prenosa mase kiseonika, odnosno na vrednost zapreminskog koeficijenta prenosa mase, k_La, jer da bi se trofazni sistemi mogli primeniti za nitrifikaciju, potrebno je prvo ispitiati fluido-mehaničke karakteristike na prenos mase kiseonika u ovim sistemima.

U trofaznim sistemima, na prenos mase kiseonika, kao jednog od limitirajućih parametara procesa nitrifikacije, ključnu ulogu imaju karakteristike čvrstih čestica. Pravilnim odabirom čvrste faze, odnosno inertih nosača za nitrifikacione bakterije, aktere nitrifikacionog procesa, može se uticati na povećanje efikasnosti procesa uklanjanja azota iz otpadnih voda.

EKSPERIMENTALNI DEO

U eksperimentima su korišćene dve kolone od pleksiglasa, različitih dimenzija. Prva kolona je bila cilindrična, 3D kolona, prečnika 64 mm i visine 2000 mm,

Prepiska: D.S. Povrenović, Univerzitet u Beogradu, Tehnološko–metalurški fakultet, Karnegieva 4, Beograd, Srbija.
E-pošta: povrenovic@tmf.bg.ac.rs
Rad primljen: 29. jun, 2013
Rad prihvaćen: 25. septembar, 2013

dok je druga bila 2D kolona, dimenzija 278 mm×20,4 mm i visine 500 mm. Na slici 1 prikazana je šema eksperimentalnog sistema korišćenog u ovom radu i izgled 2D i 3D kolona.

Voda i vazduh su uvođeni na dnu kolone, preko distrubutora, a izlazili su na vrhu kolone. Distributor, kod obe kolone je bio obrazovan od pakovanog sloja staklenih, sferičnih čestica prečnika 4 mm. Kao čvrsta faza trofaznog sistema, korišćene su čestice različitih karakteristika, koje su prikazane u tabeli 1.

Tabela 1. Karakteristike čestica
Table 1. Particle characteristics

Tip čestice	Prečnik, mm	Gustina, kg/m^3
Sferične staklene čestice	3	2500
Sferične staklene čestice	6	2500
Sferične keramičke čestice	6	2311

Eksperimentalna ispitivanja su vršena sa različitim visinama pakovanog sloja čestica, 10, 20, 30 i 40 cm. Brzina vazduha kroz kolonu se kretala od 0,03 do 0,09 m/s, a protok vazduha je meren rotametrom. Protok vode je meren pomoću elektromagnetnog merača, a brzina vode kroz kolonu se kretala u intervalu od 0 do 0,09 m/s. U ovim ispitivanjima, širok opseg protoka fluida, obuhvatio je različite slojeve čestica, od nepokretnog pakovanog sloja do fluidizovanog sloja.

Pod pretpostavkom da je u kolonama uspostavljeno idealno mešanje, za izračunavanje zapreminskog koeficijenta prenosa mase korišćena je jednačina (1):

$$\frac{dC}{dt} = k_L a\left(C^* - C_t\right) \quad (1)$$

Ispitivanja prenosa mase kiseonika su rađena sa česmenskom vodom, na sobnoj temperaturi, iz koje je pomoću natrijum-sulfita prethodno uklanjan rastvoren kiseonik do koncentracija ispod 1 mg/l. Promena koncentracije rastvorenog kiseonika u koloni sa vremenom merena je pomoću oksimetra, WTW Oxi 340i. Uvođenje vazduha je vršeno do postizanja najmanje 90% koncentracije zasićenja. Takođe u eksperimentu je praćena distribucija i veličina mehurova pomoću analize slika. Na poleđinu kolona je bio zalepljen paus papir, na koji je usmeren reflektor, što je omogućilo jasnije uočavanje mehurova na slikama, a potom su prečnici mehurova na slikama odredjivani pomoću programa ″Sigma Scan″.

REZULTATI I DISKUSIJA

Uticaj brzine gasa na k_La

U trofaznom sistemu, bez proticanja vode, sa povećanjem brzine vazduha, generalno raste i vrednost zapreminskog koeficijenta prenosa mase, što se vidi na slici 2.

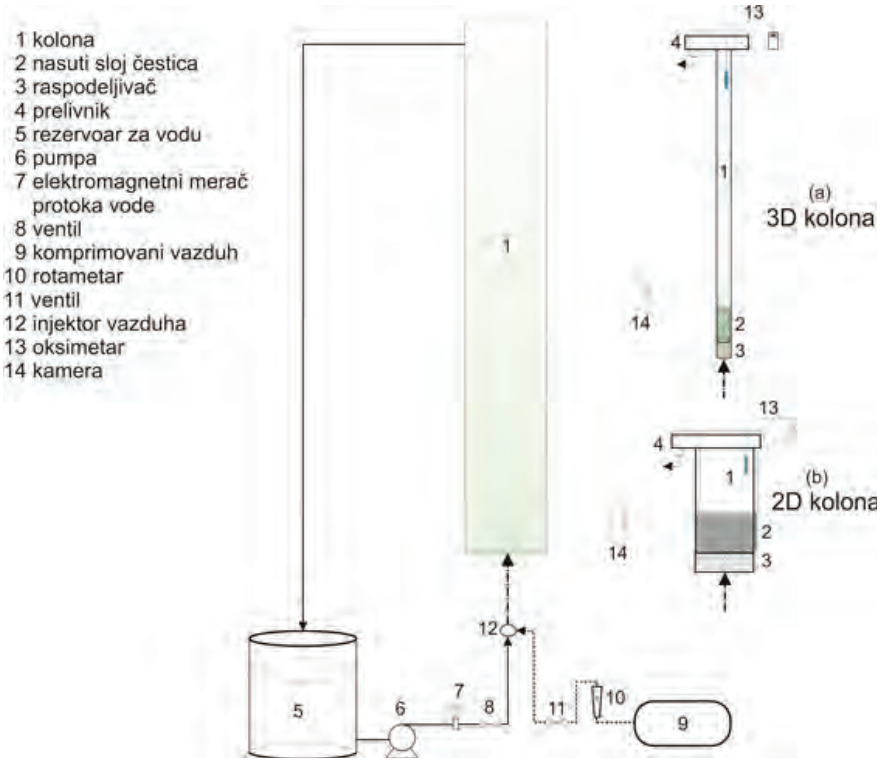

Slika 1. Šeme eksperimentalnih aparatura: a) Cilindrična kolona; b) 2D kolona.
Figure 1. Scheme of the experimental system: a) Cylindrical column; b) 2D column.

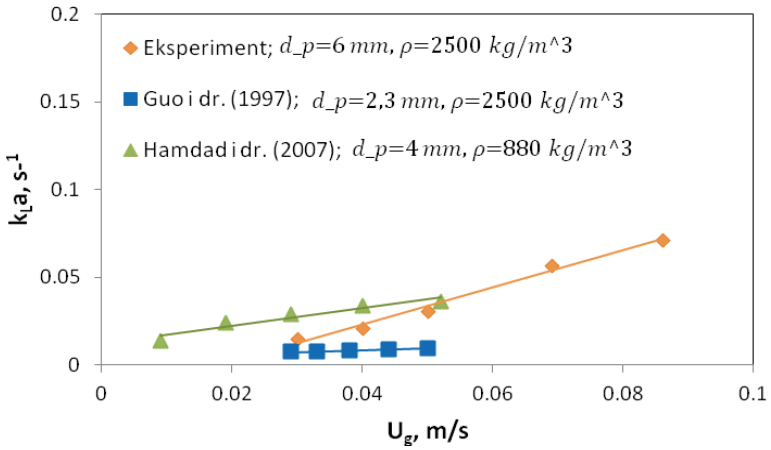

Slika 2. Zavistnost k_La od brzine proticanja vazduha.
Figure 2. Magnitude of k_La as a function of gas velocity.

Ovo se objašnjava time da sa povećanjem brzine gasa, obe veličine i specifična međufazna površina, *a* i koeficijent prenosa mase, k_L rastu, jer velika brzina gasa, odnosno njegov fluks ($m^3/s\ m^2$), utiče na povećanje „*hold-up*"-a gasa u sistemu i na smanjenje prečnika mehura, što dovodi do povećanja međufazne površine, a time i do boljeg prenosa mase, [9]. Na slici 3 se vidi da povećanje brzine gasa dovodi do povećanja broja mehurova, odnosno količine gasa u sistemu kao i to da su formirani mehurovi sitniji pri većoj brzini gasa. Da povećanje brzine gasa utiče na povećanje „*hold-up*"-a gasa i k_La, potvrđeno je i od strane drugih istraživača koji su ispitivali i druge tipove čestica [4,6,9,16,27,28].

Pored ovoga, porast brzine gasa u trofaznom sistemu dovodi do drobljenja mehurova i smanjenja njihovog prečnika, pa iako bi se očekivao suprotan efekat, usled povećanja turbulencije dolazi do povećanja njihove brzine dizanja u koloni, a time i povećanja turbulencije tečnosti oko mehurova. U tom slučaju otpor prenosu mase od strane filma tečnosti opada, a što utiče na povećanje vrednosti koeficijenta prenosa mase, k_L, što je i eksperimentalno potvrđeno u rezultatima [9].

Uticaj brzine tečnosti na k_La

Brzina tečnosti ima značajan hidrodinamički uticaj u trofaznim sistemima. Uticaj brzine tečnosti na formiranje mehurova gasa i zapreminski koeficijent prenosa mase se ogleda preko povećane turbulencije u sistemu, koja doprinosi da film tečnosti postane tanji a otpor prenosu kiseonika manji, što utiče na povećanje koeficijenta prenosa mase od strane tečnosti k_L. Na slici 4 je prikazana zavisnost zapreminskog koeficijenta prenosa mase od brzine tečnosti kroz kolonu.

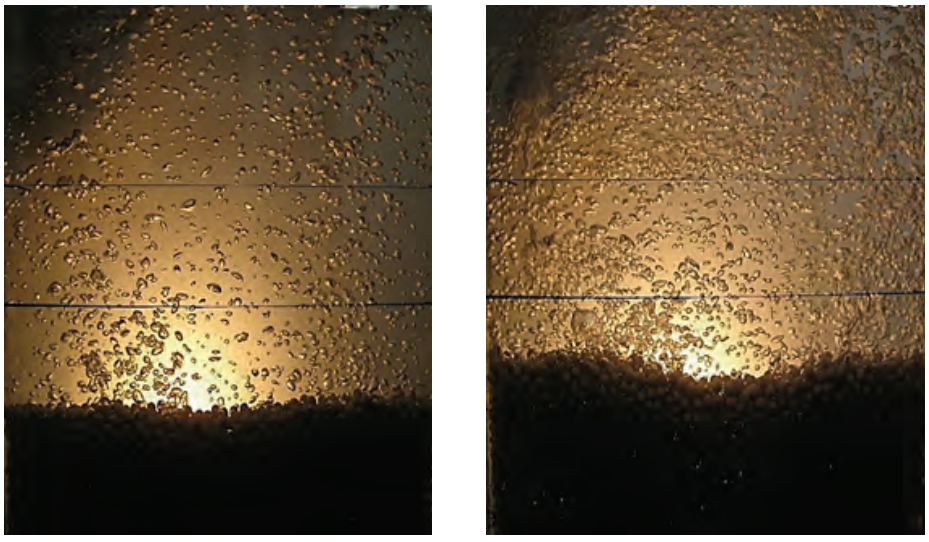

(a) (b)

Slika 3. Veličina mehurova u 2D koloni sa sferičnim česticama od keramike, prečnika 6 mm, pri različitim brzinama gasa: a) U_g = 0,02 m/s; b) U_g = 0,05 m/s.
Figure 3. Bubble size in a 2D column with 6 mm diameter ceramic spherical particles at: a) U_g = 0.02 m/s; b) U_g = 0.05 m/s.

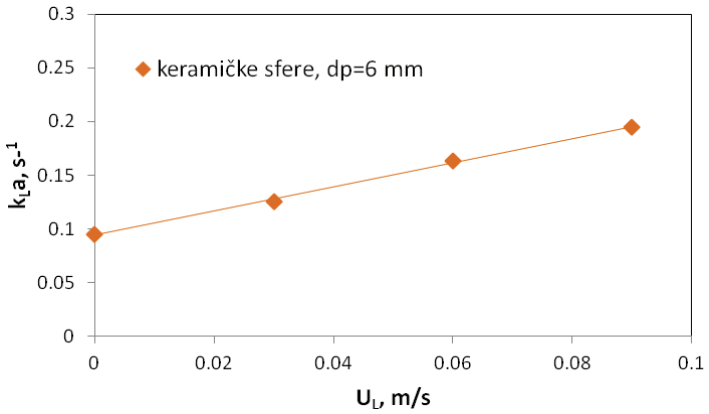

Slika 4. Uticaj brzine tečnosti na zapreminski koeficijent prenosa mase u sistemu sa keramičkim sferama prečnika 6 mm, pri brzini gasa od 0,09 m/s.
Figure 4. Effects of liquid velocity on the volumetric mass transfer coefficient at U_g = 0.09 m/s in column with 6 mm diameter ceramic spherical particles.

Turbulencija, odnosno povećanje brzine tečnosti u sistemu takođe doprinosi i cepanju mehurova, odnosno smanjivanju njihovog prečnika. U cilju određivanja dimenzija mehorova, praćena je promena u broju i veličini mehurova u 2D koloni (slika 1b), snimanjem pomoću kamere. Dobijene slike su skenirane i zatim analizirane u softverskom paketu za analizu slika „Sigma-Scan“. Analizom slika, dobijena je vrednost srednjeg prečnika mehura u koloni pri određenim operativnim uslovima, a zavisnost veličine mehura od brzine tečnosti je prikazana na slici 5.

Pri većim brzinama tečnosti dolazi do formiranja većeg broja uniformnih mehurova (homogen režim protoka mehura), dok je pri manjim vrednostima brzine tečnosti izraženije njihovo srastanje, pa dolazi do formiranja heterogenog režima proticanja mehurova, slika 6.

Rezultati nekih eksperimentalnih ispitivanja, dostupni u literaturi, pokazuju da se zapreminski koeficijent prenosa mase povećava sa povećanjem protoka tečnosti [9,12,29], dok drugi rezultati govore suprotno, da se zapreminski koeficijent prenosa mase smanjuje sa povećanjem brzine tečnosti [6,10,30].

Rezultati naših eksperimentalnih ispitivanja pokazuju da povećanje brzine tečnosti i gasa, utiču na povećanje zapreminskog koeficijenta prenosa mase, što je prikazano na slici 7.

Uticaj karakteristika čestica na k_La

Kao što je već rečeno, pri većim brzinama gasa postiže se homogen režim protoka mehurova, koji se odlikuje boljim karakteristikama procesa prenosa mase, za razliku od heterogenog režima. U dvofaznim sistemima bez prisustva čestica, homogeni režim se jedino može postići pri niskim protocima gasa jer pri višim protocima dolazi do koalescencije [7]. Međutim, zbog presudne uloge rastvorenog kiseonika u aerobnim mikrobiološkim procesima, velika količina vazduha u sistemu je neophodna za adekvatno odvijanje procesa. Istraživanja su pokazala, da odgovarajuća prisutna čvrsta faza u sistemu ima mogućnost da pri visokim protocima gasa utiče na formiranje homogenog režima

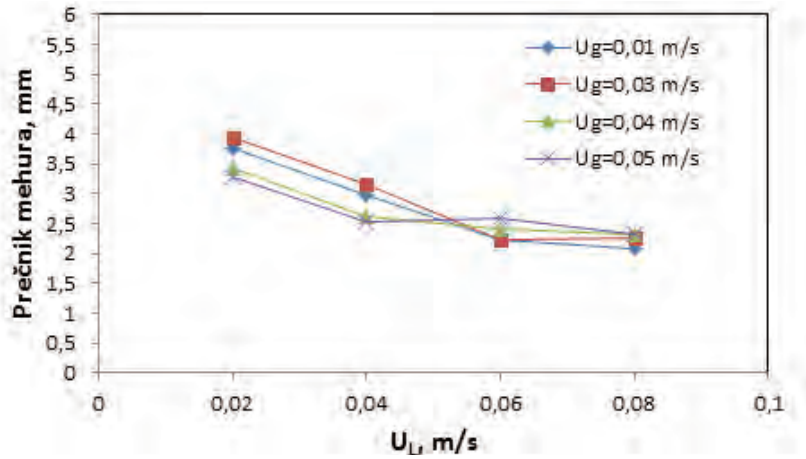

Slika 5. Uticaj brzine tečnosti na prečnik mehura, pri konstantnim brzinama gasa u sistemu sa staklenim kuglicama prečnika 6 mm.
Figure 5. Effects of liquid velocity on bubble diameter, at constant gas velocity in column with 6 mm diameter glass particles.

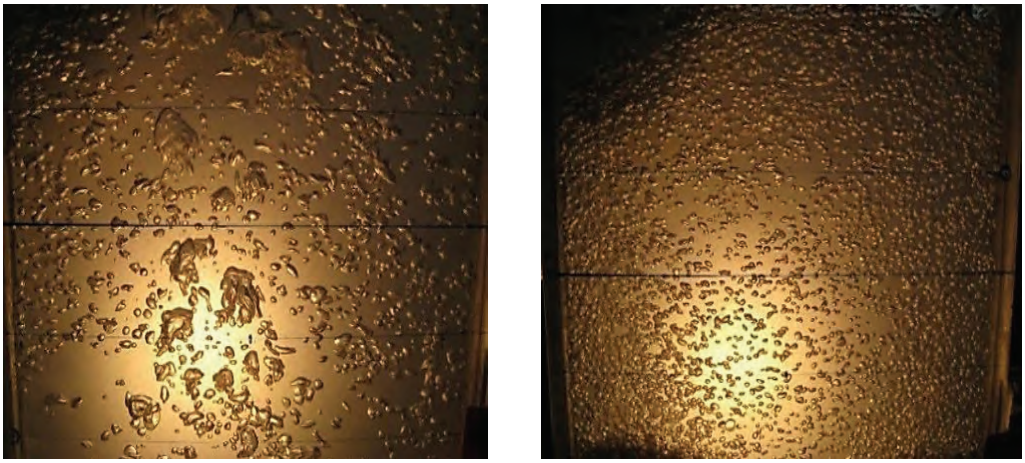

(a) (b)

Slika 6. Veličina mehurova u 2D koloni sa keramičkim česticama od 6 mm pri istoj brzini gasa a pri različitim brzinama tečnosti od a) 0,02 i b) 0,1 m/s.
Figure 6. Bubble size in a 2D column with 6 mm diameter ceramic spherical particles at same gas velocity and different liquid velocity: a) U_L =0,02 m/s, b) U_L = 0,1 m/s.

mehurova. Na osnovu ovoga je istaknuto da važnu ulogu na formiranje mehurova imaju osobine čestica koje čine ispunu. Uticaj osobina čestica potrebno je detaljno ispitati jer, pri određenim uslovima, čestice mogu da suzbiju koalescenciju, ali isto tako mogu i da je pospeše.

Jedna od osobina čestica koja utiče na efikasnost prenosa mase kiseonika u sistemu je njihov prečnik. Sa porastom prečnika čestica raste količina zadržanog gasa u koloni, što je u skladu sa literaturnim rezultatima [6,10,30,31]. Sitne čestice utiču na povećanje koalescencije, u odnosu na sisteme sa krupnijim česticama. Pri istoj visini nasutog sloja i istim vrednostima protoka fluida, kod sitnijih čestica povećani pad pritiska uslovljava kompresiju vazduha na dnu sloja, što izaziva srastanje mehurova a time i *„by pass“* vazduha kroz nasut sloj. Veliki mehurovi imaju manju specifičnu površinu, veće brzine dizanja kroz kolonu i kraće vreme zadržavanja, što dovodi do smanjenog prenosa mase. Povećanje prečnika čestica utiče na bolje cepanje muhurova što dovodi do povećanja sadržaja gasa u koloni kao i do povećanja vrednosti zapreminskog koeficijenta prenosa mase, k_La [6,11,12]. Uticaj prečnika čestica na zapreminski koeficijent prenosa mase u sistemu sa staklenim sferama prečnika 3 i 6 mm, prikazan je na slici 8.

Ukoliko je u sistemu uspostavljeno i proticanje tečnosti, zabeleženo je isto ponašanje, da sa povećanjem prečnika čestica raste i zapreminski koeficijent prenosa mase, slika 9.

Druga bitna osobina čestica koja utiče na efikasnost prenosa mase kisenika je gustina čestica. Rezultati eksperimentalnih ispitivanja, prikazani na slici 10, pokazuju da su vrednosti zapreminskog koeficijenta prenosa mase veće u sistemu sa keramičkim sferama prečnika 6 mm i gustine 2311 kg/m^3 od vrednosti dobijenih u sistemu sa staklenim sferama istog prečnika 6 mm, a gus-

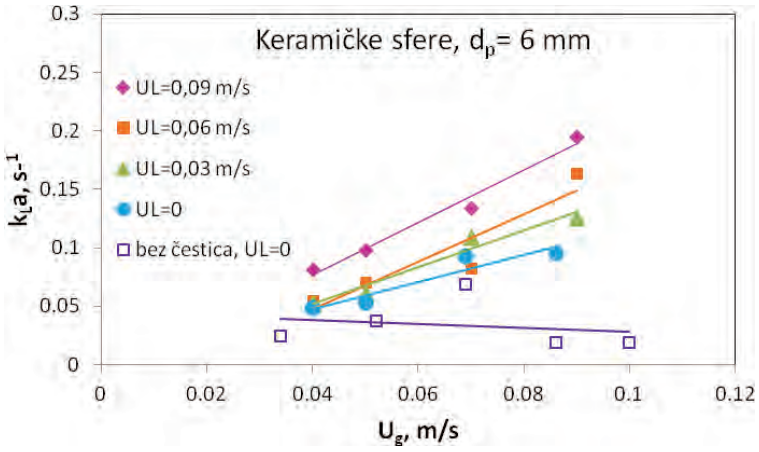

Slika 7. Uticaj brzine gasa i tečnosti na zapreminski koeficijent prenosa mase (H_{sloja} = 40 cm).
Figure 7. Effects of gas and liquid velocity on (H_{bed} = 40 cm).

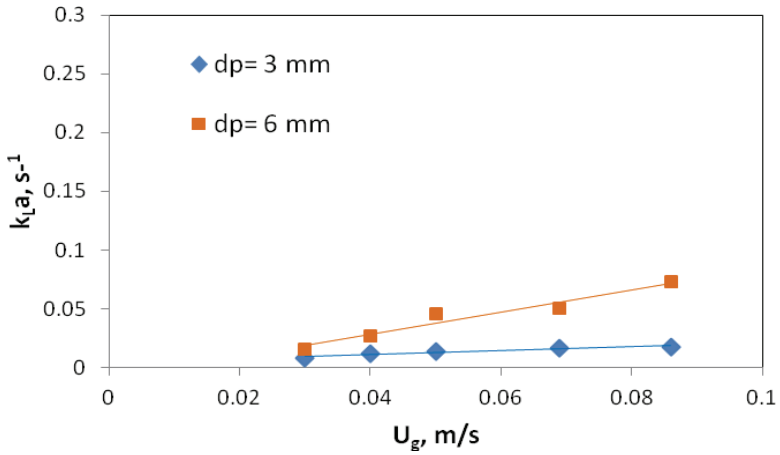

Slika 8. Uticaj prečnika staklenih čestica na k_La u zavisnosti od U_g, U_L = 0 m/s, H_{sloja} = 30 cm.
Figure 8. Influence of glass particle diameter on k_La as a function of U_g, U_L = 0 m/s, H_{bed} = 30 cm.

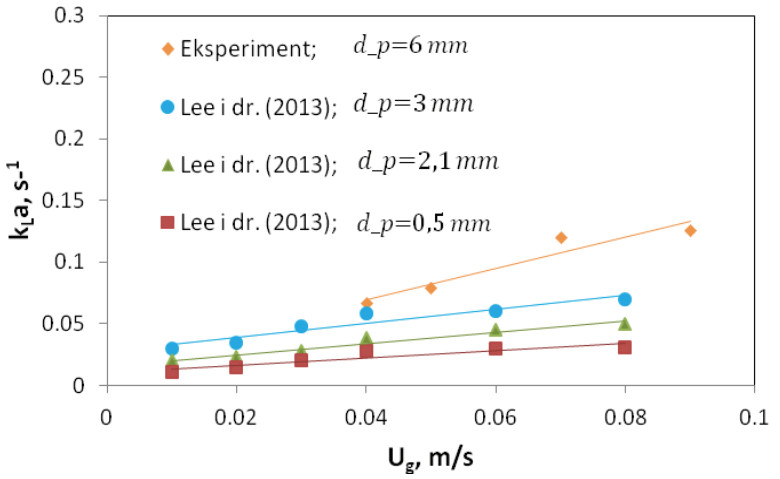

Slika 9. Uticaj prečnika staklenih sferičnih čestica na zapreminski koeficijent prenosa mase u zavisnosti od brzine gasa. Eksperiment: U_L = 0,09 m/s ; Lee i dr. (2013): U_L = 0,3 m/s.
Figure 9. Influence of glass particle diameter on k_La as a function of U_g. Experiment: U_L = 0.09 m/s ; Lee et al. (2013): U_L = 0.3 m/s.

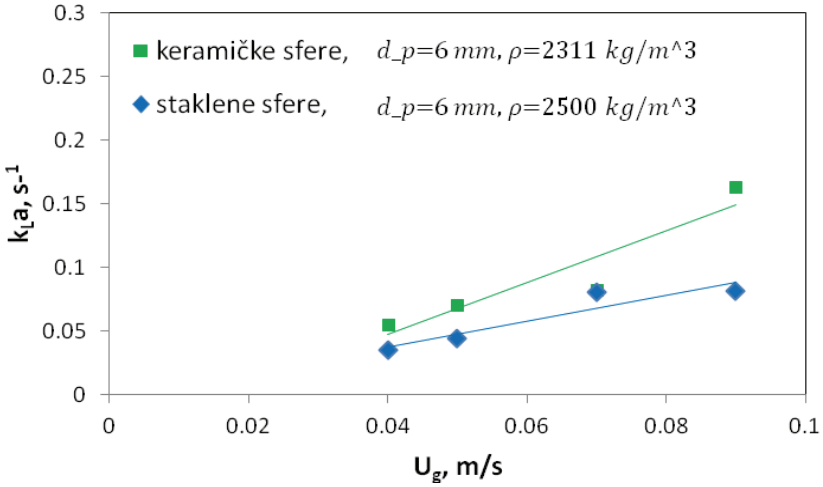

Slika 10. Uticaj gustine čestica na zavisnost zapreminskog koeficijenta prenosa mase od brzine proticanja gasa, pri brzini tečnosti od 0,06 m/s (H_{sloja} = 40 cm).
Figure 10. Influence of particle density on k_La as a function of gas velocity at liquid velocity 0,06 m/s (H_{bed} = 40 cm).

tine 2500 kg/m^3, pod istim operativnim uslovima. Ovako mala razlika u gustinama čestica dovela je do značajne razlike u vrednostma k_La u ova dva ispitivana sistema. Freitas i Teixeira [13] koji su ispitivali čestice prečnika 2,1 mm, gustine 1023 i 1048 kg/m^3, su došli do istog zaključka, da mala razlika u gustini čestica ima uticaj na vrednosti zapreminskog koeficijenta prenosa mase.

ZAKLJUČAK

U ovom radu je ispitivan uticaj karakteristika različitih tipova čestica na distribuciju mehurova i zapreminski koeficijent prenosa mase u trofaznom sistemu.

Pokazano je da prisustvo čvste faze u sistemu doprinosi znatnom povećanju vrednosti zapreminskog koeficijenta prenosa mase u odnosu na vrednosti koeficijenta koje su dobijene u dvofaznom sistemu. Povećanje brzine vazduha i tečnosti doprinose povećanju prenosa mase kiseonika iz gasovite u tečnu fazu dok karakteristike čestica igraju presudnu ulogu za prenos mase kiseonika u trofazom sistemu. Sa povećanjem prečnika čestice raste i zapreminski koeficijent prenosa mase. Poređenjem čestica istog prečnika uočeno je da malo smanjenje u gustini čestice utiče na povećanje k_La. Dobijene vrednosti u ovom eksperimentu za k_La se kreću u opsegu 0,011-0,195 s^{-1}, u zavisnosti od protoka fluida i tipa čestica.

Dobijeni rezultati predstavljaju osnov za dalja istraživanja procesa nitrifikacije u trofaznim disperznim sistemima.

Simboli

k_La	zapreminski koeficijent prenosa mase, s^{-1}
C^*	koncentracija zasićenja kiseonikom, mg/L
C_t	koncentracija rastvorenog kiseonika u vremenu t, mg/L
d_p	prečnik čestice, mm
ρ	gustina čestice, kg/m^3
U_g	brzina gasa kroz kolonu, m/s
U_L	brzina tečnosti kroz kolonu, m/s
H	visina nasutog sloja, m

Zahvalnica

Ovaj rad je urađen u okviru projekta OI-172022, finansiranog od strane Ministarstva prosvete, nauke i tehnološkog razvoja Republike Srbije.

LITERATURA

[1] M.Y. Chisti, Airlift Bioreactors, Elsevier Applied Science, London, 198.

[2] J.C. Merchuk, M.H. Siegel, Airlift reactors in chemical and biological technology, J. Chem. Technol. Biotechnol. **41** (1988) 105–120.

[3] F. Benyhaia, L. Jones, D. Plantaz, Mass transfer studies in pneumatic reactors, Chem. Eng. Technol. **19** (1996) 425–431.

[4] Chia-Min Chen, Lii-Ping Leu, A highly elevated mass transfer rate process for three-phase, liquid-continuous fluidized beds, Chem. Eng. J. **81** (2001) 223–230.

[5] M. Jamnongwong, K. Loubiere, N. Dietrich, G. Hébrard, Experimental study of oxygen diffusion coefficients in clean water containingsalt, glucose or surfactant: Consequences on the liquid-side mass transfer coefficients, Chem. Eng. J. **165** (2010) 758–768.

[6] H. Miura, T. Katoh, Y. Kawase, Gas–liquid mass transfer in co-current three-phase fluidized beds with non-Newtonian fluids: Theoretical models based on the energy dissipation rate, Chem. Eng. J. **185**–**186** (2012) 337–346.

[7] E. Camarasa, C. Vial, S. Poncin, G. Wild, N. Midoux, J. Bouillard, Influence of coalescence behaviour of the liquid and of gas sparging on hydrodynamics and bubble characteristics in a bubble column, Chem. Eng. Process. **38** (1999) 329–344.

[8] W.-D. Deckwer, A. Schumpe, Improved tools for bubble column reactors design and scale-up, Chem. Eng. Sci. **48** (1993) 889–911.

[9] W. Yang, J. Wang, T. Wang, Y. Jin, Experimental study on gas–liquid interfacial area and mass transfer coefficient in three-phase circulating fluidized beds, Chem. Eng. J. **84** (2001) 485–490.

[10] D.H. Lee, J.O. Kim, S.D. Kim, Mass transfer and phase holdup characteristics in three-phase fluidized beds, Chem. Eng. Commun. **119** (1993) 179–196.

[11] A. Schumpe, W.-D. Deckwer, K.D.P. Nigam, Gas–liquid mass transfer in threephase fluidized beds with viscous pseudoplastic liquids, Can. J. Chem. Eng. **67** (1989) 873––877.

[12] V. Sivasubramanian, Gas–liquid mass transfer in three-phase inverse fluidized bed reactor with Newtonian and non-Newtonian fluids, Asia-Pacific J. Chem. Eng. **5** (2010) 361–368.

[13] C. Freitas, J.A. Teixeira, Oxygen mass transfer in a high solids loading three-phase internal-loop airlift reactor, Chem. Eng. J. **84** (2001) 57–61.

[14] M. Herskowitz, J.C. Merchuk, A loop three-phase fluidized bed reactor, Can. J. Chem. Eng. **64** (1986) 57–61.

[15] D.B. Bukur, S.A. Patel, J.G. Daly, Gas holdup and solids dispersion in a threephase slurry bubble column, AIChE J. **36** (1990) 1731–1735.

[16] Imran Hamdad, Shahrzad Hashemi, Dano Rossi, Arturo Macchi,Oxygen transfer and hydrodynamics in three-phase inverse fluidized beds, Chem. Eng. Sci. **62** (2007) 7399–7405.

[17] D. Bougard, N. Bernet, D. Cheneby, J. P. Delgenes, Nitrification of a high-strength wastewater in an inverse turbulent bed reactor: Effect of temperature on nitrite accumulation, Process Biochem. **41** (2006) 106–113.

[18] U.J. Strotmann, G. Windecker, Kinetics of ammonium removal with suspended and immobilized nitrifying bacteria in different reactor systems, Chemosphere, DOI: 10.1016/S0045-6535(97)00341-X.

[19] J.L. Shore, W.S. M'Coy, C.K. Gunsch, M.A. Deshusses, Application of a moving bed biofilm reactor for tertiary ammonia treatment in high temperature industrial wastewater, Bioresour. Technol. (2012), doi: 10.1016/ /j.biortech.2012.02.045.

[20] B. Tartakovsky, E. Kotlar, M. Sheintuch, Coupled nitrification-denitrification processes in a mixed culture of coimmobilized cells: analysis and experiment, Chem. Eng. Sci. **51** (1996) 2327–2336.

[21] M. Andalib, G. Nakhla, D. Sen, J. Zhu, Evaluation of biological nutrient removal from wastewater by Twin CirculatingFluidized Bed Bioreactor (TCFBBR) using a predictive fluidization model and AQUIFAS APP, Bioresour. Technol. **102** (2011) 2400–2410.

[22] H.J. Lars, B. Rusten, H. Odergaard, Nitrification in a moving bed biofilm reactor, Water Res. (1994) 1425– –1433.

[23] Y. Dong, Z. Zhang, Y. Jin, Z. Li, J. Lu, Nitrification performance of nitrifying bacteria immobilized in waterborne polyurethane at low ammonia nitrogen concentrations, J. Environ. Sci. **23** (2011) 366–371.

[24] R. Nogueira, L. F. Melo, U. Purkhold, S. Wuertz, M. Wagner, Nitrifying and heterotrophic population dynamics in biofilm reactors: effects of hydraulic retention time and the presence of organic carbon, Water Res. **36** (2002) 469–481.

[25] S. Aslan, M. Dahab, Nitritation and denitritation of ammonium-rich wastewater using fluidized-bed biofilm reactors, J. Hazard. Mater. **156** (2008) 56–63.

[26] B. Wang, W. Wang, H. Han, H. Hu, H. Zhuang, Nitrogen removal and simultaneous nitrification and denitrification in a fluidized bed step-feed process, J. Environ. Sci. **24** (2012) 303–308.

[27] Y.X. Guo, M.N. Rathor, H.C. Ti, Hydrodynamics and mass transfer studies in a novel external-loop airlift reactor, Chem. Eng. J. **67** (1997) 205–214.

[28] J.S. Lee, H.R. Jin, H. Lim, D.H. Lim, Y. Kang, S.D. Kim, K.W. Jun, Interfacial area and liquid-side and overall mass transfer coefficients in a three-phase circulating fluidized bed, Chem. Eng. Sci. (2013), http://dx.doi.org/ /10.1016/j.ces.2013.02.012i

[29] K. Ramesh, T. Murugesan, Minimum fluidization velocity and gas holdup in gas–liquid–solid fluidized bed reactors, J. Chem. Technol. Biotechnol. **77** (2002) 129–136.

[30] H.M. Jena, B.K. Sahoo, G.K. Roy, B.C. Meikap, Characterization of hydrodynamic properties of a gas–liquid–solid three-phase fluidized bed with regular shape spherical glass bead particles, Chem. Eng. J. **145** (2008) 50–56.

[31] H.M. Jena, B.K. Sahoo, G.K. Roy, B.C. Meikap, Characterization of hydrodynamic properties of a gas–liquid–solid three-phase fluidized bed with regular shape spherical glass bead particles, Chem. Eng. J. **145** (2008) 50–56.

SUMMARY

THE INFLUENCE OF FLUID-MEHANICAL CHARACTERISTICS OF THE SYSTEM ON THE VOLUMETRIC MASS TRANSFER COEFFICIENT AND GAS DISPERSION IN THREE-PHASE SYSTEM

Milena M. Knežević, Dragan S. Povrenović

University of Belgrade, Faculty of Technology and Metallurgy, Belgrade, Serbia

(Scientific paper)

Distribution of gas bubbles and volumetric mass transfer coefficient, k_La in a three phase system with different types of solid particles at different operation conditions were studied in this paper. The ranges of superficial gas and liquid velocities used in this study were 0.03–0.09 m/s and 0–0.1 m/s, respectively. The three different types of solid particles were used as a bed in the column (glass, d_p of 3 and 6 mm and ceramic, d_p of 6 mm). The experiments were carried out in 2D plexiglas column, 278 mm×20.4 mm×500 mm, and in cylindrical plexiglas column with the diameter of 64 mm and hight of 2000 mm. The k_La coefficient increases with gas and liquid velocities. The results show that the volumetric mass transfer coefficient has higher values in three phase system with solid particles in comparison to two phase system. The particles' properties (diameter and density) have major impact on oxygen mass transfer in three phase systems.

Keywords: Volumetric mass transfer coefficient • Three phase system • Glass and ceramic particles

Wet flue gas desulphurisation procedures and relevant solvents thermophysical properties determination

Nikola V. Živković[1], Slobodan P. Šerbanović[2], Emila M. Živković[2], Mirjana Lj. Kijevčanin[2], Predrag Lj. Stefanović[1]

[1]*Institute for Nuclear Sciences "Vinča", University of Belgrade, Laboratory for Thermal Engineering and Energy, P.O. Box 522, 11001 Belgrade, Serbia*
[2]*Faculty for Technology and Metallurgy, University of Belgrade, Karnegijeva 4, 11120 Belgrade, Serbia*

Abstract

In order to mitigate climate change, the priority task is to reduce emissions of greenhouse gases, including sulfur oxides, from stationary power plants. The legal framework of the European Union has limited the allowable emissions of gases with harmful effects and fulfillment of this obligation is also ahead of the Republic of Serbia in the following years. In this paper the categorization of wet procedures for sulfur oxides removal is given. Wet procedure with the most widespread industrial application, lime/limestone process, has been described in detail. In addition, the procedures with chemical and physical absorption and solvent thermal regeneration, which recently gained more importance, have been presented. Experimentally determined thermophysical and transport properties of commercially used and alternative solvents, necessary for the equipment design and process optimization, are also given in the paper. The obtained values of densities and viscosities of pure chemicals - solvents, polyethylene glycol 200 (PEG 200), polyethylene glycol 400 (PEG 400), tetraethylene glycol dimethyl ether (TEGDMA), N-methyl-2-pyrolidon (NMP) and dimethylaniline (DMA), measured at the atmospheric pressure, are presented as a function of temperature.

Keywords: removal of sulfur oxides, flue gases, thermal power plant, density, viscosity, climate change.

Available online at the Journal website: http://www.ache.org.rs/HI/

SCIENTIFIC PAPER

UDC 621.311.22:628.53:502.3:504.5

Hem. Ind. **68** (0) 491–500 (2014)

doi: 10.2298/HEMIND130610074Z

The sulfur oxides, generated by combustion of fuels containing sulfur (coal, oil), are the greenhouse gases with indirect effect. It is well known that these gases have a harmful impact on the environment, causing the occurrence of acid rains and respiratory problems. The flue gas desulphurization (FGD) processes had no commercial application, until the importance to protect the environment was understood, and consequently, the national legal regulations were adopted [1,2].

The EU regulations limited emissions of greenhouse gases and developed strategies to adapt to climate change. Republic of Serbia is facing a number of obligations, including the reduction of emissions of greenhouse gases, in the process of joining the European Union. Having this in mind, the processes used for flue gas desulphurization gained its importance.

This paper gives an overview of wet processes used for the removal of sulfur oxides from stationary power plants. Wet processes can be classified in non-regenerative (once-through) and regenerative procedures. The most important among them and also the most common in general practice is non-regenerative lime/ /limestone process. In this process the alkaline mixture is a reagent and gypsum is a final product. In regenerative procedures, used solvent is thermally regenerated and circulated back to the process. Among the regenerative procedures the most widespread are dual alkali process, process of chemical absorption in amines and process of physical absorption in organic solvents. The regenerative processes are further divided into those whose final product is disposed on landfill, and those with a commercially useful product.

For computer simulations, equipment design and consequently implementation of FGD procedures, it is necessary to have reliable data on thermophysical and transport properties of potential solvents. This paper presents experimentally determined densities (ρ) and viscosities (η) of pure solvents, polyethyleneglycol 200 (PEG 200), polyethyleneglycol 400 (PEG 400), tetraethylene glycol dimethyl ether (TEGDME), *N*-methyl-2--pyrollidone (NMP) and dimethylaniline (DMA), in the temperature range from 288.15 to 323.15 K and at atmospheric pressure. Some of the above mentioned liquids have already found industrial application in the regenerative processes with organic solvents, while the others are suggested as alternative absorbents due to

Correspondence: E.M. Živković, Faculty for Technology and Metallurgy, University of Belgrade, Karnegijeva 4, 11120 Belgrade, Serbia.
E-mail: emila@tmf.bg.ac.rs
Paper received: 10 June, 2013
Paper accepted: 12 July, 2013

their favourable environmental impact, low toxicity or suitable physical and chemical properties.

Wet FGD processes

As stated above wet FGD processes can be classified into regenerative and once-through. Unlike once--through procedures, the regenerative processes include solvent regeneration stage. Based on the records of flue gases desulphurization processes on thermal power plants in the US, about 90% [3] of the applied procedures are once-through. Wet lime/limestone process has been used in about 78% [3] of plants in the US, and still is the most widespread FGD technology, with gypsum as the final, commercially valuable byproduct.

A general flow diagram of the non-regenerative FGD process is shown in Figure 1. The main part of the unit is the absorber, where the flue gas containing SO_2 is brought to contact with alkaline slurry. Before alkaline slurry enters the absorber, the sorbent solid particles are crushed (at desired particle size) in a crushing station. This is inevitable step, since crushing of the solid particles will increase dissolution rate in the preparation tank. The alkaline slurry is then fed to the reaction tank and transported to the top of the absorber, usually constructed as a spray tower or tray tower. The most common configuration of the absorber is vertical with counterflow of the phases, where the flue gas containing SO_2 is flowing upwards, and set of nozzles spray alkaline slurry (lime/limestone) downwards. In the process of removing SO_2, two mechanisms take place, the sorption in the absorber and chemical reaction with the alkaline slurry in the reaction tank.

Lime/limestone process

Lime/limestone is by far the most common FGD process. The method was patented by Eschellman in 1909. The first commercial application of lime process was in London, England, and the first unit of the Battersea Power Station was put into operation in 1931. This once-through process used small amount of chalk added to water from River Thames as solvent. Many modern and improved lime/limestone processes [3,4] were based on this process.

Babcock & Wilcox Power Generation Group developed wet flue gas desulfurization systems based on standard lime/limestone process [5]. The reagent is an alkaline mixture of lime (calcium oxide (CaO) and calcium hydroxide ($Ca(OH)_2$)) or limestone (calcium carbonate ($CaCO_3$)) in water. The alkaline mixture as a reagent is introduced in absorber and brought into contact with flue gases containing SO_2. Insoluble sulfates and sulfites ($CaSO_4$ and $CaSO_3$) formed in the reaction are removed as sludge. Gas, purified after passing through the separator, is released to the atmosphere. Used sludge from absorber is sent to the reaction tank, then to a dewatering stage where water is removed and finally to the landfill. The chemical reactions and process equipment are very similar regardless of whether the alkaline mixture of water with lime or limestone is used. Schematic representation of wet lime/limestone is similar to the general flow diagram presented in Figure 1.

For some applications, and under particular operating conditions, it is allowed to leave sulfite to sulfate oxidation process intact, in so-called natural oxidation mode. For most applications, however, it is necessary

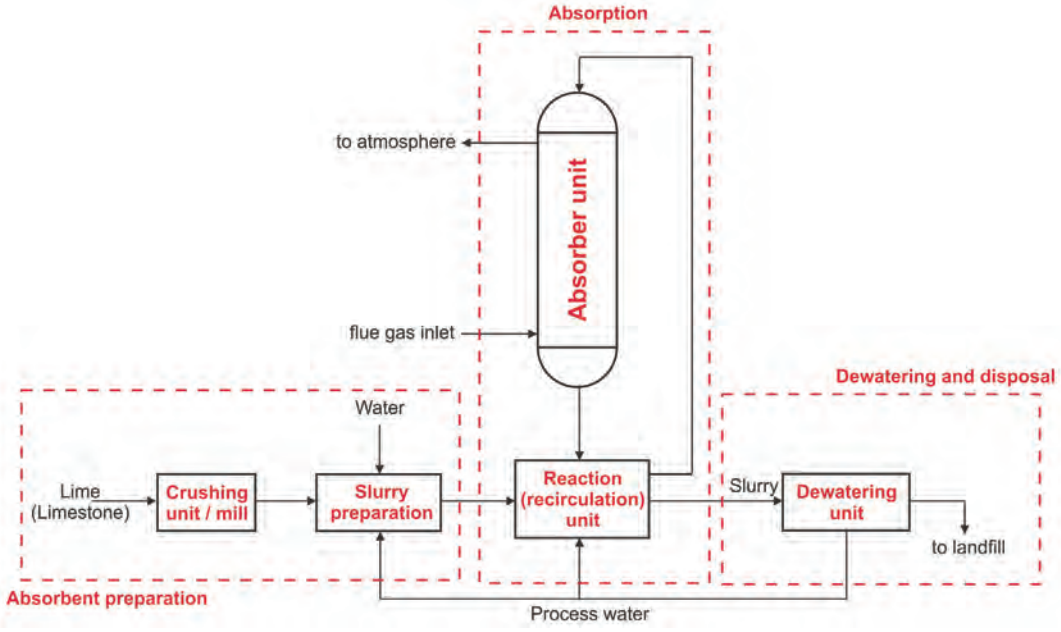

Figure 1. Wet FDG process – general flow diagram.

to control the oxidation process. One of the parameters that affects the process of oxidation in the absorber is liquid to gas phase flow rate ratio (L/G). Slurry pH is another process parameter that determines the amount of SO_2 removed. In order to improve reliability of the process it is necessary to control the oxidation process, so the limestone forced oxidation (LSFO) is most widespread subvariant. In order to prevent scaling problems, deposition of calcium sulfate - gypsum in the absorber, mist eliminator and piping, and to simplify slurry dewatering, air is usually blown through the absorbent slurry to force controlled oxidation outside the absorber. The air have to be blown through the reaction tank (in-situ oxidation) or through additional hold tank (ex-situ oxidation). Since market demand for gypsum has been reduced over the years and a wastewater treatment became a requirement, FGD technology with inhibited oxidation (LSIO) was offered as a solution.

In order to avoid scaling problems, sulfur and sodium thiosulfate emulsion could be added to the reaction tank, thus reducing oxidation rate below 15%. This variant of the process can be used with various reagents, lime, limestone, magnesium-enhanced lime and sodium. The advantages of LSIO are low investment and reagent costs and no necessity for wastewater treatement, which lead to lower overall operational costs.

Another sub-variety of lime/limestone procedure is a process enhanced by the presence of magnesium. As a sorbent, lime sludge is used, which is a mixture of water, lime and 5–8% magnesium oxide, or a mixture of water, lime and dolomite lime (with about 20% magnesium oxide). The enhanced process is very efficient compared to classic procedure and the final product is high-quality gypsum.

Since limestone is less reactive than lime, it requires slightly modified process equipment. The advantage of limestone compared to lime is in its market value (about 3 times cheaper than lime) which makes it more acceptable for use in large systems.

Wet lime/limestone process parameters are: flue gas velocity (residence time) through the absorber, L/G ratio, lime/limestone milk pH value, SO_x concentration and solid particles concentration. Flue gas velocity through the absorber depends on the type of absorber. For absorber with countercurrent flow, increasing the speed of the flue gases, can lead to lower SO_2 removal efficiency. Required alkalinity of the process rises with the increase of L/G ratio. Efficiency of the process is influenced by pH value, while the concentration of particles and their residence time in the tank affect the reliability of the process. Typical values of concentration of solids in the mixture are 10–15% by weight, while the residence time of solids in the tank is 12–14 h. Higher values of these parameters can lead to unwanted particles' deposition in the equipment.

Removal efficiency for standard wet lime/limestone process is in range from about 60 to 97%, while for subvariety of enhanced lime/limestone process with magnesium, SO_2 removal efficency can be increased to 99%. Basic operational parameters for lime/limestone systems on utility boilers in United States are given in Table 1.

Dual alkali process

Process name is derived due to presence of two types of components during absorption. Dual alkali process uses alkaline solution based on sodium as sorbent. Process also includes a stage of sorbent regeneration in which limestone is used. Calcium sulfite and sulfate formed in this stage are separated as sludge, while the regenerated sodium solution is reused in the absorption step (Figure 2). The chemistry of the process is very similar to the lime/limestone process.

Sodium-based solution (NaOH, Na_2CO_3 and Na_2SO_3) is brought into contact with the flue gas in the absorber. The used liquid solution is transported to the reactor within regeneration step, where the mixing with limestone, formation of calcium salts and sorbent regeneration take place. The sludge from the reactor is directed to the clarifier or thickener where it is filtered, water washed and emptied from the bottom. The regenerated sodium solution is sent to a mixing tank where sodium chemical compounds (soda ash or caustic soda) and water are added, and directed back to the absorber.

Table 1. Basic operational parameters for lime/limestone systems on utility boilers in US [3]

Alkaline mixture	Company/plant name	Power, MW	Fly ash control	Sulphur content in coal, %	L/G ratio, l/m^3
Water + CaO	Columbus & Southern Ohio Electric/ Conesvill #5	411	Electrostatic precipitator	4.7	6.7
	Duquesne Light/Elrama	510		2.2	5.3
	Utah Power & Light/Hunter #1, Hunter #2	400		0.6	5.7
Water + $CaCO_3$	Alabama Electric/Tombigbee #2, Tombigbee #3	255		1.2	9.4
	Commonwealth Edison/Powerton	450		3.5	8.0

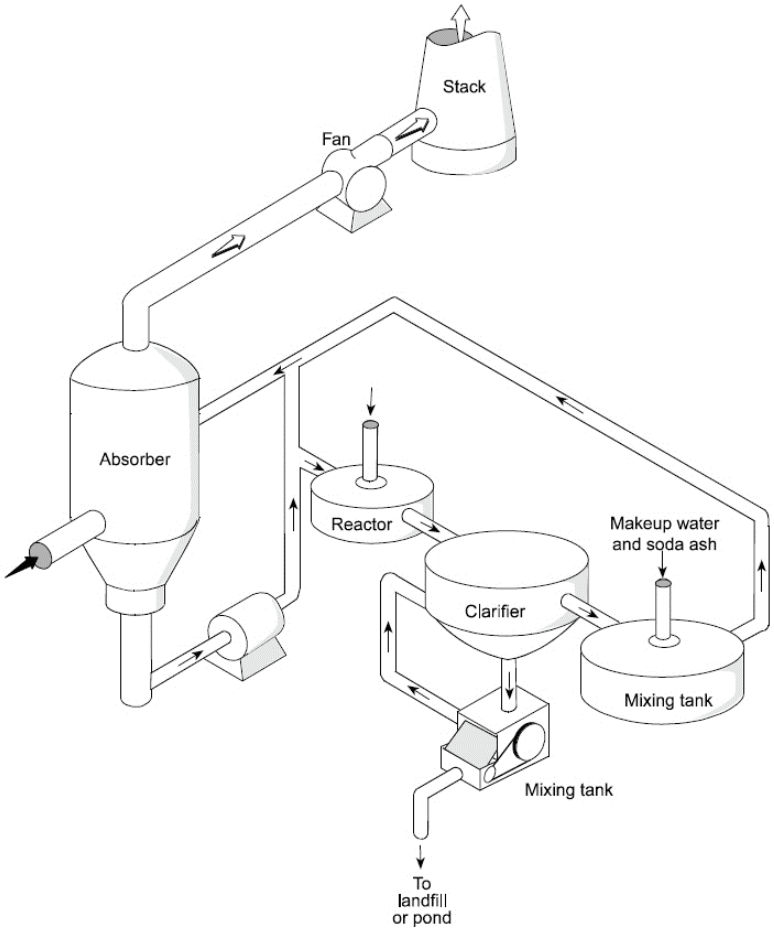

Figure 2. Schematic representation of the dual alkali process [3].

An alkaline solution of sodium is more efficient than lime/limestone solution. The required liquid to gas flow rate ratio (L/G) is much lower compared to the lime/ /limestone process, as can be concluded from Tables 1 and 2. Due to the lower L/G ratio, the process equipment is smaller in size. The process efficiency is about 95%. As a result of good solubility of sulfur oxides in sodium based alkaline solution, problems such as corrosion, erosion and deposit formation inside the equipment and installation are avoided.

Basic operational data for systems using dual alkali FGD process on utility boilers in the United States are given in Table 2 [3].

Amine processes with thermal regeneration

Processes based on chemical absorption in amines, already have applications for purification of outgoing gases from smelters (with SO_2 content higher than 3.5%). Three aromatic amines, dimethylaniline (DMA), xylidine and toulidine, are commonly used as sorbents. DMA has a lower boiling point than the other two, a higher vapor pressure and its losses during the absorption process are higher. Xylidine is preferable than toulidine, due to its higher boiling point, however it has some undesirable properties. For low SO_2 concentrations, a mixture of xylidine and water as sorbent is more suitable, while for higher SO_2 concentrations, DMA is more appropriate. The examples of amine processes with thermal regeneration that already found commercial application are Sulphidine process, ASARCO process, Dow process and CANSOLV process. This paper briefly describes the CANSOLV process.

CANSOLV process [6], owned by Cansolv Technologies Incorporated, A Shell Global Solutions Company,

Table 2. Operational data for systems using dual alkali FGD process on utility boilers in the US [3]

Company/plant name	Power, MW	Fly ash control	Sulphur content in coal, %	L/G ratio, l/m^3
Central Illinois Public Service/Newton #1	617	Electrostatic precipitator	2.5	1.3
Louisville Gas & Electric/Cane Run #6	299		4.8	1.3
Southern Indiana Gas & Electric/A.B. Brown #1	265		3.6	1.3

schematically is presented on Figure 3. It has a wide commercial application for purification of outgoing gases in industrial and utility boilers, smelters, refineries and chemical plants. The process has two steps, absorption and amine regeneration step. Flue gases come in contact with the amine solution in counter-current absorber, and treated gas exits with lower SO_2 content. Rich amine solution (with high absorbed SO_2 content) flows to the regeneration stage, and comes out as lean amine (with a lower sulfur content). Lean amine solution is regenerated by indirect steam stripping, clean SO_2 is set aside, dried and transported to sulfuric acid production unit. Lean amine leaves the regeneration unit and returns to the absorption unit.

CANSOLV process advantages are:

- Final products have its market value (pure SO_2, sulfur and sulphuric acid).
- The process does not produce solid waste.
- Low investment and operating costs.
- High flexibility in terms of gas flow rate fluctuations and SO_2 concentration in flue gases.

Physical (organic) solvent processes

Processes with organic solvents are among the most cost-effective and efficient processes for purification of flue gases with high or fluctuating SO_x content. Some organic solvents have excellent selectivity towards SO_2, in relation to other flue gas components (N_2, O_2 and CO_2). Physical solvent for SO_2 removal should have temperature dependent solubility, high selectivity to SO_2, high chemical and thermal stability, low vapor pressure, should be environmentally friendly, not harmful to human health and cost effective. Solubility of SO_2 increases almost linearly with the increase of the physical solvent partial pressure, while solubility trend in chemical solvents has minimal growth or in some cases near zero.

Advantages of physical solvents in relation to chemical solvents are:

- Cost-effective process (lower energy requirements for solvent regeneration).
- Lack of heat released due to the chemical reactions.
- Useful and commercially valuable product.

Solinox process developed by the Linde AG group, is a practical application of the physical absorption in organic solvents. In United States Solinox process is offered by Lotepro Corporation, using tetraethyleneglycol dimethylether for SO_2 removal. Detailed description of the process and operating data from plants purifying flue gas streams that emanate from lead and

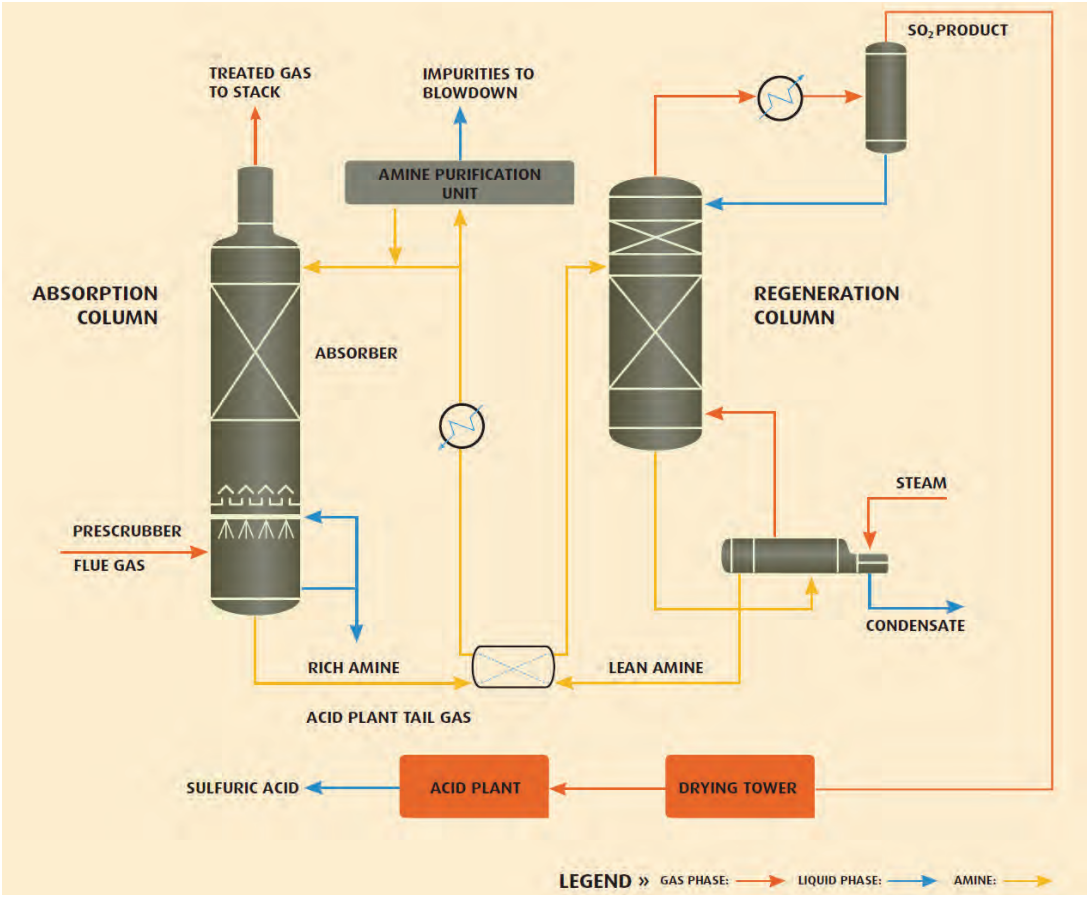

Figure 3. CANSOLV process, schematic representation [6].

zinc smelters is given by Sporer [7]. Before entering the absorber, flue gases have to be water washed, in order to lower the flue gas temperature and remove the impurities. The specific feature of this procedure is that it can remove hydrocarbons from outgoing gases, within the requirements for the air pollution control. The obtained removal efficiency for the process is 95-99.3%. Basic Solinox process has absorption and regeneration stage. The absorption stage takes place in countercurrent absorber, while regeneration stage (for separation of SO_2 from the solvent) takes place in countercurrent stripper with a reboiler.

However, investigations have shown that selectivity of TEGDME to sulfur dioxide is not satisfactory [8] and NMP as an alternative solvent has been proposed. Industrially, NMP has already been applied is in Lurgi's Purisol process with excellent results in selective desulfurization of flue gasses from oil refineries and power plants.

As an alternative to above mentioned solvents several polymers, including PEG 200 and PEG 400, have been investigated [9]. The main advantages of PEG for desulfurization processes are high solubility and desorption capability for SO_2 which lead to lower energy requirements for absorption and regeneration processes.

Ionic liquids have been recently suggested as physical solvents for FGD processes [10–12]. Due to its favorable properties (high stability, low vapor pressure, excellent selectivity towards certain gases and non-toxicity) ionic liquids have found application in various separation processes. The preliminary investigations have shown that ionic liquids could also be used as an alternative to organic solvents in the processes of physical absorption and solvent regeneration.

Determination of thermodynamic and transport properties

In order to develop an absorption process for flue gases desulfurization and to set a numerical case for computer process simulation or work on equipment design, it is necessarry to have reliable data on chemical, physical and transport properties of potential solvents. In this work the experimental densities and viscosities of five potential solvents for SO_2 removal, PEG 200, PEG 400, TEGDME, NMP and DMA, are reported at ten temperatures (288.15, 293.15, 298.15, 303.15, 308.15, 313.15, 318.15, 323.15, 328.15 and 333.15 K) and atmospheric pressure.

PEG 200, PEG 400 (99.5 mass%), NMP (99.0 mass%), DMA were supplied by Merck and TEGDME (99.0 mass%) by Acros Organics. Chemicals were kept in dark bottles in an inert atmosphere, used without further purification and degassed just before a sample preparation.

Densities, ρ, of the pure substances were measured using an Anton Paar DMA 5000 digital vibrating U-tube densimeter (with automatic viscosity correction) having a stated accuracy of $\pm 5\times10^{-6}$ g·cm^{-3}. The temperature in the cell was regulated to ±0.001 K with a built in solid-state thermostat. Temperature in the cell was measured by means of two integrated Pt 100 platinum thermometers and temperature stability was better than ±0.002 K. Calibration of the apparatus was performed daily using ambient air and Milipore quality water. The combined expanded uncertainty in the density is within $\pm 2\times10^{-5}$ g·cm^{-3} with a 0.95 level of confidence ($k \approx 2$).

Viscosities, η, of the pure substances were measured with a digital Anton Paar Stabinger viscometer (model SVM 3000/G2). The instrument contains two measuring cells; one of them is used for measuring the density of the sample. U-tube is filled with the sample liquid and excited to oscillate using magnetic coils. Density measurement is based on the relation between oscillation period and sample density. The other cell, used for dynamic viscosity measurements contains a straight tube filled with sample. The tube rotates at a constant speed. In this tube, centered by the centrifugal force, floats a measuring rotor made of low density material, with a built-in magnet. A rotating magnet in SVM 3000 induces an eddy current field with a speed dependant brake torque. Shortly after the start of the experiment the rotor reaches a constant speed determined by the equilibrium between the viscosity-dependent driving torque, proportional to the speed difference between the tube and the rotor, and the brake torque caused by eddy currents. The kinematic viscosity is calculated from the measured density and dynamic viscosity. The stated reproducibility of the dynamic viscosity and density measurements is 0.35% and 5×10^{-4} g·cm^{-3} in the temperature interval 288.15 to 333.15 K. The temperature in the cell was regulated to ±0.01 K with a built in solid-state thermostat. The relative uncertainty in dynamic viscosity measurements was estimated to be within ±0.8%.

RESULTS AND DISCUSSION

Experimental data of density (ρ) and viscosity (η) for pure chemicals PEG 200, PEG 400, TEGDME, NMP and DMA at ten temperatures, 288,15, 293,15, 298,15, 303,15, 308,15, 313,15, 318,15, 323,15, 328,15 and 333,15 K, and atmospheric pressure, are presented in Tables 3 and 4.

In Table 5, densities and dynamic viscosities of pure PEG 200, PEG 400, TEGDME, NMP and DMA have been compared with literature values at 298.15 and 303.15 K [13–24]. The agreement between literature and our experimental values is very good with differences less than 6.5×10^{-4} g·cm^{-3} for density measurements and

Table 3. Measured density values (ρ / g·cm^{-3}) of pure PEG 200, PEG 400, TEGDME, NMP and DMA at atmospheric pressure

T / K	PEG 200	PEG 400	TEGDME	NMP	DMA
288.15	1.128778	1.13009	1.01563	1.037298	0.960062
293.15	1.124828	1.126001	1.010995	1.03284	0.955975
298.15	1.120865	1.121905	1.006359	1.028382	0.951878
303.15	1.116909	1.117802	1.001732	1.023925	0.947778
308.15	1.112945	1.113711	0.997104	1.019462	0.943669
313.15	1.108981	1.109622	0.992481	1.015	0.939552
318.15	1.105016	1.105536	0.987859	1.010533	0.935426
323.15	1.101043	1.101461	0.983234	1.006061	0.931291
328.15	1.097068	1.09739	0.978613	1.001583	0.927142
333.15	1.093088	1.093324	0.973989	0.997096	0.92298

Table 4. Measured viscosity values (η / mPa·s) of pure PEG 200, PEG 400, TEGDME, NMP and DMA at atmospheric pressure

T/K	PEG 200	PEG 400	TEGDME	NMP	DMA
288.15	86.442	161.67	4.3415	1.9896	1.5247
293.15	64.815	119.54	3.8338	1.8232	1.403
298.15	49.724	90.582	3.3801	1.6795	1.2965
303.15	38.912	70.145	3.0042	1.5546	1.2035
308.15	31.006	55.365	2.6913	1.4443	1.1205
313.15	25.102	44.463	2.4258	1.3464	1.0462
318.15	20.602	36.262	2.1994	1.2593	0.97959
323.15	17.136	29.981	2.0063	1.1816	0.91971
328.15	14.424	25.097	1.8382	1.1099	0.86528
333.15	12.343	21.247	1.6914	1.0427	0.81953

Table 5. Densities ρ *and dynamic viscosities* η *of pure components at atmospheric pressure*

Component	T / K	ρ / g·cm^{-3}		η / mPa· s	
		Exp.	Lit.	Exp.	Lit.
PEG 200	298.15	1.120865	1.12098 [13]	49.724	48.157 [13]
PEG 400	298.15	1.121905	1.12249 [13]	90.582	92.797 [13]
			1.12230 [14]		
			1.1218 [9]		
			1.12162 [15]		
TEGDME	298.15	1.006359	1.0063 [16]	3.3801	3.394 [16]
			1.0067 [17]		3.313 [18]
			1.0059 [18]		
			1.00653 [19]		
NMP	298.15	1.028382	1.02872 [20]	1.6795	1.656 [20]
			1.0283 [21]		1.67 [21]
DMA	303.15	0.947778	0.9484 [22]	1.2035	1.174 [23]
			0.948 [23]		1.170 [24]
			0.94833 [24]		

within 7×10^{-2} mPa·s for viscosity measurements of less viscous fluids. The differences between experimental and literature values of viscosity are somewhat higher for more viscous fluids but still under 3% deviation.

Densities of pure components decrease with temperature increase, as expected. Measured density data show linear temperature dependence and can be correlated with linear expression (1):

$$\rho = A_0 + A_1 T \quad (1)$$

With the temperature increase viscosities behave in the same manner as densities, their values decrease

with temperature increase and can be correlated with polynomial expression (2):

$$\eta = B_0 + B_1T + B_2T^2 + B_3T^3 \quad (2)$$

Parameters A_0, A_1, B_0, B_1, B_2 and B_3 in expressions (1) and (2) are presented in Table 6.

Table 6. Polynomial parameters A_p and B_p for pure solvents (expressions (1) and (2))

Property	A_0, B_0	A_1, B_1	B_2	B_3
		PEG 200		
ρ / g·cm^{-3}	1.3573	-0.0008	-	-
η / mPa s	33739	-310.01	0.9516	-0.001
		PEG 400		
ρ / g·cm^{-3}	1.3656	-0.0008	-	-
η / mPa s	68033	-626.54	1.9271	-0.002
		TEGDME		
ρ / g·cm^{-3}	1.2822	-0.0009	-	-
η / mPa s	440.97	-3.8412	0.0113	-1 10^{-5}
		NMP		
ρ / g·cm^{-3}	1.2947	-0.0009	-	-
η / mPa s	125.22	-1.0819	0.0032	-3 10^{-6}
		DMA		
ρ / g·cm^{-3}	1.1975	-0.0008	-	-
η / mPa s	72.575	-0.6057	0.0017	-1.7 10^{-6}

CONCLUSION

In the years to come, Republic of Serbia will be faced with the need and obligations to reduce emissions of greenhouse gases, including sulfur oxides. In view of this fact, particular attention has to be focused on emissions from major polluters – the stationary power plants.

In this paper, review of wet flue gas desulphurization technologies has been presented. The most common technology for flue gas desulfurization is wet lime/limestone process. With development of flue gas desulphurization technology, wet procedures with solvent regeneration attract more attention, because of their advantages, in terms of efficiency, solvent use and environmental impact. Among regenerative procedures the most widespread are dual alkali process and processes based on absorption in amines or absorption in organic solvents.

The transport properties of potential solvents for FGD processes are of great importance for computer simulation and equipment design. Thermophysical and transport properties (density and viscosity) of pure solvents, PEG 200, PEG 400, TEGDME, NMP and DMA have been measured and presented in the paper.

Acknowledgment

The authors gratefully acknowledge the financial support received from the Research Fund of Ministry of Education, Science and Technology Development of the Republic of Serbia and the Faculty of Technology and Metallurgy, University of Belgrade (project No. 172063).

REFERENCES

[1] Sulfur Dioxide, EPA – United States Environmental Protection Agency, (http://www.epa.gov/air/sulfurdioxide/).

[2] European Commission, Climate Action, EU greenhouse gas emmissions and targets, (http://ec.europa.eu/clima/policies/g-gas/index_en.htm).

[3] Flue Gas Desulfurization (Acid Gas Removal) Systems, Lesson 9, United States Environmental Protection Agency (www.epa.gov).

[4] R.K. Srivastava, W. Jozewicz, C. Singer, SO_2 Scrubbing Technologies: A Review, Environ. Prog. **20**(4) (2001) 219–228.

[5] Wet Gas Desulfurization (FGD) Systems, Advanced Technology For Maximum SO_2 Removal, Babcock & Wilcox Power Generation Group (www.babcock.com).

[6] Cansolv Technologies Incorporated, A Shell Global Solutions Company, State of the Art Gas Absorption Solutions (www.cansolv.com).

[7] J. Sporer, The Linde Solinox Process: Gypsum-free fluegas desulphurization, Gas Separ. Purif. **6**(3) (1992) 133–140.

[8] M.H.H. van Dam, A.S. Lamine, D. Roizard, P. Lochon, C. Roizard, Selective Sulfur Dioxide Removal Using Organic Solvents, Ind. Eng. Chem. Res. **36** (1997) 4628–4637.

[9] F. Han, J. Zhang, G. Chen, X. Wei, Density, Viscosity and Excess Properties for Aqueous Poly(ethylene glycol) Solutions from (298.15 to 323.15) K, J. Chem. Eng. Data **53** (2008) 2598–2601.

[10] X.L. Yuan, S.J. Zhang, X.M. Lu, Hydroxyl Ammonium Ionic Liquids: Synthesis, Properties, and Solubility of SO_2, J. Chem. Eng. Data **52**(2) (2007) 596–599.

[11] K.Y. Lee, G.T. Gong, K.H. Song, H. Kim, K.D. Jung, C.S. Kim, Use of Ionic Liquids as absorbents to separate SO_2 in SO_2/O_2 in thermochemical processes to produce hydrogen, Int. J. Hydrogen Energy **33**(21) (2008) 6031–6036.

[12] J. Huang, A. Riisager, P. Wasserscheid, R. Fehrmann, Reversible physical absorption of SO_2 by ionic liquids, Chem. Commun. (2006) 4027–4029.

[13] S. Ottani, D. Vitalini, F. Comelli, C. Castellari, Densities, Viscosities, and Refractive Indices of Poly(ethylene glycol) 200 and 400 + Cyclic Ethers at 303.15 K, J. Chem. Eng. Data **47** (2002) 1197–1204.

[14] E.A. Mueller, P. Rasmussen, Densities and excess volumes in aqueous poly(ethylene glycol) solutions, J. Chem. Eng. Data **36** (1991) 214–217.

[15] C. Aucouturier, G. Roux-Desgrenges, A.H. Roux, Excess Molar Volumes and Excess Molar Heat Capacities of Poly (ethylene glycols)+Water at Temperatures between *T* = 278 K and *T* = 328 K, J. Chem. Thermodyn. **31** (1999) 289–300.

[16] A. Pal, G. Dass, A. Kumar, Excess Molar Volumes, Viscosities, and Refractive Indices of Tetraethylene Glycol Dimethyl Ether + Dimethyl Carbonate, + Diethyl Carbonate and + Propylene Carbonate at 298.15 K, J. Chem. Eng. Data **44** (1999) 2–5.

[17] J.N. Real, T.P. Iglesias, S.M. Pereira, M.A. Rivas, Analysis of temperature dependence of some physical properties of (*n*-nonane + tetraethylene glycol dimethyl ether), J. Chem. Thermodyn. **34** (2002) 1029–1043.

[18] M.E. Ferreyra de Ruiz Holgado, C.R. de Schaefer, E.L. Arancibia, Densities and Viscosities of Binary Mixtures of Polyethylene Glycol 350 Monomethyl Ether with *n*-Butanol and *n*-Pentanol and Tetraethylene Glycol Dimethyl Ethers with *n*-Propanol, *n*-Butanol and *n*-Pentanol from 278.15 K to 318.15 K, J. Chem.Eng. Data **47** (2002) 144––148.

[19] F.J. Carmona, F.J. Arroyo, I.D. de la Fuente, J.A. Gonzales, J.C. Cobos, Excess Molar Volumes of Methanol or Ethanol + *n*-Polyethers at 298.15 K, Can. J. Chem. **77** (1999) 1608–1616.

[20] A. Henni, J.J. Hromek, P. Tontiwachwuthikul, A. Chakma, A. Volumetric Properties and Viscosities for Aqueous *N*-Methyl-2-pyrrolidone Solutions from 25 °C to 70 °C, J. Chem. Eng. Data °C (2004) 231–234.

[21] D.D. McDonald, D. Dunay, G. Manlon, J.B. Hyne, Properties of the *N*-methyl-2-pyrrolidinone-water system, Can. J. Chem. Eng. **49** (1971) 420–423.

[22] V. Pandiyan, S.L. Oswal, P. Vasantharani, Thermodynamic and acoustic properties of binary mixtures of ethers. IV. Diisopropyl ether or oxolane with *N*,*N*-dimethylaniline or *N*,*N*-diethylaniline at 303.15, 313.15 and 323.15 K, Termochim. Acta **518** (2011) 36–46.

[23] M. Kondaiah, D. Sravana Kumar, K. Sreekanth, D. Krishna Rao, Densities and Viscosities of Binary Mixtures of Propanoic Acid with *N*,*N*-Dimethylaniline and *N*,*N*-Diethylaniline at *T* = (303.15, 313.15, and 323.15) K, J. Chem. Eng. Data **57** (2012) 352–357.

[24] A.G. Oskoei, N. Safaei, J. Ghasemi, Densities and Viscosities for Binary and Ternary Mixtures of 1,4-Dioxane + 1-Hexanol + *N*,*N*-Dimethylaniline from *T* = (283.15 to 343.15) K, J. Chem. Eng. Data **53** (2008) 343–349.

IZVOD

PREGLED MOKRIH POSTUPAKA ZA ODSUMPORAVANJE DIMNIH GASOVA I ODREĐIVANJE TERMOFIZIČKIH SVOJSTAVA NJIMA ODGOVARAJUĆIH RASTVARAČA

Nikola Živković[1], Slobodan Šerbanović[2], Emila Živković[2], Mirjana Kijevčanin[2], Predrag Stefanović[1]

[1]*Institut za Nuklearne Nauke "Vinča", Univerzitet u Beogradu, Laboratorija za termotehniku i energetiku, p. pr. 522, 11001 Beograd,Srbija*

[2]*Tehnološko–metalurški fakultet, Univerzitet u Beogradu, Karnegijeva 4, 11120 Beograd, Srbija*

(Naučni rad)

Za ublažavanje klimatskih promena, neophodno je izvršiti smanjenje emisija gasova sa efektom staklene bašte među koje spadaju i sumporni oksidi iz stacionarnih termoenergetskih postrojenja. Ublažavanje promena je uslovljeno zakonskim okvirom Evropske Unije. Ispunjenje ove obaveze je i pred Republikom Srbijom u narednim godinama. S obzirom na prioritete i aktuelnost navedene problematike, u radu je data kategorizacija mokrih postupaka za uklanjanje sumpornih oksida iz dimnih gasova iz termoelektrana i prikazane su karakteristike odgovarajućih solvenata za regenerativne postupke. Opisan je u praksi najzastupljeniji mokri krečni postupak. Predstavljeni su postupci sa termalnom regeneracijom solventa zasnovani na hemijskoj ili fizičkoj apsorpciji, koji u poslednje vreme imaju sve veći značaj. Prikazani su rezultati eksperimentalnog određivanja termofizičkih svojstva komercijalno primenjenih i alternativnih solvenata, koja su od primarnog značaja za projektovanje opreme i optimizaciju procesa. Izmerene vrednosti gustine i viskoznosti čistih rastvarača, polietilenglikol 200 i 400 (PEG 200 i PEG 400), tetraetilenglikola–dimetil-etar (TEGDME), *N*-metil-2-pirolidona (NMP) i dimetilanilina (DMA), na atmosferskom pritisku, predstvljene su u funkciji temperature.

Ključne reči: Uklanjanje sumpornih oksida • Dimni gasovi • Termoelektrana • Gustina • Viskoznost • Klimatske promene

Mineral composition of different basil (*Ocimum* spp.) genotypes

Vlado Đ. Ličina, Slavica Ć. Jelačić, Damir V. Beatović, Svetlana B. Antić Mladenović

University of Belgrade, Faculty of Agriculture, Zemun, Serbia

Abstract

This experiment investigated mineral composition of 13 basil genotypes (*Ocimum* spp.) in order to find varieties supporting human dietary intake of essential minerals and to evaluate basil genotypes which could serve for herbal production as raw material in pharmaceutical or food processing industry. In addition, this study tested a potential risk of the accumulation of heavy metals during the commercial production of basil on agricultural soil. Mineral composition of basil genotypes was found to be in association with its genetic potential, where some of them can be used in human nutrition as an additional source of several minerals, particularly micronutrients (Fe, Mn and Zn), which generally improve human immune system. Iron-rich basil genotypes were identified in this experiment, like Compact (3576.0 mg/kg), with Lattuga (1585.6 mg/kg) and Blue spice (1167.9 mg/kg) genotypes, containing more than 1000 mg/kg of Fe in herbal part on dry basil (d.m.). This attract a special attention as a source of iron, especially for humans with low Fe intake, and consequently, for people with low level of hemoglobin. Basil grown on agricultural soil was tested on the accumulation of heavy metals (Cu, Co, Cu, Ni, Cr and Pb), which were not found to be excessive in herbal parts of the plants. Cluster analysis (CA) distinguished *Ocmium* spp. genotypes in two separate groups. Despite of significant differences among the genotypes, content of Fe, Mn, Co, Cr, Ni and Pb made a clear distinction between the clusters.

Keywords: basil, genotyp, mineral composition, iron, heavy metals, cluster analysis.

Available online at the Journal website: http://www.ache.org.rs/HI/

SCIENTIFIC PAPER

UDC 635.71:575:54:51

Hem. Ind. **68** (4) 501–510 (2014)

doi: 10.2298/HEMIND130314075L

Basil (*Ocimum* spp.) falls within Labiates mint family plant that usually grows in tropical and subtropical countries and it is widely used in human nutrition as a spice, improving aroma in meat, vegetable and other meals. However, the primary culinary interest in this herb has decreased to be substituted by its medicinal properties, since it is widely used in health treatments [1–3]. Recently, basil studies get all the more attention due to organic compounds containing aroma compounds which are to be found in volatile extracts exhibiting potent antioxidant activity comparable to the known antioxidants [4]. In considering the abundance of these aroma chemicals in basil plants, we can say that the total activity is either comparable or higher to the known antioxidants [5]. In fact, the obvious antioxidant potential of basil are based on the presence of polyphenolic compounds and essential oils extracted from the above ground herbal parts, in which rosmarinic acid is the most prevalent basil phenol [3,6–8]. Therefore, in recent years a great commercial interest in this crop increased after such assigned antioxidant health benefit of basil for humans [9], so that basil is now globally grown as a medicinal plant species. Its commercial cultivation usually tends to sustain growth originating from its natural eco system [10], thus limiting fertilizer use, especially the use of nitrogen which affects its antioxidant potential [11,12], while increased potassium application can alter antioxidant capacity and phenolic concentration of basil in a positive way [13].

Despite the fact that people's interest in basil as a medicinal plant increases all the time, all around the world there is also a strong interest in aromatic plants due to their dietary minerals [14–16]. Green parts of basil can provide additional amount of several minerals in human nutrition, particularly micronutrients [17] which play a critical role in some protein synthesis and essential enzyme system which can improve resistance to diseases in people [18]. The importance of mineral content of basil has been recognized in several recent studies, imposing environmental factors (locality) as the one playing an important role in accumulation of mineral nutrients [19–22]. However, genetic diversity of basil species may also significantly change the mineral and chemical composition of the plant, especially in secondary metabolite products of herbal parts, sometimes strictly related to its taxonomy species [23]. This is usually related to basil morphological variability, expressed as differences in steam and leaves shape, making it difficult to use morphological traits as a reliable indicator for its selection in commercial use.

This study, which included 13 different basil genotypes grown in the same soil substrate under the iden-

Correspondence: V.Đ. Ličina, University of Belgrade, Faculty of Agriculture, Nemanjina 6, 11080 Zemun, Serbia.

E-mail: licina@agrif.bg.ac.rs

Paper received: 14 March, 2013

Paper accepted: 1 October, 2013

tical nutritional regimes, gives an opportunity to evaluate each genotype according to the presence/excess of essential elements in herbal tissue and to select basil species recommendable for further growth. Besides, concerning other important parameters like a basil herbal yield and its morphological appearance, this study can significantly contribute to its selection for pharmaceutical and food processing industry purposes. Although many studies have focused on the characterization of volatile oils and phenol compounds of different genotypes within this species [24–26], the obtained results could be also used to describe genotype diversity and to indicate to chemical polymorphism in mineral composition of this herbaceous and medical plant. Apart from the fact that they contain essential minerals, the main constraint of each plant species of wild origin is the presence of heavy metals in their herbal tissues, varying among the species and growing conditions [27,28], so that this study also highlights the specific heavy metal (Cu, Cd, Co, Cr, Ni and Pb) accumulation in each tested genotype during its growth for commercial purpose.

Mineral composition may serve to identify similarities or differences between basil cultivars, therefore one can draw certain conclusions regarding the classification of individual samples. In order to obtain useful biological information from a complex spectral data set, mineral composition can be combined with cluster analysis. Previously, CA has been used to evaluate different basil collections [29–31].

Therefore, the analyzed data can be useful in the selection of varieties, where excessive heavy metal accumulation is one of the most limiting factors when it comes to the use thereof by humans, while the goal of cluster analysis was to detect relations between the genotypes.

EXPERIMENTAL

Material

The experimental plot was located in Belgrade at the "City nursery" in NE part district – Zemun (longitude 44.8500° N, latitude 20.4000° E) throughout 2011. The nursery was used for city's decorative and herbal plants production, covering 4 ha area. The field experiment was established based on the system of a random block arrangement with 4 repetitions. The experimental crop was established through the nursery. Plants were transplanted at the distance of 50 cm in the basic plot, so that plants were set at the distance of 50 cm (50 cm×50 cm). The size of the basic plot was 6 m^2 and it contained 35 plants in each. The total number of basic plots was 52, and the surface covered by the experiment was 312 m^2. They used basil genotypes labelled by numbers 01 to 13 in which: Lime, Hollander, Purple Ruffles, Lattuga, Cinnamon, Osmin, Blue Spice, Siam Queen, Fino Verde, Purple Opal, Compact, Genovese, belong to *Ocimim basilicum* L., while Holy Red belongs to *Ocimim sanctum* L. The used basil genotypes have been derived from the national collection of germ-plasma (Plant Gene Bank of the Republic of Serbia) and its genotype collection of Institute of Crop Science (Faculty of Agriculture, University of Belgrade) as described by Beatović *et al*. [32].

Soil analysis

Representative soil sampling was carried out to the depth of 30 cm, with 3 sub-samples from each experimental block merged in a single sample, the quantities thereof necessary for the analyses were brought to the laboratory in appropriate polyethylene bags. For the analyses, a representative sample of each 4 replicate was made upon the mixing and homogenization of 20 spade probes, which was thereafter air dried (20 °C), and sieved through a 2 mm stainless-steel mesh.

Particle-sized distribution combined wet sieving (coarse, medium and fine sand) and pipette sedimentation technique (silt and clay). Prior to separation, 1:4 soil/water suspension was ultrasonically treated (40 MHz, 120 W) for 30 min following the procedure described by Hereter *et al*. [33]. Collected fractions were dried at 40 °C and weighed.

Basic chemical properties of soil were analyzed using standard soil analysis methods: pH was measured in a suspension characterized by a residue/water ratio of 1:2.5. Inorganic $CaCO_3$ was quantified by Scheibler method [34], organic C by dichromate method. Total N was determined using a Kjeldahl method [35], available N forms (NH_4^+ and NO_3^-) were extracted with 2M KCl and determined by hot distillation with MgO and Devarda alloy for NO_3^- determination [36]. Available P was determined using spectrophotometry upon the extraction in AL solution (0.1 M ammonium lactate and 0.4 M HOAc) [37], Available K was quantified by flame photometry from the same extraction solution as K. Determination of available boron was done after its extraction with hot water and used cucurmin method for colorimetric determination [38].

Pseudo-total metal concentrations (Fe, Mn, Cu, Zn, Co, Pb, Ni and Cd) in nursery soil were quantified using atomic absorption spectrophotometry AAS (Varian SpectrAA 202 FS), in flame acetylene/air, after digestion using HNO_3 (70%) + H_2O_2 (33%) [34]. This digestion is considered useful if complete metal recovery is not essential [35] where metals in residuum are not expected to be released in a solution over a reasonable time span under the conditions normally encountered in nature [36]. Detection limits, calculated as analytic concentration greater than three times standard deviation, obtained after eight measurements of the blank solution, were (μg/ml): 0.010 Fe, 0.003 Mn, 0.001 Cu,

0.015 Zn, 0.002 Co, 0.002 Pb, 0.002 Ni, 0.007 Cr and 0.001 Cd. The certified reference material, BCR No. 141, was analyzed to ensure accuracy. Labile pool of heavy metals in soil samples was determined by flame AAS after extraction with 0.005 M DTPA solution (diethylenetriaminopentaacetic acid), as proposed by Lindsay and Norvell [37].

Plant analysis

The yield of fresh and dry basil herb was determined on the sample of plants per genotype (4×10). Plants were cut at the height of 5 cm above the soil surface, and the fresh herb yield (g/plant) above the soil surface was measured on the scale (KERN MH5K5) for field measurements. Dry herb yield was determined upon drying fresh herb at the temperature of 40 °C.

The plant material (basil herbs) collected from field was brought into the lab and then prepared for analyses: washed with tap water, rinsed with distilled water, submerged in 0.1 M HCl to ensure that leaf surface was free of adhering soil particles, and finally carefully rinsed with de-ionized water. Prior to mineral and metal analysis, all plant material was oven-dried (80 °C) for 15 h, weighed and grounded into powder in a plant lab sample grinder (Retsch). The analytical method applied for macronutrient and B determination was the same method applied for the soil, while metal content in the plant material was also determined by AAS, after the digestion in concentrated acids: HNO_3 and $HClO_4$, with the addition of 33% H_2O_2.

Statistical analyses

Analysis of variance (ANOVA) was carried out. All ANOVAs were performed using treatments as statistical parameters at a significance level of $P \leq 0.05$. The least significant difference (*LSD*), if necessary, was used to determine whether the difference between two accessions was big enough to be considered real at a fixed level of confidence (*LSD* 0.05 = 95% confidence and *LSD* 0.01 = 99% confidence). Data referring to the content of elements in the plant material, as well as the weight of fresh and dry basil herb, were expressed in the average value and the standard deviation value.

All the properties were used to cluster accessions into similarity groups using the unequal pair group method with arithmetic mean (UPGMA). Statistical analyses were conducted using STATISTICA for Windows 6.0 (StatSoft Inc., Tulsa Okla).

RESULTS AND DISCUSSION

Soil properties and metal concentration

The intended experimental nursery plot, stipulated for basil growth, is located on chernozem soil type [38], and it obtains seedling production of different agricultural and decorative plant species. Main properties of the soil have been analyzed, as shown in Table 1, in order to determine physical, chemical and nutritional properties thereof. Soil texture is sandy loam, with a strong predominance of silt fraction (41.65%), and significant presence of fine sand (36.52%). Investigated chernozem is of slightly alkaline pH (7.66) reaction, generally in optimal values for the growth of the most plants. A slight amount (0.33%) of $CaCO_3$ was present in this soil. In comparison with the total nitrogen, the total organic matter is not so high for this soil type (2.98 and 0.174%), while available phosphorus is low (< 10 mg/100 g) and available potassium in the medium range (18.4 mg/100 g). In the analyzed samples, the available nitrogen content (14.0 mg/kg) is also low, as a result of missed fertilization, which should keep the herbal quality of basil as good as possible.

Table 1. Soil properties with pseudo-total (aqua regia) and DTPA-extractable metal concentrations (means ± standard deviation) collected from experimental field used for growth of different basil (Ocimum spp.) genotypes

Soil property	Values
pH_{H2O}	7.66
pH_{KCl}	6.47
Organic matter, %	2.98
$CaCO_3$, %	0.3
Coarse sand (0.2–2.0 mm), %	1.4
Fine sand (0.05–0.2 mm), %	36.52
Silt (0.05–0.002 mm), %	41.65
Clay (<0.002 mm) , %	21.33
Total N, %	0.174
NH_4+NO_3, mg kg^{-1}	14.0
P_2O_5, mg/100 g	6.6
K_2O, mg/100 g	18.4
B, mg/kg	0.5±0.05
Fe, mg/kg	1440±51.0[a], 11.5±1.8[b]
Mn, mg/kg	183.4±10.12[a], 3.9±0.8[b]
Cu, mg/kg	10.9±0.31[a], 2.53±0.42[b]
Zn, mg/kg	46.2±7.11[a], 0.51±0.02[b]
Cd, mg/kg	–[c], 0.08±0.01[b]
Co, mg/kg	8.9±0.03[a], 0.05±0.01[b]
Ni, mg/kg	28.1±6.4[a], 0.23±0.01[b]
Pb, mg/kg	22.8±2.16[a], 2.39±0.05[b]
Cr, mg/kg	23.9±5.43[a], –[d]

[a]Pseudo-total (*aqua regia*); [b]DTPA-extractable concentrations; [c]HNO_3 is an appropriate media for pseudo total Cd detection; [d]DTPA extraction of available Cr under detection limit (0.007 μg Cr/ml)

Analysis of pseudo-total (*aqua regia*) metal content is usual for this soil type [39]. The level of heavy metals was mainly below the critical values for soils and substrates, and analyzed chernozem should be treated unpolluted. Heavy metal content (mg/kg) slightly varied

among collected samples, according to applied block system, with the average of 10.9 Cu, 46.2 Zn, 8.9 Cd, 28.,1 Ni, 22.8 Pb and 23.9 Cr, while HNO_3 was an appropriate media for pseudo total Cd detection. At all sampling locations, the average content of heavy metals in each soil sample was under the critical threshold background.

Micronutrients and heavy metals are phytoavailable as DTPA extracted values in Table 2. DTPA-extractable proportion of heavy metals pseudo-total concentration decreases in order Cu > Pb > Zn > Ni > Co, while DTPA extractable Cr was under the detection limit (0.007 μg Cr/ml). A very low phytoavailable proportion of pseudo total content was found in all samples for Ni (0.23%), Zn (0.51%) and Co (0.05%), possibly influenced by relatively high pH (>6.5) [40] and high organic content (2.98%) [41], while Cu and Pb had considerably higher available amounts (2.53 and 2.39%, respectively). However, positive correlation between pseudo-total and available amounts of heavy metals in soil was not found.

Yield and morphology issue

The taxonomy of *Ocimum* was complex due to the interspecies hybridization and polyploidy of the species in genus, but now we can speak about 65 basil species, where the *Ocimum basilicum* L. should be treated as a major genus aimed as crop and grown in many countries [42]. There was no matching in genotype and habitus appearance among investigated basil genotypes (13). In fact, there was no clear connection between any available shape of basil aboveground part and its genotype status. However, the obtained basil biomass yield significantly varied between genotypes, both as a fresh or dried biomass, pointing out that primary basil yield depended on its genotype origin (Table 2).

Fresh basil herb yield was calculated at the sample of 40 plants per genotype (4×10). In the experiment, two genotypes had the biggest herbal yield: Fino verde (65.85 g) and Hollander (67.0 g), both as a linalool chemotype, however with different habitus, intermediarius and upright, respectively. The biomass variation among investigated genotypes were rather high, sometimes double or even tree times (3.78) higher (e.g., Holy Red: 17.7 g *versus* Holandjanin: 67.0 g), which provided useful information for basil selection for cultivation.

Comparing our results to those of other researchers, regarding the same genotypes and different agroecological conditions, we can say that the experiment was set up at the advantageous conditions for basil production. Namely, the experiments carried out in Europe, on the same genotypes, have resulted in basil herb yields somewhat below the average values [43–46].

Macronutrient issue

Since there was no significant interaction between macronutrient and micronutrient accumulation in examined basil genotypes, the presence of this minerals in dry tissue was discussed separately. Two approaches could be used to summarize a review about plant tissue macronutrient accumulation: their percentage in tissue or their uptake by plant yield (g/plant) (Table 3).

A significant variation has been found between the content of elements in the plant of each investigated basil genotype, showing the substantial mineral diversity of examined species. Two elements (N and Ca) participate with the highest amount in basil biomass, where the level of the former could be easily changed

Table 2. Herbal biomass yield (g/plant of fresh and dried biomass) of different basil (Ocimum spp.) genotypes with chemotype classification grown in field experiment

Genotype	Chemotype	Habitus	Fresh herba, g/plant	Dried herba, g/plant
Holy Red	Caryophyllene	Upright	85.5±2.14	17.7±0.32
Lime	Geranial – neral	Intermediarius	106.75±3.66	20.05±0.41
Hollander	Linalool	Upright	318.5 ±3.56	67.0±0.70
Purple Ruffles	Linalool	Upright	138.75±2.71	19.85±0.41
Lattuga	Linalool	Intermediarius	208.0±2.92	31.0±0.52
Cinnamon	Linalool – methyl cinnamate	Upright	242.5±4.21	43.2±0.73
Osmin	Linalool	Intermediarius	168.75±2.17	25.5 ±0.74
Blue Spice	Bisabollene	Intermediarius	205.75±2.06	35.15±0.43
Siam Queen	Methyl chavicol	Intermediarius	232.5±3.53	43.65±0.65
Fino Verde	Linalool	Intermediarius	311.0±2.85	65.85±0.60
Purple Opal	Linalool	Intermediarius	141.75±4.16	22.3±0.39
Compact	Linalool	Roundish	276.0±3.45	55.2±0.70
Genovese	Linalool	Upright	260.0±3.64	44.9±0.32
LSD = 0.05			5.35	2.75
LSD = 0.01			7.45	4.25

Table 3. Macronutrient content (%) and their uptake by plant yield (g/plant) of different genotypes of basil (Ocimum spp.) grown in field experiment

Genotype	N		P_2O_5		K_2O		Ca		Mg	
	%	g/plant	%	g/plant	%	g/plant	%	g/plant	%	g/plant
Holy Red	3.22±0.11	0.57	0.63±0.08	0.11	1.11±0.05	0.20	1.92±0.03	0.34	0.46±0.11	0.08
Lime	2.75±0.18	0.55	0.76±0.04	0.15	1.52±0.17	0.31	1.94±0.04	0.39	0.84±0.08	0.17
Hollander	3.33±0.10	2.23	0.84±0.03	0.57	1.45±0.06	0.97	2.56±0.11	1.71	0.54±0.04	0.36
Purple Ruffles	3.33±0.22	0.66	0.81±0.01	0.16	1.64±0.08	0.33	2.78±0.09	0.55	0.87±0.08	0.17
Lattuga	3.52±0.13	1.09	0.99±0.12	0.31	1.76±0.34	0.55	3.60±0.10	1.12	0.75±0.15	0.23
Cinnamon	3.81±0.10	1.64	1.08±0.07	0.47	2.07±0.03	0.89	2.46±0.22	1.06	0.70±0.07	0.30
Osmin	3.29±0.01	0.84	0.85±0.19	0.22	2.03±0.17	0.52	3.18±0.14	0.81	0.62±0.04	0.16
Blue Spice	2.40±0.34	0.86	0.80±0.03	0.28	1.86±0.05	0.65	1.92±0.12	0.68	1.53±0.19	0.54
Siam Queen	2.91±0.49	1.27	0.93±0.06	0.40	2.15±0.15	0.94	2.64±0.67	1.15	0.81±0.04	0.35
Fino Verde	2.74±0.12	1.81	0.68±0.02	0.45	1.40±0.25	0.92	3.65±0.07	2.41	0.67±0.12	0.44
Purple Opal	2.27±0.16	0.51	0.97±0.12	0.22	1.55±0.10	0.35	3.29±0.05	0.73	0.84±0.20	0.19
Compact	1.97±0.33	1.09	0.80±0.03	0.44	1.94±0.03	1.07	3.22±0.11	1.78	0.73±0.04	0.40
Genovese	3.45±0.11	1.55	0.81±0.01	0.36	1.13±0.08	0.51	3.42±0.09	1.54	0.84±0.08	0.38
LSD = 0.05	0.07		0.01		0.05		0.06		0.05	
LSD = 0.01	0.05		0.005		0.04		0.04		0.04	

by fertilization [47], but the uptake of the latter is genetically controlled [48]. In addition, potassium fertilization during the basil production is still necessary and considered desirable [49]. The "dilution effect" in mineral analyses [50] could be successfully overcome by the calculation of nutrient uptake by the formed biomass. This usually provides more obvious data about the potential and capability of each genotype to accumulate these minerals from the soil. Therefore, formed plant biomass sometimes is crucial for nutrient accumulation, where low or high nutrient content in tissues does not portray a realistic picture of the plant's needs. This is illustrated by our results: certain genotypes with the smallest growth between tested species (Holy red, Lattuga and Osmin), have had a relatively small accumulation of nitrogen, dispute N high concentration in analyzed tissues (3.22, 3.52 and 3.29%, respectively) (Table 3). Among others, two genotypes stand out for the highest N accumulation in tissues (Hollander and Fino Verde), assuming that this genotype feature has the biggest impact on organic compound synthesis.

Micronutrient issue

Monitored medicinal, aromatic and spice plants grown in different regions usually show differences in the concentration of elements, as a consequence of soil composition and the climate in which the plant is grown [51]. However, the presence of micronutrients in green parts of the plants support a synthesis of organic compounds in plant tissues [52], providing organic and mineral substances which act as an enzyme activator in human body [53]. So far, in recent years, with enhanced awareness of the importance of trace elements on health, an increasing number of reports on the role of trace elements in medicines has been published in different countries [54–56]. According to the results obtained from this investigation, some genotypes of examined basil should be regarded as a rich source of micronutrients for humans (Table 4).

A significant variation in microelement content was identified among basil genotypes, which can be related to different biomass growth of tested basil species, or to its genotype adaptation to the growing conditions. Consequently, this could possibly induce the presence of different chemical compounds in herbal tissues [57]. In fact, some elements were detected in substantial amounts, like Fe and Mn in Compact and Zn in Lattuga variety, qualifying these genotypes as extraordinary for human use. The ability of plants to make Fe organic chelating in tissues [52] is another basil advance for medical use. Therefore, found Fe-rich basil genotypes (Blue Spice – 1167.9 mg/kg, Lattuga – 1585.6 mg/kg and especially Compact, with 3576.0 mg/kg of Fe on dry basis) could be of special interest as iron source for humans with extreme hemoglobin deficit. Dispute that basil is classified as a spice and usually used in human nutrition in very small amounts, its effects as a Fe source in human food can be illustrate on the basis of its daily intake by salad. The result of Fe fresh tomato salad use could be taken into account. If dry mater of tomato fruits contain the highest 2.41±0.34 mg/kg of Fe according to investigation [59], due to its very high water content (92.84–94.76%) [58], the amount of 1000 g of this vegetable will provide 0.1446 mg of iron in nutrition. The addition of only 1 g of d.m. of basil spice (Compact variety) to this salad, however, can

Table 4. Micronutrient and heavy metal content (mg/kg) in basil of different basil genotypes (Ocimum spp.) grown in field experiment

Genotype	Fe	Mn	Cu	Zn	B	Cd	Co	Cr	Ni	Pb
Holy Red	766.5±40.0	73.2±9.5	13.78±1.01	28.60±3.19	25.83±1.26	0.21±0.02	1.75±0.38	3.11±0.13	1.97±0.06	1.08±0.03
Lime	477.4±8.7	74.4±14.6	15.64±2.44	44.36±5.59	19.67±0.76	0.17±0.02	1.78±0.40	4.19±0.13	1.62±0.17	0.69±0.17
Hollander	202.1±17.7	78.5±9.6	24.19±3.66	52.87±5.68	20.67±2.57	0.21±0.08	1.90±0.05	2.15±1.02	2.77±0.83	0.51±0.10
Purple Ruffles	719.1±92.8	92.6±31.8	16.91±3.29	42.28±7.06	27.00±3.77	0.07±0.03	2.55±0.44	5.82±0.45	2.40±0.24	0.30±0.02
Lattunga	1126.0±101.6	126.4±36.3	19.14±4.61	124.6 ±21.6	30.33±1.26	0.23±0.05	2.97±0.28	4.50±0.71	3.39±0.60	0.85±0.18
Cinnamon	290.1±61.7	77.5±5.3	19.36±1.92	47.89±3.59	23.17±2.02	0.35±0.08	2.20±0.15	3.23±0.10	1.65±0.14	0.73±0.08
Osmin	686.0±62.8	87.4±8.3	18.92±2.89	54.35±5.50	30.67±2.25	0.25±0.02	2.68±0.03	3.22±0.29	2.82±0.33	0.72±0.07
Blue Spice	1507.2±251.7	94.5±15.1	15.72±4.31	36.82±4.07	21.67±3.55	0.16±0.05	2.10±0.28	4.97±1.11	2.87±0.24	0.29±0.04
Siam Queen	508.4±15.5	88.6±2.9	22.60±3.92	78.57±10.8	27.17±1.61	0.23±0.03	2.33±0.20	2.62±0.50	2.53±0.38	0.14±0.11
Fino Verde	540.5±146.1	130.8±22.2	21.71±3.06	68.32±2.52	24.50±0.87	0.08±0.10	2.72±0.28	2.20±0.22	3.42±0.20	0.53±0.13
Purple Opal	740.3±125.2	114.2±12.0	18.88±4.42	70.76±1.90	30.33±3.40	0.32±0.07	2.50±0.20	3.08±0.09	2.50±0.45	1.01±0.15
Compact	3576.0±275.6	234.9±44.8	24.75±5.19	60.91±3.91	22.67±4.86	0.20±0.02	5.07±0.98	8.42±0.77	10.2±1.06	2.84±0.23
Genovese	1010.9±140.8	126.2±10.6	23.31±2.73	57.21±11.61	25.83±4.75	0.16±0.05	3.05±0.17	3.17±0.10	1.96±0.50	0.55±0.08
LSD = 0.05	0.051	7.02		7.67	3.14	0.03	0.11	0.07	0.33	0.05
LSD = 0.01	0.037	5.09		5.52	2,28	0.02	0.08	0.05	0.24	0.03

enrich this food with additional 0.2794 mg of Fe. Such high content of iron (10814, 9043 and 2465 mg/kg) in dray weight of basil leaf has been found in some basil genotypes (*O. basilicum*, *O. sanctum*, *O. minimum*, respectively) grown in Indian arid areas [59], but this results should be accepted with reserve, because this analytical material was obtained using a manual grinder. Similarly, high iron content in basil with over 1000 mg/kg of d.m., should be found only in the seed, if this species is grown in arid areas as a wild plant [60].

The tree-plot obtained by the cluster procedure (UPGMA) showed basil genotypes grouped in the clusters with their respective distances. Cluster analysis classified 13 *Ocimum* genotypes into two distinct groups (Figure 1). In fact, one cluster included almost all genotypes studied, while the second one included only one. The average genotype distance (*D*) among the osmium cultivars based on the examined traits was 799, ranging from 36.4 (the most related accessions, Purple Ruffles and Osmin) to 3377.6 (the most distantly related, Hollander and Compact).

Cluster I. This group included 12 genotypes (all but Compact) this cluster was split off into three distinct sub-groups, defined as cluster IA, IB and IC. Sub-

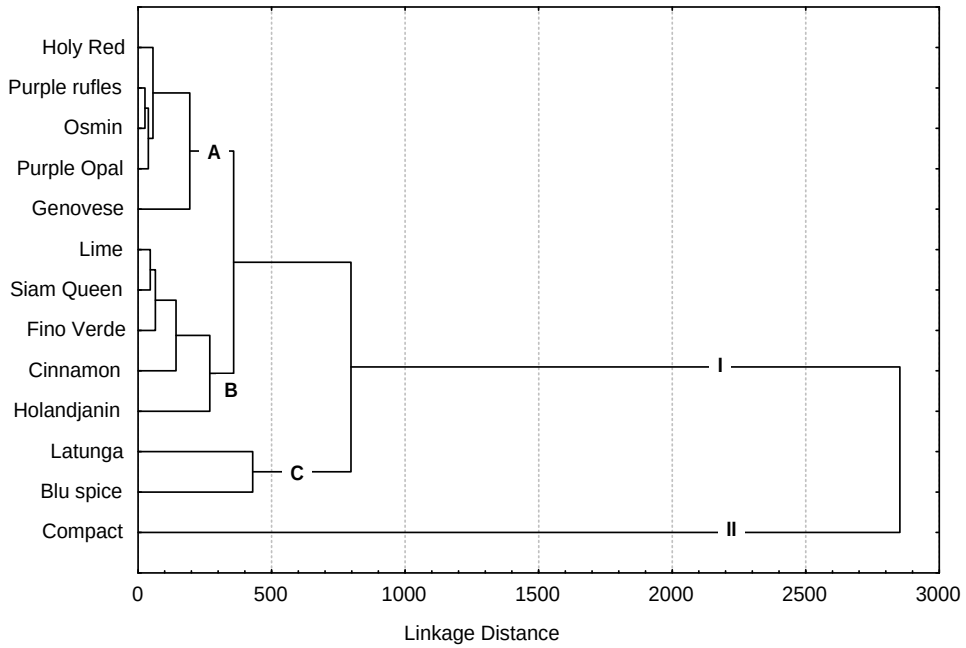

Figure 1. Cluster analyses of present minerals in herbs in basil genotypes.

clustering was done according to the Fe content. Subgroup (IA) consisted of five genotypes (Holy Red, Purple Ruffles, Osmin, Purple Opal and Genovese) with higher content of Fe than in the following genotypes: Lime, Siam Queen, Fino Verde, Cinnamon and Hollander, which formed sub-group (IB). IC sub-group separated Latunga and Blu Spice, with relatively high content of Fe.

Cluster II. It consisted only of one genotype, Compact. This cultivar is characterized by a very high content of Fe, Mn, Co, Cr, Ni and Pb. Cluster analysis pointed out to a considerable diversity in the *Ocumum* cultivars where the content of some heavy metals (Fe, Mn, Co, Cr, Ni and Pb) was a determinant criterion for genotypes clustering. This points out that even different genotypes of plant species accumulate a different amount of heavy metals, which should be of concern [61,62].

Heavy metal issue

Like all other plant species, medicinal plant growing in nature can accumulate heavy metals through complex absorption process, governed by numerous mutually influencing factors. Accumulation to certain extent depends on individual properties and genotype, while the total concentration of heavy metals in various soil is less important than their availability and mobility, which greatly depends on soil properties such as: pH, organic matter, clay content, etc. [41]. As heavy metals pose a hazard to human health, dispute that some of them are essential for people and plants (Fe, Mn, Cu, Co and Zn), monitoring of these metals in herbal parts is of great importance for public protection against the hazards with possibly toxic effects [63]. Heavy metal contamination of agricultural soil should especially be of concern as one of major environmental problems that can reduce a plant production and safety of plant products used as food [64]. Therefore, it is of crucial importance that the commercial production of this plant species take place at unpolluted or potentially uncontaminated agricultural soil, and it should be tested to the level of presence of heavy metals (Table 1) [65].

Heavy metal concentrations in basil plants grown on agricultural soil (chernozem) are shown in Table 4. Presented results reveal considerable variations in concentration depending on the element and basil genotype, simultaneously demonstrating that metal absorption significantly depends on genetic properties of tested types.

Heavy metals accumulate in plant tissue by the following order: Cu > Cr > Ni > Co > Pb > Cd, while the total uptake greatly depends on genotype biomass. Estimated concentration, mg/kg, in investigated genotypes varied for Cu 13.78–24.75, Cr 2.15–8.42, Ni 1.6––10.2, Co 1.75–5.07, Pb 0.14–2.84 and Cd 0.07–0.35, having values in the range as was proved in earlier basil studies [66]. Since these plants were grown under field conditions, the contamination level with the toxic heavy metals, Cr, Ni, Co, Pb and Cd, can be classified as very low, as expected. This investigation of contamination level is very important because some of herbal plants have a phytoremediation potential [67] where the genotype variation of heavy metal accumulation in herbal plants exists as well [68]. Hence, as recommended by the World Health Organization, all medicinal/herbal plant material should be tested to the presence of heavy metals and other pollutants, regardless of the place they have been grown [69].

Basil samples contain less than 0.3 mg/kg Cd and less than 3 mg/kg Pb measured in dry weight basis, as recommended for these toxic metals in medicinal plants by EC Regulation [70]. Besides, for this medicinal plant, toxic Ni content in the herb does not depend on soil pH [70], as found in this experiment. The tested genotype variety (Compact), which collects above 5 mg/kg at the soil pH > 7.0, has pointed out that genetic tendency of basil could have a stronger influence on Ni accumulation than soil pH property. The question of toxic Cr is still open; Cr content of analyzed herbal parts of the majority of genotypes is more than 2–3 mg/kg, which is regarded excessive, however non-toxic, concentration for cultivated plants [72]. Chromium content in the investigated basil plant is much lower (3.40–4.46 mg/kg), as found in some medicinal plants, which is considered non-toxic content (Khan 2013). Possible Co toxicity in basil tissues has not been estimated.

CONCLUSION

Mineral compositions of different basil (*Ocimim* spp.) genotypes vary, based on different genetic potential of investigated basil types. There is no reliable connection between shapes of the basil aboveground parts and its mineral content. According to dried herbal biomass, where average of 40 plants per basil genotype was tested, two genotypes should be recommended for further cultivation practice (Hollander and Fino Verde). However, the investigated basil mineral composition, promote some other basil genotypes (Compact, Lattuga and Blue spice) as a good raw material for further processing. According to the content of micronutrients, especially Fe, Mn and Zn, basil can support human dietary intake with this organically bound minerals. Especially the iron concentration in some basil genotypes was proved by statistical evaluation as genotypes with distinct mineral properties. Hence, Fe-rich genotype Compact (3576.0 mg/kg), which is in the cluster II with two other genotypes (Lattuga and Blue Spice) from cluster IC, with more than 1000 mg/kg of Fe (d.m.), could be treated as iron source originating from plant material and used for humans with low level Fe, consequently, with low level of hemoglobin.

Hierarchical cluster analysis allowed the assessment of similarity or dissimilarity and clarified some of the relationships among basil cultivars. Obtained dendrogram had two main clusters, the first one was split-off into three sub-groups. Further accumulation of data across the years might result in better precision of cultivar assessment.

According to the present study, commercial growth of basil was shown as a good practice, which can obtain a constant supply of herbal material for different purposes in pharmaceutical or food processing industry with no excess of heavy metal in herbal parts.

Acknowledgements

This study is financially supported by the Ministry of Education, Science and Technological development of Republic of Serbia, Project No. III46001.

REFERENCES

[1] J. Javanmardi, A. Khalighi, A. Kashi, H.P. Bais, J.M. Vivanco, Chemical characterization of basil (*Ocimum basilicum* L.) found in local accessions and used in tradetional medicines in Iran, J. Agric. Food Chem. **50** (2002) 5878–5883.

[2] A. Chanwitheesuk, A. Teerawutgulrag, N. Rakariyatham, Screening of antioxidant activity and antioxidant compounds of some edible plants of Thailand, Food Chem. **92**(3) (2005) 491–497.

[3] A. Rusaczonek, M. Żebrowska, B. Waszkiewicz-Robak, E. Ślusarczyk, Evolution of phenolic compounds content and antioxidant capacity of herbs, Pol. J. Food Nutr. Sci. **57** (2007) 483–488.

[4] K.G. Lee, T. Shibamoto, Determination of antioxidant potential of volatile extracts isolated from various herbs and spices. J. Agri. Food Chem. **50** (2002) 4947–4952.

[5] S-J. Lee, U. Katumi, S. Takayuki, L. Kwang-Geun, Identification of volatile components in basil (*Ocimum basilicum L*.) and thyme leaves (*Thymus vulgaris L*.) and their antioxidant properties. Food Chem. **91** (2005) 131–137.

[6] M. Peterson, M.S.J. Simmonds, Rosmarinic acid, Phytochemistry **62** (2003) 121–125.

[7] V. Katalinic, M. Milos, T. Kulisic, M. Jukic, Screening of 70 medicinal plant extracts for antioxidant capacity and total phenols, Food Chem. **94** (2006) 550–557.

[8] O. Politeo, M. Jukic, M. Milos, Chemical composition and antioxidant capacity of free volatile aglycones from basil (*Ocimum basilicum* L.) compared with its essential oil, Food Chem. **101** (2007) 379–385.

[9] T.P.A. Devasagayam, J.C. Tilak, K.K. Boloor, K.S. Sane, S.S. Ghaskadbi, R.D. Lele, Free radicals and antioxidants in human health: current status and future prospects, J. Assoc. Physicians India **52** (2004) 794–804.

[10] E. Klimánková, K. Holadová, J. Hajšlová, T. Čajka, J. Poustka, M. Koudela, Aroma profiles of five basil (*Ocimum basilicum* L.) cultivars grown under conventional and organic conditions, Food Chem. **107** (2008) 464––472.

[11] P.M. Nguyen, E. D. Niemeyer, Effects of nitrogen fertilization on the phenolic composition and antioxidant properties of basil (*Ocimum basilicum* L.), J. Agric. Food Chem. **56** (2008) 8685–8691.

[12] A. Biesiada, A. Kuś, The effect of nitrogen fertilization and irrigation on yielding and nutritional status of sweet basil (*Ocimum basilicum* L.), Acta Sci. Pol., Hort. Cult. **9** (2010) 3–12.

[13] P.M. Nguyen, E.D. Niemeyer, Effects of nitrogen fertilization on the phenolic composition and antioxidant properties of basil (*Ocimum basilicum* L.), J. Agric. Food Chem. **56** (2008) 8685–8691.

[14] Y. Miyamoto, A. Kajikawa, J. H. Zaidi, T. Nakanishi, K. Sakamoto, Minor and trace element determination of food spices and pulses of different origins by NAA and PAA, J. Radioanal. Nucl. Chem. **243** (2000) 747–765.

[15] V. Singh, A.N. Garg, Availability of essential trace elements in Indian cereals, vegetables and spices using INAA and the contribution of spices to daily dietary intake, Food Chem. **94** (2006) 81–89.

[16] C. Karadaş, D. Kara, Chemometric approach to evaluate trace metal concentrations in some spices and herbs, Food Chem. **130** (2012) 196–202.

[17] P.F. Leal, N. B. Maia, Q. A.C. Carmello, R. R. Catharino, M.N. Eberlin, M.A.A. Meireles, Sweet basil (*Ocimum basilicum*) extracts obtained by supercritical fluid extraction (SFE): global yields, chemical composition, antioxidant activity, and estimation of the cost of manufacturing, Food Biopro. Tech. **1** (2008) 326–338.

[18] C.G. Fraga, Relevance, essentiality and toxicity of trace elements in human health, Mol. Asp. Med. **26** (2005) 235–244.

[19] M.M. Özcan, Mineral contents of some plants used as condiments in Turkey, Food Chem. **84** (2004) 437–440.

[20] M.M., Özcan, M. Akbulut, Estimation of minerals, nitrate and nitrite contents of medicinal and aromatic plants used as spices, condiments and herbal tea. Food Chem. **106** (2007) 852–858.

[21] M.M. Özcan, A. Űnver, T. Ucar, D. Arslan, Mineral content of some herbs and herbal teas by infusion and decoction, Food Chem. **106** (2008) 1120–1127.

[22] M.E. Ghanjaoui, M.L. Cervera, M.E.I. Rhazi, M. Guardia, Validated fast procedure for trace element determination in basil powder, Food Chem. **125** (2011) 1309–1313.

[23] R.F. Vieira, R.J. Grayer, A. Paton, J.E. Simon, Genetic diversity of *Ocimum gratissimum* L. based on volatile oil constituents, flavonoids and RAPD markers, Biochem. Syst. Ecol. **29** (2001) 287–304.

[24] I. Telci, E. Bayram, G.Yılmaz, B. Avcı, Variability in essential oil composition of Turkish basils (*Ocimum basilicum* L.) Biochem. Syst. Ecol. **34** (2006) 489–497.

[25] E.M. Kwee, E.D. Niemeyer, Variations in phenolic composition and antioxidant properties among 15 basil (*Ocimum basilicum* L.) cultivars, Food Chem. **128** (2011) 1044–1050.

[26] S. Jelačić, D. Beatović, S. Prodanović, S. Tasić, Đ. Moravčević, A. Vujošević, S. Vučković, Chemical composition of

the essential oil of basil (*Ocimum basilicum* L. Lamiaceae), Hem. Ind. **65** (2011) 465–471.

[27] M.O. Ajasa, M.O. Bello, A.O. Ibrahim, I.A. Ogunwande, N.O. Olawore, Heavy trace metals and macronutrients status in herbal plants of Nigeria, Food Chem. **85** (2004) 67–71.

[28] U. Gasser, B. Klier, A.V. Kühn, B. Steinhoff, Current findings on the heavy metal content in herbal drugs, Pharmeuropa Scien. Not. **1** (2009) 37–49.

[29] M. Sahu Geda, A.K., A. Shrivastava, P. Nirmodh, Analysis of genetic divergence in basil (*Ocimum* spp.), J. Spices Aromatic Crops **17** (2008) 244–246.

[30] Z. Huang, B. Wang, D.G. Mortley, T. Mindingall, C.K. Bonsi, W.A. Hill, C.E. Morris, Chemical characteristics of essential oil from five basil cultivars grown hydroponically in a controlled environment using the nutrient film technique. Int. J. App. Sci. Tech. **1** (2011) 42–49.

[31] N Amoli, Investigation on yield and some agronomic and breeding characteristics of basil masses. Int. J. Agri. Crop Sci. **4** (2012) 1017–1020.

[32] D. Beatović, S. Jelačić, N. Menković, Collection, and evaluation of basil (*Ocimum basilicum* L.) genotypes in Serbia (in Serb.), Agroznanje **9** (2008) 35–41.

[33] A. Hereter, R. Josa, X. Candela, Changes in particle-size distribution influenced by organic matter and mechanical or ultrasonic dispersion techniques, Comm. Soil Sci. Plant Anal. **33** (2002) 1351–1362.

[34] U.S. EPA. Method 3050, in: Test Methods for Evaluating Solid Waste, 3rd ed., IA, Environ. Prot. Agency Washington DC, 1986.

[35] M.C. Amacher, Nickel, cadmium, and lead. In Methods of soil analysis, Part 3 – Chemical methods, Madison, WC, Soil Sc. Soc. Amer., Amer. Soc. Agron., 1996, pp. 739–768.

[36] A. Tessier, P.G.C. Campbell, M. Bisson, Sequential extraction procedure for the speciation of particulate trace metals, Anal. Chem. **51** (1979) 844–851.

[37] W.L. Lindsay, W.A. Norvell, Development of a DTPA soil test for zinc, iron, manganese and copper. Soil Sci. Soc. Am. J. **42** (1978) 421–428.

[38] FAO/ISRIC/ISSS, World Reference Base for Soil Resources, World Soil Resources Report, FAO, Rome, 1998, Vol. 84.

[39] S. Jakšić, P. Sekulić, J. Vasin, Content of heavy metals in gleyic chernozem of Srem loess terrace (Serbia) under alfalfa, Ratarstvo i povrtarstvo **49** (2012) 189–194.

[40] G. Siebielec, R. Chaney, Liming to remediate Ni contaminated soils with diverse properties and a wide range of Ni concentrations, Plant Soil **299** (2007) 117–130.

[41] A. Kabata–Pendias, A.B. Mukherjee, Trace Elements from Soil to Human, Springer-Verlag, Berlin, 2007.

[42] A. Paton, R.M. Harley, M.M. Harley, *Ocimum* – an overview of relationships and classification, in: Y. Holm, R. Hiltunen (Eds.), Medicinal and Aromatic Plants – Industrial Profiles, Harwood Academic, Amsterdam, 1999, pp. 1–38.

[43] L. De Masi, P. Siviero, C. Esposito, D. Castaldo, F. Siano, B. Laratta, Assessment of agronomic, chemical and genetic variability in common basil (*Ocimum basilicum* L.), Eur. Food Res. Technol. **223** (2006) 273–281.

[44] M. Habán, S. Barátova, P. Otepka, B. Kocourkova, J. Fojtová, Selected cultivars of *Ocimum basilicum* L. introduced to the growing conditions of warm agri-climatic macro region and their evaluation. Unapređenje poljoprivredne proizvodnje na Kosovu i Metohiji. Poljoprivredni fakultet, Priština-Lešak, 2007, pp. 131–141.

[45] M. Labra, M. Miele, B. Ledda, F. Grassi, M. Mazzei, F. Sala, Morphological characterization, essential oil composition and DNA genotyping of *Ocimum basilicum* L. cultivars, Plant Sci. **167** (2004) 725–731.

[46] M. Marotti, R. Piccaglia, E. Giovanelli, Differences in essential oil composition of Basil (*Ocimum basilicum* L.) Italian cultivars related to morphological characteristics. J. Agr. Food Chem. **44** (1996) 3926–3929.

[47] M.I. Sifola, G.Barbieri, Growth, yield and essential oil content of three cultivars of basil grown under different levels of nitrogen in the field. Sci. Hort. **108** (2006) 408––413.

[48] K. Mengel, E. A. Kirkby, Principles of plant nutrition, 5th ed., Kluwer Academic Publishers, Dordrecht, 2001.

[49] P.M. Nguyen, E.M. Kwee, E.D. Niemeyer, Potassium rate alters the antioxidant capacity and phenolic concentration of basil (*Ocimum basilicum* L.) leaves, Food Chem. **123** (2010) 1235–1241.

[50] W.M. Jarrell, R.B. Beverly, The dilution effect in plant nutrition studies, Adv. Agron., N.C. Academic Press, NY, 1981, pp. 197–224.

[51] R. Chizzola, H. Michitsch, C. Franz, Monitoring of metallic micronutrients and heavy metals in herbs, spices and medicinal plants from Austria, Euro Food Res. Tech. **216** (2003) 407–411.

[52] L. Taiz, E. Zeiger, Plant Physiology, 4th ed., Sinauer Associates, Sunderland, MA, 2006.

[53] C.G. Fraga, Relevance, essentiality and toxicity of trace elements in human health, Mol. Asp. Med. **26** (2005) 235–244.

[54] P. Masson, T. Dalix, S. Bussière, Determination of major and trace elements in plant samples by inductively coupled plasma-mass spectrometry, Comm. Soil Sci. Plant Anal. **41** (2010) 231–243.

[55] D. Donatella, A.M. Maria, R. Carla, Determination of essential and non-essential elements in some medicinal plants by polarised X ray fluorescence spectrometer (EDPXRF), Microchemical J. **95** (2010) 174–180.

[56] R. Subramanian, S. Gaythri, C. Rathnavel, V. Ray, Analysis of mineral and heavy metals in some medicinal plants collected from local market, Asian Pacific J. Trop. Biomed. **2** (2012) 74–78.

[57] E. Klimánková, K. Holadová, J. Hajšlová, T. Čajka, J. Poustka, M. Koudela, Aroma profiles of five basil (*Ocimum basilicum* L.) cultivars grown under conventional and organic conditions. Food Chem. **107** (2008) 464––472.

[58] D.M. Barrett, C. Weakley, J.V. Diaz, M. Watnik, Qualitative and nutritional differences in processing tomatoes grown under commercial organic and conventional production Systems, J. Food Sci. **72** (2007) 441–451.

[59] A. Demirbus, Oil, micronutrients and heavy metal content of tomatoes, Food Chem. **118** (2010) 504–507.

[60] T.M. Ansari, N. Ikrim, M.najam-ul-Haq, I. Fayyaz, Q. Fayyaz, I.Ghafoor, N.Khalid, Essential trace metal (zinc, manganese, copper and iron) levels in plants of medicinal importance, J. Biolog. Sci. **4** (2004) 95–99.

[61] J. Barthwal, S. Nair, P. Kakkar, Heavy metal accumulation in medicinal plants collected from environmentally different sites, Biomed. Environ. Sci. **21** (2008) 319–324.

[62] Y. Zhu**,** H. Yu, J. Wang, W. Fang, J. Yuan, Z. Yang, Heavy metal accumulations of 24 asparagus bean cultivars grown in soil contaminated with Cd alone and with multiple metals (Cd, Pb and Zn), J. Agric. Food Chem. **55** (2007) 1045–1052.

[63] D. Kostić, S. Mitić, A. Zarubica, M. Mitić, J. Veličković, S. Randjelović, Content of trace metals in medicinal plants and their extracts, Hem. Ind. **65** (2011) 165–170.

[64] A. Kabata-Pendias, A.B. Mukehrjee, Trace Elements from Soil to Human, Springer-Verlag, Berlin, 2007.

[65] B.J. Alloway, Heavy Metals in Soil, 2nd ed., Blackies Academic & Professionals, London, 1995.

[66] M.E. Ghanjaoui, M.L. Cervera, M.E.L. Rhazi, G. Mdela, Validated fast procedure for trace element determination in basil powder, Food Chem. **125** (2011) 1309––1313.

[67] V.D. Zheljazkov, L.E. Craker, B. Xing, Effects of Cd, Pb, and Cu on growth and essential oil contents in dill, peppermint, and basil, Environ. Exper. Botany **58** (2006) 9–16.

[68] H. Diawin, A. Ahmad, M. Iqbal, Genotypic variation in the phytoremediation potential of Indian mustard for chromium. Environ. Manag. **41** (2008) 734–741.

[69] World Health Organization, Quality Control Methods for Medicinal Plant Materials, WHO, Geneva, 1998.

[70] Commission Regulation (EC) No. 1881/2006, Current Findings on the Heavy Metal Content in Herbal Drugs certain contaminants in foodstuffs as regards heavy metals. Official J. Eur. Union **49** (2006) 5–24.

[71] D. Radanović, S. Antić Mladenović, M. Jakovljević, M. Kresović, Content of heavy metals in *Gentiana lutea* L. roots and galenic forms, J. Serb. Chem. Soc. **72** (2007) 133–138.

[72] A.K. Shankera, C. Cervantesb, H. Loza–Taverac, S. Avudainayagamd, Chromium toxicity in plants, Environ. Internat. **31** (2005) 739–753.

IZVOD

MINERALNI SASTAV RAZLIČITIH GENOTIPOVABOSILJKA (*Ocimum* spp.)

Vlado Ličina, Slavica Ć. Jelačić, Damir V. Beatović, Svetlana B. Antić Mladenović

Univerzitet u Beogradu, Poljoprivredni fakultet, Zemun, Srbija

(Naučni rad)

U radu je ispitan mineralni sastav 13 različitih genotipova bosiljka (*Ocimum spp.* L.), sa ciljem da se odrede tipovi koji bi mogli da posluže kao dopunski izvori esencijalnih elemenata u ljudskoj ishrani, kao i da se odrede genotipovi koji bi poslužili za proizvodnju herbe kao sirovine za farmaceutsku ili prehrambenu industriju. Takođe, u ovom istraživanju je testiran i potencijalni rizik vezan za zagađenje bosiljka teškim metalima pri njegovom komercijalnom gajenju na poljoprivrednom zemljištu. Mineralni sastav ispitivanih genotipova uglavnom je uslovljen njegovim genetskim karakteristikama, ukazujući da u ishrani čoveka ova lekovita biljna vrsta može poslužiti kao značajan izvor nekih od esencijalnih elemenata, naročito mikroelemenata (Fe, Mn i Zn), koji generalno doprinose jačanju ljudskog imuno sistema. Posebno je važno što su u ovom istraživanju identifikovani neki genotipovi bogati gvožđem, kao što je to Compact, kao genotip sa ekstremno visokim nivom Fe u herbi (3576,0 mg/kg), a koji bi zajedno sa genotipovima *Lattuga* (1585,6 mg/kg) i *Blue Spice* (1167,9 mg/kg) koji sadrže više od 1000 mg/kg Fe u suvoj materiji herbe, trebali da privuku posebnu pažnju kao izvori ovog elementa u ishrani ljudi kod kojih je evidentiran njegov nedostatak, načešće ispoljen sa pojavom anemije, odnosno, slabom sintezom hemoglobina. Gajenje bosiljka na poljoprivrednom zemljištu nije uslovilo povećanu akumulaciju teških metala (Cu, Co, Cu, Ni, Cr i Pb) u herbi, pa se može reći da su ovi proizvodi sa aspekta zagađenosti teškim metalima potpuno bezbedni. Klaster analiza je podelila ispitivane genotipove bosiljka (*Ocmium* spp.) u dve grupe. Uprkos različitosti između genotipova, sadržaj Fe, Mn, Co, Cr, Ni i Pb uticao je na jasnu podelu između klastera.

Ključne reči: Bosiljak • Genotip • Mineralni sastav • Gvožđe • Teški metali • Klaster analiza

Optimization of extraction of antioxidant components from Yarrow herb

Ivana A. Arsić[1], Vanja M. Tadić[2], Sofija M. Đorđević[2], Ana R. Žugić[2], Zorica B. Vujić[3], Slobodan D. Petrović[4]

[1]*University of Niš, Faculty of Medicine, Department of Pharmacy, Niš, Serbia*
[2]*Institute for Medicinal Plant Research "Dr Josif Pančić", Belgrade, Serbia*
[3]*University of Belgrade, Faculty of Pharmacy, Institute for Pharmaceutical Chemistry, Belgrade, Serbia*
[4]*University of Belgrade, Faculty of Technology and Metallurgy, Belgrade, Serbia*

Abstract

Recently, research efforts have been directed toward medicinal plants and their extracts, as important sources of natural antioxidant. Lots of biologically active compounds are responsible for the antioxidant effects of yarrow – *Achillea millefilium* L. extracts. The aim of our study was to determine which of the process parameters of pressure enhanced solvent extraction of *Millefolii herba* is significant for its efficiency and weather there are interactions between the examined parameters. Compression time, decompression time and the number of cycles were identified as independent variables, while the content of total flavonoids, tannins and total polyphenols were selected as dependent variables. For obtaining the extract of *M. herba*, rich in antioxidative ingredients, compression time should be set on its higher level (2.0 min), decompression time on its lower level (1.30 min) and the number of cycles on its higher level (99).

Keywords: timatic micro-extractor, Yarrow, optimization, polyphenols, tannins, flavonoids.

Available online at the Journal website: http://www.ache.org.rs/HI/

SCIENTIFIC PAPER

UDC 66.061.18:582.998.1:615.279

Hem. Ind. **68** (4) 511–517 (2014)

doi: 10.2298/HEMIND130910076A

The functional food designates all sorts of food containing, along with their own nutritive value, constituents that may have positive effects on human health and its psychophysical condition. Modern community is changing the concept of foods. The aim of science, today, is development of such food products, which assume prevention and simultaneous reduction of risks of appearance of different diseases [1]. Oxidation reactions and the decomposition of oxidation products are major causes of deterioration of various food products. To prevent these processes, antioxidants are widely used as additives in some foods. Owing to increased safety concerns about synthetic antioxidants and their possible involvement in chronic diseases, research efforts have been directed toward natural antioxidants [2]. Medicinal plants and their extracts constitute one of the most important targets to search for new sources of natural antioxidants for consideration as components for functional ingredients and nutraceuticals, as well as feasible and natural alternatives to synthetic antioxidants in the food industry. Since plant-derived antioxidants are generally considered to be multifunctional and their activity depends on various parameters, any herb or its extract should be thoroughly tested involving several methods of assessing antioxidant activity [3].

Correspondence: I.A. Arsić, University of Niš, Faculty of Medicine, Department of Pharmacy, Dr Zoran Đinđić Boulevard 81, 18000 Niš, Serbia.
E-mail: ivana.arsic@medfak.ni.ac.rs
Paper received: 10 September, 2013
Paper accepted: 21 October, 2013

The genus *Achillea* L. (Yarrow) comprises over 100 perennial herb species indigenous to the Northern Hemisphere [4]. In Serbia, the *Achillea millefolium* L., the best-known and most widespread species of Yarrow, is listed among the most commonly used plant species in both folk and conventional medicine [5]. Yarrow is primarily a bitter tonic, but it can also be used to treat atonic forms of stomach disease [6]. Aerial part of *A. millefolium* contains terpenes, alkaloids and bases, tannins, coumarins, saponins, sterols, vitamins, amino and fatty acids [6,7]. Phenolic compounds, such as flavonoids and phenolcarbonic acids, constitute one of the most important groups of pharmacologically active principles in yarrow. It is suggested that anti-inflammatory [6], choleretic [8] and cytotoxic [9] activities of species of *Achillea* genus are mainly attributed to the flavonoid and phenolcarbonic acid complex. It has been shown that the anti-diabetic [10] and gastroprotective [11] properties of different extracts from *Achillea* sp. may be linked to their antioxidant potential. Therefore, it is of high importance to investigate their antioxidant effectiveness. Recent reports indicate that the *Achillea* genus displays a relevant antioxidant activity that is associated or correlated well with its flavonoid and total phenolic contents [12,13]. However, the observed similarities or close correlation between the profiles of the antioxidant capacity and of the total phenolic and flavonoid contents must be interpreted with care, since the latter parameter is usually measured using traditional spectrophotometric assays, which are based on non-specific reaction of phenolic compounds with Folin–Ciocalteu reagent and complexation of flavonoids with Al(III) ion [14].

The interest in the use of medicinal plants in food industry is continuously growing and accordingly the efforts in the improvement of the conventional solvent based extraction are made. The traditional techniques of solvent extraction of plant materials are mostly based on the correct choice of solvents and the use of heat and/or agitation to increase the solubility of the desired compounds and improve the mass transfer [15]. For each device and/or each method of extraction, it is necessary to experimentally determine optimal conditions for making the extracts which are the richest in relevant active substances. Other researchers have presented the definition of optimal conditions for extraction of bioactive compounds (crocin, geniposide, total phenolic compounds, phenolic acids and proteins) using different extraction methods, different extractors and different optimization methodologies [15-17]. In the present study, Timatic micro-extractor was used for the extraction [18]. The aim of our study was to determine which of the process parameters of pressure enhanced solvent extraction of aerial parts of *A. millefolium* (*Millefolii herba)*, is significant for its efficiency and weather there are interactions between the examined parameters.

EXPERIMENTAL

Samples of *A. milefollum* (upper parts of the herb ~12 cm in length) were collected at full flowering stage, during the flowering period on the mountain Rtanj, Serbia (in the end of June 2009). A voucher specimen's No. 174/09 has been deposited at the Institute for Medicinal Plant Research "Dr Josif Pančić". The raw material was air dried at room temperature (20–25 °C), in a ventilated lodge, avoiding direct sunlight for two weeks. Dry material was packed into paper bags and stored in a dark room at ambient temperature. The air-dried aerial parts of *A. millefolium* were milled at room temperature and sieved using a lab sieve with 355 μm mesh.

All chemicals were of analytical grade. Folin–Ciocalteu reagent was purchased from Merck (Germany), gallic acid from Sigma–Aldrich Chemie GmbH (Germany). Acetonitrile, labelled as HPLC grade, was supplied by Sigma–Aldrich (Buchs, Switzerland). Ethanol 96.3% (*V*/*V*) was provided by Crvenka, Serbia.

For the pressure enhanced solvent extraction we used Timatic micro-extractor (Tecnolab, Spello, PG, Italy) [18]. The rapid series extractors Timatic are technologically advanced and dedicated to the extraction of active ingredients from medicinal plants. This is an alternative method for extraction in comparison to traditional methods, such as maceration or percolation. The extraction was carried out under controlled conditions (defined by temperature, pressure and time of solvent circulation). Plant material was filled into the filter bag, which was sealed and placed into the extraction chamber. Appropriate solvent is circulating through the filter bag and can be controlled by the speed of circulation and the number of cycles during the extraction process. The working cycle is fully automatic and alternates between dynamic and static phases. During the extraction, plant material is compacted under pressure, which allows better extraction efficiency. With respect to our preliminary research (data not shown), fixed amounts of the drug and 70% (*V*/*V*) ethanol, as an extraction solvent were used. The drug: extract ratio was 1:3 and the operating pressure was set between 1 and 9.9 bar. A 2^3 factorial design consisting of eight experimental points was applied to evaluate the effect of three process parameters as independent variables, namely compression time (*TP1*), decompression time (*TP0*) and the number of cycles (*CL*) on the extraction efficiency in terms of obtaining the extract with the best properties. Prepared extracts were marked as YE_1–YE_8. Characterization of extracts included determination of physicochemical characteristics: dry residue (*DR*), refractive index (*RI*), relative density (*RD*), ethanol content (*EC*) and pH value as well as determining the content of total flavonoids (*TF*), tannins (*TN*) and polyphenols (*PY*) as active compounds, important for the extract quality definition.

The total content of phenols was determined by the Folin–Ciocalteu method. A total of 100 μl of a methanolic solution of dry extract (17.5, 13.1, and 8.8 μg ml^{-1} final quantity) was mixed with 0.75 ml of Folin–Ciocalteu reagent (previously diluted 10-fold with distilled water) and allowed to stand at 22 °C for 5 min; 0.75 ml of sodium bicarbonate (60 g l^{-1}) solution was added to the mixture. After 90 min at 22 °C, the absorbance was measured using a Hewlett Packard 8453 UV–Vis spectrophotometer (Agilent Technologies, Santa Clara, CA) at λ_{max} 725 nm. Results are expressed as gallic acid equivalents (GAE), and presented as mean value of three determinations.

The percentage content of tannins was calculated using the method described in the European Pharmacopoeia [19]. The content of tannins, expressed as pyrogallol percentage, is presented as the mean value of three determinations.

The percentage content of flavonoids expressed as hyperoside was calculated using the method described in the Deutsches Arzneibuch, DAB 10 [20]. Briefly, the sample was extracted with acetone/HCl under a reflux condenser; the $AlCl_3$ complex of the flavonoid fraction was extracted with ethyl acetate and measured by a UV–Vis spectrophotometer at λ_{max} 425 nm. The content of flavonoid, expressed as the hyperoside percentage, is presented as the mean value of three determinations.

Statistical analysis

The statistical analysis of experimental results was performed by the software Design Expert 7.0 (Stat-Ease, Inc., Minneapolis, MN, USA) [21].

RESULTS AND DISCUSSION

Independent variables are presented in Table 1. The conditions of making YE_1–YE_8 extracts are presented in Table 2. Dependent variables were dry residue (*DR*), refractive index (*RI*), relative density (*RD*), ethanol content (*EC*), pH value, content of total flavonoids (*TF*), tannins (*TN*) and polyphenols (*PY*).

Table 1. Process parameters/independent variables

Factor	Level	
	–1	+1
X1 (*TP1*) compression time, min	1.00	2.00
X2 (*TP0*) decompression time, min	1.30	2.00
X3 (*CL*) number of cycles	20	99

Table 2. The conditions of making YE_1–YE_8 extracts

Sample of YE	*TP1* / min	*TP0* / min	*CL*
YE_1	1.00	1.30	20
YE_2	2.00	1.30	20
YE_3	1.00	2.00	20
YE_4	2.00	2.00	20
YE_5	1.00	1.30	99
YE_6	2.00	1.30	99
YE_7	1.00	2.00	99
YE_8	2.00	2.00	99

Various extraction conditions, resulted in some differences in the physicochemical characteristic of the manufactured extracts and different contents of total phenols, flavonoids and tannins (Table 3). Value of dry residue of manufactured extracts varied within the limits from 2.17 to 3.86. Dry residue content depended on the number of cycles. Increasing the number of cycles led to an increase in the value of dry residue (the maximum value of *DR* was registered in YE_5). The same extract had the highest value of relative density. There was no significant difference in the refractive index and pH values between manufactured extracts. Ethanol content in extracts YE_1–YE_8 varied within the limits from 63.28 (YE_1) to 69.88 (YE_3) and did not depend on the number of cycles.

Statistical analysis of the experimental data indicated that all three examined process parameters generally have the greatest impact on *DR*, while individually, *TP1* influences mostly *TF* and *RI*, *TP0*, *TF* and *RD*, and *CL*, *DR*, pH, *TN* and *PY*. When considering active principle content, it may be noted that *TP1* and *TP0* have the biggest influence on *TF* (except that *TP1* has a positive, and *TP0* negative effect on *TF*), while *CL* on *TN* (positive effect) and *PY* (negative effect). Comparing active principle contents among themselves, the greatest impact of all three process parameters is on *PY*. Nevertheless, interactions observed between *TP1* and *TP0* indicate that with *TP0* set on its lower value (1.30 min) the increase of *TP1* increases *TN* and *PY*. Taking all of this in consideration, it can be concluded that for obtaining the extract of *A. millefolium* rich in active ingredients, *TP1* should be set on its higher level (2.0 min), *TP0* on its lower level (1.30 min) and *CL* on its higher level (99).

Since the selected responses were not affected in the same manner an additional optimization procedure was needed. In order to optimize eight responses with different targets, the multicriteria methodology was employed by means of Derringer's desirability function [22–24].

The Derringer's desirability function, *D*, is defined as the geometric mean, weighted, or otherwise, of the individual desirability functions (d_i). The expression that defines the Derringer's desirability function is:

$$D = \sqrt[n]{\prod_{i=1}^{n} d_i^{p^i}} \quad (1)$$

where n is the number of responses, p^i is the weight of the responses and d_i is the individual desirability function of each response. The scale of the individual desirability function ranges between 0 for a completely undesired response, to 1 for a fully desired response.

Table 3. Physicochemical characteristics and contents of total phenols, flavonoids and tannins of YE_1–YE_8

Sample of YE	*DR* / %	*RI*	pH	*RD* / g cm^{-3}	*EC* / vol.%	*TF* / %	*TN* / %	*PY* / μg GA mg^{-1}
YE_1	2.31	1.3647	5.59	0.9098	63.28	0.0216	0.077	0.23
YE_2	2.50	1.3676	5.69	0,8999	67.64	0.0206	0.094	0.27
YE_3	2.52	1.3674	5.64	0.8993	69.88	0.0230	0.115	0.27
YE_4	2.17	1.3662	5.64	0.9016	65.44	0.0200	0.076	0.24
YE_5	3.86	1.3667	5.44	0.9292	66.84	0.0310	0.108	0.20
YE_6	3.61	1.3667	5.49	0.9060	66.20	0.0290	0.094	0.26
YE_7	3.27	1.3667	5.48	0.9065	65,44	0.0220	0.102	0.18
YE_8	3.15	1.3679	5.62	0.9031	67.64	0.0326	0.108	0.18

Weight of the response is the relative importance of each individual functions d_i and may range from 0.1 to 10. Weights lower than 1 give less emphasis to the goal, whereas weights greater than 1 give more emphasis to the goal (in both cases, d_i varies in a non-linear way while approaching to the desired value). In the present report, weights equal to 1 for all the eight responses was chosen.

The value of *D* close to 1 means that the combination of different criteria is globally optimal. If any of the responses or factors falls outside their desirability range, the overall function becomes zero.

The criteria for the optimization of each individual response are shown in Table 4. Desirability function calculations were performed using Design-Expert® 7.0. Obtained results are graphically presented (Figure 1). For better visualization of the results, the global desirability function, *D*, was presented in a form of a three-dimensional plot and presented in Figure 2. The coordinates related to the functions maximum are selected as the best operating conditions. The coordinates producing the maximum desirability value (*D* = 0.846) were: compression time (*TP1*), 2.00 min; decompression time (*TP0*), 1.30 min; number of cycles (*CL*), 99.0.

CONCLUSION

In the present study, Timatic micro-extractor was used for the extraction of yarrow and it may be concluded that various extraction conditions result in some differences in the physicochemical characteristic of the manufactured extracts and content of active substances. When considering active principle content with

Table 4. Criteria for multivariate optimization of the individual responses

Response	Goal	Weight	Lower limit	Upper limit	Importance
TF	Maximize	1	0.02	0.0326	5
DR	In range	1	2.17	3.86	3
RI	In range	1	1.3647	1.3679	3
pH	In range	1	5.44	5.69	3
RD	In range	1	0.899	0.9292	3
EC	In range	1	53.28	69.88	3
TN	Maximize	1	0.076	0.115	5
PY	Maximize	1	0.18	0.27	5

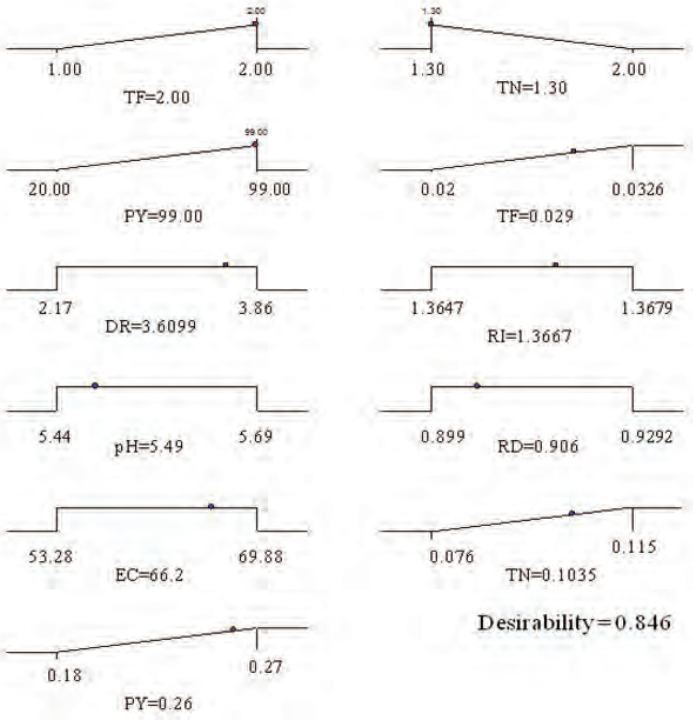

Figure 1. Graphical representation of the constraints accepted for the determination of global desirability and obtained optimal conditions.

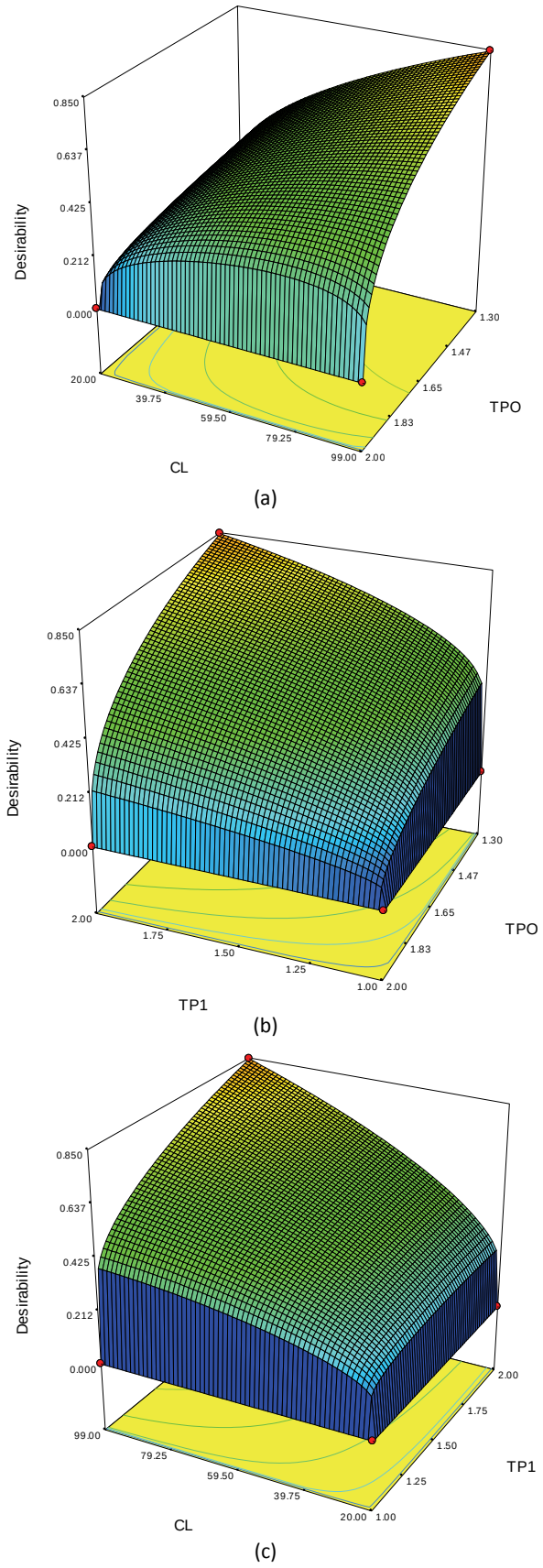

Figure 2. 3-D plots of the Derringer's desirability function in correlation with number of cycles and decompression time (a), decompression time and compression time (b) and compression time and number of cycles (c).

antioxidative effects (total phenols, flavonoids and tannins content), it may be noted that *TP1* and *TP0* have the biggest influence on *TF* (except that *TP1* has a positive, and *TP0* negative effect on *TF*), while *CL* on *TN* (positive effect) and *PY* (negative effect). Taking all of this in consideration, it can be concluded that using Timatic micro-extractor, for obtaining the extract of *A. millefolium* rich in active ingredients, *TP1* should be set on its higher level (2.0 min), *TP0* on its lower level (1.30 min) and *CL* on its higher level (99).

Acknowledgment

The authors wish to thank Serbian Ministry of Education, Science and Technological Development for financial support (Projects TR 31029 and III 45017).

REFERENCES

[1] I. Arsić, S. Đorđević, M. Ristić, D. Runjaić-Antić, Medicinal herbs in production of functional foods, Lek. Sirov. **23** (2003) 15–22.

[2] F. Shahidi, Antioxidants in food and food antioxidants, Nahrung **44** (2000) 158–163.

[3] I. Arsić, V. Tadić, S. Đorđević, D. Runjaić-Antić, G. Marković, S. Pavkov, A. Žugić, Comparative characterisation of different Blackberry leaf extracts, Lek. Sirov. **29** (2009) 51–59.

[4] X.T. Si, M.L. Zhang, Q.W. Shi, H. Kiyota, Chemical constituents of the plants in the genus *Achillea*, Chem. Biodivers. **3** (2006) 1163–1180.

[5] M. Sarić, Medicinal Plants of SR Serbia, SASA, Belgrade, 1989.

[6] M. Blumenthal, A. Goldberg, J Brinckmann, Herbal Medicine, Expanded Commission E Monographs, The American Botanical Council, Austin, TX, 2000.

[7] PDR for Herbal Medicines, 3rd ed., Thomson PDR at Montvale, 2004.

[8] B. Benedek, N. Geisz, W. Jager, T. Thalhammer, B. Kopp, Choleretic effects of yarrow (*Achillea millefolium*) in the isolated perfused rat liver, Phytomedicine **13** (2006) 702–706.

[9] S. Trifunović, V. Vajs, I. Juranić, Z. Žižak, V. Tešević, S. Macura, Cytotoxic constituents of *Achillea clavennae* from Montenegro, Phytochemistry **67** (2006) 887–893.

[10] R. Yazdanparast, A. Ardestani, S. Jamshidi, Experimental diabetes treated with *Achillea santolina*: Effect on pancreatic oxidative parameters, J. Ethnopharmacol. **112** (2007) 13–18.

[11] F.B. Potrich, A. Allemand, L.M. da Silva, A.C. Dos Santos, C.H. Baggio, C.S. Freitas, Antiulcerogenic activity of hydroalcoholic extract of *Achillea millefolium* L. Involvement of the antioxidant system, J. Ethnopharmacol. **130** (2010) 85–92.

[12] S. Konyalioglu, C. Karamenderes, The protective effects of *Achillea* L. species native in Turkey against H_2O_2-induced oxidative damage in human erythrocytes and leucocytes, J. Ethnopharmacol. **102** (2005) 221–227.

[13] S. Trumbeckaite, R. Benetis, L. Bumblauskiene, D. Burdulis, V. Janulis, A. Toleikis, P. Viškelis, V. Jakštas, *Achillea millefolium* L. s.l. herb extract: Antioxidant activity and effect on the rat heart mitochondrial functions, Food Chem. **127** (2011) 1540–1548.

[14] M. Naczk, F. Shahidi, Extraction and analysis of phenolics in food. J. Chromatogr., A **1054** (2004) 95–111.

[15] M. Vivekananda, M. Yogesh, S. Hemalatha, Microwave Assisted Extraction – An Innovative and Promising Extraction Tool for Medicinal Plant Research, Pharmacogn. Rev. **1** (2007) 7–18**.**

[16] A.A. Wani, D. Kaur, I. Ahmed, D.S. Sogi, Extraction optimization of watermelon seed protein using response surface methodology, LWT-Food Sci. Technol. **41** (2008) 1514–1520.

[17] I.M. Savić, V.D. Nikolić, I.M. Savić, Lj.B. Nikolić, M.Z. Stanković, K. Moder, Optimization of total flavonoid compound extraction from *Camellia sinensis* using the artificial neural network and response surface methodology, Hem. Ind. **67** (2013) 249–259.

[18] http://www.timatic.it/index.php/en/products/extractors-of-active/timatic-micro (Accessed 05 Dec 2012).

[19] European Pharmacopoeia, 7.0 ed., Council of Europe, Strasbourg, 2011.

[20] Weißdornblätter mit Blüten, In Deutsches Arzneibuch, Band 2, DAB 10, *Monographien R-Z.* Amlitche Ausgabe Deutscher Apotheker Verlag, Govi-Verlag GmbH, Stuttgart, 1991.

[21] B. Ivić, S. Ibrić, N. Cvetković, A. Petrović, S. Trajković, Z. Djurić, Application of Design of Experiments and Multilayer Perceptrons Neural Network in the Optimization of Diclofenac Sodium Extended Release Tablets with Carbopol® 71G, Chem. Pharm. Bull. **58** (2010) 947–949.

[22] R.H. Myers, D.C. Montgomery, Response Surface Methodology: Process and Product Optimization Using Designed Experiments, 2nd ed., John Wiley & Sons, New York, 2002.

[23] Z. Vujić, N. Mulavdić, M. Smajić, Simultaneous Analysis of Irbesartan and Hydrochlorothiazide: An Improved HPLC Method with the Aid of a Chemometric Protocol, Molecules **17** (2012) 3461–3474.

[24] P. Venkatesan, V.S. Janardhanan, C. Muralidharan, K. Valliappan, Improved HPLC Method with the Aid of Chemometric Strategy: Determination of Loxoprofen in Pharmaceutical Formulation, Acta Chim. Slov. **59** (2012) 242–248.

IZVOD

OPTIMIZACIJA EKSTRAKCIJE ANTIOKSIDANTNIH KOMPONENATA IZ HERBE HAJDUČKE TRAVE

Ivana A. Arsić[1], Vanja M. Tadić[2], Sofija M. Đorđević[2], Ana R. Žugić[2], Zorica B. Vujić[3], Slobodan D. Petrović[4]

[1]*Univerzitet u Nišu, Medicinski fakultet, IAS Farmacije, Niš, Srbija*
[2]*Institut za proučavanje lekovitog bilja"Dr Josif Pančić", Beograd, Srbija*
[3]*Univerzitet u Beogradu, Farmaceutski fakultet, Institut za farmaceutsku hemiju, Beograd, Srbija*
[4]*Univerzitet u Beogradu, Tehnološko-metalurški fakultet, Beograd, Srbija*

(Naučni rad)

Oksidativna degradacija sastojaka hrane dovodi do promene njenog mirisa i ukusa, čime se narušava njen nutritivni i senzorni kvalitet. Iz navedenog razloga je neophodno dodavati antioksidante tokom tehnološkog procesa izrade namirnica. Lekovito bilje i njihovi izolati predmet su istraživanja, pored ostalog i kao izvor antioksidantnih materija i alternativa sintetičkim antioksidansima za primenu u industriji hrane. Istraživanja velikog broja biljaka ukazala su da skoro sve poseduju određena antioksidativna svojstava. Hajdučka trava – *Achillea millefilium* L. (Asteraceae) i njeni ekstrakti, zahvaljujući prisustvu, pre svega, polifenola, flavonoida i tanina, ispoljavaju antioksidativni efekat. Sadržaj ovih materija u izolatima zavisi od njihove koncentracije u polaznom biljnom materijalu ali i od načina/uslova ekstrakcije. Cilj našeg ispitivanja bio je da utvrdimo optimalne vrednosti procesnih parametara za izvođenje pritiskom ubrzane ekstrakcije iz herbe hajdučke trave (*Millefolii herba*), radi dobijanja ekstrakata bogatih antioksidativnim materijama, kao i da utvrdimo zavisnost koja postoji između procesnih parametara. Ekstrakcija je obavljena u Timatic mikro ekstraktoru. Takozvano vreme kompresije, vreme dekompresije i broj ciklusa kruženja ekstrakcionog sredstva predstavljaju nezavisno promenljive veličine, dok su sadržaj ukupnih flavonoida, tanina, ukupnih polifenola kao i indeks refrakcije, suvi ostatak, relativna gustina, sadržaj etanola i pH vrednost zavisno promenljive veličine. Vreme kompresije bilo je 1 odnosno 2 minuta, vrednost vremena dekompresije 1,3 i 2 min, dok su ekstrakcije obavljene uz minimalno 20 odnosno maksimalno 99 ciklusa. Kao ekstragens korišćen je 70% (*V*/*V*) etanol. Droga: ekstrakt odnos iznosio je 1:3. Radni pritisak kretao se u opsegu od 1 do 99 bar. Primenjen je 2^3 faktorski dizajn, odnosno urađeno je osam ekstrakcija herbe hajdučke trave. Statistička analiza eksperimentalnih rezultata izvršena je upotrebom softvera *Design Expert* 7.0. U cilju potpune optimizacije primenjena je multivarijantna metodologija upotrebom *Derringer* funkcije poželjnih odgovora. Proces optimizacije postupka ekstrakcije pokazao je da je za izradu ekstrakata herbe hajdučke trave bogatih sadržajem antioksidativnih materija (flavonoidi, tanini i polifenoli), potrebno podesiti vreme kompresije na najviši nivo (2,0 min), vreme dekompresije na najniži (1,30 min) i vršiti ekstrakciju uz maksimalni broj ciklusa (99).

Ključne reči: *Timatic* mikroekstraktor • Hajdučka trava • Optimizacija • Polifenoli • Tanini • Flavonoidi